Dwarfs among Giants: Exploring Environmental Impacts on Dwarf Galaxies with the Solo Survey

by

Clare R. Higgs
B.Sc., Queen's University, 2012
M.Sc., University of Victoria, 2016

A Dissertation Submitted in Partial Fulfillment of the
Requirements for the Degree of

DOCTOR OF PHILOSOPHY

in the Department of Physics and Astronomy

We acknowledge with respect the lək̓ʷəŋən peoples on whose traditional territory the university stands, and the Songhees, Esquimalt and W̱SÁNEĆ peoples whose historical relationships with the land continue to this day.

Dwarfs among Giants: Exploring Environmental Impacts on Dwarf Galaxies with the Solo Survey

by

Clare R. Higgs
B.Sc., Queen's University, 2012
M.Sc., University of Victoria, 2016

Supervisory Committee

Dr. A. McConnachie, Co-Supervisor
(Department of Physics & Astronomy)

Dr. K. Venn, Co-Supervisor
(Department of Physics & Astronomy)

Dr. T. Darcie, Outside Member
(Department of Electrical & Computer Engineering)

ABSTRACT

This thesis attempts to untangle, as best as possible, the importance of internally-driven evolutionary mechanisms relative to externally-driven effects, in shaping the structure and properties of the smallest observable galaxies. All galaxies are influenced by internal processes, such as feedback from star formation and the infall of gas or lack thereof, as well as environmental processes, like tides and ram pressure stripping. The smallest galaxies – dwarfs – are highly susceptible to all such processes, and their resulting structure is the summation of all prior events.

I use nearby dwarf galaxies of the Local Group as test cases, focusing on those which are separated from the massive galaxies (like the Milky Way) and can be considered as "isolated". These dwarfs are observed as part of the *So*litary *Lo*cal (Solo) Dwarf Galaxy Survey. Solo dwarfs will have spent the majority of their time as isolated systems, hence their properties should generally reflect their "intrinsic nature", unperturbed and unaffected by interactions with other systems. This survey was designed to focus on the old stellar populations present in these galaxies, in order to characterize their faint and extended structures. These old stellar populations should carry the hallmarks of the dwarfs' histories. By comparing the observed properties of Solo dwarfs with dwarfs currently in close proximity to a large host galaxy (i.e., the M 31 and Milky Way satellites), it should be possible to determine what aspects of the properties of dwarfs are most affected by environmentally-driven processes.

The Local Group is the ideal regime in which to study these faint features, as the dwarfs' close proximity to us presents an opportunity to fully characterize these galaxies. However, the number of dwarfs in the Local Group is limited, with several galaxies (e.g. IC 10 or Sag dSph) being the unique example of their "type" locally observable. This limited sample emphasizes the need for careful, homogeneous observations and analysis, such that comparisons between this small, yet highly diverse, snapshot of galaxies accurately reflects the true nature of these dwarfs.

I have homogeneously analyzed the 12 closest Solo dwarfs observable from the northern hemisphere, resulting in a consistently derived dataset. I determine fundamental properties, like distances, and characterize the structure of the dwarfs. I explore the possibility that the dwarfs may be more consistent with a two component profile, rather than one, finding that they are largely well characterized by a single Sérsic profile.

I then compare these isolated dwarfs with the well-studied satellites of the Milky

Way and M 31, primarily using two other homogeneous surveys; the MegaCam Survey of Outer Halo Objects and the Pan-Andromeda Archaeological Survey respectively. Examining each property (e.g. ellipticity, central surface brightness, or Sérsic radius) individually, we find no statistically significant differences between each group. However, when considering parameters in combination (e.g. absolute magnitude as a function of Sérsic radius), we see increased scatter in the satellite population, indicative of the impact of a massive host galaxy on the dwarfs, likely via tidal effects.

The comparison between satellites and isolated dwarfs hones in on the impact of a massive galaxy in close proximity. Of course, processes within and surrounding the dwarf itself can also alter the dwarf. I look at the star formation histories and gas content of the dwarfs to explore the connection between internal and external processes in these small galaxies. Finally, I search for substructure in the form of satellites of dwarf galaxies, globular clusters and extended tidal features, all which inform about the dwarf's isolation, environment and history. Collectively, I generate comprehensive and detailed inspections of Local Group dwarfs and aim to understand them as products of their environment.

Contents

List of Tables

List of Figures

ACKNOWLEDGEMENTS

First and foremost, I would like to acknowledge with respect the Indigenous Peoples upon whose land observations were obtained and this research was conducted. Specifically, I acknowledge with respect the lək̓ʷəŋən peoples on whose traditional territory the University of Victoria stands, and the Songhees, Esquimalt and W̱SÁNEĆ peoples whose historical relationships with the land continue to this day.

I also recognize and acknowledge the very significant cultural role and reverence that the summit of Maunakea has always had within the Indigenous Hawaiian community. As an astronomer, I am fortunate to have the opportunity to conduct observations from this mountain. Without the mauna, there would be no astronomy in Hawai'i and no graduate thesis today. I owe the Indigenous Hawaiian community a great debt for sharing their skies with the world. As I explore the shared sky, I acknowledge our responsibilities to honour those who were here before us, and their continuing relationships to these lands.

It clearly takes a village to raise up a student with a (rough) idea into a fully fledged PhD candidate and there are many people to whom I owe many thanks.

I would like to thank my supervisor Alan for his endless encouragement (and patience), wisdom, insights, guidance and enthusiasm throughout my work. I deeply appreciate the support, freedom and time given to explore the avenues of my curiosity, to develop my own ideas and understanding and find my way through this academic journey. I am also extremely grateful for the numerous opportunities, both close to home and further afield, provided - I can't say thank you enough! I would also like to extend a huge thank you to Kim for her support and endless encouragement, both in regards to my science and my space in our broader community.

A big thank you to the Solo Collaboration for the wonderful observations on which this thesis is built. I am grateful to the Canada France Hawaii Telescope, both for the outstanding observations (thanks MegaCam!) and for the nurturing and supportive community they build and foster. Special thanks to Todd Burdullis and Mary Beth Laychak. My thanks to the Institute of Astronomy at the University of Cambridge and Prof. Mike Irwin for my extended visit and all the insights gained.

Thank you to the astro grad community. Working alongside you all and sharing offices and lunch tables (and Zoom calls) has been a pleasure and wishing you all the best! In particular, a big thanks to Mara, Maan, Azi, Nick, Collin, Kyle, Zack,

Charlie and Jaclyn for all your help and support (and games of Hanabi).

Last but most definitely not least, I would like to thank my friends and family for their support, encouragement and patience as I have slowly trudged my way through this journey. Particularly huge thank you's to Sandra (for the unwavering support, pep talks and consistent source of snacks), Frances (for being an amazing role model and also for the snacks), Kyle (for seeing me through the homestretch and being an additional source of snacks), and the whole "crew" (for keeping me sane and all the weekend adventures). I am so grateful to my parents and my brother for their love, help and learning more astronomy than they ever expected. For friends old and new, near and far who's words and encouragement have been the consistent tides that have carried me through - thank you!!

My grandmother once gave me some advice: if you put the word *just* in front of anything, it won't seem so impossible. So without further ado, I will just finish my PhD...

DEDICATION

To all those who helped and supported me along the way, whether they knew it or not (especially Wiz).

Chapter 1

Introduction

Dwarf galaxies are central to this thesis. Due to their small sizes, their study poses both an opportunity and a challenge. In this chapter, I first define what I classify as a dwarf galaxy, and then place them in the overall context of galaxies of all masses. I go on to discuss our general understanding of the relevant processes that affect dwarf formation and evolution, and connect these processes to the larger picture. I close this chapter with discussion of the opportunities and challenges in dealing specifically with Local Group dwarfs, and how to determine whether a dwarf is truly isolated or not. This discussion motivates the Solo Survey, which is described in full in Chapter 2.

Throughout, I refer to "host" galaxies as those massive galaxies which dominate their local environment (like the Milky Way or Andromeda/M 31); "satellites", which refer to dwarfs residing in close proximity to a host; "isolated dwarfs", synonymous with field dwarfs, which refers to those dwarfs at large separations from any potential host. I use "dwarfs" when referring to both isolated dwarfs and satellites together, and "galaxy" when referring to galaxies across all mass scales, from the smallest satellites to the most massive hosts.

1.1 Introducing Dwarf Galaxies

A galaxy is a sophisticated amalgamation of baryons – stars, gas and/or dust – and dark matter. The absolute and relative contributions of each of these components, and the chemistry and composition of the baryons, is a result of the integrated effects of a multitude of processes governing the initial formation of the system and its subsequent evolution. Correspondingly, the structure and chemistry of a galaxy can, in principal,

provide important insights into the major events and major physical processes that form the galaxy we now observe. However, in this approach, complexity arises due the large number of processes possibly at play, potentially simultaneously.

By definition, dwarf galaxies are all low mass, but local examples range from the more sizeable Large Magellanic Cloud (LMC - with a stellar mass of $2.7 \times 10^9 M_\odot$; van der Marel 2006) to tiny systems like Segue 1 (with a stellar mass of only $\approx 1000 M_\odot$; Geha et al. 2009). Dwarfs are plentiful in our Universe – the galaxy luminosity function is such that small mass systems are far more common than high mass systems – and it is believed that dwarfs form the "building blocks" of more massive galaxies via hierarchical galaxy formation (e.g., White & Rees 1978). Indeed, the number of known nearby dwarfs has increased significantly in the last decade (e.g., see Figure 1 in Simon 2019 with respect to the Milky Way satellites alone), and as the numbers have increased, so too has their morphological diversity. Dwarfs exhibit a wide array of morphologies and properties, that suggest complex and varied formation and evolutionary pathways.

Dwarfs are particularly interesting laboratories for galaxy evolution as their low masses cause their baryonic components to potentially be very sensitive to individual events (e.g. feedback from star formation). A good example is Reticulum II, a dwarf satellite of the Milky Way. Typically, the metal abundance of stars observed in a galaxy will reveal the integrated impact of all star formation and stellar feedback events throughout a galaxy's history, with earlier stellar populations impacting the composition of those that form later. Large galaxies will have many such events, and the impact of any individual event can get lost. However, detailed chemistry of individual stars in Reticulum II shows the signature of a single, dominant r-process event, likely a neutron star merger (Ji et al. 2016; Safarzadeh et al. 2019 among others). In larger galaxies, the hopes of observing such a signature become increasingly unlikely, since the impact of this one event may easily be lost amongst the accumulated impacts of many.

1.1.1 Classification, and the perils thereof

Binggeli (1994) writes about the complexity of naming and classifying dwarfs, asking what defines the "dwarfishness" of dwarfs. He expands that classifications based on the absolute magnitude – central surface brightness trends ($M - \mu$, Kormendy relations; Kormendy 1985) are perhaps premature as "there is much *terra incognita* in

the $M - \mu$ plane left to be explored". Since this work, the complexity of classifying and defining dwarfs has only increased, with the known population of nearby dwarfs rapidly expanding. Simon (2019) shows that the number of Milky Way (MW) satellites has risen from ~ 10 to > 50 since Binggeli (1994). In addition, the *terra incognita* has held numerous surprises. Recent examples include the highly unusual Crater II and Antlia II, (Torrealba et al. 2016, 2019 respectively) which have exceptionally low surface brightnesses and exceptionally large scale radii. New classifications, such as ultra-faint and ultra-diffuse, have been introduced and are now in common usage (e.g. Simon 2019). New discoveries have shown that previous individual "outliers" are, in fact, representative of previously unknown groups that share similar morphological features.

While it is natural to try to categorize like-with-like when describing dwarfs, as with any classification procedure, it can complicate the picture. Classification encourages strong distinctions to be made between systems that might actually occupy the same continuum of properties. Further, without understanding the range of physical processes that lead to certain appearances, it is equally possible that we can group together systems that have, in fact, had completely different evolutionary histories. For instance, consider systems classed as "old", based on their stellar populations. These galaxies must have, inevitably, previously stopped forming stars. The cessation of star formation at early times in different systems may be due to the removal of gas by reionization, or infall of the dwarf into the halo of a more massive galaxy, or via the expulsion of gas from stellar feedback from the star formation episode. Each of these scenarios is quite different, with different implications for the interplay between the dwarf and its local or cosmic environment. By simply grouping all dwarfs which only show an old stellar population together, we are at risk of becoming blind to these possible distinctions.

With these important caveats in mind, we show in Figure 1.1 a selection of galaxies with a range of masses in terms of V-band absolute magnitude (M_v), central surface brightness (μ_v) and effective radius (r). To encompass the diversity, I have complied various surveys and samples, creating an illustrative, but far from exhaustive, sampling of galaxies in an effort to place dwarfs in context. Figure 1.1 shows the Virgo Cluster galaxies from the Next Generation Virgo Survey, with a diverse range of galaxy sizes and types from Ferrarese et al. (2020). Similarly, the Local Group dwarfs complied in McConnachie (2012), with a mixture of dwarf types. The Milky Way globular clusters from Muñoz et al. (2018b) are shown. On larger scales, spiral

and elliptical galaxies from the Carnegie - Irvine Galaxy Survey (CGS) (Ho et al., 2011; Li et al., 2011).

Various regions of these diagrams are distinct, indicating where certain "classes" of objects lie, and each will be expanded on in the following sections. Briefly, we see ultra diffuse galaxies selected from van Dokkum et al. (2015) and Cohen et al. (2018) and ultra compact dwarfs from Evstigneeva et al. (2008). Ultra faint dwarfs identified as spectroscopically confirmed by Simon (2019) are shown (using values from McConnachie 2012).

1.1.2 Dwarfs versus globular clusters

Figure 1.1 shows that, with the discovery of very faint dwarf galaxies around the Milky Way (e.g., Segue 1, Canes Venatici II and Hercules from Belokurov et al. 2007; Willman 1 from Willman et al. 2005; Boötes II Walsh et al. 2007), the distinction between dwarfs and globular clusters (GCs) is not clearly defined. Gilmore et al. (2007) define "the valley of ambiguity" as that region of overlap in the effective radius and absolute magnitudes of these systems, and suggests that it is a challenge to distinguish between them using photometry alone. The presence of multiple stellar populations within GCs (see reviews by Gratton et al. 2012 and Bastian & Lardo 2018, or D'Ercole et al. 2008) further confuses the distinction.

A defining distinction of a GC is that it is not believed to be at the center of its own dark matter halo (e.g. Willman & Strader 2012). Fundamentally, the formation mechanisms of GCs must therefore be distinct from the formation of a galaxy (see Brodie & Strader 2006 for a review or more recently Kruijssen 2015, for an example of a globular cluster formation scenario). Observationally, however, it can be challenging to distinguish the more extreme or unusual examples of both GCs and dwarfs, and extreme examples of either population may need their own special formation channel. For example, some GCs, such as ω Cen (see Freeman 1993; Ideta & Makino 2004 among others), are thought to be the stripped cores of dwarf galaxies.

For the bulk of both populations, the existence of a significant dark matter halo would be sufficient to distinguish a dwarf from a GC. This can usually be determined via measurement of its velocity dispersion for a stellar system in equilibrium. The dynamical mass can be calculated and compared to its stellar mass, given the scale radius of the stellar system. However, for very faint stellar systems, there are sometimes very few stars that can be easily accessed for spectroscopy. Often, this means

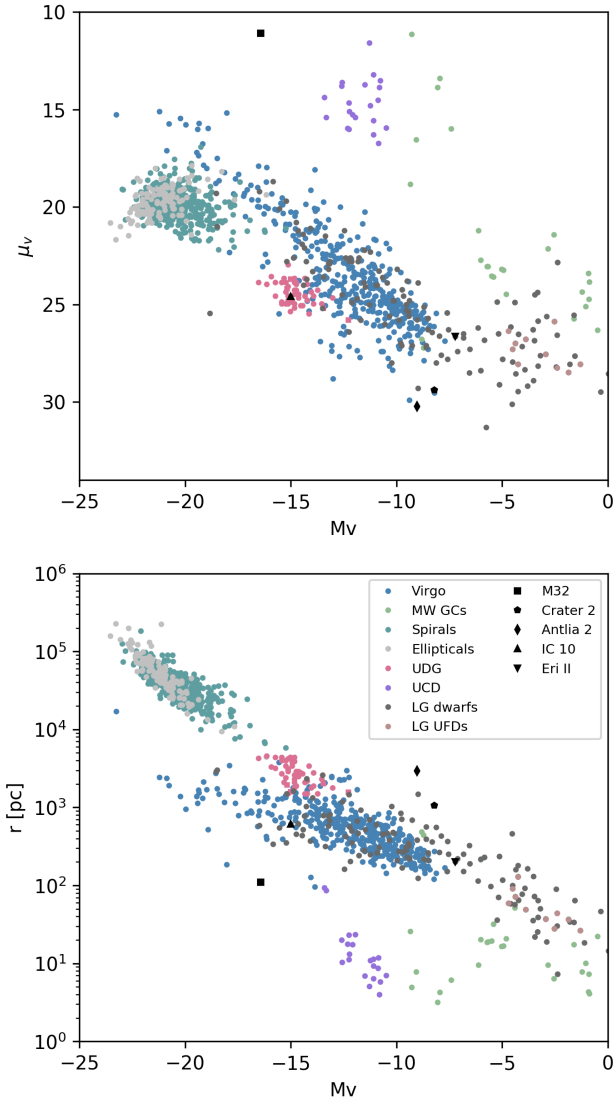

Figure 1.1: Based on Tolstoy et al. (2009), various galaxy types and globular clusters (GCs) shown as function of V-band absolute magnitude (M_v), central surface brightness (μ_v) and effective radius (r). Various individual galaxies of interest (discussed specifically in this introduction) are noted in black using values from McConnachie (2012). Details of each group is given in the text. Virgo galaxies: Ferrarese et al. (2020), MW GCs: Muñoz et al. (2018b), spirals & ellipticals: Ho et al. (2011) and Li et al. (2011), ultra diffuse galaxies: van Dokkum et al. (2015) (circles) and Cohen et al. (2018) (squares), ultra compact dwarfs: Evstigneeva et al. (2008), ultra faint dwarfs: Simon (2019), Local Group dwarfs:McConnachie (2012). Where necessary, conversions to the V-band using Thomas et al. (2021) and the effective surface brightness (μ_e) to central surface brightness using Graham & Driver (2005).

velocity dispersions are unable to be calculated without very significant uncertainties. In the absence of a robust velocity dispersion, a spread in metallicities is often used as an indirect indicator of a gravitational potential well deep enough that the outflows from star formation can be retained in order to enrich future generations of stars. Thus, the metallicity spread implies the presence of a massive dark matter halo for systems with low stellar mass. GCs and dwarfs are distinguished into two unique classes using this fundamental difference.

1.1.3 Dwarfs versus larger galaxies

Are dwarfs simply small counterparts of more massive systems? Figure 1.1 shows a trend famously noted by Kormendy (1985), which is the change in the direction of slope of the $M - \mu$ relation as a function of magnitude, around $M_B \sim -18$. When first noted, there were few galaxies at these intermediate magnitudes, and the scaling relations of these systems appeared particularly distinct from one another. However, more recent studies, such as those by the Next Generation Virgo Survey (Ferrarese et al. 2012; also see Graham & Guzmán 2003) show a continuum in surface brightness as a function of magnitude. The absence of any strong discontinuity in surface brightness means distinct formation scenarios for dwarfs and giants are likely not required. We therefore expect, unlike the case for GCs, the fundamental formation scenario for dwarfs and larger galaxies are possibly (likely) the same.

Where dwarfs and more massive galaxies diverge in their evolution results from the fact that the same processes likely have very different impacts on the system. For example, the presence and impact of active galactic nuceli (AGN) on massive galaxies is substantial (e.g., Di Matteo et al. 2005; Bower et al. 2006 among many others or review by Harrison 2017). The diagram in Figure 1.2 illustrates how star formation is quenched in large galaxies, and highlights the numerous pathways through which AGN regulate their host galaxies.

However, AGN are not observed in the smallest dwarf galaxies. For example, Mezcua & Domínguez Sánchez (2020) find AGN candidates in 37 dwarfs in the MANGA Survey, the smallest of which have stellar masses $\sim 10^9 M_\odot$. Similarly, Bradford et al. (2018) have a sample of gas depleted, isolated dwarfs possibly with AGN selected from SDSS with masses $> 10^{9.2-9.5} M_\odot$. Reines et al. (2020) looks for "wandering" black holes in dwarfs (not lying at the centers of their potential wells) finding three candidates below $3 \times 10^8 M_\odot$ (the previously lowest mass AGN identified

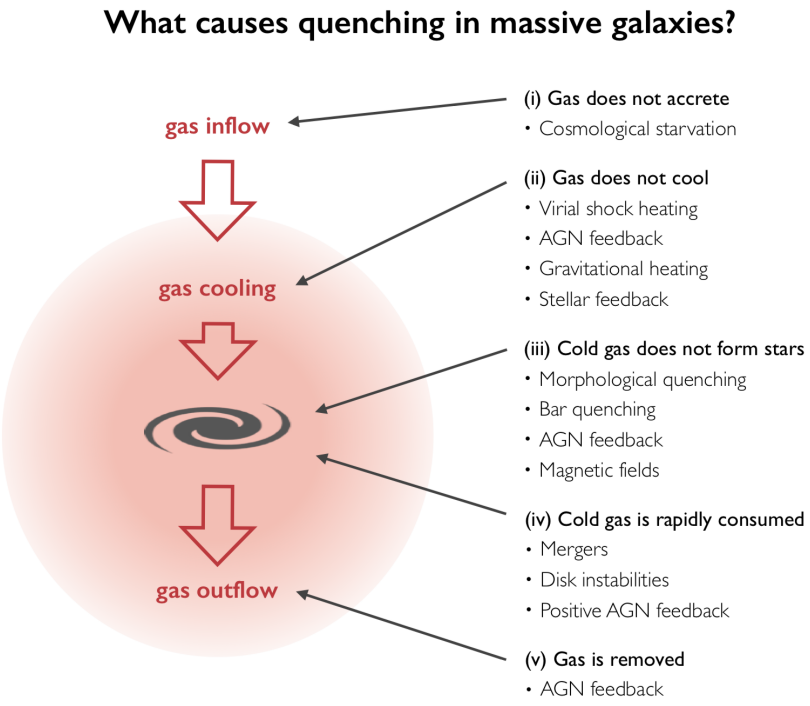

Figure 1.2: Diagram from Man & Belli (2018), showing the mechanisms via which star formation is halted in massive galaxies. Note the emphasis on the role of an active galactic nucleus (AGN).

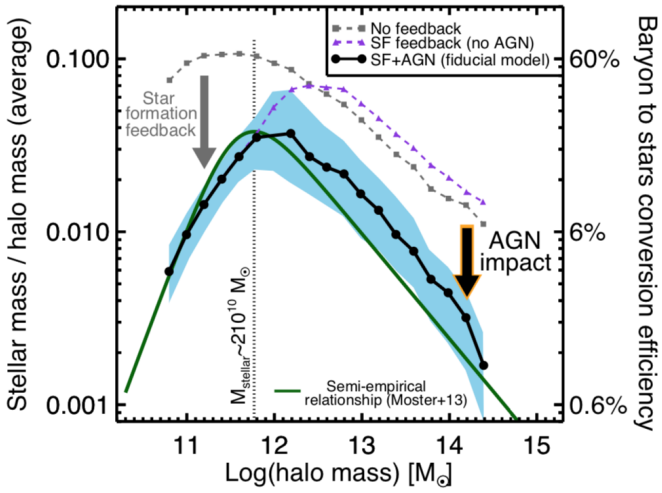

Figure 1.3: Diagram from Harrison (2017), showing the stellar to halo mass ratio as a function of halo mass. The distinction in star formation efficiency in the dwarf regime (left side) and more massive galaxies (right side) is clear.

by Reines et al. 2013). These detections are at the more massive end of the Local Group dwarfs which are our focus here.

Without AGN, there are fewer mechanisms by which a dwarf can halt star formation in isolation. Indeed, Geha et al. (2012) show that there is a mass threshold (around $\sim 10^9 M_\odot$), below which no isolated quenched dwarf galaxies have been found in the SDSS. Dwarfs do, however, lie in a mass regime where quenching by supernova is believed to be effective (e.g. Behroozi et al. 2013). Figure 1.3 from Harrison (2017) shows the star formation efficiency as a function of halo mass. The two different regimes contrasting dwarf and more massive galaxies are highlighted, with the different drivers (AGN or star formation feedback) highlighted. Polzin et al. (2021) suggest they have detected an isolated quenched dwarf, located 1.4 Mpc from a host, possibly demonstrating this "self quenching" in the field. These differences in evolution may result in significant distinctions in observed properties of dwarfs and more massive galaxies.

There are also some structural differences that reveal themselves between dwarf and giants. For star forming systems, dwarf galaxies are frequently irregular in morphology, whereas more massive galaxies often exhibit more order (like spiral arms). The irregular appearance of dwarfs implies that pressure support and turbulence may, typically, be of greater importance, rather than rotational support. El-Badry et al. (2018b) show the importance of rotation and pressure support on HI gas through a

range of masses in the FIRE simulations, finding that gas is less rotationally supported with decreasing mass. Observationally, Roychowdhury et al. (2010) observe larger ratios of velocity dispersion to rotational velocity in dwarf galaxy HI disks as compared to spiral galaxies. Kaufmann et al. (2007) model the formation of low mass dwarfs, and show that lower mass dwarfs are more likely to form as puffy disks, with significant pressure support. Simply, dwarfs are not straight analogs of larger systems, and pressure support is usually important (Chowdhury & Chengalur, 2017; Butler et al., 2017). However, this does not mean dwarfs are not lacking rotation completely, as there are numerous examples of rotation in Local Group (e.g. WLM - Leaman et al. 2009, Carina - Muñoz et al. 2006, Sculptor - Battaglia et al. 2008, Leo I - Mateo et al. 2008, and Tucana - Fraternali et al. 2009 to name a few).

Despite this contrast in the presence/lack of spiral arms and rotation, dwarfs and more massive galaxies do sometimes show some analogous features in terms of their structures. For example, Vansevičius et al. (2004) examine Leo A in detail, and propose that exhibits a complex structure, similar to a more massive, disky galaxy. Further, large galaxies often exhibit stellar halos, and the presence of an analogous structure in low mass dwarfs is presently unclear. The allure of detecting halos around dwarfs lies in our desire to better understand their formation, whether they are a result of mergers or in-situ star formation. Pucha et al. (2019) claim they identify a "halo" in IC 1613, finding the older, extended stellar component exhibits a different density profile to the more compact stellar component. However, the stellar densities in question are very low and they caution against over interpretation as a halo. In a similar vein, Chiti et al. (2021) claim the detection of stars very far from the center of the ultra faint dwarf Tucana II, suggestive of a halo. Clearly, the definitive detection of a dwarf's halo is elusive, in contrast to the detailed and extensive halo studies of more massive galaxies (e.g. GAIA study of the Milky Way: Bland-Hawthorn & Gerhard 2016, M 31's extended structure with PAndAS: McConnachie et al. 2009, HST study of 6 edge-on spirals with the GHOSTS Survey: Monachesi et al. 2016 to name but a few).

Finally, there is also an observational difference in the study of dwarfs compared to giants: survey completeness is much more of an issue for dwarf galaxies rather than massive galaxies. The discoveries of ever fainter systems (described below) means we are forced to observe at the extremes of detectable surface brightness. These are not generally challenging issues for larger galaxies, where our census of galaxy types is consequently more robust. Completeness is an issue I will return to again in this

thesis.

Tollerud et al. (2011) find that dispersion-supported galaxies follow the same fundamental mass-radius-luminosity plane over 8 orders of magnitude in luminosity, and that this plane does not include GCs and ultra compact dwarfs (defined in the next section). This conclusion is in keeping with the idea that dwarfs are, indeed, the smaller counterparts of more massive galaxies, yet we must bear in mind how differences in observations (completeness/detection of halos) and structure (rotation/AGN) impact dwarfs and our interpretations.

1.1.4 On the diversity of dwarfs

What of all the dwarfs in Figure 1.1? This population breaks down into many subclasses. We broadly define "classical dwarfs" as those with $M_\star \approx 10^{5-7} M_\odot$ (following Bullock & Boylan-Kolchin 2017). Those with gas are typically called dwarf irregulars (dIrrs) and those without are dwarf elliptical (dE). Classical dE galaxies fainter than $M_V \simeq -15$ are typically referred to as dwarf spheroidals (dSphs). Usually, dIrrs are seen to be actively star forming, with young, bright, bluer stellar populations, while dSphs generally have only older, redder stellar populations. There is a clear and well observed distance – morphology relation in the Local Group and elsewhere, showing that dwarfs close to a host are typically dSphs and those at greater distances are dIrrs (Einasto et al., 1974; Spekkens et al., 2014; Putman et al., 2021). A "transition-type" dwarf is sometimes defined as a dwarf with gas but without active star formation. The distinction of transition-type dwarfs from dIrrs in particular is not clear. For example, a dwarf with low-level star formation may be observed in a quiescent period and classed as a transition-type, but it would be difficult to argue that it is fundamentally distinct from dIrrs in morphology or evolution. Figure 1.4 shows examples of dwarfs with a range of morphological types and masses within the Local Group (LG) from the LMC ($3 \times 10^9 M_\odot$) to Pictoris I ($3 \times 10^3 M_\odot$).

Beyond the classical dwarfs, other dwarf types highlighted in Figure 1.1 include "ultra compact" and "ultra faint". Ultra compact dwarfs are generally identified with half light radii between $10 - 100\,\mathrm{pc}$ and masses larger than $2 \times 10^6 M_\odot$ to $10^8 M_\odot$ (Saifollahi et al., 2021), meaning they lie in the mass range between "normal" dwarfs and globular clusters. They were first identified in the Fornax cluster (Hilker et al., 1999; Drinkwater et al., 2000). They have since been found in other environments, like the Virgo cluster (Ferrarese et al., 2016). There are two proposed formation

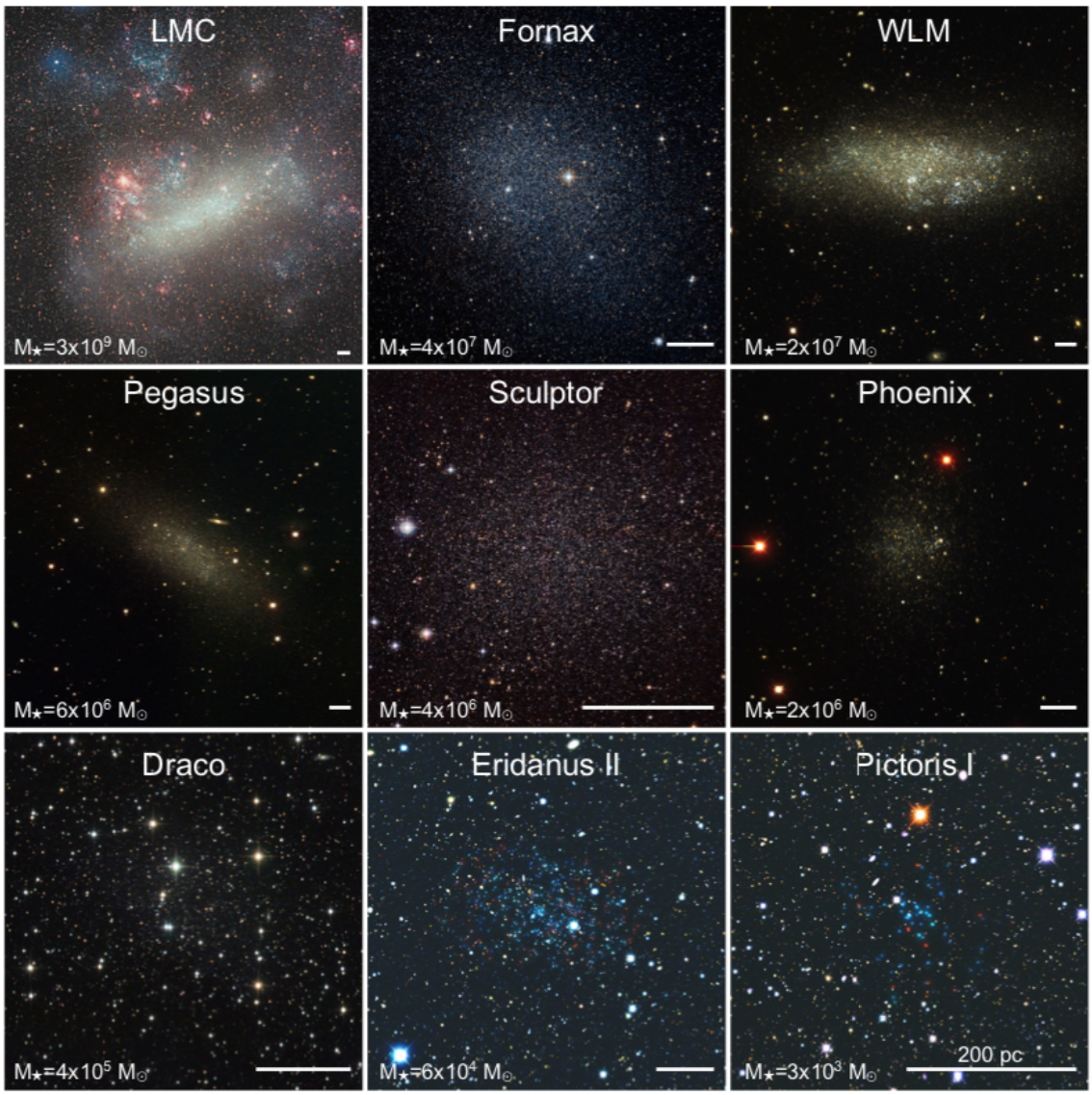

Figure 1.4: From Bullock & Boylan-Kolchin (2017) (image references within), dwarfs at a range of stellar masses (LMC: $3 \times 10^9 M_\odot$ to Pictoris I: $3 \times 10^3 M_\odot$). The scale bar shows 200 pc.

scenarios, either ultra compact dwarfs are the remnants of heavily stripped galaxies and therefore occur primarily in dense environments, or they are the very brightest star clusters, i.e. globular clusters. Saifollahi et al. (2021) perform a systematic, expanded search in the Fornax cluster, and find ultra compact dwarfs outside the core of the cluster. However, they conclude that the majority ($\sim 87\%$) are likely heavily stripped, lending weight to the origin scenario that UCDs are the stripped remnants rather than star clusters.

Ultra faint dwarfs are, as the name implies, very low luminosity. Simon (2019) suggest a limit of $M_v = -7.7$ ($L < 10 \times 10^5 L_\odot$) consistent with Bullock & Boylan-Kolchin (2017), who define ultra faints as $M_\star \approx 10^{2-5} M_\odot$. Willman et al. (2005) first used the term "ultra faint" with the discovery of Willman I (then identified as SDSSJ1049+5103), signifying that it appeared to be a dwarf but significantly fainter than any of the then-known Milky Way dwarf satellites. As detailed by Simon (2019), ultra-faint dwarfs distinguish themselves from star clusters as they have generally extended star formation episodes, are implied to contain significant fractions of dark matter, and are generally more extended than star clusters. However, they do appear to overlap with globular clusters in the parameter space shown in Figure 1.1, and detailed observations are often required to distinguish them from globular clusters. Simon (2019) list 21 spectroscopically confirmed ultra faint dwarfs, including Draco II and Eridanus II (recently discovered and, surprisingly, containing a surprising stellar cluster; Zoutendijk et al. 2020).

Ultra diffuse galaxies (UDGs) are also worth noting. A recent addition, UDGs were first defined after detection with the unique Dragonfly telescope (Abraham & van Dokkum, 2014). They generally have stellar masses comparable to dwarfs, but have physical sizes much more comparable to the Milky Way. This combination results in them being very low surface brightness. van Dokkum et al. (2015) report 47 ultra diffuse galaxies in the Coma cluster with effective radii of $\sim 1.5 - 4.6\,\mathrm{kpc}$, comparable to $L_\star$ galaxies (e.g. Milky Way- or M31–sized), with a median stellar mass of $6 \times 10^7 M_\odot$ (comparable to dwarf galaxies). They propose the definition that "ultra-diffuse" galaxies should apply to those galaxies with $r_e > 1.5\,\mathrm{kpc}$ and $\mu_{g,o} > 24\,\mathrm{mag.\,arcsec^{-2}}$. These recently detected, highly spatially extended objects do not have any direct analogues in the Local Group, although Antlia II and Crater II ("feeble giants") are much lower stellar mass systems that bear similarities to this population (see discussion in Collins et al. 2021). All of these objects illustrate the diversity of dwarfs and the yet-undiscovered possibilities of *terra incognita*.

1.2 From Origin to Observation

To understand the dwarfs observed today, we must take into account their initial formation as well as the internal and external processes that have since shaped them. The number and complexity of the processes involved results in the wide variety of dwarf morphology and types observed today. There is no one single characteristic, be it halo mass or environment or other, that will singularly predict the properties of a dwarf observed today; this is not a one parameter problem.

1.2.1 The formation of dwarfs

The general picture of galaxy formation in the ΛCDM (Λ Cold Dark Matter) is a hierarchical model, by which successively larger dark matter halos and their associated baryons are built through a series of mergers and in-situ star formation (foundationally, White & Rees 1978; Blumenthal et al. 1984; White & Frenk 1991 and many others). Baryonic matter accretes into the dark matter halos, triggering star formation, enriching and impacting successive generations of stellar populations. In such a model, it is reasonable to suggest that there is a mass limit below which the halo is not massive enough to acquire and retain gas for star formation (Efstathiou 1992 and others), and so the smallest dwarfs represent the limits of the galaxy formation process.

Fitts et al. (2018) suggest the role mergers play in the assembly of dwarfs is less than that for large galaxies. In the FIRE simulations (Hopkins et al., 2018), they find that $>90\,\%$ of stars are formed in-situ for most dwarfs (stellar masses $10^{5-7}M_{\odot}$). This result agrees with Moster et al. (2013) who also find that the role of mergers is more significant for more massive galaxies, for which roughly half of their stars may have formed ex-situ.

While mergers may not be as significant for the build-up of dwarfs as for the build-up of massive galaxies, ΛCDM nevertheless suggests that dwarf galaxies can themselves host satellite galaxies, in keeping with the hierarchical nature of dark matter halos. Wheeler et al. (2015) have also used the FIRE simulations to predict the numbers of satellites that dwarfs should have, as seen in Figure 1.5. They find dwarfs with masses $10^{6}M_{\odot}$ typically have $1-2$ well resolved satellites. This figure also shows the abundance of substructure in these dark matter halos and the number of small halos which do not have a stellar counterpart. Indeed, Dooley et al. (2017) have estimated the likelihood of the Solo dwarfs (discussed in this thesis) hosting an

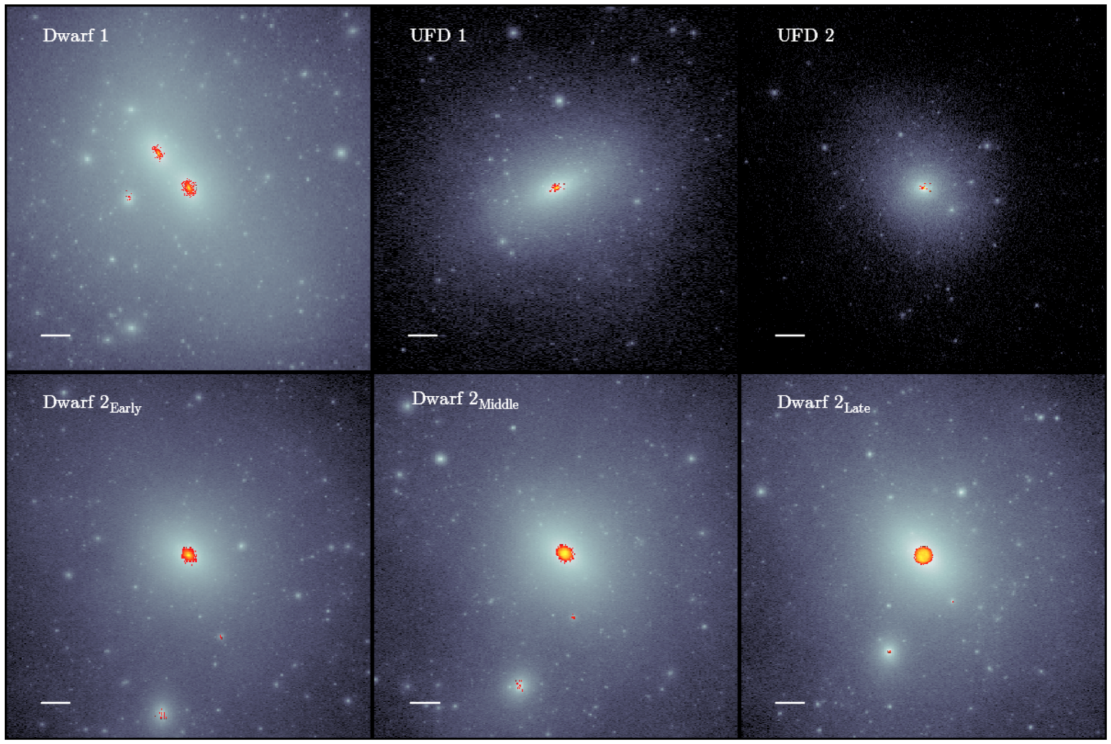

Figure 1.5: Diagram from Wheeler et al. (2015), showing the formation of dwarfs. Dark matter is shown in the grey scale and stellar density in colour. The scale bar is 5 kpc.

observable satellite within the field of view of our observations, finding a non-zero possibility of an observable satellite within our data.

Overall dwarfs fit the hierarchical ΛCDM picture, with the mergers and in-situ star formation building and growing galaxies, like all galaxies on all scales.

1.2.2 The evolution of dwarfs

There are numerous evolutionary processes that impact galaxies. These processes are expected to be relevant, to varying degrees, in the dwarf mass regime as well as the regime of massive galaxies, with the exception of feedback from AGN. They include: gas accretion, reionization, star formation (including supernovae and other feedback), strangulation, ram pressure stripping, tidal stripping, tidal shocking, resonant stripping, tidal stirring, galaxy harassment, mergers and dark halo interactions.

Gas accretion into a dark matter halo is necessary in order to acquire the fuel to form stars, both initially as the galaxy is forming and throughout its lifetime, if there

is to be continued star formation. This accretion requires the gravitational potential of the halo to be massive enough to retain any gas that cools. Indeed, the ability of a halo to retain fuel for star formation is a critical aspect of galaxy evolution, and small, dwarf-like halos are clearly less able to retain gas than more massive halos.

Early on in the Universe, **reionization** has a critical effect on the gas content of young galaxies (e.g. Bullock et al. 2000, Tollerud & Peek 2018, Kang & Ricotti 2019, or Rodriguez Wimberly et al. 2019). It is believed that star formation in high redshift dwarf galaxies were a significant (but not the only) source of the reionizing photons (e.g., Boylan-Kolchin 2018, Ma et al. 2021 or Wise et al. 2014) that acted to heat gas. In low mass halos, this heating could cause any gas not already formed into stars to escape the gravitational potential of the halo, and therefore stop any subsequent star formation. As a result, reionization is believed to be a major reason for a mass limit below which dark matter halos do not host galaxies. Again, see Figure 1.5 with the dark matter halos missing their baryonic counterparts. However, by its very nature, reionization is unlikely to have been homogeneous (e.g. Miralda-Escudé et al. 2000), and so its impact on low mass galaxies may differ depending on the dwarf's local environment at early times.

Wheeler et al. (2015) use simulations with a resolution that can resolve low mass UFDs, to look for the mass floor at which a dark matter halo no longer forms stars. They argue that there is a mass cutoff ($\sim 3 \times 10^4 M_\odot$) below which star formation will be halted via reionization, resulting in strictly old stellar populations. The LCID (Local Cosmology from Isolated Dwarfs) survey used HST ACS observations of 6 isolated dwarfs (Cetus, Leo A, IC 1613, Tucana, LGS 3 and Phoenix) to obtain deep photometry of the oldest main sequence turn off in these galaxies (Monelli et al. 2010b,a; Hidalgo et al. 2011; Skillman et al. 2014). For each of these galaxies, their results showed that star formation was able to continue after reionization for systems with stellar masses greater than $10^6 M_\odot$, well above the cut off from Wheeler et al. (2015). Brown et al. (2014) looked at the star formation histories of 6 UFDs in a similar way. In contrast to the more massive LCID systems, they found that UFDs have predominately old stellar populations consistent with the general idea of the cessation of star formation at around the time of reionisation. Brown et al. (2014) also finds that some systems have slightly younger stars, and discuss, using the terminology of Ricotti & Gnedin (2005), "true fossils" (those systems that are consistent with reionisation ending all star formation in the galaxy), "survivors" (those which have substantial star formation after reionization), "polluted fossils" (those showing

comparable star formation before and after star formation) and "rejuvenated fossils" (e.g. Leo T, where gas is believed to have been recently reaccreted and triggered a new wave of star formation).

For those systems that are able to accrete/retain gas, **star formation** plays a critical role in regulating the gas/stellar content of galaxies. Specifically, the stars that form provide feedback to the gas, either by heating the gas, by providing high velocity winds through supernovae that can push out the gas, or via less energetic but still significant winds from evolved stars, such as AGB stars. These feedback processes change the amount of gas that is available for the next generation of star formation. As before, the effects of stellar feedback are more pronounced for low mass dwarfs that for high mass galaxies. Almost all dwarf galaxies generally have a dominant old stellar population, showing most stars formed early in the life of the dwarf soon after the first gas was accreted. This early star formation is evident in Figure 1.6, reproduced from Weisz et al. (2014). These authors show that dSphs and dIrrs generally have very similar star formation histories at early times, and most of the morphological distinction between these two "classes" is a result of the presence of very recent star formation in dIrrs, that is generally absent in the dSphs.

Figure 1.6 suggests the major distinction between dSph and dIrr galaxies hinges on the latter have been able to retain, or re-acquire, gas to fuel recent star formation. Considering galaxies of roughly equivalent masses, what other effects not yet discussed might cause one system to lose its gas and the other to retain it? The position-morphology relation in the Local Group suggests such processes might be environmental (depending on the surroundings like the presence of another galaxy), for which there are a few candidates. **Ram pressure stripping** (Gunn & Gott 1972) can occur when a dwarf galaxy with its own gas passes through a hot halo of a galaxy, group or cluster. The efficiency with which the gas is stripped depends on the density of the medium, the density of the gas and stars in the dwarf, and the velocity of the dwarf with respect to the medium. Within the Local Group, the Pegasus dIrr is a good candidate for a system actively being ram pressure stripped (McConnachie et al., 2007b). Numerous other examples are known in the Local Universe, including Phoenix (Gallart et al., 2001), the 9 new Milky Way satellites discovered by Dark Energy Survey and devoid of HI (Westmeier et al., 2015), the Virgo cluster spiral galaxy NGC 4522 (Vollmer et al., 2000), NGC 1427A, a dIrr in the Fornax Cluster (Mastropietro et al., 2021).

Alternatively (or in addition), **strangulation** (or starvation) is the process by

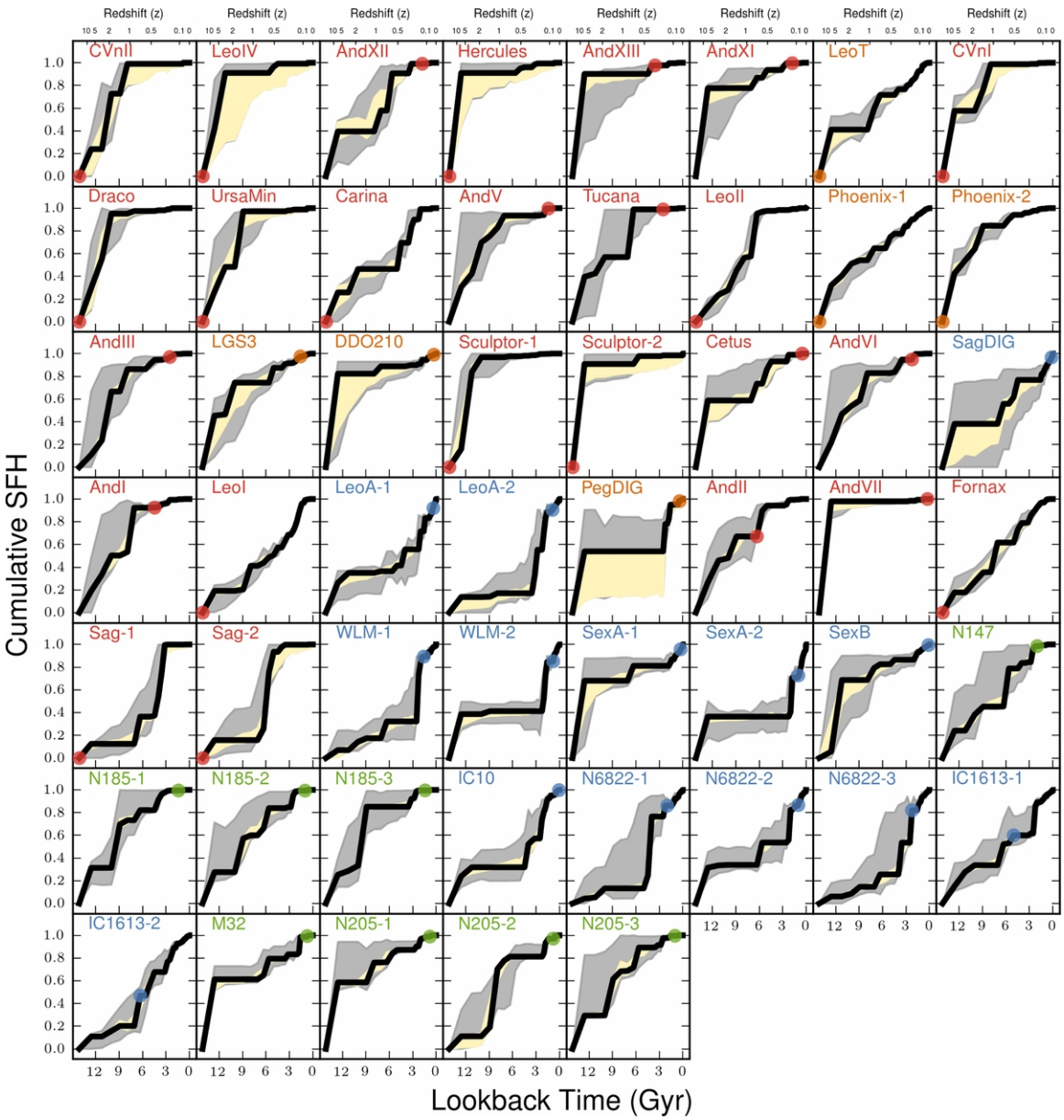

Figure 1.6: Cumulative star formation histories (SFH) for Local Group dwarfs from Weisz et al. (2014), with blue labelling dIrrs and red for dSphs.

which the infall of gas into the halo is prevented, effectively halting the possibility for future star formation (e.g. Larson et al. 1980, Balogh et al. 2000 or Bekki et al. 2002). While often discussed in the context of galaxy clusters or groups, Kawata & Mulchaey (2008) suggests this can happen in lower mass groups, generally with a central elliptical galaxy (not applicable to our Local Group). Strangulation is sometimes used as an umbrella term, encompassing various mechanisms of gas removal, hence ram pressure stripping and mergers may cause strangulation (e.g. Peng et al. 2015). However, Bekki et al. (2002) describe the mechanism for strangulation as predominantly the hydrodynamical interaction between the halo gas and the hot intracluster gas. Peng et al. (2015) highlight a key aspect of strangulation: the process happens slowly, with star formation using up the remaining gas, resulting in more metal rich galaxies. Koutsouridou & Cattaneo (2019) use differing timescales and metallicities to untangle the effects of strangulation, ram pressure stripping and tides on star formation in dwarf galaxies. Weak impacts from ram pressure stripping and tides will stop the infall of gas but not remove the gas already present in the galaxy, so star formation will continue (but decline), resulting in increasingly metal rich populations. With a strong effects from tides and ram pressure stripping, gas is rapidly removed and star formation is halted and the metallicity is "frozen".

In contrast to ram pressure stripping, **tidal stripping** can act not just on the gas, but also on the stars and dark matter. Tidal stripping is the removal of mass from a system as a result of differential gravitational forces experienced by that system from a more massive companion. Stars far from the center of the dwarf's potential will generally be the first to become unbound. Read et al. (2006b) explore tidal stripping in detail and show that the radius at which a particle (star) becomes unbound is dependent on four parameters: the potentials of both the satellite and host, the orbit of the satellite and the orbits of the stars within the dwarf. Ordered from least to most bound, stars on prograde, radial, and retrograde orbits are actually stripped differently. Clearly, tidal effects are most significant for satellites near pericenter, and can have negligible effects for dwarfs far from a host galaxy. The impacts of tidal stripping on the resulting structure is varied. Łokas et al. (2011) study the results in various simulations. They find some expected results, such as the fact that the half light radius decreases. Some results are more complicated, like the ellipiticity which can increase or decrease depending on the orbital parameters and initial conditions of the dwarf. Fattahi et al. (2018) use the APOSTLE simulations to study how tidal stripping changes the observed properties of dwarfs in the LG. They find "cold

faint giants" (e.g. Crater II and And XIX) within the LG are likely heavily stripped dwarfs. They investigate the necessary properties of the progenitor population, and find that their dynamical properties are in agreement with the isolated LG dwarfs. Borukhovetskaya et al. (2021) looks at a specific example of tidal stripping on Fornax, which does not appear to reside in as massive a dark matter halo as might be expected given its luminosity. Fornax can be brought into agreement with the ΛCDM framework with the inclusion of tidal stripping. This stripping predominantly impacts its dark matter halo, reducing its mass by $\sim 50\%$ while the stellar component is only reduced by about 5% of its initial mass.

The difference between tidal stripping and **tidal shocking** is the latter is the impulsive limit, meaning the timescale of the gravitational interaction is much shorter than the dynamical time of the dwarf (Gnedin et al., 1999a). As a result of this impulse, the kinetic energy of the system is changed without changing the potential energy, and the system is out of virial equilibrium. As equilibrium is re-established, the system (stars) are less tightly bound, resulting in a more "puffy" satellite.

Tidal shocking generally occurs in two scenarios, either as a dwarf passes through the disk of a massive galaxy, or as a dwarf on a highly eccentric orbit passes through the Galactic Center (Gnedin & Ostriker 1997; Gnedin et al. 1999a,b). Read et al. (2006a) details the factors that establish the resulting impact of the tidal shocks, and they depend on the host's potential, the satellite's mass distribution and the satellite's orbit. Given the (Milky Way) potential employed in their analysis, Read et al. (2006a) find that tidal shocks are negligible for satellites which never pass closer than $\approx 20\,\mathrm{kpc}$ from the center of the massive galaxy. Interestingly, they also note that there is a regime in which tidal shocks can be significant, but where tidal stripping is not, meaning these two effects can, but may not always, act in concert.

Another variant on tidal stripping is **resonant stripping**. This process has been investigated by D'Onghia et al. (2009), who suggest that 80% of the stars can be removed from a disky dwarf, without significantly altering its dark matter halo. In this scenario, there is a resonant interaction that occurs between the stellar disk of the dwarf in its orbit around a massive host halo or other dwarf. The resonance cause disk stars to be preferentially removed, whereas the dark matter halo is largely unaffected due to the fact that its particle motions are randomly distributed, running counter to the example of tidal stripping in Fornax discussed previously.

While tidal stripping undoubtedly occurs for satellites, its major effect is to remove mass, be it stellar, gaseous or dark. However, the density–morphology relation exists

in the Local Group, meaning there is an absence of dIrr galaxies around large hosts. Dwarf spheroidal galaxies are generally all pressure supported systems; however, the gas in most Local Group galaxies shows some rotation. For some time, this led to the view that dIrrs were rotationally supported systems. However, more recent observations of the older stellar populations in dIrr galaxies shows that they are often pressure supported too (e.g., see Kirby et al. 2014). Prior to these more recent observations, however, the prevailing view was that to turn a dIrr galaxies into a dSph galaxy required removing the cold gas, removing (redistributing) the angular momentum, and heating the stellar disk. Mayer et al. (2001a) propose **tidal stirring** to do just this. Here, ram pressure stripping and tidal stripping both act, but in addition the tidal interactions cause a bar to form in the disk of the dwarf. This bar becomes unstable and acts to redistribute the angular momentum in the dwarf, moving it to larger radius. Mayer et al. (2001a) suggest a dIrr galaxy can be turned into a dSph galaxy in only 2 or 3 orbits. More recent work by Kazantzidis et al. (2011) find that tidal stirring is effective for turning rotationally supported disks into dSphs, although its efficiency depends both on the orbital parameters of the dwarf, and also on the properties of the original disk (mass loss is increased for a more compact, thinner disk). They further note that bar formation is an effective mechanism to redistribute the angular moment but tidal shocking can also result in a dSph with minimal rotation in a few cases.

Of course, the extreme result of tidal stripping of a satellite is its eventual merger with the host. Indeed, **mergers** are a core element of ΛCDM models of galaxy growth. Depending on the mass ratio of the merger, they can alter the galaxy morphology, cause increased star formation (and possibly increase the AGN activity). Dwarfs fit into this framework both as the objects that contribute to the build up of larger systems (e.g., the Sagittarius stream; discovery in Ibata et al. 1994, now with Gaia Early Data Release 3 kinematics, Ibata et al. 2020), as well as systems that are themselves built up via this process (i.e., dwarf-dwarf mergers). There is ample evidence of the former scenario in action, even in just the Milky Way system (e.g. the Styx Stream - Grillmair 2009, which is possibly associated with Boötes III dwarf Carlin & Sand 2018; the Cetus Polar Stream - Newberg et al. 2009; the Aquarius Stream - Williams et al. 2011; or the very recently discovered Nyx Stream - Necib et al. 2020). Indeed, with the advent of Gaia (Gaia Collaboration et al., 2021), merger remnants do not even need to form a coherent stream on the sky to be detected, for example see the discovery of the Gaia-Enceladus-Sausage (Belokurov et al. 2018;

Helmi et al. 2018, Sequoia (Myeong et al., 2019), the Milky Way "family tree" of mergers (Kruijssen et al., 2020) and the numerous discoveries from STREAMFINDER (Ibata et al., 2021). Figure 11 from the review by Helmi (2020) shows the extended features detected, listing a total of 72 known, spatially coherent stellar streams and overdensities.

Evidence for dwarf-dwarf mergers is not copious, but it does exist, for example in Local Group dwarf galaxies like Sextans (Cicuéndez & Battaglia, 2018), Andromeda II (Amorisco et al., 2014), and Fornax (Amorisco & Evans, 2012), and further afield (e.g., the blue compact dwarf VCC 848 located on the outskirts of the Virgo cluster Zhang et al. 2020). Paudel et al. (2018) complies a catalog of 177 merging dwarfs ($M_\star = 10^7 - 10^{10} M_\odot$), finding tentative evidence that dwarf-dwarf mergers are more likely in low density environments. Interactions between dwarfs that have not fully merged have also been seen, for example, in the increased star formation observed in pairs of dwarfs in the TiNy Titans Survey (Stierwalt et al., 2015).

Deason et al. (2014) look at minor mergers in dwarf galaxies in the Local Group using the ELVIS simulations. In general, they find 10% of dwarfs have likely experienced a major merger since $z \simeq 1$. They find that dwarfs that are near to a host (<1.4 Mpc), but outside the viral radius, are twice as likely to have had a major merger than those inside the virial radius, consistent with the idea that more isolated dwarfs are more likely to undergo minor mergers. Thus, at the distances where interactions with the MW are less likely, dwarf-dwarf mergers appear to be more likely. In related work, Benítez-Llambay et al. (2016) use the CLUES simulations and examine galaxies with stellar masses in the range $10^6 - 10^7 \mathrm{M}_\odot$. They select six dwarfs which each exhibit two distinct stellar populations (old and young). They find the old stellar component is always less centrally concentrated than the young, and they argue that the old component is actually a result of a merger event. However, while simulations and observations both suggest that dwarfs do indeed undergo mergers, like more massive galaxies, recall again Fitts et al. (2018) and their result with the FIRE simulations, finding that mergers do not play as significant a role in dwarf evolution as for massive galaxies.

Given that there is a proposed mass limit below which dark matter halos are not able to retain enough mass to form stars, and given that this mass limit is close to the mass of the faintest dwarfs, **"dark halo interactions"** (interactions with a dark matter halo devoid of a luminous, baryonic component) have been proposed to be relevant for dwarf galaxies and stellar streams, and is a natural extension of the

dwarf-dwarf interaction idea. Erkal & Belokurov (2015) proposed that cold stellar streams can hold evidence of interactions with such halos, and there is considerable research looking for signs of interactions between the streams with these hitherto undetected dark matter halos. For example, Bonaca et al. (2019) argue that gaps and "spurs" in the thin and dynamically cold GD-1 stream are most likely due to interactions with a dark halo. In the same vein, it is plausible that an apparently isolated dwarf galaxy could interact with such a dark substructure: Helmi et al. (2012) discuss the impact of this type of interaction on dwarfs, suggesting that they can trigger star formation and could even act as a mechanism to turn dIrrs to dSphs.

Finally, in more dense environments than those found in the Local Group, **galaxy harassment** (Moore et al., 1996, 1998) can be important for satellites. This phrase refers to the continued gravitational interactions felt by a galaxy due to all the other nearby galaxies in its vicinity, not just the main host or central cluster galaxy. This can be a source of heating, and affects all components, as it is gravitational effect. This harassment can possibly alter a dIrr into a dSph, removing both mass and angular momentum (Mayer et al., 2001a).

1.2.3 Key variables

The plethora of processes potentially at work in galaxy evolution and their interdependency results in a challenging landscape in which to determine what, if any, is the dominant process for a particular dwarf. For example, there are multiple ways in which star formation might be suppressed. The cold gas can be removed (ram pressure stripping), or hot gas can be prevented from in-falling (strangulation). Feedback from supernovae are an effective mechanism via which to remove the gas from a dwarf and therefore reduce star formation, but such a process requires there to be star formation in the first place. Early on in the Universe, reionization might be the culprit that stops subsequent generations of star formation. Each scenario is distinct in its implications for a dwarf's history and the resulting morphology.

There are a couple of dominant variables that should be considered when examining a dwarf. Given the central role that star formation plays in galaxy evolution (with the associated considerations of how much gas has been accreted and retained), the first of these variables is baryonic mass. The baryonic mass includes the current mass of the galaxy in gas – a measure of the galaxy's ability to retain and/or re-accrete gas through its history – as well as the current mass of the galaxy in stars – a measure

of how much gas has been successfully transformed into stars over its history.

The second variable that needs to be considered is environment. The impact of environment can clearly be profound, since ram pressure stripping, all tidal processes, galaxy harassment and all merger-related processes depend upon the environment. Indeed, for a truly isolated dwarf, likely the only processes that can quench star formation are reionization or feedback from star formation. We note that AGN would play a significant role in more massive galaxies, but not for dwarfs (see Figure 1.2). While Geha et al. (2012) find isolated, quenched, massive galaxies where AGN are credited with quenching the galaxy, they do not see the same isolated, quenched, ("red and dead") galaxies at smaller mass scales. Geha et al. (2012) discusses the minimum mass for which we find isolated quenched dwarfs and find no quenched field (isolated) dwarfs with $M_\star < 1.0 \times 10^9 M_\odot$.

Peng et al. (2010) identify the two main drivers of quenching as mass or environment. The first is closely tied to the star formation (and AGN), while the latter is a consequence of the hierarchical nature of galaxy evolution as galaxies (of all sizes) are distributed throughout the cosmic web.

By moving to isolated locales, we can therefore hope to minimise the number of processes at play for any particular dwarf galaxy, especially by then comparing findings to analogous systems in different environments. Such an idea is not new, of course. With respect to the star formation histories of the Local Group galaxies, there are a few important HST-based studies. For example, the Lifetimes of Andromeda Satellites (ISLAndS) project studied Andromeda XVI (Monelli et al., 2016), a system that is thought to be a recent arrival to the Local Group (see Letarte et al. 2009) so has evolved largely in isolation. It shows similarities to Leo T, Leo A and VV 124 (UGC 4879), all relatively isolated dwarfs (see papers by Irwin et al. 2007; Vansevičius et al. 2004; Kopylov et al. 2008 for example). This group of (relatively low mass) dwarfs all lie around the virial mass limit proposed by Wheeler et al. (2019) of $\sim 5 \times 10^9 M_\odot$, below which dwarfs should be quenched by reionization. Instead, these dwarfs all quenched post-reionization, raising hard questions on what mechanisms could cause the quenching. Using the rest of the ISLAndS sample of dwarfs (six satellites of M 31), Skillman et al. (2017) find no trends in quenching time with mass or distance from the M 31, suggesting local environment within a satellite system may not have a big impact on quenching timescales.

This current study's purpose is to better understand the structural properties of Local Group isolated dwarfs, with the aim of conducting similar comparative studies

of structural characteristics among the entire Local Group population, like those that have already been done targeting their star formation histories.

1.3 Why study dwarfs in the Local Group?

Understanding dwarf galaxies is intrinsically complex due to the underlying physical processes involved. However it is further complicated, as not only do dwarfs have a diverse array of properties, but the methodology used to determine their observational characteristics are equally diverse. Whether we estimate size using integrated light or resolved stars, whether we are using a small field of view and going deep (e.g. observation from HST-ACS), or a wide-field of view going shallower, whether we estimate kinematics based on the gas or stellar components, all these choices can introduce biases in the subsequent analysis and each are best suited to a subset of studies.

Many dwarf galaxies are so faint that they can only be observed in the nearby Universe, and integrated light observations are insufficient to even detect these systems. Instead, most analyses must be based on their resolved stellar content. While these dwarfs at the extreme faint end of the luminosity function are the most challenging to observe, they are worth the effort, since they represent the true limits of galaxy formation as it is currently understood.

As such, Local Group observations of dwarf galaxies are critical to many key aspects of modern ideas of galaxy formation and evolution (e.g. Tolstoy et al. 2009). The dwarf regime presents big challenges, like the current and extensively studied core-cusp problem, the missing satellite problem and the "too big to fail" problem:

- The core-cusp problem (concisely defined and summarized by de Blok 2010) questions the shape of a galaxy's dark matter halo density profile and whether it has a classic NFW halo with a "cuspy center" or a core with a reduced central density. It has been suggested that feedback from star formation can alter a cusp into a core (Pontzen & Governato, 2012), and would be most effective in lower mass galaxies (e.g. $M_\star \sim 10^{8.5} M_\odot$; Di Cintio et al. 2014).

- The missing satellite problem, as the name implies, is the discrepancy between the number of observed dwarfs to the number of dark matter halos predicted by ΛCMD simulations. Klypin et al. (1999) and Moore et al. (1999) reported a significant difference, with substantially more halos predicted in simulations

than galaxies observed in reality. This problem lies at the intersection of cosmological simulations (are there too many halos?) and observations studies (are we missing a significant number of dwarfs?). This tension has been reduced with the inclusion of processes in the simulations that impact a halo's ability form a galaxy. At the other extreme, by including some versions of these processes, Kim et al. (2018) and Graus et al. (2019) present dark matter and reionization models which can, in fact, reverse this "problem", with too many observed satellites. However, a number of missing dwarfs perhaps remain to be detected (e.g. Newton et al. 2018, Fattahi et al. 2020), and the number of newly discovered dwarfs suggest there are still unknown dwarfs in our Local Group. Peñarrubia et al. (2012) also point out the tension between these two challenges – with the cusp-core problem requiring a high star formation efficiencies and the missing satellites requiring the opposite. This tension is increased if increasingly low mass dwarfs are detected to have cores.

- Finally, "too big to fail" was first defined by Boylan-Kolchin et al. (2011) and is the result that the halos (and corresponding galaxies) predicted in simulations are far too massive to match the bright ($L_v > 10^5 L_\odot$) Milky Way satellite population. That is, there is a lack of massive satellites in the Milky Way, which cannot be explained by the absence of stars (like the missing satellites problem) as they should have deep potential wells. Proposed solutions include the impacts of tidal stirring and feedback from star formation (e.g. Tomozeiu et al. 2016; Verbeke et al. 2017).

These three challenges in the dwarf regime have generated a wealth of insight and refinement in our understanding of our Local Group and galaxies on all scales. However, there are perhaps more challenges yet to be unearthed in this regime, like Safarzadeh & Loeb (2021) proposed "too-dense-to-be-satellites" based on Horologium I and Tucana II, which may (or may not) test our models and understanding. Collectively, these three challenges highlight some of the needs to understand these "extreme" galaxies, despite the observational challenges and the relatively small number of systems within our observational grasp.

1.4 Isolated dwarfs in the Local Group

The Local Group is populated by a diverse and plentiful collection of dwarfs, but inevitably their numbers are not statically large compared to studies of more distant galaxies. The population of known nearby dwarfs has increased dramatically in recent years, especially at the faint end, and especially for the satellite populations of the Milky Way (e.g. numerous dwarfs discovered in the Dark Energy Survey - Bechtol et al. 2015; Drlica-Wagner et al. 2015; Crnojević et al. 2019; Drlica-Wagner et al. 2020; Crater III and Bootes IV from the Hyper Suprime-Cam Subaru Strategic Program - Homma et al. 2018, 2019; Sagittarius II, Draco II and Laevens 3 from the Pan-STARRS 1 3π Survey - Laevens et al. 2015, among others) and M 31 (e.g. And XXIX - Bell et al. 2011; Lacerta I/And XXXI and Cassiopeia III/And XXXII - Martin et al. 2013a; Andromeda XVIII, XIX, and XX - McConnachie et al. 2008).

There have been far fewer discoveries of new isolated dwarf galaxies in the Local Group. This population of galaxies lies at the intersection of two useful characteristics. First, their isolation suggests that the evolutionary pathway cannot have been significantly influenced by processes, such as tidal or ram pressure stripping, and so largely their evolution should have been dominated by more internally-driven, or intrinsic, properties. Secondly, even although they are isolated, they are still relatively close (generally, as close as the M 31 satellite population, on which there has been extensive recent work). Their close proximity thus allows for detailed analysis of their faint stellar structures, and permits studies of their older, extended stellar populations, not just their young and bright stellar populations. Bluntly, we can hope to know as much about them, in as much detail as we know about the M 31 satellites, and even some of the Milky Way satellites. These critical considerations motivate the Solo Survey, on which this thesis is based.

Solo targets all dwarf galaxies in the Local Group and beyond, so long as they lie within 3 Mpc. At these distances, at least some of their stellar populations can be resolved from the ground, and all the Local Group dwarfs can have their older stellar populations resolved. Solo dwarfs are also selected to be more than 300 kpc from a massive galaxy (the Milky Way or M 31), given that this is the approximate value of the virial radius for these two galaxies (e.g. Klypin et al. 2002).

The threshold in distance from a host does not ensure a clean selection of "truly isolated" galaxies. Using only their current positions, we cannot determine whether a dwarf has always been isolated (without knowing its orbit). As such, a necessary

caveat to consider is the presence of "backsplash" galaxies in the isolated sample. These galaxies are often discussed in the context of galaxy clusters, where a significant fraction of galaxies at $1-2$ virial radii have had a previous pericentric passage through the center of the cluster (see Balogh et al. 2000; Gill et al. 2005; Smith et al. 2015 among others). It is difficult to rule out the same type of scenario for some of the "isolated" Local Group dwarf galaxies without access to the full three-dimension velocities of the dwarfs (however, see Buck et al. 2019; Teyssier et al. 2012, and Blaña et al. 2020 for careful endeavours to do so). Most recently, McConnachie et al. (2021)(hereafter Paper III) combines our Solo photometry of isolated Local Group galaxies with astrometry from Gaia Data Release 2 (Gaia Collaboration et al. 2018) in order to determine the proper motions, and consequently the orbits, for that small subset of Solo galaxies that have enough bright supergiants that are visible to the Gaia spacecraft (NGC 6822, WLM, IC 1613 and Leo A). For NGC 6822, the proper motions strongly favour a scenario where it has never interacted with either of the massive galaxies. For the rest, future Gaia data releases are required in order to provide proper motions with sufficient accuracy to discern their orbital histories.

The purpose of Solo is to obtain, and analyze, wide-field imaging of isolated, nearby, dwarf galaxies. Whereas most Local Group galaxies now have high quality HST imaging (e.g., the ISLAndS project and LCID - Bernard et al. 2009, both discussed earlier), the same is not true with respect to modern wide-field imaging. This results in many of the key properties of the systems, such as luminosity, sizes, surface brightness profiles, being based on studies by de Vaucouleurs et al. (1991) and others, where the stellar content is not resolved and where the estimates available are not easily comparable to similar parameters for the Milky Way and M 31 populations.

1.5 Summary

In this chapter, I have introduced dwarf galaxies, and placed them in context with their larger counterparts and globular clusters. I have then discussed the formation and evolutionary processes which a dwarf may undergo. I have discussed why the dwarf regime is an interesting regime to study, in particular, the unique possibilities presented in the Local Group. This complex picture for the nature versus nurture of dwarfs motivates the necessity for the Solo Survey's focus on isolated dwarfs.

This thesis is organized as follows: Chapter 2 introduces the Solo Survey, its goals, observations and data processing. Chapter 3 is the homogeneous analysis and

parameterization of 12 Solo dwarfs, generating a consistent dataset. Chapter 4 takes this dataset and uses comparisons to Milky Way and M 31 satellites to distinguish between these population. Chapter 5 explores the star formation histories, gas and substructure in and around the dwarfs (including both satellites of dwarfs and globular clusters) and finally Chapter 6 summarizes and concludes.

Chapter 2

The Solo Survey

In this chapter, I introduce the Solo Survey and the dwarfs observed. Some of this discussion is similar to the introduction to Solo provided in Higgs et al. (2016). I detail the data processing used to generate the images and stellar catalogues used in the ensuing analysis. I then provide some general background on both the resolved stellar and integrated light techniques which form the backbone of this thesis.

2.1 The survey and its targets

The Solitary Local Dwarf Galaxy (Solo) Survey is a volume limited, wide-field imaging survey of all known dwarf galaxies that are within 3 Mpc and more than 300 kpc from either M 31 or the Milky Way. Galaxies are observed with either CFHT/Megacam in the northern hemisphere or Magellan/Megacam or IMACS in the southern hemisphere. Some targets are observed with multiple instruments for calibration purposes. The total survey area per galaxy is approximately one square degree, regardless of telescope/instrument (for Magellan, multiple pointings are used to cover this area, whereas only a single pointing is required for CFHT). All dwarfs were observed in $g-$ and $i-$bands. Additionally, almost half (21 out of 44 dwarfs) were also observed in the $u-$band. Some of the $u-$band observations were taken as part of the Canada France Imaging Survey (CFIS; Ibata et al. 2017) or are from archival data. The observed dwarfs are listed in Table 2.1.

Figure 2.1 shows a spatial projection of all dwarf galaxies within 3 Mpc. The isolated Solo sample in Table 2.1 is shown along with the satellites of M 31 and the Milky Way. As discussed in the previous chapter, the Solo sample may include some

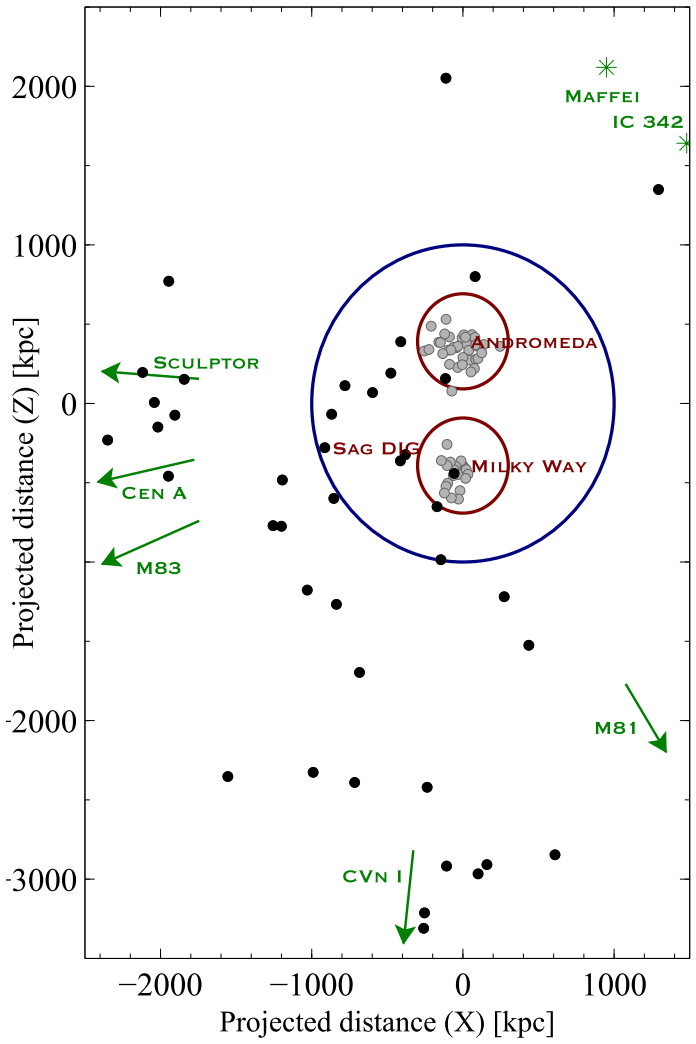

Figure 2.1: From Higgs et al. (2016), showing the Solo dwarfs in black and satellite dwarfs in grey, relative to the Milky Way and M 31. The blue circle indicates 1 Mpc and 300 kpc (the approximate virial radius of the Local Group and MW/M31 respectively). The green points/arrows indicate the direction/location of the closest groups.

dwarfs that are on very long period orbits, or "backsplash" galaxies that are at very large distances but which have had a previous pericentric passage with one of the two large bodies (e.g. Gill et al. 2005). Timing arguments suggest that most galaxies located near or beyond the periphery of the Local Group will not have had time to have had a close interaction at any point in their history (McConnachie, 2012). All of the Solo dwarfs are close enough to resolve their brighter stellar populations (at least in their outskirts) from the ground.

Many of the closest targets in this list are reasonably well studied. However, a systematic, modern survey including more distant dwarfs is lacking. Arguably the most systematic study of a subset of these galaxies is Massey et al. (2006), who surveyed ten star-forming, Local Group galaxies to determine certain properties relating to star formation activity. In addition, the Local Cosmology from Isolated Dwarfs (LCID) survey studied six nearby isolated dwarf galaxies in the Local Group using deep HST imaging (see Gallart et al. 2015 and references within). The HST imaging reaches the main-sequence turn-off for these dwarfs, and has provided some of the most detailed insights into the star formation histories and stellar content of these galaxies available (e.g. Monelli et al. 2010a,b; Hidalgo et al. 2011, 2013; Skillman et al. 2014; Gallart et al. 2015).

Despite the presence of excellent HST imaging, many of the more distant dwarfs listed in Table 2.1 are relatively poorly studied in the era of modern wide-field CCD studies. For example, an examination of the data tables in McConnachie (2012) reveal that many of the dwarfs' basic properties are derived from the Third Reference Catalogue survey by de Vaucouleurs et al. (1991), and a homogeneous wide-field study of the entire sample has not been conducted recently. It is this important niche that Solo is designed to filled, while being complementary to the ground- and space-based studies that have been undertaken of individual targets

2.2 Data Processing

For the CFHT/MegaCam data analyzed here, the image processing steps were similar to those followed by Richardson et al. (2011). Data were preprocessed by the Elixir system at CFHT, including de-biasing, flat-fielding and fringe-correcting the $i-$band data in addition to determining the photometric zero-points. The data were then transferred to the Cambridge Astronomical Survey Unit where the overscan region was first trimmed off, then all images and calibration frames were run through a

Name	Alt. Name	RA	Dec.	Distance [kpc]	Tel.	Filt.	Notes
WLM	DDO221	$00^h01^m58.2^s$	$-15^o27'39"$	933 ± 34	M	*gi*	2014B
					C	*gi*	2013B/2016B
AndXVIII		$00^h02^m14.5^s$	$+45^o05'20"$	1355 ± 81	C	*ugi*	2013A, PAndAS
ESO410-G005	KK98	$00^h15^m31.6^s$	$-32^o10'48"$	1923 ± 35	M	*ugi*	2012B
Cetus		$00^h26^m11.0^s$	$-11^o02'40"$	755 ± 24	M	*gi*	2014B
					M	*gi*	2017B, IMACS
					C	*g*	2016B
					C	*gi*	2014B
ESO294-G010		$00^h26^m33.4^s$	$-41^o51'19"$	2032 ± 37	M	*gi*	2014B
IC1613	DDO8	$01^h04^m47.8^s$	$+02^o07'04"$	755 ± 42	M	*ugi*	2012B
					M	*gi*	2017B, IMACS
					C	*gi*	2016B
KKs3		$02^h24^m44.4^s$	$-73^o30'51"$	2120 ± 70	M	*gi*	2017A
Perseus		$03^h01^m22.8^s$	$+40^o59'17"$	785 ± 65	C	*gi*	2016B
Eridanus II		$03^h44^m21.1^s$	$-43^o32'00"$	785 ± 65	M	*gi*	2017B, IMACS
HIZSS3A(B)		$07^h00^m29.3^s$	$-04^o12'30"$	1675 ± 108	M	*ugi*	2012A
					C	*g*	2012A, 2012B
UGC4879	VV124	$09^h16^m02.2^s$	$+52^o50'24"$	1361 ± 25	C	*ugi*	2016A
LeoT		$09^h34^m53.4^s$	$+17^o03'05"$	417 ± 19	C	*ugi*	2016A, CFIS
LeoA		$09^h59^m26.5^s$	$+30^o44'47"$	798 ± 44	C	*gi*	2016A, CFIS
SextansB		$10^h00^m00.1^s$	$+05^o19'56"$	1426 ± 20	C	gi	2016A
NGC3109	DDO236	$10^h03^m06.9^s$	$-26^o09'35"$	1300 ± 48	M	*ugi*	2012A
Antlia		$10^h04^m04.1^s$	$-27^o19'52"$	1349 ± 62	M	*gi*	2015A, IMACS
SextansA	DDO75	$10^h11^m00.8^s$	$-04^o41'34"$	1432 ± 53	M	*ugi*	2012A
LeoP		$10^h21^m45.1^s$	$+18^o05'17"$	1620 ± 150	C	*gi*	2014A
NGC4163		$12^h12^m09.1^s$	$+36^o10'09"$	2860 ± 39	C	gi	2016A
IC3104		$12^h18^m46.0^s$	$-79^o43'34"$	2270 ± 188	M	*ugi*	2012A
DDO113		$12^h14^m57.9^s$	$+36^o13'08"$	2950 ± 82	C	*gi*	2014A, 2016A
DDO125		$12^h27^m40.9^s$	$+43^o29'44"$	2580 ± 59	C	gi	2016A
GR8	DDO155	$12^h58^m40.4^s$	$+14^o13'03"$	2178 ± 120	M	*gi*	2015A, IMACS
UGC8508		$13^h30^m44.4^s$	$+54^o54'36"$	2580 ± 36	C	*gi*	2014A, 2016A
KKH86		$13^h54^m33.5^s$	$+04^o14'35"$	2590 ± 190	M	*ugi*	2012A
DDO190		$14^h24^m43.4^s$	$+44^o31'33"$	2790 ± 93	C	*gi*	2014A
KKR25		$16^h13^m48.0^s$	$+54^o22'16"$	1905 ± 61	C	*gi*	2014A
IC4662		$17^h47^m08.8^s$	$-64^o38'30"$	2440 ± 191	M	*gi*	2017A
SagDIG		$19^h29^m59.0^s$	$-17^o40'51"$	1067 ± 88	C	*ugi*	2012B, 2013A
NGC6822	DDO209	$19^h44^m56.6^s$	$-14^o47'21"$	459 ± 17	C	*ugi*	2013A
Phoenix		$19^h44^m56.6^s$	$-14^o47'21"$	415 ± 19	M	*ugi*	2012B
DDO210	Aquarius	$20^h46^m51.8^s$	$-12^o50'53"$	1072 ± 39	M	*ugi*	2012B
					M	*gi*	2017B, IMACS
					C	*ugi*	2013A
IC5152		$22^h02^m41.5^s$	$-51^o17'47"$	1950 ± 45	M	*ugi*	2012B
AndXXVIII		$22^h32^m41.2^s$	$+31^o12'58"$	661^{+152}_{-61}	C	*ugi*	2012B, 2013A, CFIS
KK258		$22^h40^m43.9^s$	$-30^o47'59"$	2230 ± 50	M	*gi*	2017A
Tucana		$22^h41^m49.6^s$	$-64^o25'10"$	887 ± 49	M	*ugi*	2012B
					M	*gi*	2017B, IMACS
UKS2323-326	UGCA438	$23^h26^m27.5^s$	$-32^o23'20"$	2208 ± 92	M	*ugi*	2012B
PegDIG	DDO216	$23^h28^m36.3^s$	$+14^o44'35"$	920 ± 30	C	*ugi*	2012B, 2013A
KKH98		$23^h45^m34.0^s$	$+38^o43'04"$	2523 ± 105	C	*ugi*	2013A,2015B
UGCA86		$03^h59^m48.3^s$	$+67^o08'19"$	2960 ± 232	C	*ug*	2012B
DDO99		$11^h50^m53.0^s$	$+38^o52'49"$	2590 ± 167	C	*i*	2014A
KKR3		$14^h07^m10.5^s$	$+35^o03'37"$	2188 ± 121	C	*g*	2014A
UGC9128		$14^h15^m56.5^s$	$+23^o03'19"$	2291 ± 42	C	*g*	2014A
Antlia B		$09^h48^m56.1^s$	$-25^o59'24"$	1294 ± 99	C	g	2016B

Table 2.1: The Solo Survey dwarfs, with their right ascension (RA), declination (Dec.), observed distance, telescope (C - CFHT, M - Magellan), filters used and the semester observed (with additional notes).

variant of the data reduction pipeline originally developed for processing Wide Field Camera (WFC) data from the Isaac Newton Telescope (INT). For further details, see Irwin (1985, 1997), Irwin & Lewis (2001) and Irwin et al. (2004).

Prior to deep stacking, catalogues were generated for each individual processed science image to further refine the astrometric calibration and also to assess the data quality. For astrometric calibration, a Zenithal polynomial projection (Greisen & Calabretta 2002) was used to define the World Coordinate System (WCS). A fifth-order polynomial includes all the significant telescope radial field distortions leaving just a six-parameter linear model per detector to completely define the required astrometric transformations. The Two Micron All Sky Survey (2MASS) point-source catalogue (Cutri et al. 2003) was used for the astrometric reference system.

Quality control assessment for each exposure was based on the average seeing and ellipticity of stellar images, together with the sky level and sky noise, all determined from the object catalogues. During the stacking process, the individual catalogues from each MegaCam image were used, in addition to the standard WCS solution. The images were aligned to a sub-pixel level for the stacked images. The common background regions in the overlap area from each image in the stack were used to compensate for sky variations during the exposure sequence and the final stacks for each band included seeing weighting, confidence (i.e. variance) map weighting and clipping of cosmic rays.

As a final image processing step, catalogues were derived from the deep stacks for each detector and their WCS astrometry was updated. All objects detected in the catalogues are morphologically classified (stellar, non-stellar, noise-like) before creating the final band-merged $g-$ and $i-$products. The morphological classification is done using a ratio of fluxes within apertures around each source. This ratio determines how point-like or extended the source appears. Using the ratio, stellar (point-like) sources are distinguished from background extended sources or cosmic rays. The final catalog includes a classification where objects are either noise-like, extended (i.e., galaxy-like, within 1 or 2σ of the locus of extended objects) or point-like (i.e., stellar sources, within 1 or 2σ of the locus of point sources). The catalogues provide additional quality control information and the classification step also computes the aperture corrections required to place the photometry on an absolute scale. The $g-$ and $i-$catalogues for each field are typically combined to form an overall single $g-$, $i-$entry for each detected object. In this process, objects lying within 1 arcsec of each other are taken to be the same and the entry with the higher signal-to-noise

measure is retained. Objects present only in $g-$ or $i-$band are retained throughout this process.

For a few galaxies, the $g-$band data was taken in sub-optimal seeing conditions. In these cases, the $i-$band data is used to generate a list-driven version (i.e. forced photometry) for the $g-$band catalogue. This catalogue was used to provide an alternative band - merged product for further analysis.

During the course of the Solo Survey, the filters available at CFHT were updated, resulting in two different $u-$,$i-$ and $g-$band filters used (see Table 2.1 for details). Each of the old filters is transfomed to the new filter system using Equations 2.1 and 2.2 (S. Prunet, private communication):

$$g - gS = 0.022 + 0.078(gS - iS) \tag{2.1}$$

$$i - iS = 0.001 - 0.0015(gS - iS) \tag{2.2}$$

The magnitudes are presented in their natural instrumental (AB) system. The $g-$ and $i-$magnitudes of each source are corrected for Galactic dust using values interpolated from the Schlegel et al. (1998) dust extinction maps, assuming that $A_g = 3.793 \times E(B-V)$ and $A_i = 2.086 \times E(B-V)$. No corrections are applied for extinction internal to the dwarfs.

2.3 Techniques

A significant component of the work presented in this thesis relies on combining resolved stellar analysis with integrated light from the dwarfs in order to understand their structure from their dense, crowded centers to the faint, extended outskirts. Here, I provide some background information on some of the important techniques used in this analysis. The specific implementation of these techniques on the Solo dwarfs is detailed in Chapter 3.

2.3.1 Resolved stars: a clear picture

By resolving stars, we can separate the different stellar populations of dwarf galaxies using their temperature/colour and luminosity/apparent magnitude. Figure 2.2 shows the evolution of a $1M_{\odot}$ star on a Hertzsprung Russel diagram, after formation on the

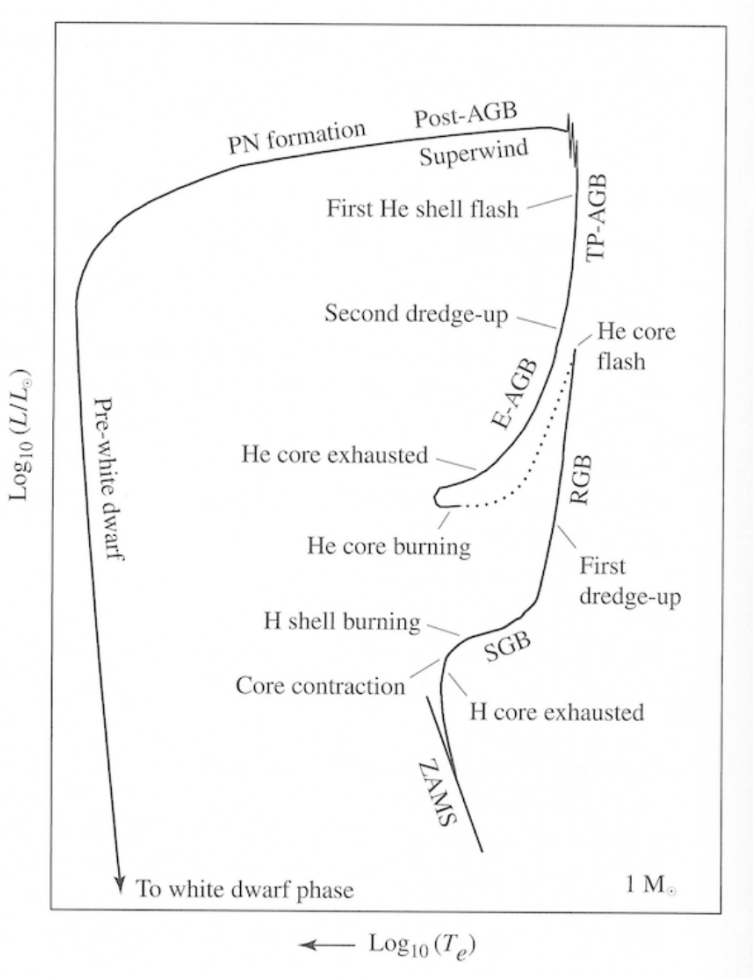

Figure 2.2: The evolution of a 1 $M_\odot$ star from Carroll & Ostlie (2006). (Abbreviations include ZAMS: zero age main sequence, SGB: sub giant branch, RGB: red giant branch, AGB: asymptotic giant branch, PN: planetary nebula.)

zero age main sequence (ZAMS), through to its final white dwarf phase.

While the specific evolution of any star is highly dependent on its mass (and metallicity), the important point to take away from Figure 2.2 is that it is possible to distinguish different evolutionary phases of a star by measuring its magnitude (luminosity) and color (temperature). If we now consider a stellar population with the same age, we can examine a color- magnitude diagram (CMD) and so distinguish stars in different evolutionary phases using their colour and observed brightness. Indeed, we can do this even if there are a mix of ages or metallicites in the stellar population. For stars in the Solo survey, located more than hundreds of kiloparsecs away, we can only see the brighter stars, namely young blue stars, asymptotic giant branch (AGB)

stars, and older red giant branch (RGB) stars. Given that most stars in dwarf galaxies are generally old (older than a few gigayears), we are most interested in the tracers of the older stellar populations, the RGB stars. These are also the most numerous stars we observe, given that stars spend longer on the RGB than on the AGB, and we will use this RGB population to trace the extended structure of the dwarf, in the same way as studies of Milky Way and M 31 satellite galaxies use RGB stars to trace their global structures (e.g. larger surveys of the satellite populations like Muñoz et al. 2018b or Martin et al. 2016, and more focused studies like Brasseur et al. 2011 of And X and And XVII).

The power of Solo comes from its wide field aspect, combined with its moderate depth. Figure 2.3 shows a CMD of the globular cluster M 92 from Paust et al. (2007), where the shaded region shows the approximate depth of CMDs observed in Solo. M 92 is dominated by a single, older stellar population, with no young blue stars and AGB stars (which are bright enough to be observed in the Solo observations). This figure highlights the details in the CMD unattainable from Solo, but which are generally accessible using HST-ACS. These deeper CMDs are key for understanding the star formation histories of the dwarfs, but have a much more limited field of view. Unlike HST, however, Solo observations span the entirety of nearly every dwarf, and in many cases reach out to many tens of half light radii or more. This makes Solo ideal to focus on the extended features of the dwarfs.

Isochrones are models of a single age stellar population, which can be placed on a CMD. The age and metallicity of a given population can be determined by matching key features to the observed CMD. There are numerous limitations on this technique such as reddening within the dwarf, the accuracy of the models employed, and that dwarfs rarely (never) consist of a truly simple, single age population. However, comparison of CMDs to isochrones is a good way to determine some average properties of the stellar populations in which we are interested, especially metallicity. Throughout, we generally use Dartmouth isochrones from Dotter et al. (2008), that are particularly good matches to the RGBs of older stellar populations (e.g., see discussion in McConnachie et al. 2010, especially their Figure 5).

The processed Solo object catalogs contain morphological information (especially, point sources, extended sources, noise sources). To clearly observe the stellar populations of the dwarfs, we first remove non-point sources and then isolate the RGB population using color/magnitude cuts, which helps to separate the dwarf's stars from point sources in the image, like foreground Milky Way stars or background

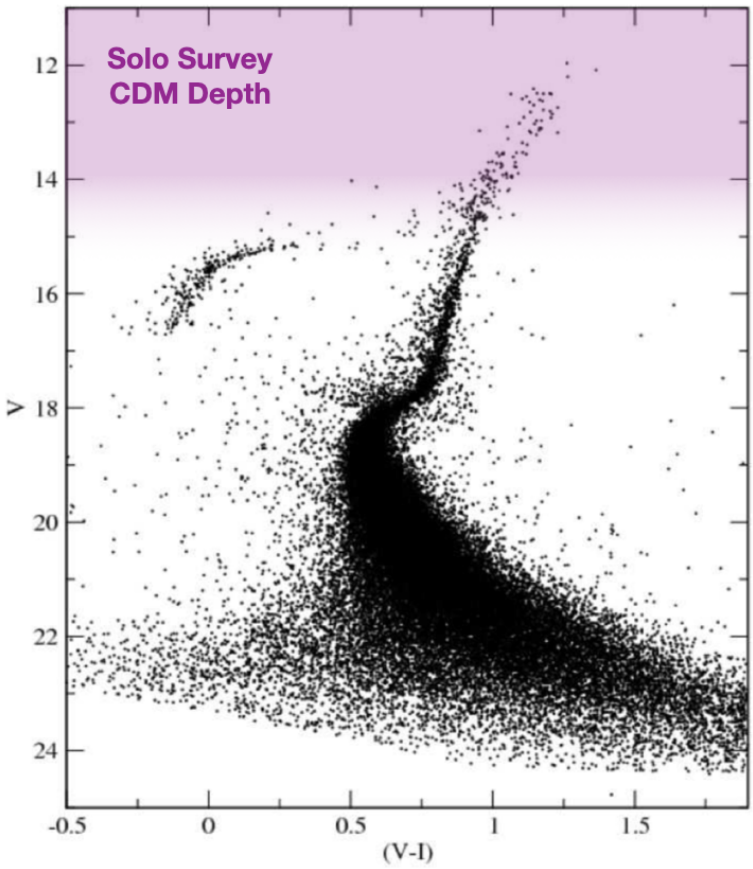

Figure 2.3: A CMD of the globular cluster M 92 from Paust et al. (2007), overlaid with the approximate depth of CMDs observed in the Solo Survey.

sources which appear star-like. Figure 2.4 demonstrates this processes using Leo A, with all the sources (panel A), star-like sources (panel C) and RGB stars selected via color/magnitude cuts (panel E). These color/magnitude cuts do not uniquely identify RGB stars given the overlapping loci of RGB stars, background sources, and Milky Way foreground stars. However, they do boost the "signal" from the dwarf, and can reveal faint features with significantly reduced contamination levels.

Distances using the Tip of the RGB

In what follows, we use the tip of the red giant branch (TRGB) as a standard candle to estimate distances to the Solo dwarfs (Figure 2.2 labels this feature the "He core flash" on the HR diagram.) For RGB stars, the luminosity of the He core flash is largely independent of stellar metallicity or age (for older, metal-poor stellar populations). Thus, we can compare its absolute magnitude with the observed magnitude in each dwarf to determine the distance. An extensive literature for this technique exists, with Lee et al. (1993) and Madore & Freedman (1995) notably establishing it as a robust method, and further examination in detail by Bellazzini et al. (2001); McConnachie et al. (2004); Madore et al. (2009); Freedman et al. (2020), among many others. Interestingly, Freedman et al. (2020) explains that the TRGB is an important distance calibrator for easing the tension surrounding estimates of the Hubble Constant (H_o) (summarized in Freedman 2017), from the Local Universe versus cosmological measurements. The TRGB is a robust measurement that can be applied to many galaxy types (unlike Cepheid variable stars which are only in spiral galaxies) in an interesting distance regime in which to further explore this tension.

Figure 2.5 show the luminosity of the TRGB in the $i-$band[1] from the Dartmouth isochrones (Dotter et al., 2008) as a function of metallicity and age. As expected, for stars older than ~ 6 Gyrs and [Fe/H] <-0.5 dex, m_i does not vary significantly, with a variation on the order of only 0.01 magnitudes. In what follows, I use a value of $M_i^{TRGB} = -3.49$ when computing distances for the Solo Survey (note that Figure 2.5 shows the old filter values and does not reflect this value used). The uncertainty in location of the TRGB in the CMDs is on the order of 0.1 magnitudes (an order of magnitude larger than the uncertainty for M_i^{TRGB}), hence it dominates the uncertainties in the resulting distances.

By determining distances with this method, we are inherently assuming that the

[1]This is the old CFHT $i-$filter plotted, I convert to the new filters.

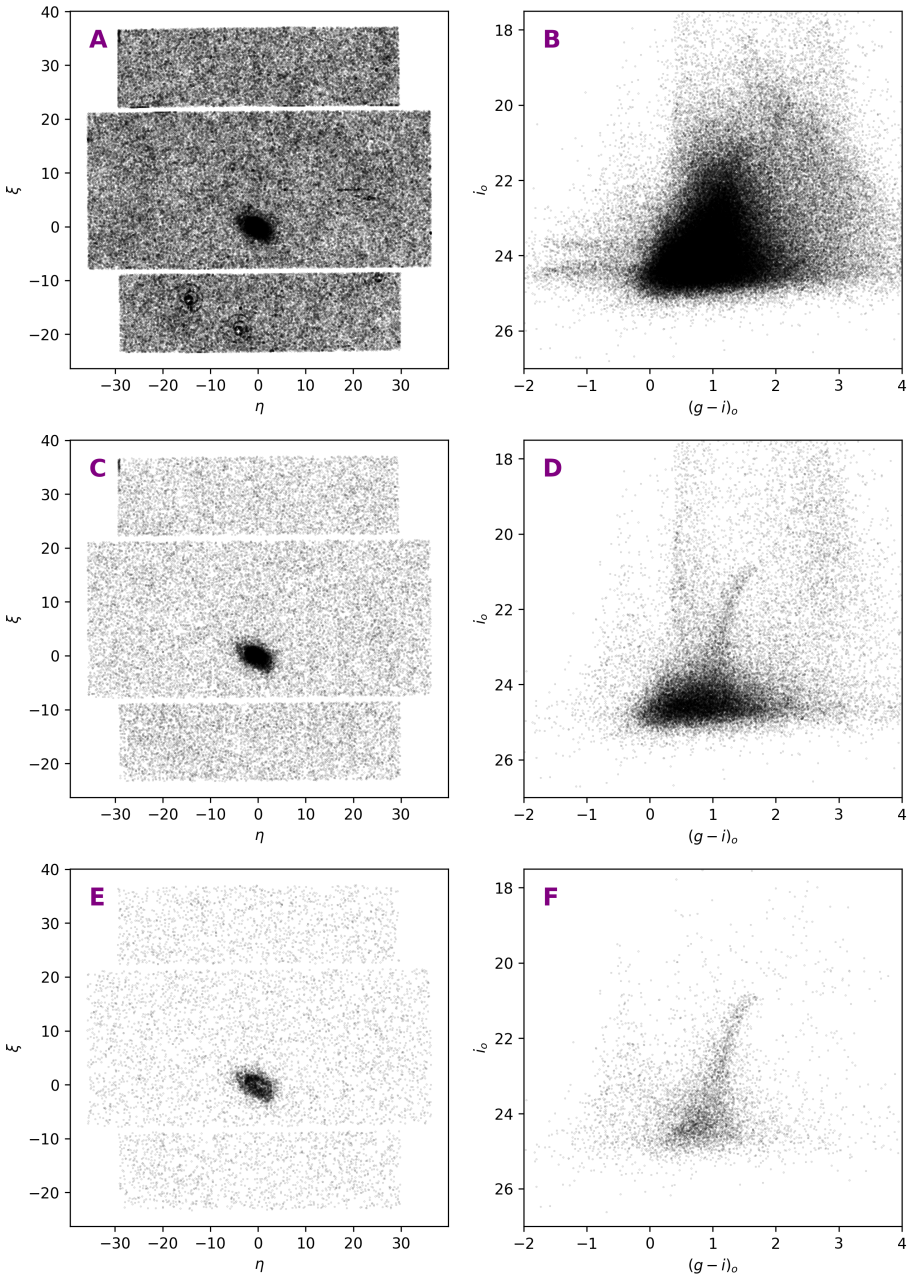

Figure 2.4: The spatial distribution of sources (*left*) and CMD (*right*) of Leo A. Panel A shows all sources detected, and B shows the corresponding CMD. Panel C selects only star-like (point) sources, and the resulting CMD in panel D. Panel E shows only RGB stars. Panel F shows sources spatially selected with the dwarf.

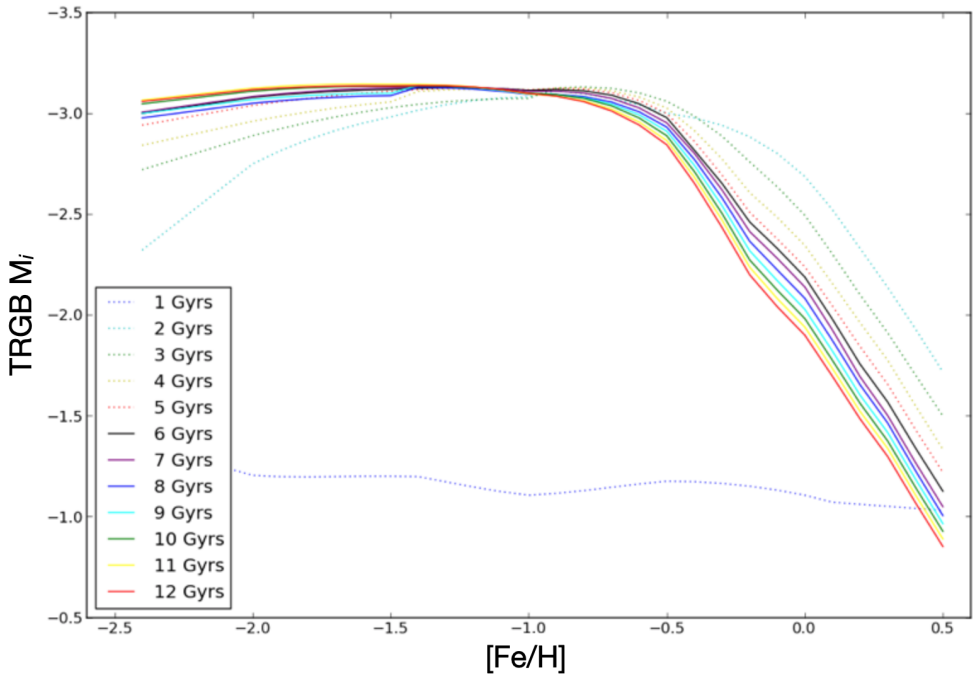

Figure 2.5: The TRGB in the i-band (old CFHT filters, corrected to new) as a function of metallicity and age from the Darthmouth isochrones Dotter et al. (2008).

RGB consists largely of older, metal-poor stars and the RGB is well populated such that there is an appreciable number of stars at the He core flash stage, generating a well defined TRGB. This first assumption is very reasonable for Solo dwarfs as they all have an old, metal poor population (e.g., see Weisz et al. 2014). The second assumption is not always true for these dwarfs, as some are very low mass, hence have an intrinsically low number of stars in the RGB. Considerable care has been taken to develop a consistent, cautious methods to address this issue and this is discussed in Chapter 3.

2.3.2 Integrated light: all together now

The focus of this work is largely on the resolved stellar content of the Solo dwarfs, which reveals the faint and extended structure of the dwarfs. In addition to reaching to low surface brightness, such an approach also removes the bias of integrated light studies towards young stellar populations (which can be considerably brighter than even the brightest RGB stars). However, crowding in many galaxies prevents us applying this technique in the very central regions of most of the Solo dwarfs.

The high stellar density in many Solo dwarfs becomes high enough that crowding causes the completeness of the resulting stellar catalogue to decline precipitously. We can clearly see when plotting a radial profile of stellar density (see Figure 3.14 for the declining central regions, or panel E of Figure 2.4 for the "doughnut" structure it produces). While a completeness correction can work in the intermediate region, where crowding is bad but not extreme, even a completeness correction cannot work if no stars are resolved at all (the hole in the doughnut). We are thus forced to use the integrated light in these regions.

An advantage of these integrated light measurements for the central regions of the dwarf galaxy is that they provide an empirical means to anchor our stellar density measurements (RGB stars per unit area) to a direct surface brightness measurements (magnitudes per square arcsecond). A caveat, of course, is that the flux we measure in the integrated light measurement is the total flux from all the stars in that region, not just RGB stars, We discuss how we approach this complex issue in more detail in Chapter 3.

2.4 Summary

Here, I have introduced the Solo Survey, with its wide-field imaging of isolated (>300 kpc from the MW and M 31) and nearby dwarfs (<3 Mpc) for a total of 44 dwarfs. Observations are taken with CFHT/MegaCam, Magellan/Megacam and Magellan/IMACS, with a field of view of one full square degree around each dwarf. This dataset is optimized for wide-field, resolved stellar populations. We use the resolved stars (particularly RGB stars) to trace the old stellar population and its underlying structure and the distances to the dwarfs themselves. As crowding in the central regions is significant for some dwarfs, we combine the resolved stellar view with the integrated light, generating a complete picture of the dwarf to very faint surface brightness limits.

In the next chapter, we use the Solo data to derive homogeneous structural parameters for all the isolated LG galaxies in our dataset.

Chapter 3

The stellar structure of isolated Local Group dwarf galaxies

This chapter is published as Higgs et al. (2021), (with the data processing section somewhat reduced as this has been largely address in the introduction). The majority of this paper is my own work, analysis and writing. The co-authors assisted in obtaining the observations for the survey, generating the stellar catalogues and provided comments/edits on the draft.

The Solo (*So*litary *Lo*cal) Dwarf Galaxy survey is a volume limited, wide-field $g-$ and $i-$band survey of all known nearby ($<$3 Mpc) and isolated ($>$300 kpc from the Milky Way or M 31) dwarf galaxies. This set of 44 dwarfs are homogeneously analysed for quantitative comparisons to the satellite dwarf populations of the Milky Way and M 31. In this chapter, an analysis of the 12 closest Solo dwarf galaxies accessible from the northern hemisphere is presented, including derivation of their distances, spatial distributions, morphology, and extended structures, including their inner integrated light properties and their outer resolved star distributions. All 12 galaxies are found to be reasonably well described by two-dimensional Sérsic functions, although UGC 4879 in particular shows tentative evidence of two distinct components. No prominent or convincing extended stellar substructures, that could be signs of either faint satellites or recent mergers, are identified in the outer regions of any of the systems examined (with the possible exception of an extremely tentative detection in Perseus).

3.1 Introduction

Dwarf galaxies are a fascinating and challenging regime in which to study galaxy evolution. Both internal and external processes dramatically impact the morphology and evolution of dwarfs as a consequence of their low masses and shallow gravitational potential wells. Star formation and the resulting feedback (e.g. El-Badry et al. 2018a), ram pressure stripping (e.g. Gunn & Gott 1972; Grebel et al. 2003), tidal stripping (e.g. Fattahi et al. 2018), tidal stirring (e.g. Kazantzidis et al. 2011; Mayer et al. 2001b), reionization (e.g. Ordoñez & Sarajedini 2015; Wheeler et al. 2019), mergers and interactions (e.g. Deason et al. 2014) are all processes which can significantly alter a dwarf's structure, morphology and stellar populations. The observational challenge then becomes understanding the complex interplay between initial formation processes and the internal and external processes that shape and reshape dwarfs.

Dwarf galaxies are the most numerous class of galaxy in the Universe and the population of known nearby dwarfs has increased dramatically in recent years (e.g. numerous dwarfs discovered in the Dark Energy Survey Bechtol et al. 2015; Drlica-Wagner et al. 2015; Crnojević et al. 2019; Drlica-Wagner et al. 2020; Crater III and Bootes IV from the Hyper Suprime-Cam Subaru Strategic Program Homma et al. 2018, 2019; Sagittarius II, Draco II and Laevens 3 from the Pan-STARRS 1 3π Survey Laevens et al. 2015 among others). The parameter space that dwarfs are known to inhabit has been broadened by these discoveries and others (e.g. Crater II and Antlia II from Torrealba et al. 2016, 2019). New terminology such as ultra-faint and ultra-diffuse is now in common usage (Simon, 2019). Many dwarf galaxies are so faint that the only detailed information obtainable for them comes through their resolved stars, with the result that the dwarfs in the nearby Universe are a critical observational sample for astronomers.

Within the Local Group, the satellite dwarfs of the Milky Way (e.g., the MegaCam Survey of Outer Halo Satellites, Marchi-Lasch et al. 2019) and those around M 31 (e.g., the Pan-Andromeda Archaeological Survey, McConnachie et al. 2009; Martin et al. 2016) are generally well studied. Typically, these ground-based, resolved stellar studies are limited to the Local Group and work in concert with the extensive number of surveys and studies at larger distances (e.g., M 101: Karachentsev & Makarova 2019; Müller et al. 2017; Cen A: Müller et al. 2019; Crnojević et al. 2019; NGC 1291: Byun et al. 2020), in other environments (e.g., NGVS Ferrarese et al. 2012, 2020 and Fornax Venhola et al. 2018), and which question the "stereotypical" nature of the

Local Group (e.g., the SAGA Survey: Geha et al. 2017; Mao et al. 2021; Carlsten et al. 2020).

The importance of environment on dwarf galaxy evolution is well known, most famously the presence of increased star formation with distance from a large companion (Einasto et al. 1974, also see McConnachie 2012 and references therein). However, while it is clear that dwarfs around a large host galaxy are affected by their companion, the interplay of these effects remain relatively poorly understood and quantified (Spekkens et al., 2014; Geha et al., 2012). The study of dwarfs well separated from large galaxies, where the current impact of the host is likely to be minimal, offer an interesting opportunity. Even here though, we must be aware that some of these dwarfs may be "backsplash" dwarfs (Buck et al. 2019 and references therein), which could have had a close pericentric passage with a massive galaxies some point in their history. The isolated dwarfs in the Local Group present a unique opportunity to study the lowest mass galaxies in great detail, largely in the absence of strong environmental influences.

Of course, isolated Local Group galaxies have been studied for many years. This includes individual dedicated studies for some of the most prominent members e.g., WLM (Wolf, 1909; Melotte, 1926; Leaman et al., 2012), IC 1613 (Hodge et al., 1991; Pucha et al., 2019), and DDO 210 (McConnachie et al., 2006); as part of catalogues like Mateo (1998); Karachentsev et al. (2013); van den Bergh (1999); McConnachie (2012); as inclusion in HI Surveys like LITTLE THINGS (Hunter et al., 2012) or FIGGS2 (Patra et al., 2016); as part of Local Group-wide studies like the star formation history analysis of Weisz et al. (2014); and as targets to understand their stellar dynamics (e.g., Kirby et al. 2014; Kacharov et al. 2017 among numerous other works). However, homogeneous, systematic studies focused on this population are generally lacking but with exceptions, such as Local Group Galaxies Survey Project (Massey et al. 2006, 2007).

Given the limited sample of galaxies available, homogeneous analyses are important in order to minimise systematic errors in what is, fundamentally, a relatively small statistical sample. It is with this intent that we began Solo, the *So*litary *Lo*cal Dwarf Galaxy Survey.

Solo is a volume limited sample of all known, nearby, and isolated dwarf galaxies, designed to study the secular evolution of dwarfs. A general introduction to the Solo Survey is given in Chapter 2 and Higgs et al. (2016). Briefly, all 44 dwarfs that are known within 3 Mpc, and which are located more than 300 kpc from the Milky

Way or M 31 are included. In this distance range, at least the outer parts of these dwarfs can usually be resolved into stars using ground-based facilities. While the adoption of 300 kpc as a threshold for isolation is somewhat arbitrary (although it does correspond to the approximate expected halo virial radius for these galaxies; e.g., Klypin et al. 2002; Posti & Helmi 2019), work by Geha et al. (2012) and Spekkens et al. (2014) suggests that it is around this distance that there is a notable change in dwarf morphology (see also Einasto et al. 1974). While there is no doubt that backsplash galaxies will be in the sample (e.g., Buck et al. 2019 suggest both IC 1613 and And XXVIII are likely backsplash systems), it is clear that most of the Solo sample of dwarfs have largely evolved in isolation, and are the best nearby systems to use to explore the faint end of the galaxy luminosity function away from the influence of massive galaxies.

The Local Group Galaxies Survey Project, Massey et al. (2006, 2007) focused on detailed analysis of the CMDs using UVBRI photometry of some of the more massive Local Volume dwarfs (M 31, M 33, NGC 6822, WLM, IC 10, Phoenix, Pegasus, Sextans A, and Sextans B). In contrast, Solo has a larger field of view by a factor of ~ 2 and deeper photometry by $\sim 2 - 3$ mags, but in only two filters. Our focus is largely on the extended structure of these galaxies rather than their detailed stellar populations, as in Massey et al. (2006, 2007).

The Solo Survey is designed to probe several questions pertaining to the role of environment in the evolution of the lowest mass galaxies. In particular, the intent is to provide observational data and parameters of a similar quality to those that exist for the Milky Way and M 31 satellite populations. This particular contribution is focused towards obtaining updated wide field structural parameters in a similar way to the corresponding M 31 and Milky Way data for galaxies in a similar luminosity range, i.e. by analysis of the distribution of the oldest stellar populations, primarily the red giant stars. This is not an insignificant point, given that many of the isolated Local Group galaxies have their light dominated by young stellar populations, which are invariably more centrally concentrated than other stellar populations. Weisz et al. (2014) presents star formation histories showing substantial recent star formation in many of these systems, and studies of radial gradients in the stellar populations of dwarf galaxies invariably show that the younger populations are more concentrated (e.g. Harbeck et al. 2001; Tolstoy et al. 2004; Bernard et al. 2008; Mercado et al. 2020 among others). Thus, in determining the physical extent of the galaxy, studies that are based solely on integrated light or young stars will generally find a smaller size for

these galaxies than studies based on the distribution of older stellar populations (as is nearly always the case for studies of Milky Way and M31 satellites). Minimising these systematic differences between observations of satellites and isolated galaxies is a primary purpose of this current study.

This chapter is structured as follows. Section 3.2 describes the survey, including the observations, data processing, calibrations, and a brief introduction to the dwarfs analysed. Section 3.3 analyses the integrated light in the central regions of the target galaxies. Section 3.4 describes the analysis of the resolved stellar components, including distance estimates and shape analysis. Section 3.5 derives radial profiles from a combined fit of the integrated light and resolved stars, and presents the associated parameters describing the dwarf galaxies. Section 3.6 compares our results to the literature, and Section 3.7 concludes.

3.2 Preliminaries

3.2.1 Solo and the Local Group subset

Solo is discussed in detail in Chapter 2 and Higgs et al. (2016) (hereafter Paper 1). While the full Solo Survey contains 44 dwarfs, this chapter explores a Local Group (LG) subset, consisting of 12 dwarfs within the zero velocity surface of the Local Group ($\approx$1 Mpc) and visible from the northern hemisphere. Table 3.1 lists these 12 galaxies (hereafter the "LG subset") and gives details of the observations relevant to this work. Other dwarfs within the zero velocity surface, but observed for Solo only from the Southern hemisphere are Cetus, Eri II, Phoenix and Tucana.

Figure 3.1 shows galactocentric radial velocity against galactocentric distance for dwarfs in and around the Local Group. Our transformation from the heliocentric values listed in McConnachie (2012) assumes $(R_\odot,\ V_c) = (8.122\,\mathrm{kpc},\ 229\,\mathrm{km\ s^{-1}})$ and $(U_\odot,\ V_\odot,\ W_\odot) = (11.1,\ 12.24,\ 7.25)\,\mathrm{km\,s^{-1}}$ (Gravity Collaboration et al. 2018; Schönrich et al. 2010). Within this plot, the LG subset can be defined as those whose motion is not affected by the Hubble flow. In contrast, those galaxies further away are clearly affected by the expansion of the Universe. The boundary, the so-called "zero velocity surface", is at approximately 1 – 1.3 Mpc from the Milky Way (about 1 Mpc from the center of the Local Group; McConnachie 2012). In Figure 3.1, the M 31 satellite population stands out as the distinct cluster of galaxies around 800 kpc (McConnachie et al., 2005).

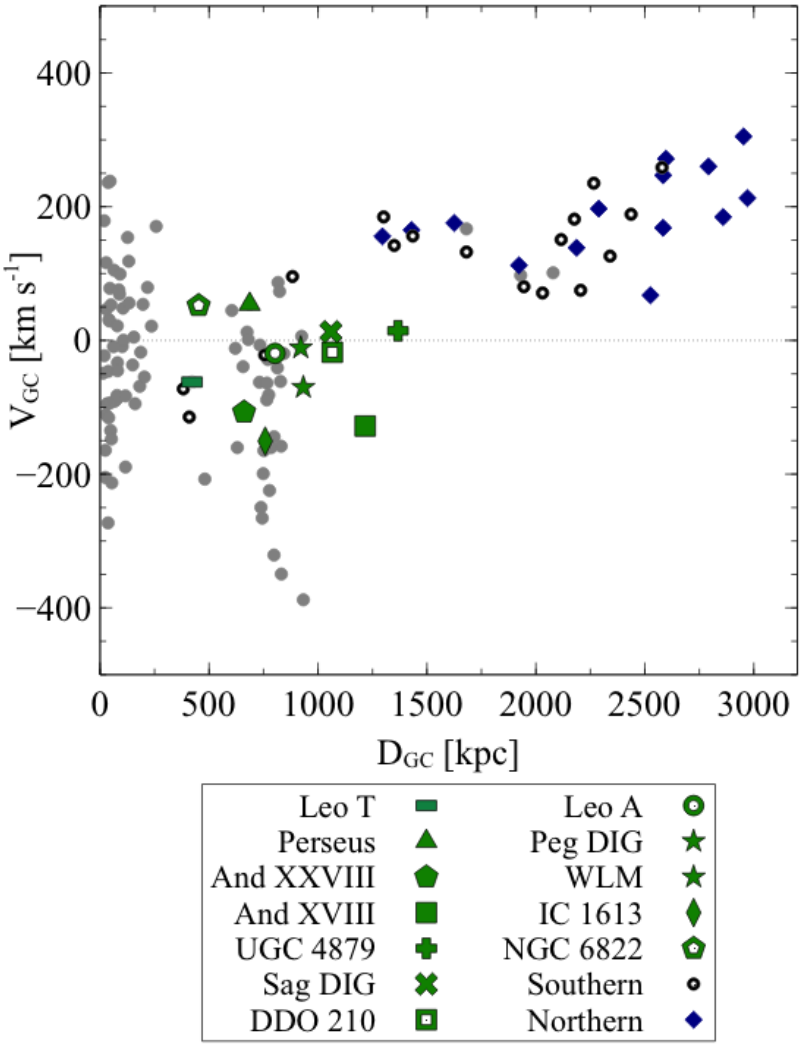

Figure 3.1: Galactocentric distance (D_{GC}) versus radial velocity relative to the Milky Way (V_{GC}) of all dwarfs in McConnachie (2012). Solo dwarfs with the Local Group subset studied in this chapter highlighted in green, with the remainder of CFHT observed Solo dwarfs shown with blue diamonds. Black hollow circles are Solo Local Group dwarfs observed with Magellan and not presented in this paper. Galaxies at large distances in this figure have their velocity dominated by the Hubble flow. The M 31 sub-group is obvious as the cluster of points around 785 ± 25 kpc (McConnachie et al., 2005).

Figure 3.2 shows colour composite images for 6 of the dwarfs in our sample, and qualitatively demonstrates the diversity of the Local Group subset. Striking differences in size, stellar density, number of bright stars, colour, and the density of the MW foreground can clearly be seen by eye. The dwarfs range from low mass, faint systems like Perseus, to large, obviously star-forming galaxies like WLM. Some dwarfs – like WLM – are well known and have been well studied (e.g., Leaman et al. 2012, Leaman et al. 2013, among others), while others in our sample, like And XXVIII, are less so.

3.2.2 Data preparation

An extensive and detailed description of the data processing is given in Chapter 2 and Paper I.

Only stellar sources are used for the subsequent analysis, using the morphological classification procedures described in Irwin (1985, 1997). Sources within 2 σ of the stellar locus in both bands are considered stellar. From the source catalogues, the positions of the sources are de-projected, converting right ascension (R.A.) and declination (Dec.) to standard plane coordinates (ξ, η). The standard plane is centered on the dwarf's coordinates as listed in McConnachie (2012).

Figure 3.3 shows photometric errors as a function of magnitude in $g-$ and $i-$band for a sample of dwarfs. These uncertainties are derived from the square root of the variance of the weighted flux measurements. They are generally less than 0.1 magnitudes at ($g \sim 24.5, i \sim 24.0$), meaning red giant branch (RGB) stars in the dwarfs are easily detectable in all cases.

WLM was observed in non-photometric conditions for the $i-$ band. As such, a correction was required and was derived from Isaac Newton Telescope (INT) Wide Field Camera observations of WLM, DDO 210 and Peg DIG (published in McConnachie et al. 2005). RGB stars in common between the two datasets for DDO 210 and Peg DIG were used to define the appropriate transformation between the two filter systems for photometric conditions. Applied to the INT data for WLM, this transformations then allowed us to determine the appropriate correction to convert the non-photometric MegaCam data to the correct photometric system.

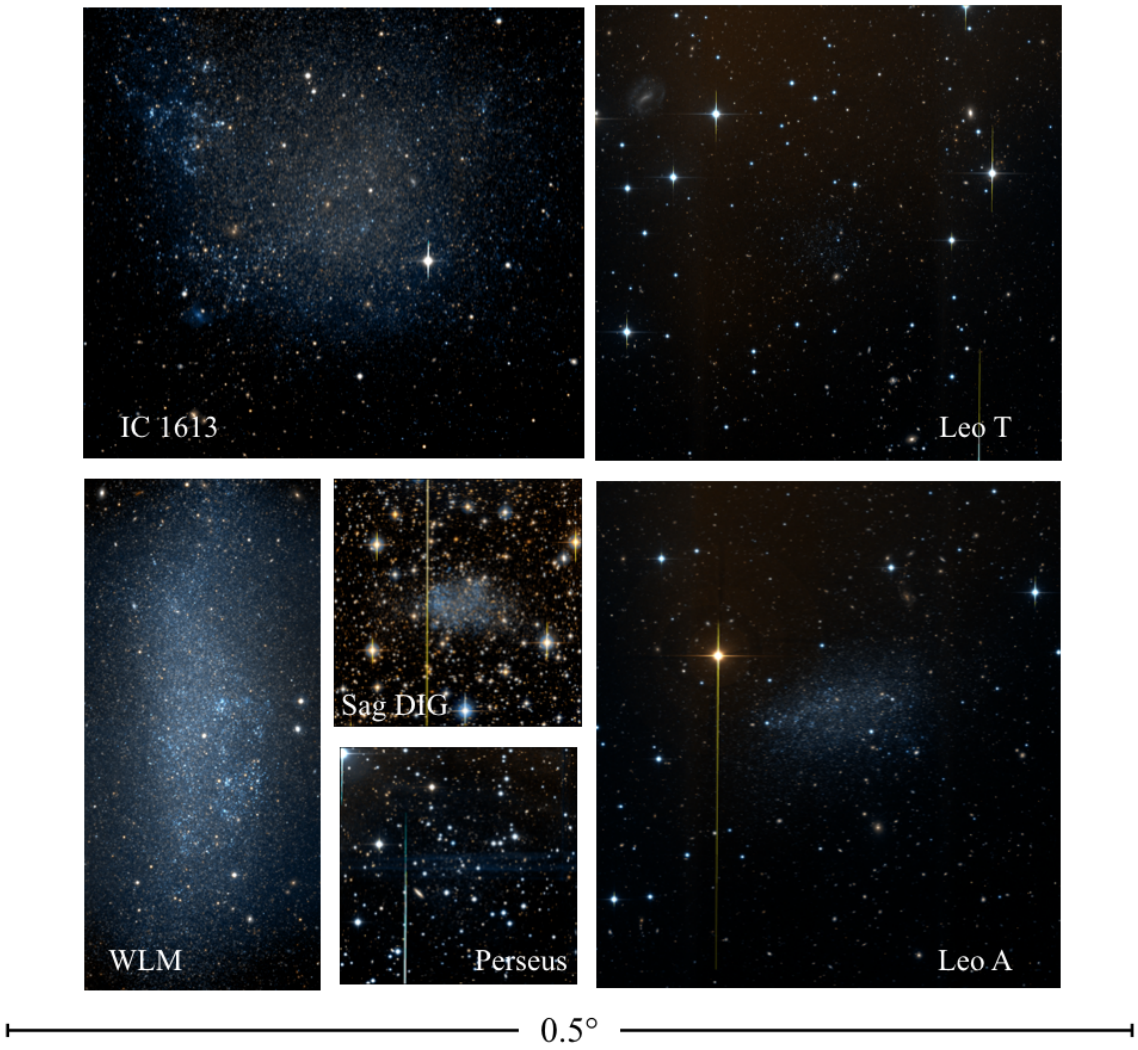

Figure 3.2: Two-colour images of 6 of the dwarfs in this chapter, showing the diversity of this small sample. The regions shown for each dwarf does not cover the full field of view, but each panel is scaled for the same angular size. The black bar at the bottom of the image is 0.5°, half of the MegaCam field of view. Each field is oriented with North at the top and East to the left.

Table 3.1: Details on filters used in observations. Those indicated with a * were taken as part of CFIS.

Name	Alt. Name	Filter	Filter ID	Year
Leo T		u	u.MP9302	2016A*
		g	g.MP9402	2016A
		i	i.MP9703	2016A
Perseus	And XXXIII	g	g.MP9402	2016B
		i	i.MP9703	2016B
And XXVIII		u	u.MP9302	2017B*
		g	g.MP9401	2012A
		i	i.MP9702	2012A
And XVIII		g	g.MP9402	2018B
		i	i.MP9703	2018B
UGC 4879	VV 124	g	g.MP9402	2016A
		i	i.MP9703	2016A
Sag DIG		u	u.MP9301	2013A
		g	g.MP9401	2012B
		i	i.MP9702	2012B
DDO 210	Aquarius	u	u.MP9301	2013A
		g	g.MP9401	2013A
		i	i.MP9702	2013A
Leo A		u	u.MP9302	2015B*
		g	g.MP9402	2016A
		i	i.MP9703	2016A
Peg DIG	DDO 216	u	u.MP9301	2013A
		g	g.MP9401	2012A
		i	i.MP9702	2012A
WLM	DDO 221	g	g.MP9401	2013B
		i	i.MP9703	2016B
IC 1613	DDO 8	g	g.MP9402	2016B
		i	i.MP9703	2016B
NGC 6822	DDO 209	u	u.MP9301	2013A
		g	g.MP9401	2013A
		i	i.MP9702	2013A

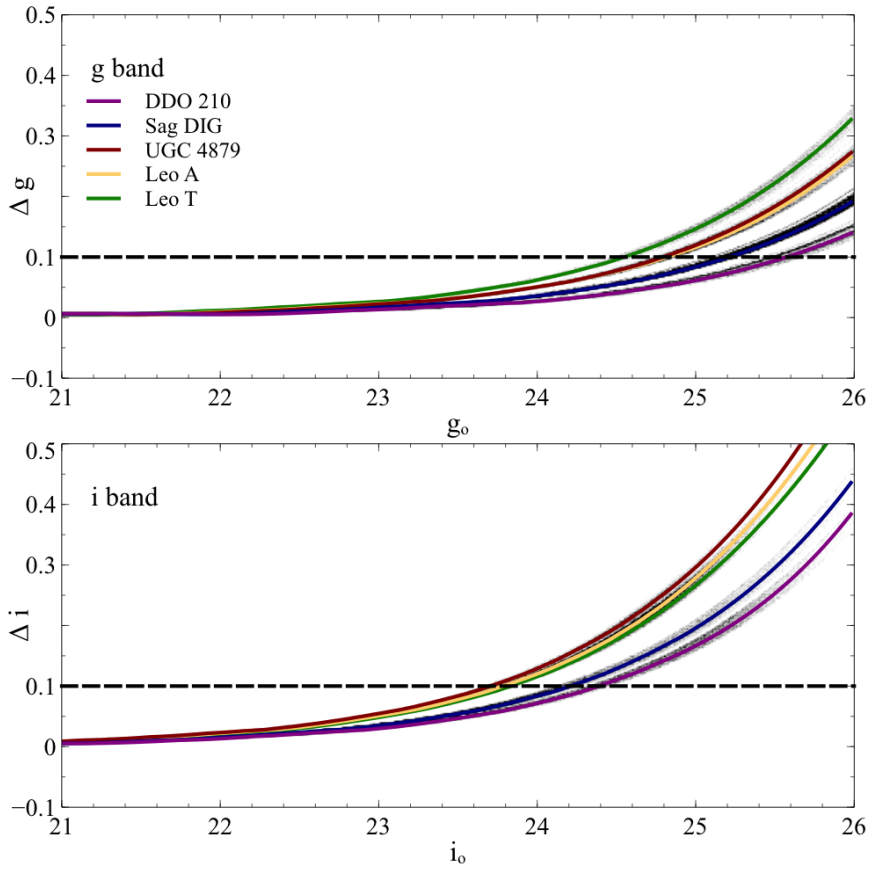

Figure 3.3: Representative photometric errors as a function of g- (*upper panel*) and i-band (*lower panel*) for DDO 210, Leo T, Leo A, Sag DIG and UGC 4879. The grey shaded background shows a histogram of all points.

3.2.3 Summary of target galaxies

Here, we briefly summarise some of the notable properties of each of our target dwarfs, and highlight the pertinent literature as it relates to their structural properties. This background is not intended to be an exhaustive summary of all previous work, but rather a useful and easy reference for the interested reader.

Andromeda XVIII

And XVIII is in the vicinity of M 31, and was discovered by McConnachie et al. (2008) as part of precursor observations for the Pan-Andromeda Archaeological Survey (PAndAS; McConnachie et al. 2009). Unfortunately, in these discovery observations, the majority of the galaxy fell in one of the large chip gaps on the detector, obscuring the central region. The dwarf's parameters were estimated under the assumption of circular symmetry to address the obscured portion. Martin et al. (2016) analysed the dwarf as part of a wider study of M 31's dwarfs, however they also used the same data. They estimated its structural parameters, and included a more robust surface brightness estimate, however its ellipticity was poorly constrained. Here, new observations, placing the dwarf well away from chip gaps, have been obtained which allow for a complete picture of its global structure.

Tollerud et al. (2012) obtained kinematics of And XVIII stars as part of the SPLASH survey. They concluded that it is a kinematically cold, dark matter dominated dwarf. Given its distance from M 31 (of order 600 kpc distant), it is unlikely to have interacted with this massive galaxy, but Tollerud et al. (2012) noted that there is a remarkable agreement between their systematic velocities.

Andromeda XXVIII

Slater et al. (2011) determined the structural parameters for And XXVIII from SDSS observations using the maximum likelihood methods described in (Martin et al. 2008; our new observations are approximately 3 magnitudes deeper than the SDSS observations). Slater et al. (2015) followed up with Gemini/GMOS and Keck/DEIMOS observations, finding no signs of recent star formation but the presence of a red clump and other features suggested an extended period of star formation. Buck et al. (2019) suggest that this dwarf has a highly likelihood (91%) of having interacted with the MW (i.e. it could be a backsplash galaxy). This estimate is based on the comparison

of observed galaxy properties (distance, radial velocity and velocity dispersion) with simulated satellite and field dwarfs in the NIHAO simulations (Wang et al. 2015).

The Pegasus Dwarf Irregular Galaxy

Peg DIG (also known as DDO 216 and UGC 12613) is a transition-type dwarf that is host to a large, central globular cluster (Cole et al., 2017; Leaman et al., 2020), making it among the lowest mass dwarfs in the Local Group with a globular cluster (in addition to Eri II; see Zoutendijk et al. 2020 and references therein). A notable population of RR Lyrae stars in the cluster have been used to derive a distance of 24.77 ± 0.08 (Cole et al., 2017).

McConnachie et al. (2007a) found an asymmetry between the gas and stellar components indicative of ram pressure stripping removing the gas from the system. However, more recent HI observations by Kniazev et al. (2009) contradict this conclusion, finding minimal evidence of interactions. These authors concluded that this dwarf has only recently joined the Local Group. The structural parameters derived by Kniazev et al. (2009) provided a good comparison to this current work, however the SDSS observations used are significantly (>3 magnitudes) shallower than the Solo data. They found the dwarf is more extended than previously thought and noted possible stellar extensions on the north-west end. In their HI observations, Kniazev et al. (2009) observed solid body like rotation. Kirby et al. (2014) found rotation in the red giant branch stars as well.

Leo T

Leo T is one of lowest mass and closest dwarfs in Solo. It is notable for being one of the few very faint dwarfs with a young stellar population, and like Peg DIG, it is often described as a transition-type dwarf, given that its other characteristics are generally typical of dwarf spheroidal galaxies. de Jong et al. (2008) determined its structural parameters based on deep, wide-field Large Binocular Telescope data, and it is also included in the MegaCam Survey of Outer Halo Satellites (Muñoz et al., 2018b,a), using CFHT *gr* photometry. Its HI structure was recently studied by Adams & Oosterloo (2018). Teyssier et al. (2012) argued that both Leo T and NGC 6822 have likely had a close pericentric passage with the Milky Way, whereas Buck et al. (2019) suggested that there is only an approximately 50% chance of Leo T being a backsplash galaxy.

Leo A

Leo A (DDO 69) shows delayed star formation, like DDO 210, and only minimal star formation happened before 10 Gyrs ago. As such, it is sometimes argued as being a possible survivor of reionization (Cole et al., 2007, 2014). Stonkutė et al. (2014, 2018) presented detailed studies of Leo A based on Subaru/SuprimeCam data, in addition to using HST ACS fields at large radius. Stonkutė et al. (2015) reported the discovery of a young star cluster in Leo A. van Zee et al. (2006) studied the HII regions in Leo A, confirming that its interstellar medium has one of the lowest metallicities of nearby galaxies (van Zee et al. 2006 find $12 + \log(\mathrm{O/H}) = 7.30 \pm 0.05$). This low metallicity makes it a useful system for calibration (e.g. for Cepheid observations Bernard et al. 2013). Leo A was also used by Ruiz-Lara et al. (2018) to test whether there are differences between star formation histories derived from colour magnitude diagrams compared to integrated light studies.

Perseus

Perseus I, also known as And XXXIII, was discovered by Martin et al. (2013b) in the Pan-STARRS1 3π survey and followed up Martin et al. (2014) with spectroscopy. The structural parameters derived are based on the maximum likelihood method (Martin et al., 2008). The Solo observations are about 2 magnitudes deeper than the PanSTARRS data. The location of this dwarf makes it an interesting object with respect to the "planes of satellites" around the Local Group (see Pawlowski & McGaugh 2014 for a discussion of Perseus in this context).

UGC 4879

UGC 4879 (also known as VV 124) was first studied in detail by Kopylov et al. (2008). Bellazzini et al. (2011b,a) performed a comprehensive analysis using HST ACS, the Large Binocular Telescope, and HI observations, and identify 2 young star clusters. Kopylov et al. (2008) and Jacobs et al. (2011) noted that it is a very isolated dwarf, and so likely not a backsplash system. Its structure is somewhat unusual, insofar as there are two "wings" on either side of an otherwise elliptical system, perhaps suggestive of a stellar disk. Kirby et al. (2012) placed an upper limit on the possible stellar disk rotation of 8.6 km s^{-1}.

DDO 210

DDO 210 (also known as Aquarius) is classified as a transition type dwarf in that there is no current star formation observed but, prior to the discovery of Leo T, it was the faintest known dwarf with a significant gaseous component. Along with Leo A, DDO 210 has a delayed star formation history (Cole et al., 2014), meaning that most of the stars are of intermediate age. Cole et al. (2014) noted a strong blue horizontal branch population which is unusual relative to similar dwarfs (like Leo A), as well as the presence of a red clump and a red bump. Its free fall time is longer than a Hubble time, hence it is likely on its first in-fall into the Local Group (McConnachie 2012). It is well separated from neighbouring galaxies.

The HI and stellar components show some offset and differences in spatial structure (McConnachie et al., 2006). Hermosa Muñoz et al. (2020) looked at the metallicity and kinematics of stars, finding significant misalignment of the HI and stellar components. They suggested that this may be due to recent HI accretion or re-accretion of gas after feedback from star formation.

The Sagittarius Dwarf Irregular Galaxy

Sag DIG was studied as the first Solo dwarf in Paper I. We previously noted differences between the HI structure and its stellar structure, similar to DDO 210 (Aquarius). There are faint extended RGB stars regions along the semi major axis of this dwarf. Qualitatively, these extensions are not found to have a HI counterpart in LITTLE THINGS observations (Hunter et al., 2012). Sag DIG lies at a low galactic latitude so the foreground contamination from the MW in the field is significant.

Wolf-Lundmark-Melotte

WLM, also known as DDO 221, is one of the more massive dwarfs in the Solo Survey. It has been extensively studied, from its discovery over 100 years ago (Wolf, 1909) to recent work presented in Albers et al. (2019). Several spectroscopic studies have been conducted. For example, RGB stars have been targeted by Leaman et al. (2009, 2012) and blue supergiants have been targeted by Venn et al. (2003); Bresolin et al. (2006); Urbaneja et al. (2008). Leaman et al. (2012) concluded that this dwarf is a highly oblate spheroid. They found good agreement, kinematically and photometrically, between the position angle and ellipticity of the RGB stars, young carbon stars and HI gas. They concluded that external environmental effects have not had a dominant role

in shaping the structure of WLM. Using HST observations, Albers et al. (2019) derived a SFH history and found relatively continuous star formation, with no dominant early episode (Gallart et al. 2015 classified the SFH of WLM as "slow"). This dwarf is one of the few with a known globular cluster, in this case a single large globular cluster located just outside the central region.

NGC 6822

NGC 6822 is one of the more massive dwarfs in Solo and has been extensively studied. Demers et al. (2006) identified this dwarf as a polar ring galaxy, based on kinematics of HI compared to asymptotic giant branch stars. This claim is disputed by Thompson et al. (2016) who found that the axis of rotation for the stars and HI are largely aligned. Battinelli et al. (2006) derived the stellar structure from wide-field CFHT observations, and noted that it has a bright central bar. NGC 6822 hosts a population of globular clusters (Huxor et al., 2013; Veljanoski et al., 2015). Hwang et al. (2014) used extended star clusters as kinematic tracers and derived a mass to light ratio of $75^{+45}_{-1}(M/L)_{\odot}$, making NGC 6822 dark matter dominated. Teyssier et al. (2012) suggested NGC 6822 is possibly a backsplash galaxy, based on its current observed position and radial velocity. In contrast, McConnachie et al. (2021) find NGC 6822 is highly likely to be isolated and on its first infall, based on orbital properties derived using Gaia Data Release 2 proper motions of the brightest stars (Gaia Collaboration et al. 2018).

IC 1613

IC 1613 is another massive dwarf in Solo and has been well studied, including by Bernard et al. (2007) and recently by Pucha et al. (2019). Pucha et al. (2019) found strong age gradients, and the young stellar population has a considerably smaller scale radius than the older stars. The SFH they determined is consistent with this picture, with a decreasing star formation rate with increasing radius. They found that the young population is off-center, and the star forming regions are distributed in a ring, coincident with areas of high HI column densities. Buck et al. (2019) suggests that this dwarf, along with And XXVIII, has a highly likelihood of having previously interacted with the Milky Way.

3.3 Characterizing Solo Dwarfs using Integrated Light

The Solo Survey selects dwarfs such that at least their outer regions can be resolved into stars from the ground in reasonable seeing. In the central parts of most of these dwarfs, crowding becomes a significant issue and the stellar catalogues become increasingly incomplete. As a result, these central regions are better analysed using the integrated light rather than resolved stars, particularly with respect to their radial profiles in both bands (and which allows identification of any colour trends present).

The integrated light profile is determined in both the $g-$ and $i-$bands. Here, elliptical annuli with the median position angle and ellipticity as derived from the resolved RGB stars (see next section) is used. All bright sources and their surrounding pixels are masked to reduce contamination from other sources, including saturated objects and diffraction spikes. Figure 3.4 shows an example of an $i-$band image and the applied mask for DDO 210. Note, the central regions of each galaxy fit within a single CCD, and so therefore we only do the integrated light analysis for a single CCD per galaxy. This helps to minimise systematic uncertainties due to detector responses and other instrumental effects.

To estimate the background, the median luminosity is found within annuli that are well separated from the galaxy i.e., that are outside of a large ellipse centered on the galaxy. The size of this ellipse varies from galaxy to galaxy from 2 to 4 R_s (where R_s is the Sérsic scale radius fitted to the radial profile as described in Section 3.5). The inner bound of this background region is shown in Figure 3.4 for DDO 210 as the blue ellipse. To determine the uncertainty on the background estimation, we look at the variation between annuli. This technique accounts for the non-uniformity of the background and acknowledges that systematic errors are dominant compared to Poisson uncertainties. These systematic errors have spatial scales associated with them, depending on the source, and so it is important that the annuli we use to measure these variations are the same width as are used for the main profile. For example, some galaxies like Leo A have a bright star in the image. Consequently, internal reflections within the MegaCam instrument can create large halos, hence the background across the image is not expected to be uniform. The radial profile of DDO 210 is shown in ADUs in Figure 3.5, along with the background estimate and the adopted uncertainty.

The background subtracted profiles for all Solo dwarfs are shown in Figure 3.6.

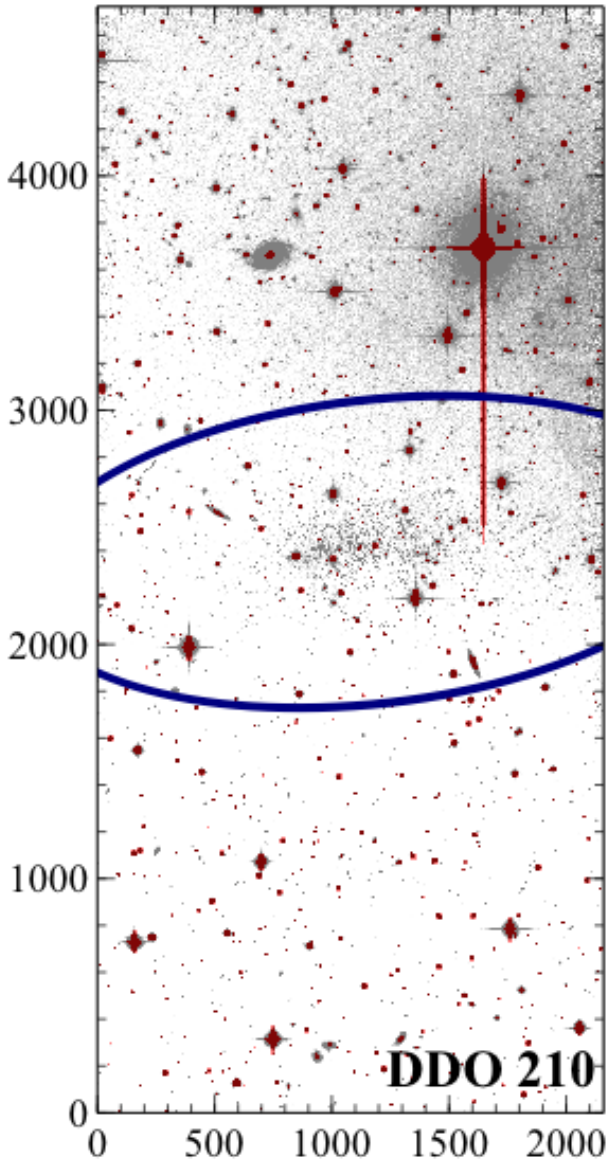

Figure 3.4: The central chip in the $i-$band for DDO 210. The grey scale shows the integrated flux, scaled to highlight the brighter stars in the dwarf. The red regions are masked out when determining the integrated light profile. The blue ellipse shows the inner edge of the region used to determine the background in the integrated light. The relative inhomogeneity of the background as well as the presence of very bright stars is obvious and highlights the necessity of carefully selecting the background region.

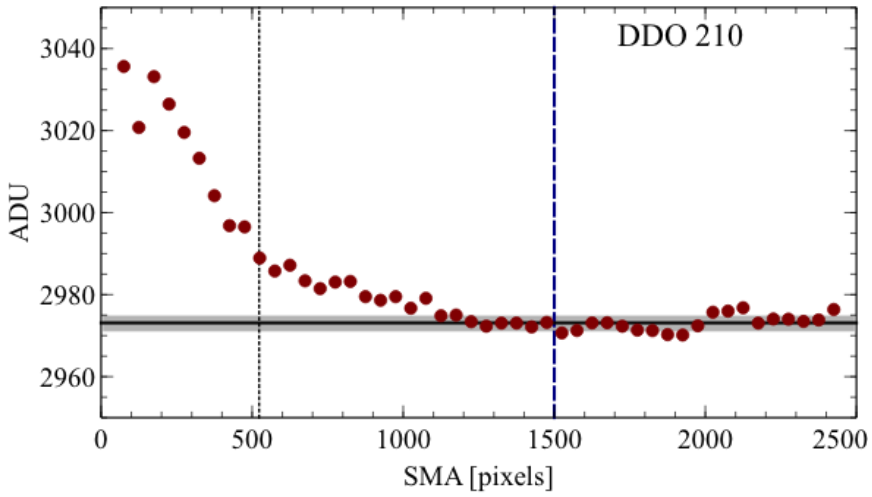

Figure 3.5: The radial semi-major axis (SMA) profile in ADUs for DDO 210 in the $i-$band. The black line indicates the mean background and the standard deviation is shown as the grey shaded region. This background is determined using the points outside the blue dashed line (corresponds to the blue ellipse in 3.4). The black dotted line is R_s, the Sérsic scale radius as defined in Section 3.5.

For some of the faintest systems, there is no discernible $i-$band integrated light component above the background. We show the colour profiles as sub-panels to the main panels for those dwarfs where both $g-$ and $i-$band profiles were determined.

For all nine galaxies with observable colour profiles, the colour profiles are largely flat or slightly rising, indicating blue centers and increasingly red toward larger radii. This structure is consistent with the fact that the Solo dwarfs are dwarf irregulars, with recent or ongoing star formation.

3.4 Characterizing Solo Dwarfs using Resolved Stars

3.4.1 Colour magnitude diagrams and distance estimates

Figure 3.7 shows the colour magnitude diagrams (CMDs) of two Solo galaxies to illustrate the different degrees of contamination from the Milky Way foreground. Perseus is relatively low apparent luminosity ($m_V = 14.1 \pm 0.7$) at a relatively low Galactic latitude ($b = 147.8°$), whereas Peg DIG is brighter ($m_V = 12.6 \pm 0.2$) at a higher latitude ($b = 94.8°$). Note, in what follows, the term "background" is used to describe foreground contamination arising from the Milky Way as well as from true background sources (generally distant, compact galaxies misidentified as stars at faint magnitudes). In both cases in Figure 3.7, the stellar populations of the dwarf are most easily discerned by selecting only stars near the center of the galaxy.

The CMDs for all of our sample are shown in Figures 3.8 and 3.9. The main feature visible in all CMDs are RGB stars. Young, blue stars are also present (for those with recent star formation), and can be seen as vertical sequences around $(g-i)_o \simeq -0.5$. Sag DIG, Leo A, WLM, IC 1613 and NGC 6822 show a clear blue sequence, where as DDO 210, Peg DIG (and tentatively Leo T and Perseus) show a few stars which may be young, blue stars. Foreground contamination makes distinguishing individual stars associated with the dwarfs not possible in this region without additional observations. Asymptotic giant branch (AGB) stars may also be present for some of the galaxies, although these are hard to distinguish from RGB stars, except at brighter magnitudes, where they are brighter than the tip of the RGB (e.g., WLM). On each panel, a Dartmount isochrone (Dotter et al., 2008) is shown, adjusted to the correct distance using our tip of the RGB measurements (see below) and with a metallicity selected to match the average colour of the RGB. The metallicities are listed in the upper right of each plot, ranging from [Fe/H] = -0.9 dex (UGC 4879) to -1.7 dex (Sag DIG).

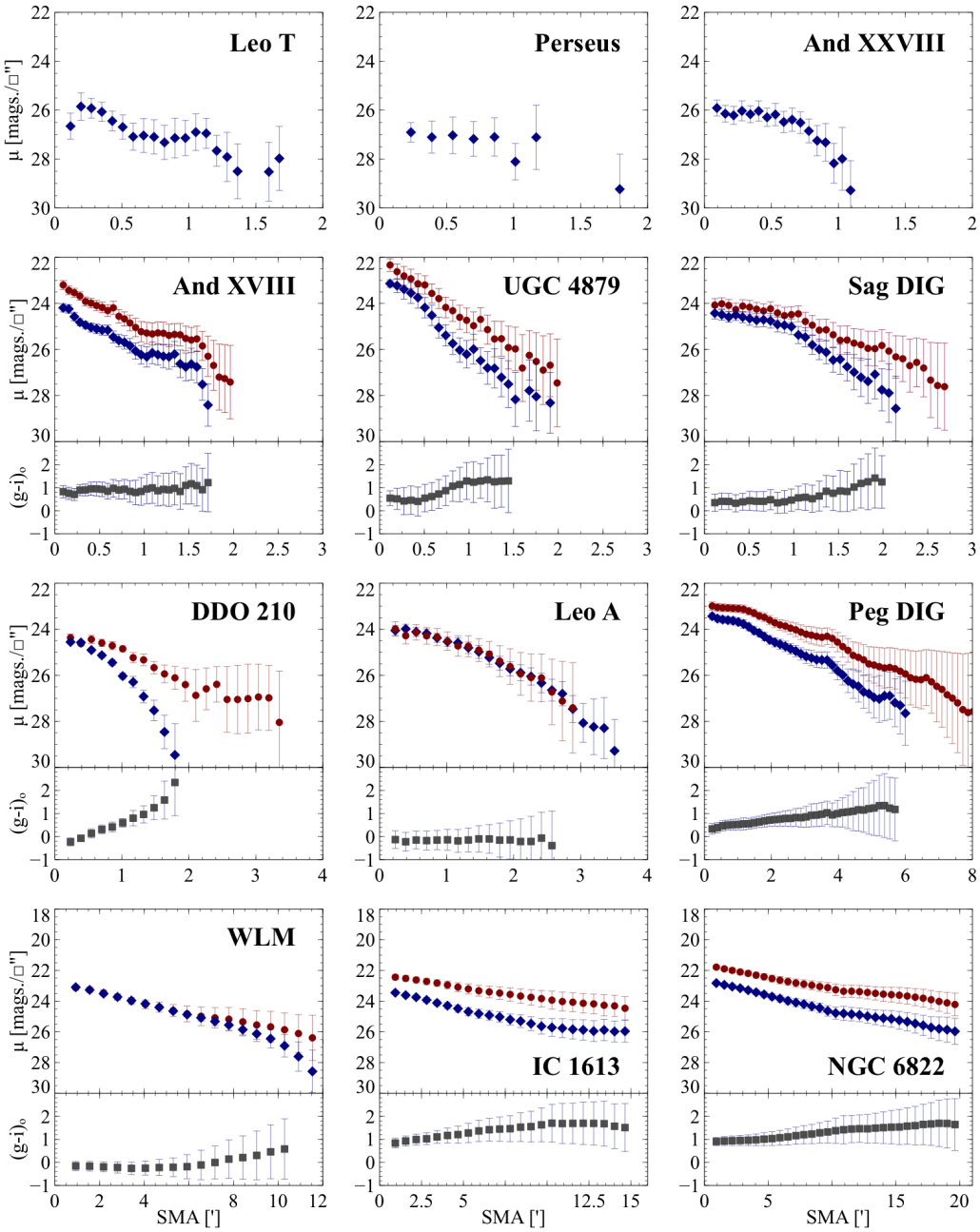

Figure 3.6: Each panel shows the surface brightness profile (shown per square arcsecond - □″) from the integrated light in the $g-$ (blue diamonds) and $i-$ (red circles) bands as a function of radius semi-major axis (SMA). In 3 cases there is no discernible $i-$band profile (top row). The sub-panels below each main panel shows the colour profile for all cases where both $g-$ and $i-$band profiles exist.

This range is broadly similar to the satellites of the Milky Way and M31 with the satellites tending to have additional lower metallicity dwarfs (from values listed in the updated tables of McConnachie 2012 and respective references). The isochrones plotted are selected to be old ($\sim$ 12 Gyrs) and intended to help visualize the RGB. As these dwarfs are irregulars, they are not necessarily simple, old stellar populations. For instance, the Perseus is not ideally matched, however this does not impact the distance estimate.

The distance to each dwarf is found using the tip of the RGB (TRGB) as a standard candle. The TRGB is ideal as its luminosity is insensitive to small variations in age or metallicity given an older, metal poor population (Lee et al., 1993). Indeed, using the Darthmouth isochrones (Dotter et al., 2008), the difference between a 10 Gyrs, 11 Gyrs or 12 Gyrs stellar population is on the order of $\Delta i = 0.002$. This uncertainty is not significant given that the uncertainties in identifying the TRGB from the CMD are on the order of $\Delta i = 0.1$.

First, the RGB stars are selected from a CMD using parallel "tram-lines". These tram-lines are visually selected and generously encompass the RGB branch. If the RGB branch is well populated, the TRGB is apparent by a significant "break" in the RGB luminosity function. The location of this break is identified using a 5 point Sobel filter, similar to Sakai et al. (1996). As the luminosity function is binned, we remove the dependence of the choice of bin locations and widths by repeating the analysis with different binning choices, similar to the method used by Battaglia et al. (2012). Note that we adopt upper and lower bounds on the region in which the TRGB may be found, to avoid spurious signals due to structures like the red clump or random stars clearly unassociated with the TRGB. These limits are chosen visually and generously encompass the whole region in which the TRGB is located. For low mass dwarfs with poorly populated RGBs, the limits are selected cautiously as to avoid biasing results. The distribution of resulting TRGB values (10 000 combinations of bin width and location in total) is shown with the median values and 1σ interquartile range highlighted.

In the above analysis, we do not find it necessary to subtract a reference luminosity function (due to the Milky Way contamination), except in the case of Sag DIG. Typically, the contamination is fairly uniform near the TRGB and due to the low number of stars in some galaxies, subtracting a background did not help in identifying the TRGB, but rather just added more noise. However, for Sag DIG, which has a reasonably well populated RGB branch and substantial contamination we found it

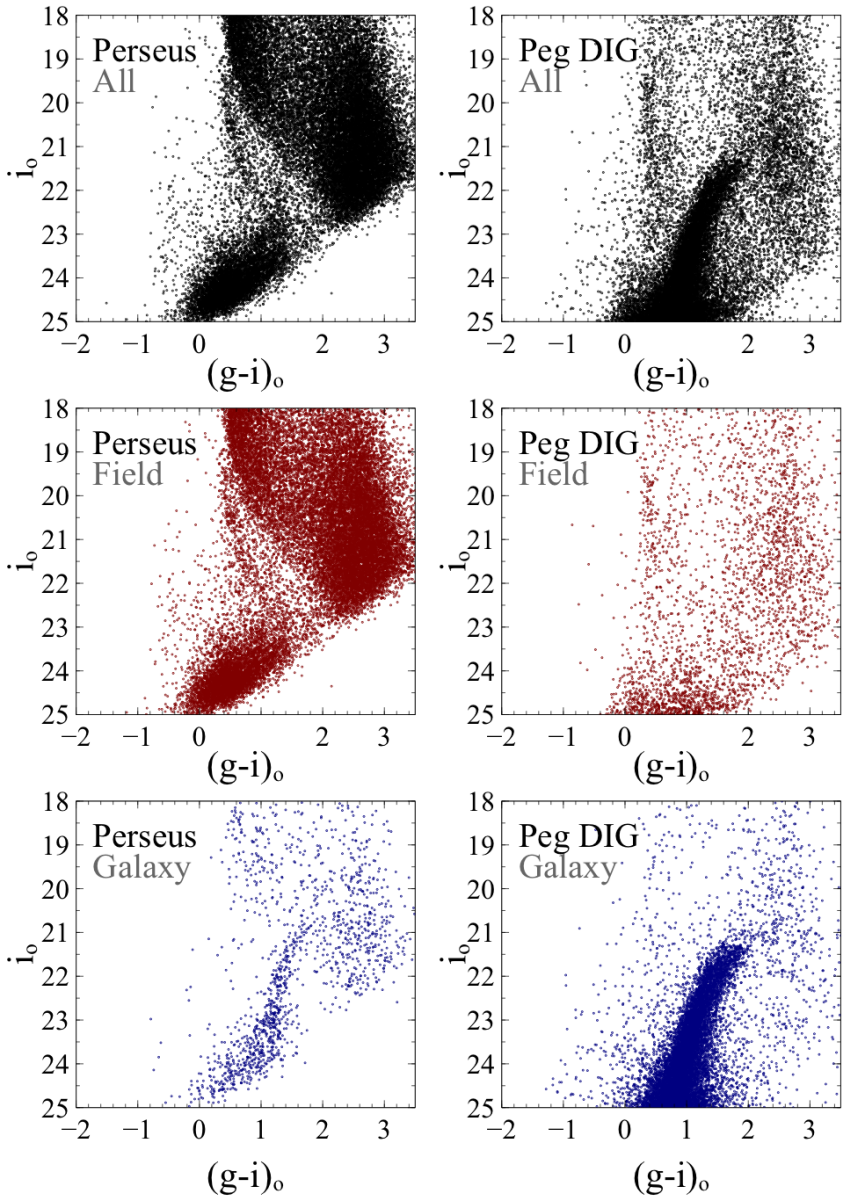

Figure 3.7: Examples of contamination in the CMDs of Solo dwarfs. *Top panels:* All stars in the full 1 sq. degree field of view for Perseus (*left*) and Peg DIG (*right*). *Middle panels:* All stars in the field far ($> 5R_s$) from the dwarf galaxy, showing the different levels of foreground contamination from MW stars, as well as the different structure of the foreground populations. Bright stars around $(g-i)_o = 0.5$ are Milky Way main sequence turn-off stars. Stars in the large cloud of points around $(g-i)_o \sim 2.5$ are generally low mass Milky Way main sequence stars. For Perseus, the sequence of stars extending from the main sequence turn-off region to $(g, (g-i)_o) = (0.5, 23)$ is a Milky Way halo overdensity. At faint magnitudes, increasing numbers of background galaxies are misidentified as stars. *Lower panels:* All stars in the field close to the centers of the galaxies, clearly showing the RGB of the two galaxies.

was necessary to statistically remove this background. As detailed in Paper I, a portion of the foreground structure in this direction is likely due to the Sagittarius stream.

The distance modulus, $(m - M)_o$, is computed from the TRGB using an absolute magnitude of $i_{o,MP9703} = -3.49$. This value is derived from the Darthmouth isochrones (Dotter et al., 2008) using the median value for old (12 Gyrs) stellar populations with [Fe/H] <0.0 dex (consistent with the isochrones matched previously). The TRGB value is converted to the new CFHT filters using the previous equations (Equations 2.1 & 2.2).

3.4.2 Structural analysis

Once the distance has been calculated for each dwarf galaxy, we examine their spatial distribution based on the RGB stars. These stars are selected from the full stellar catalogue (no spatial constraints) as within the tram-lines previously identified and fainter than the TRGB. Figures 3.10 and 3.11 show the distribution of these stars in the entire field of view for each dwarf in the subset. The fields of view were positioned so that the galaxies were slightly off-center to avoid the small detector gaps between CCDs. The two large gaps in the detector between CCD rows 1 & 2 and rows 2 & 3 are clearly visible. Note that those observations taken with the newer filter set at CFHT have a different footprint. The new filters are physically larger, and the "ears" of the detector can now be used whereas previously they were not (increasing the total number of science CCDs from 36 to 40).

The main panels of Figures 12 and 13 show the corresponding density maps for each of our dwarfs, where contour levels are set at a minimum of $2\,\sigma$ above the background, and pixels are 1 arcmin in each dimension. To estimate the background, we examine the density of stars outside of an ellipse corresponding to 5 x R_s centered on the galaxy (recall R_s is the Sérsic scale radius fitted to the radial profile as described in Section 3.5). This criteria is modified for the largest three galaxies as 5 x R_s does not lie within the 1° field of view. For WLM and IC 1613, we estimate the background at 3 and 2 x R_s respectively. For NGC 6822, no background is estimated; RGB stars belonging to the dwarf dominate over the entire full field of view.

Considering each galaxy as an ellipsoidal distribution of stars, the appropriate position angle and ellipticity is calculated for each galaxy using the moments of the corresponding unsmoothed RGB density maps. Specifically, from McConnachie &

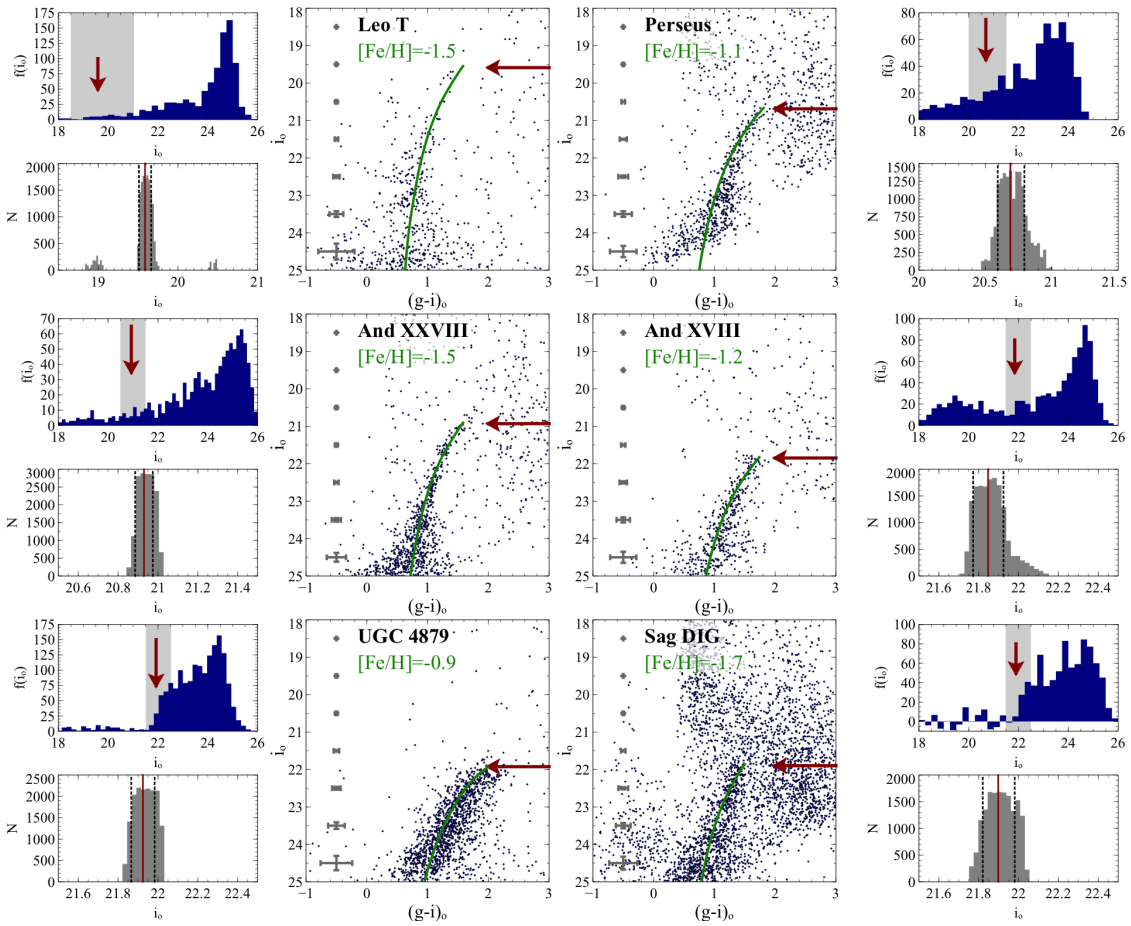

Figure 3.8: CMDs and luminosity functions for each of the dwarfs. The large panel for each galaxy is the CMD for stars selected to be within 2 R_s of the galaxy center. Mean errors as a function of magnitude are shown, and the TRGB is indicated with the red arrow. The upper small panel is the luminosity function for the RGB, and the lower small panel is the resulting distribution of the measured position of the TRGB (see text for details). The grey shaded region in the upper panel indicates the range shown the lower panel. Here, the red solid line indicates the median value and the dashed lines show a 16% and 84% quartile range (approximating 1σ).

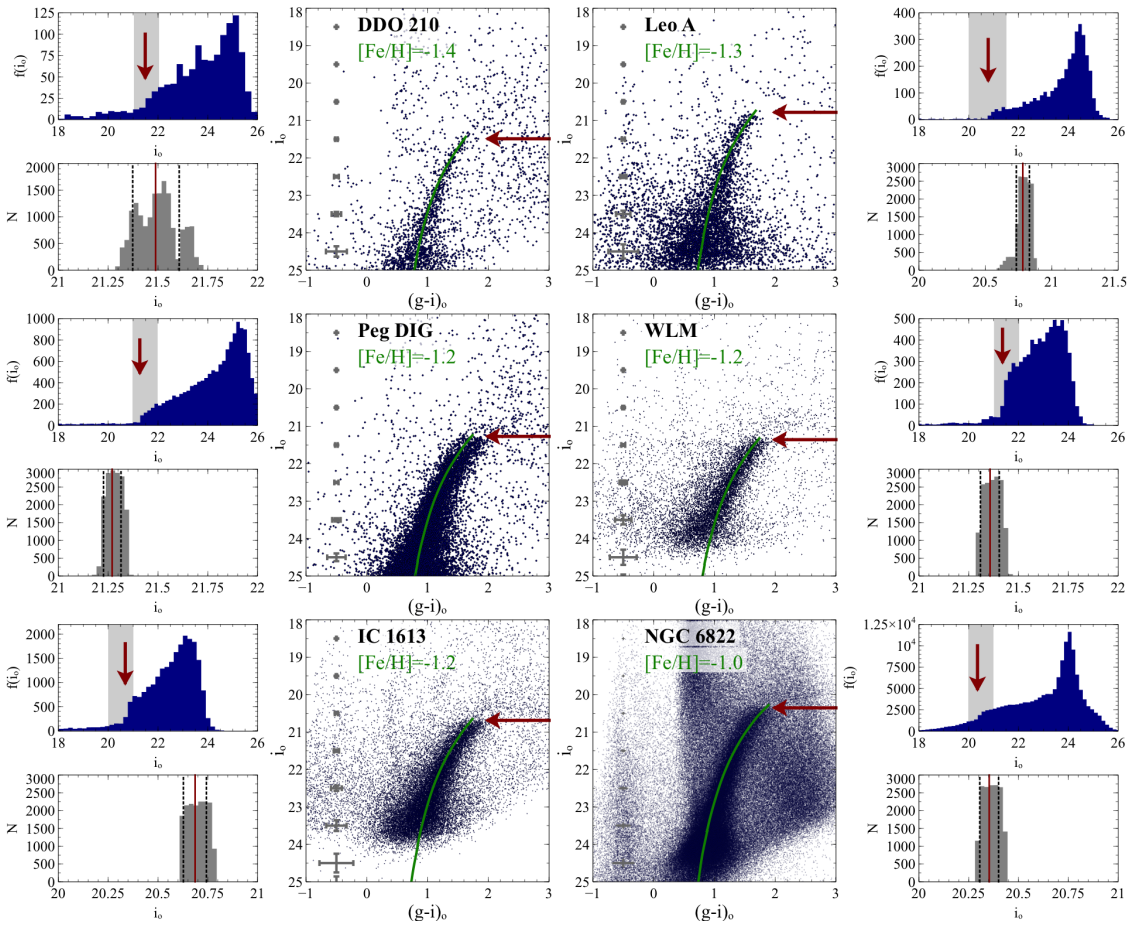

Figure 3.9: The same as Figure 3.8, CMDs and luminosity functions for each of the dwarfs. The large panel for each galaxy is the CMD for stars selected to be within 2 R_s of the galaxy center. Mean errors as a function of magnitude are shown, and the TRGB is indicated with the red arrow. The upper small panel is the luminosity function for the RGB, and the lower small panel is the resulting distribution of the measured position of the TRGB (see text for details). The grey shaded region in the upper panel indicates the range shown the lower panel. Here, the red solid line indicates the median value and the dashed lines show a 16% and 84% quartile range (approximating 1σ).

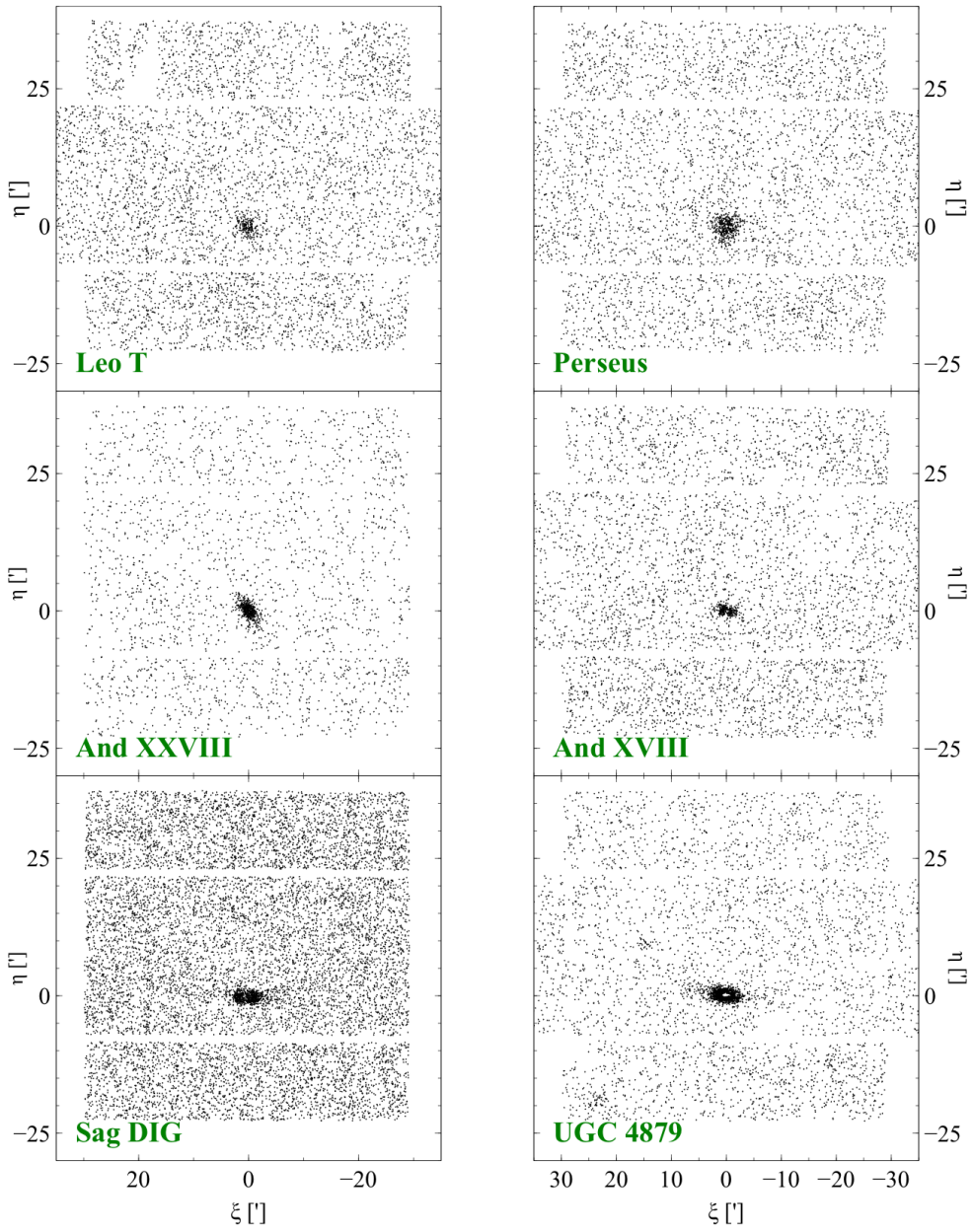

Figure 3.10: Spatial distribution of RGB stars for 6 of the dwarfs in the Local Group subset over the entire MegaCam field of view. The remaining dwarfs are shown in Figure 3.11.

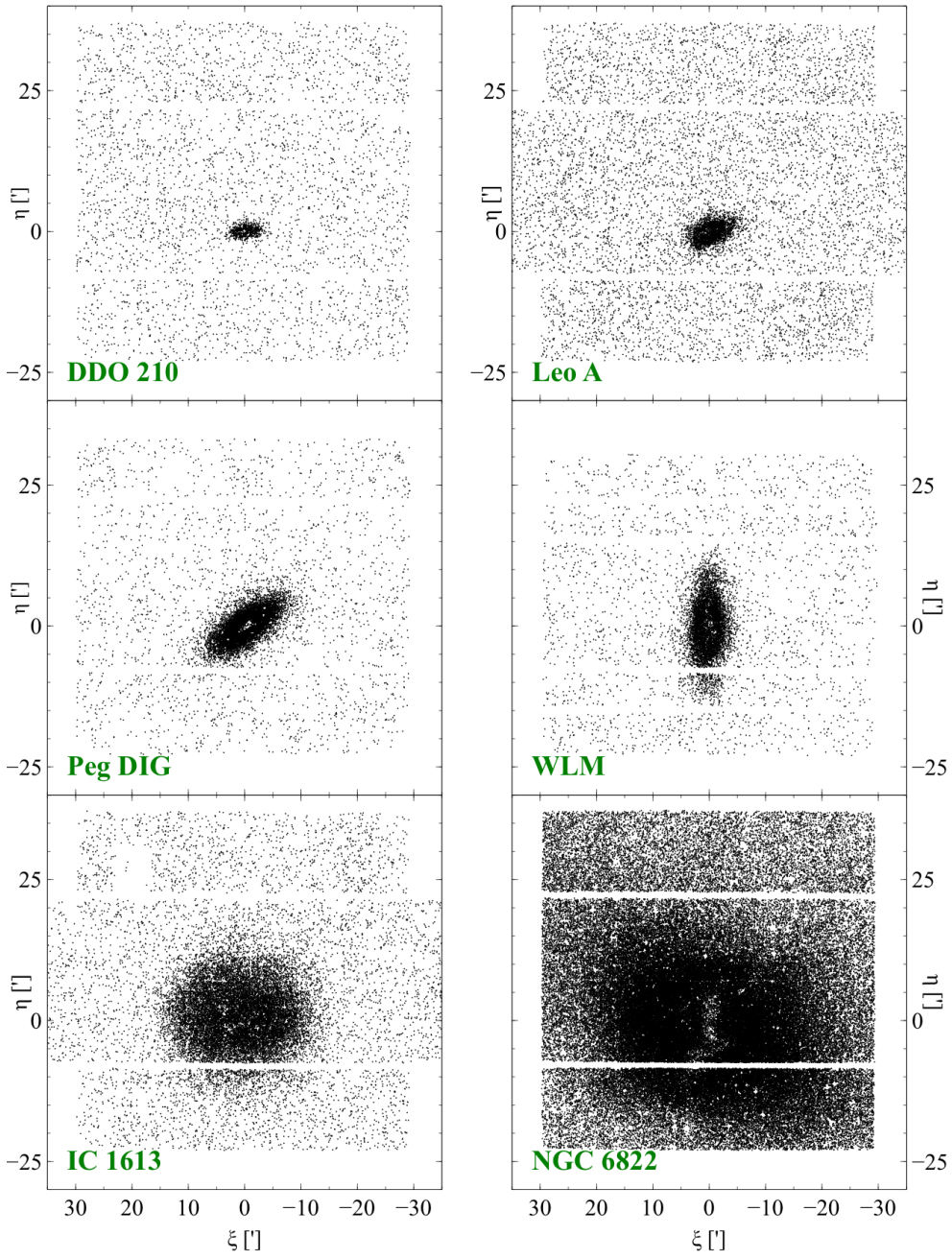

Figure 3.11: Spatial distribution of RGB stars for 6 of the dwarfs in the Local Group subset over the entire MegaCam field of view. The other dwarfs are shown in Figure 3.10.

Irwin (2006), the position angle (P.A.) and ellipticity (e) are given by:

$$P.A. = \frac{1}{2} arctan\left(\frac{2\sigma_{xy}}{\sigma_{yy} - \sigma_{xx}}\right) \tag{3.1}$$

$$e = \frac{\sqrt{(\sigma_{xx} - \sigma_{yy})^2 + \sigma_{xy}^2}}{\sigma_{yy} + \sigma_{xx}} \tag{3.2}$$

where σ_{xx}, σ_{xy}, and σ_{yy} are the intensity weighted second moments. These moments are given by:

$$\sigma_{xx} = \frac{\sum_i (x_i - X)^2 I_i}{I_{tot}} \tag{3.3}$$

$$\sigma_{yy} = \frac{\sum_i (y_i - Y)^2 I_i}{I_{tot}} \tag{3.4}$$

$$\sigma_{xy} = \frac{\sum_i (x_i - X)(y_i - Y) I_i}{I_{tot}} \tag{3.5}$$

where (X, Y) is the center of the galaxy, and (x_i, y_i) is the location of the i^{th} pixel with intensity I_i.

Starting with a circular aperture, the P.A., e, and center are determined as a function of radius, in 0.5' steps, using these relationships. The analysis is then repeated, but this time only using those pixels that are contained within an ellipse with the newly derived P.A. and e. This process is repeated until the values converge.

The resulting position angle and ellipticity profiles are shown as a function of semi major axis radius (SMA) in the side panels of Figures 3.12 and 3.13. These profiles are fairly regularly behaved in the uncrowded regions of the galaxy (indicated by the unshaded regions in Figures 3.12 and 3.13) for all but the faintest galaxies. A single P.A and e is adopted for each galaxy by determining the values between R_s and 3 $\times R_s$ for use the the following analysis. We include the standard deviation within this range as uncertainties on these quantities.

Radial profiles based on star counts alone are determined using the median values for the P.A., ellipticity and center. When computing the radial profile, a mask is used to ignore areas of our field with chip gaps, edge regions, and areas where detection of stars was not possible due to the presence of highly saturated foreground stars.

In all cases except NGC 6822, the profile is background subtracted using the background values estimated previously, generally using the area beyond $5R_s$. The

appropriate multiplicative factor for R_s, however, is estimated in the next section. In practice, this resulted in an iterative process, whereby we adopted an initial value for R_s to estimate the background, and then derived a new value of R_s based on the resulting profile. The entire process was repeated and continued until convergence. The final radial profiles based on star counts alone are shown in Figure 3.14. These radial profiles clearly extend to larger radii that the integrated light profiles shown in Figure 3.6. The impacts of crowding and the resulting incompleteness of the stellar catalogues is apparent at small radii, most strongly for the more massive dwarfs (for example, WLM very clearly shows this feature). In the case of NGC 6822, the dwarf dominates over background sources across the entire image so no background is subtracted. The resulting R_s is still robustly measured.

3.5 Dwarf galaxy profiles

3.5.1 Profile fitting

Extended radial profiles are now generated using the RGB stellar density profiles as tracers of the outskirts of the galaxies and the integrated light profiles as tracers of the inner regions of the galaxy. A significant assumption behind this approach is that the integrated light and the RGB stars trace the same populations. This is clearly incorrect in detail. However, it is a reasonable and necessary assumption to connect the outer stellar profile to the inner integrated light region. The systematic effects are limited by matching the $i-$band profile to the RGB stars, since younger stars contribute more heavily to bluer bands. For some of the smaller dwarfs – And XXVIII, Leo T and Perseus – the dwarf does not appear in the $i-$band via integrate light and we can only detect the integrated light in the $g-$band. For these dwarfs, we instead match the stellar density profiles in the $g-$band and adjust them to the $i-$band using the median colour of the RGB from the CMD for these dwarfs.

The RGB stellar density profiles, measured in stars per unit area (derived in Section 3.4.2) are matched with the integrated light profiles, measured in flux per unit area (as derived in Section 3.3) by determining the appropriate scaling factor, γ_{rgb}. This factor is a multiplicative term that includes a factor due to the difference in units as well as containing information on the contribution of the RGB stars to the total integrated light of the galaxy. We fit γ_{rgb} as an unknown parameter alongside the parameters for a Sérsic function (e.g. Graham & Driver 2005):

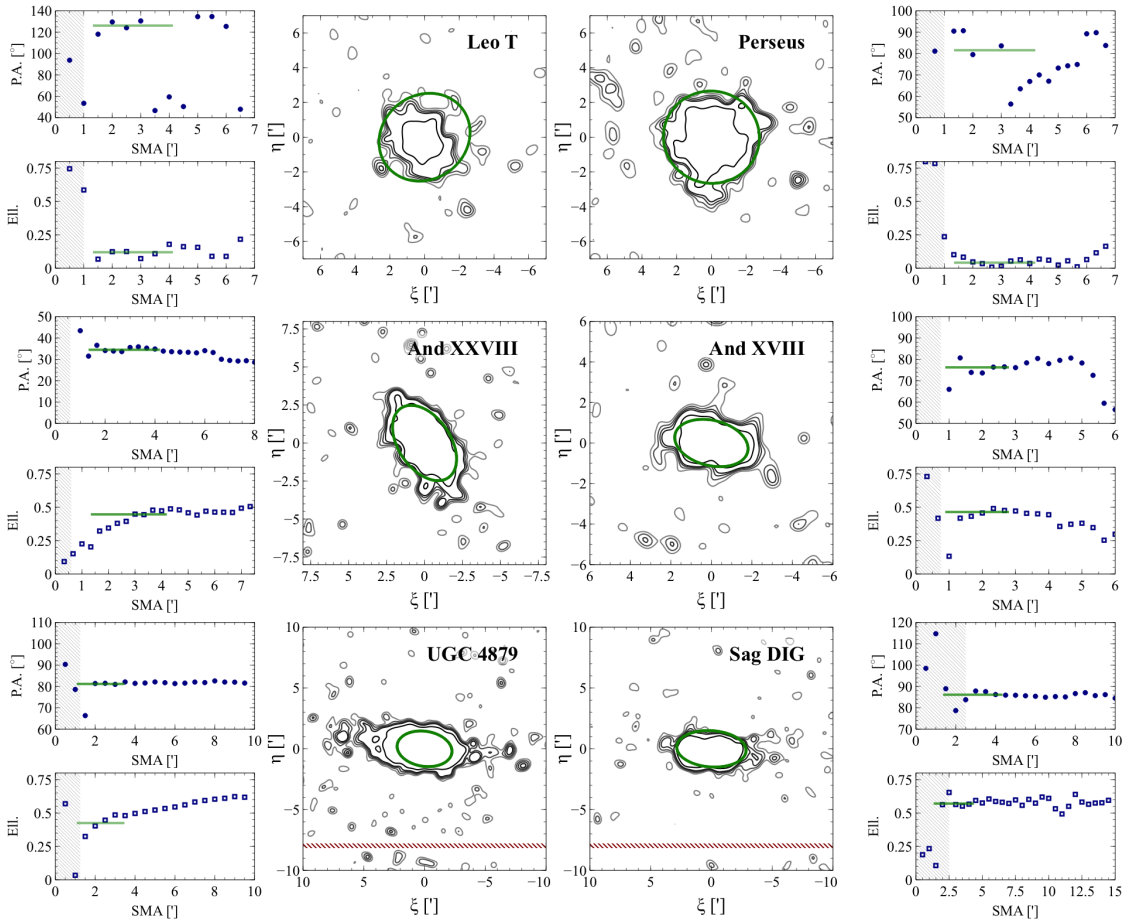

Figure 3.12: For each dwarf, the upper and lower small panels show the position angle (P.A.) and ellipticity (Ell.) as a function of radius semi-major axis (SMA). The green line indicates the adopted median from 1–3 R_s. The large panel shows a zoomed-in region showing RGB stars in contours. Contours of RGB stars are at 2, 3, 4, 5, 10, 25 σ about the estimated background. An ellipse (green) is shown with the median position angle and ellipticity with a semi-major axis of $2R_s$. The grey shaded regions show the radii at which crowding is known to be significant, as shown in Figure 3.14. The red dash regions show the locations of the large chip gaps in the detector.

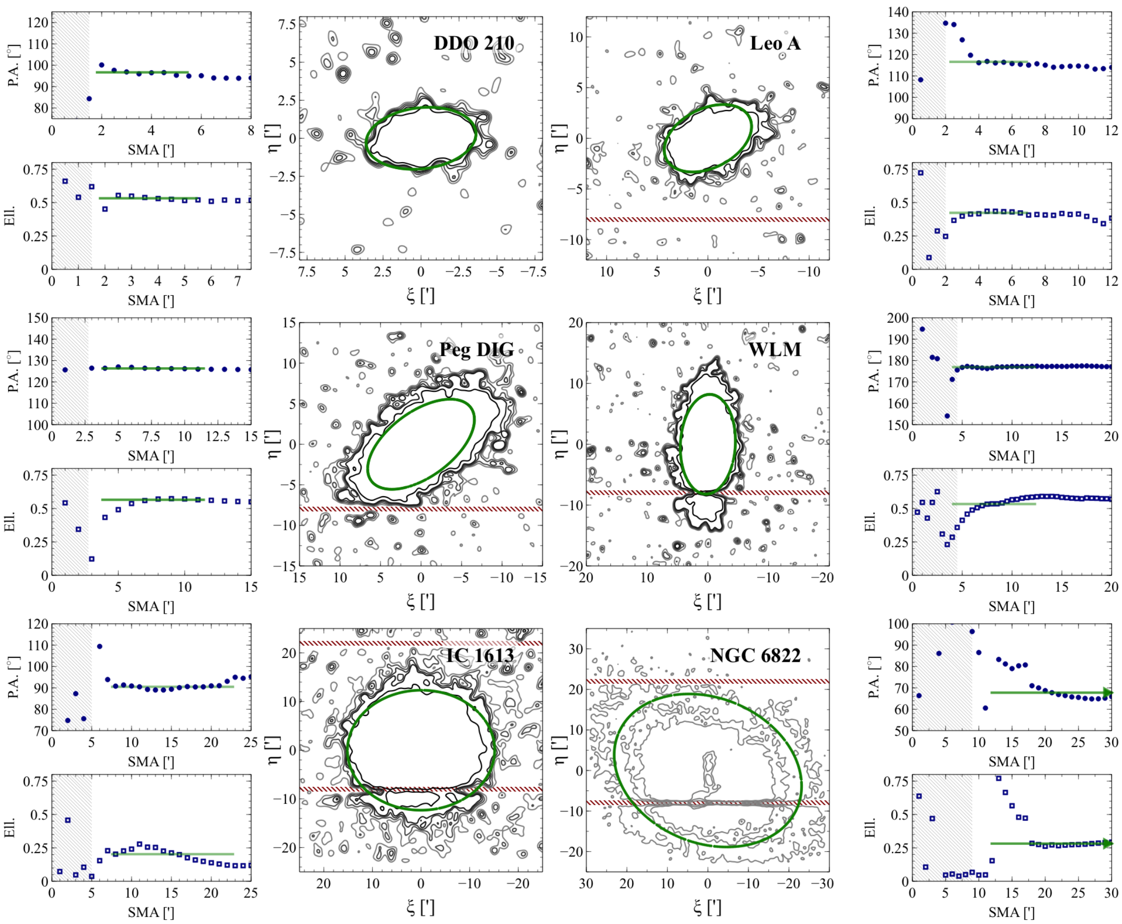

Figure 3.13: The same as Figure 3.12. For each dwarf, the upper and lower small panels show the position angle (P.A.) and ellipticity (Ell.) as a function of radius semi-major axis (SMA). The green line indicates the adopted median from 1–3 R_s. The large panel shows a zoomed-in region showing RGB stars in contours. Contours of RGB stars are at 2, 3, 4, 5, 10, 25 σ about the estimated background. NGC 6822 is dominated across the full field by RGB stars so contours shown are at 10%, 20% and 30% of the maximum stellar density. An ellipse (green) is shown with the median position angle and ellipticity with a semi-major axis of $2R_s$. The grey shaded regions show the radii at which crowding is known to be significant, as shown in Figure 3.14. The red dash regions show the locations of the large chip gaps in the detector.

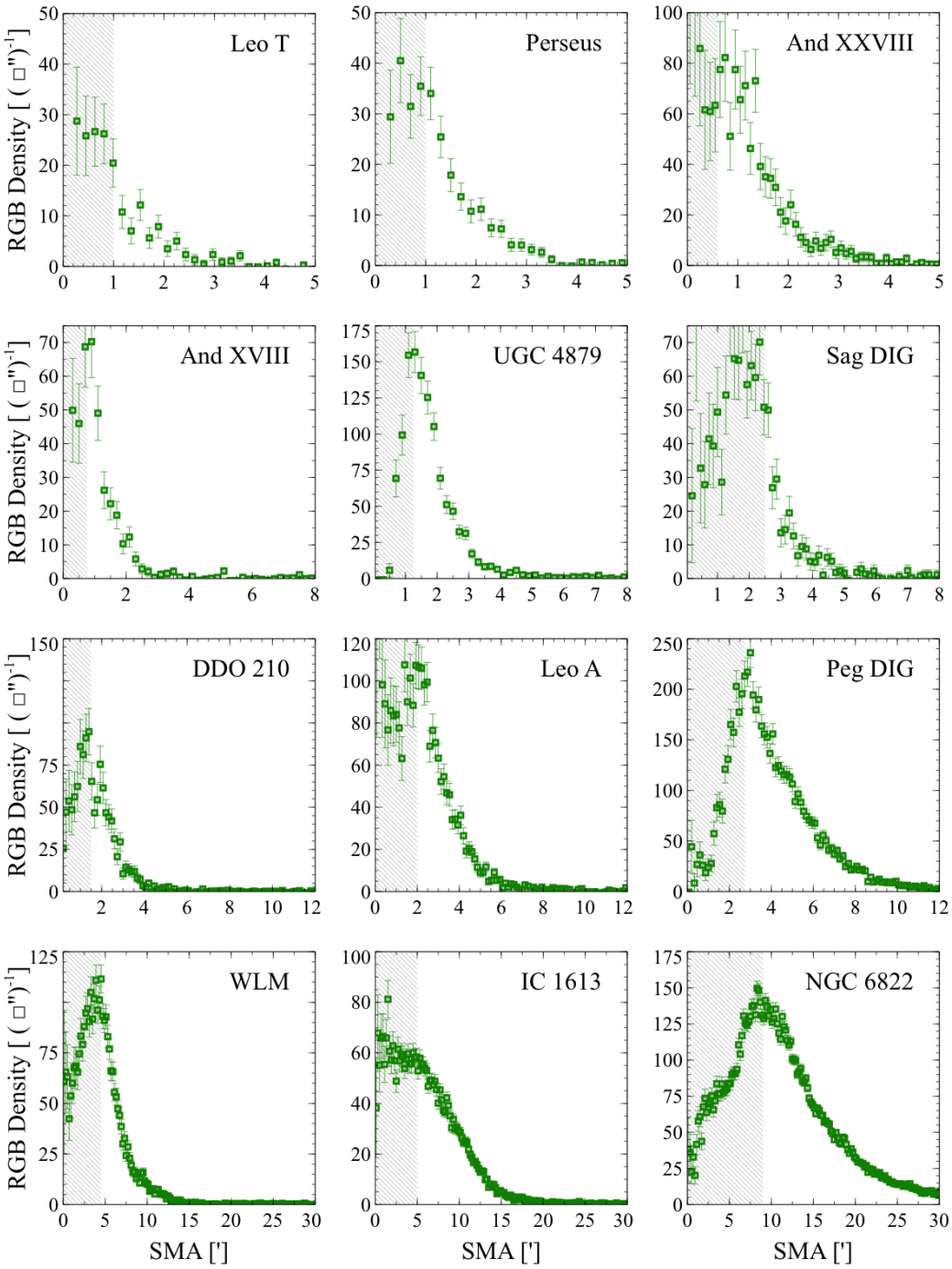

Figure 3.14: RGB stellar density profiles for each dwarf as a function of semi-major axis (SMA). The grey shaded region indicates where crowding is significant, and were excluded from our analysis.

$$I(r) = I_e exp\left(-b_n\left[\left(\frac{r}{R_s}\right)^{\frac{1}{n}} - 1\right]\right) \text{ where } b_n = 1.9992n - 0.3271 \qquad (3.6)$$

I_e is the intensity at the effective (Sérsic) radius (R_s), and n is the Sérsic index, which relates to the concentration of the galaxy. We use *emcee* (Foreman-Mackey et al., 2013) to determine the most probable values of all these unknown parameters, and this allows us to explore any degeneracy between the structural parameters and the γ_{rgb}. The resulting radial profiles are shown in Figure 3.15 and overlaid are the best-fit Sérsic functions.

3.5.2 Two component models

Each radial profile is also fit with the sum of two Sérsic profiles (again including γ_{rgb} as a free parameter) to explore any evidence for more than one component in any of these galaxies. Both Bayesian and Akaike Information Criteria (BIC, AIC, respectively; Kass & Raftery 1995) are computed to determine whether the extra parameters in the multi-component model are statistically warranted. Specifically, we compute these parameters for both the single and double-component profiles, and look at the difference. Models with lower BIC and AIC values are formally preferred, and the specific difference between the two sets of values indicates to what degree the model is preferred. These two criteria differ in how goodness-of-fit is weighted verses the number of parameters. Broadly speaking, the AIC is likely to favour models which fit well even if there are more parameters, and the BIC is likely to favour simpler models that fit less well.

Comparison of the AIC and BIC values for each dwarf for the single- and double-component models indicate that most dwarfs are clearly more suitably described by single component models. UGC 4879, DDO 210 and WLM are exceptions for which the preferred model is less clear. Figure 3.16 shows the two-component Sérsic fits for each of these systems. Also shown are the values of $\Delta(BIC) = BIC_1 - BIC_2$ and $\Delta(AIC) = AIC_1 - AIC_2$ for each galaxy, where the subscript refers to the number of components fit.

For the BIC statistic, a difference in values less than around 2 does not imply any significant preference between models, whereas differences of order 2 – 5 are indicative of moderate preference for the model with the lower BIC value. For the AIC statistic, the exponential of half of the difference in values is broadly proportional

to the probability that the model with the lower AIC value minimises the information loss. In our case, this implies that, for UGC 4879, the one component model is a factor of $\exp(-6.3/2) = 0.04$ more likely than the two component model to minimise the information loss (i.e., the two component model is significantly preferred); for DDO 210 and WLM, the corresponding numbers are 5.5×10^{-3} and 1.7×10^{-3}.

Interpretation of these results requires some caution. In particular, stellar population gradients could have a very strong effect on these profiles, because of our necessary reliance on integrated light studies for the central regions. Inspection of the CMDs of these galaxies in Figures 3.8 and 3.9 shows that young stars are present in these galaxies, and appear especially strong in the magnitude range of our observations in WLM and DDO 210. Indeed, the differences in the radial gradients of young blue stars and RGB stars has been measured by McConnachie et al. (2006), Leaman et al. (2012) and Jacobs et al. (2011) for DDO 210, WLM and UGC 4879, respectively. Thus, it is quite possible that the preference for two components in our analysis for these galaxies is a result of these differences in the spatial distribution of the stellar populations, although we note that the very few bright blue stars in our CMD for UGC 4879 suggest other factors potentially at play. Indeed, it has previously been argued (Bellazzini et al. 2011b) that UGC 4879 may host a disk-like component because of the "wings" that are visible in the 2D surface brightness map (see Figure 3.12). We will discuss this feature in more detail in Section 6.

3.5.3 Derived structural parameters

For each galaxy, Table 3.2 lists our derived positional and shape parameters, specifically: RA, Dec (from McConnachie 2012), distance modulus, distance, position angle, ellipticity, as well as offsets of the center of the RGB stellar distribution from the adopted centers.

Table 3.3 lists the fitted Sérsic parameters for each dwarf, specifically μ_e, R_s, n, as well as the adopted background density of RGB stars. Also included are the best fit parameters for the two component Sérsic profiles for DDO 210, UGC 4879 and WLM.

Table 3.4 shows derived parameters from the Sérsic fits following Graham & Driver (2005): μ_o is the central surface brightness, $\langle\mu\rangle_e$ is the mean surface brightness inside the effective radius, m_{tot} is the apparent total magnitude, and M_{tot} is the absolute magnitude using the distance modulus given in Table 3.2.

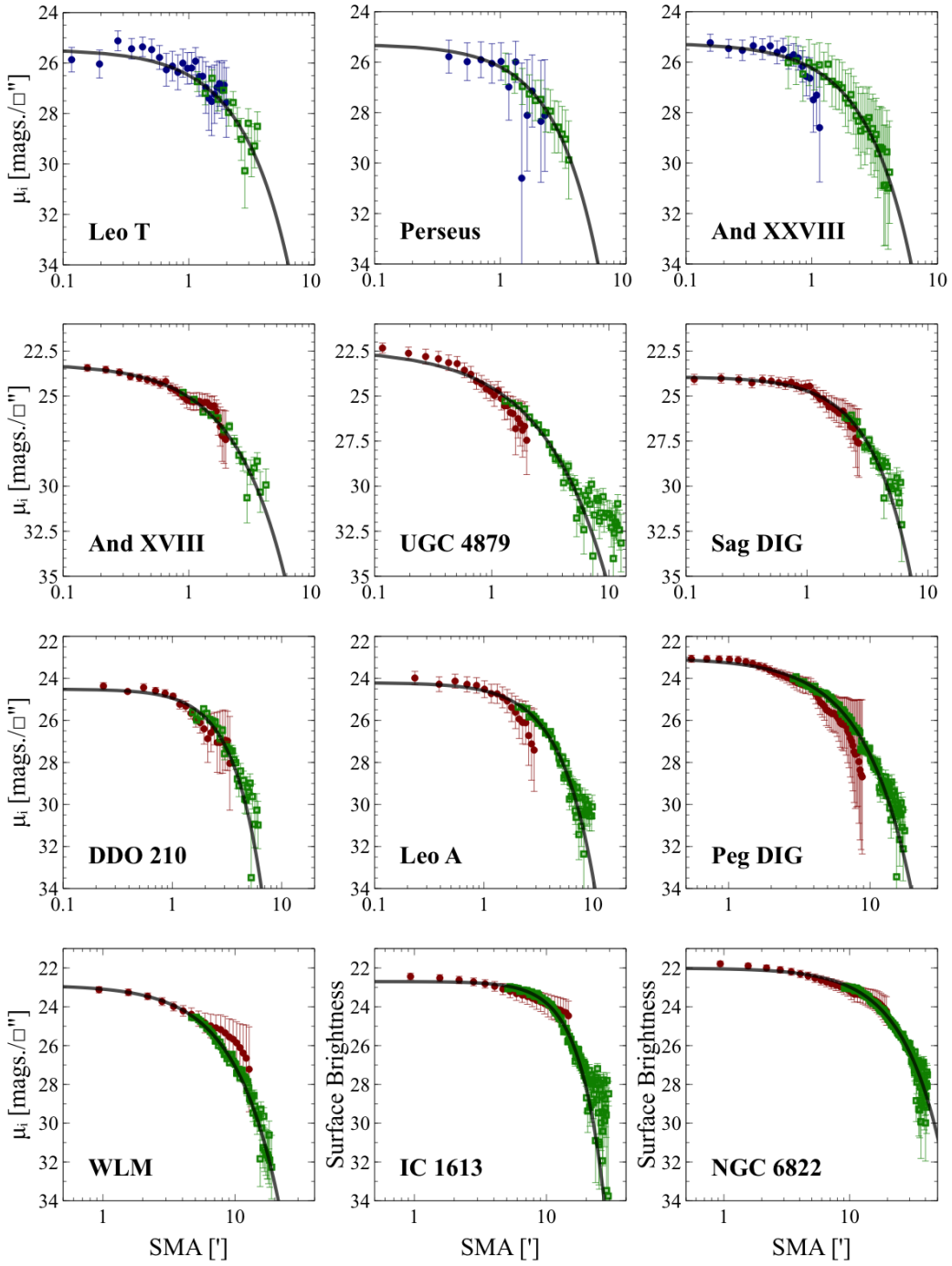

Figure 3.15: Combined radial profiles using integrated light (red circles) and star counts (green open squares) as a function of radius semi-major axis (SMA), for each galaxy. Overlaid are the best-fit Sérsic profiles (black line). For Leo T, Perseus, and And XXVIII no integrated light is detected in the $i-$band so the profile is matched to the integrated $g-$band profile and then corrected with the median colour (in the panels above, blue is adjusted $g-$band, red is $i-$band).

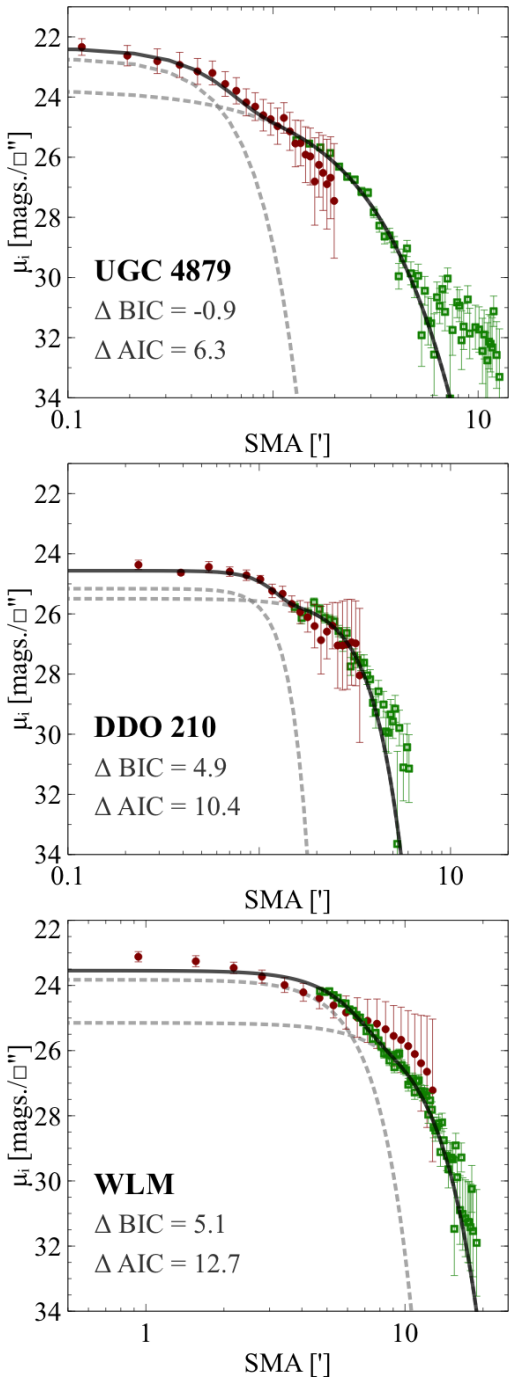

Figure 3.16: Combined radial profiles using integrated light (red circles) and star counts (green open squares) as a function of radius semi-major axis (SMA) for those galaxies for which there is some evidence of 2 components. Overlaid as solid lines are the best-fitting two component Sérsic profiles (black line), with the individual components shown as dashed grey lines. Also indicated are the AIC and BIC for each galaxy.

Table 3.2: Derived positional and shape information for each dwarf galaxy. RA and Dec. for each galaxy are taken from McConnachie (2012).

Name	RA	Dec.	$(m-M)_o$	Distance [kpc]	*P.A.* [°]	e	Δx [']	Δy [']
Leo T	$09^h34^m53.4^s$	+17°03′05”	23.08±0.08	413±15	121.13±34.66	0.12±0.08	-0.22±0.06	0.20±0.04
Perseus	$03^h01^m22.8^s$	+40°59′17”	24.18±0.11	686±34	81.56±21.43	0.04±0.08	0.07±0.01	0.18±0.02
And XXVIII	$22^h32^m41.2^s$	+31°12′58”	24.44±0.04	772±16	35.04±0.97	0.42±0.06	0.00±0.01	-0.07±0.02
And XVIII	$00^h02^m14.5^s$	+45°05′20”	25.36±0.08	1178±43	75.12±4.47	0.44±0.12	-0.01±0.17	-0.07±0.06
UGC 4879	$09^h16^m02.2^s$	+52°50′24”	25.42±0.06	1213±33	81.19±6.47	0.43±0.06	-0.23±0.02	-0.07±0.02
Sag DIG	$19^h29^m59.0^s$	−17°40′51”	25.39±0.08	1198±47	86.91±3.44	0.56±0.18	-0.17±0.38	0.35±0.05
DDO 210	$20^h46^m51.8^s$	−12°50′53”	24.97±0.09	988±43	96.58±1.44	0.53±0.05	0.25±0.09	-0.04±0.01
Leo A	$09^h59^m26.5^s$	+30°44′47”	24.28±0.05	717±17	116.40±6.11	0.42±0.05	0.49±0.18	0.12±0.10
Peg DIG	$23^h28^m36.3^s$	+14°44′35”	24.77±0.04	898±19	126.30±0.34	0.56±0.05	0.20±0.09	0.12±0.04
WLM	$00^h01^m58.2^s$	−15°27′39”	24.85±0.05	934±21	177.02±0.50	0.54±0.06	-0.17±0.01	0.05±0.10
IC 1613	$01^h04^m47.8^s$	+02°07′04”	24.18±0.06	686±19	90.49±1.02	0.20±0.05	-0.71±0.27	-0.90±0.19
NGC 6822	$19^h44^m56.6^s$	−14°47′21”	23.78±0.05	570±12	66.88±14.93	0.28±0.15	-0.60±1.60	1.08±0.80

Table 3.3: Best-fit Sérsic parameters for each dwarf, in addition to the adopted background density of RGB stars. Note that μ_e is the equivalent of I_e given in magnitudes. The two component fits (a sum of two Sérsic functions) are given for those dwarfs for which such a model appears plausible as discussed in the text.

Name		μ_e [mags/sq.arcsec]	R_s [']	n	C [RGB stars/sq.arcmin^{-1}]
Leo T		26.75 ± 0.26	1.39 ± 0.20	0.86 ± 0.36	1.43 ± 0.02
Perseus		26.96 ± 0.32	1.38 ± 0.19	0.79 ± 0.63	1.14 ± 0.02
And XXVIII		26.70 ± 0.36	1.38 ± 0.06	0.84 ± 0.13	0.64 ± 0.02
And XVIII		24.91 ± 0.09	0.92 ± 0.05	0.95 ± 0.10	1.16 ± 0.02
UGC 4879*		24.77 ± 0.16	1.13 ± 0.10	1.28 ± 0.17	0.88 ± 0.02
Sag DIG		25.19 ± 0.09	1.43 ± 0.08	0.75 ± 0.07	3.39 ± 0.04
DDO 210*		25.48 ± 0.07	1.63 ± 0.06	0.61 ± 0.05	0.99 ± 0.02
Leo A		25.42 ± 0.13	2.30 ± 0.09	0.72 ± 0.07	1.89 ± 0.03
Peg DIG		24.36 ± 0.05	3.81 ± 0.05	0.77 ± 0.03	0.64 ± 0.03
WLM*		24.20 ± 0.07	4.10 ± 0.13	0.77 ± 0.04	0.72 ± 0.02
IC 1613		23.29 ± 0.07	7.57 ± 0.05	0.43 ± 0.02	1.36 ± 0.03
NGC 6822		23.25 ± 0.05	11.95 ± 0.07	0.73 ± 0.02	–
UGC 4879	Inner	23.32 ± 0.33	0.36 ± 0.09	0.45 ± 0.20	0.88 ± 0.02
	Outer	25.37 ± 0.25	1.36 ± 0.10	0.91 ± 0.15	0.88 ± 0.02
DDO 210	Inner	25.26 ± 0.17	0.69 ± 0.08	0.22 ± 0.05	0.99 ± 0.02
	Outer	25.93 ± 0.15	1.68 ± 0.06	0.37 ± 0.05	0.99 ± 0.02
WLM	Inner	24.12 ± 0.12	3.66 ± 0.19	0.30 ± 0.06	0.72 ± 0.02
	Outer	25.56 ± 0.23	6.35 ± 0.38	0.36 ± 0.07	0.72 ± 0.02

Table 3.4: Derived parameters for each dwarf, following the relationships given in Graham & Driver (2005), $\mu_{i,o}$ is the central surface brightness in the i-band, $\langle\mu\rangle_{i,e}$ is the mean surface brightness inside the effective radius in the i-band, $m_{i,tot}$ is the total apparent magnitude in the i-band, $(g-i)$ is the median colour, and $M_{i,tot}$ is the absolute i-band magnitude.

Name	$\mu_{i,o}$	$\langle\mu\rangle_{i,e}$	$m_{i,tot}$	$(g-i)$	$M_{i,tot}$
Leo T	25.24 ± 0.82	26.14 ± 0.33	14.69 ± 0.34	0.61 ± 0.24	-8.39
Perseus	25.6 ± 1.4	26.39 ± 0.61	14.9 ± 0.62	1.13 ± 0.43	-9.28
And XXVIII	25.23 ± 0.46	26.08 ± 0.37	15.1 ± 0.38	0.68 ± 0.32	-9.34
And XVIII	23.2 ± 0.23	24.24 ± 0.10	14.17 ± 0.28	0.91 ± 0.12	-11.19
UGC 4879	22.35 ± 0.4	23.96 ± 0.17	13.42 ± 0.21	0.97 ± 0.36	-12.0
Sag DIG	23.92 ± 0.18	24.62 ± 0.1	13.85 ± 0.56	0.52 ± 0.33	-11.54
DDO 210	24.51 ± 0.13	25.0 ± 0.08	13.87 ± 0.14	0.60 ± 0.73	-11.1
Leo A	24.21 ± 0.20	24.87 ± 0.14	12.77 ± 0.17	-0.15 ± 0.07	-11.51
Peg DIG	23.04 ± 0.08	23.78 ± 0.05	10.88 ± 0.14	0.84 ± 0.28	-13.89
WLM	22.88 ± 0.11	23.62 ± 0.07	10.51 ± 0.17	-0.16 ± 0.26	-14.34
IC 1613	22.71 ± 0.08	22.93 ± 0.07	7.9 ± 0.1	1.47 ± 0.27	-16.28
NGC 6822	22.02 ± 0.07	22.69 ± 0.05	6.79 ± 0.26	1.38 ± 0.26	-16.99

3.6 Discussion

3.6.1 Structures and substructures

Together, the 2D and 1D surface brightness profiles presented in Figures 3.12, 3.13, 3.15 and 3.16 provide considerable information on the extended structures of all these isolated galaxies. Figures 3.12 and 3.13 show that nearly all of the galaxies have a relatively regular appearance, essentially appearing as large spheroids with no evidence of large scale asymmetries like tidal tails. For almost all of the dwarfs, the best-fitting Sérsic profile to the RGB distribution yields $n \sim 0.7$, i.e., the stellar distribution falls off more slowly than an exponential. This is fairly typical of many dwarf galaxies (e.g. Ferrarese et al. 2006; Gerbrandt et al. 2015; Muñoz et al. 2018b).

An exception to both of the above generalisations is UGC 4879. Here, the stellar distribution falls off faster than an exponential ($n \simeq 1.3$), and the galaxy does present evidence of extended "wings" along its major axis. This latter feature has previously been interpreted as an edge-on disk. The tentative evidence of two components in Figure 3.16 also suggests that a multi-component interpretation could be correct for this galaxy, where both components are dominated by old stars (potentially in contrast to DDO 210 and WLM; see discussion for WLM below). The extreme isolation of this system makes it extremely unlikely that such signatures are the results of a tidal interaction with a more massive galaxy (M 31 or the MW). However, it is possible that this type of structure - especially the surface brightness map - could also be the result of a merger in this galaxy. Numerous observational studies in recent years (e.g., Martínez-Delgado et al. 2012; Paudel et al. 2017; Zhang et al. 2020) - including in the Local Group (e.g., Nidever et al. 2013; Amorisco et al. 2014)- suggest that dwarf-dwarf mergers are not uncommon. In addition to UGC 4879, Sag DIG also has some evidence of a weak extension in its outer isophotes on the eastern end of its major axis (also discussed in Paper I).

Beyond the more distinct "wings" of UGC 4879 and perhaps Sag DIG, the outskirts of several dwarfs are not ideally characterized by the Sérsic fit (e.g. DDO 210, Leo A, IC 1613). In these cases, an excess of stars is found in the outskirts, rather than a deficit. Irwin & Hatzidimitriou 1995 discuss these "extra-tidal" stars extensively in the context of Milky Way dwarf spheroidals, whether these stars are being stripped or are evidence that the system is not in dynamic equilibrium. For Solo dwarfs, the likelihood of tidal interactions is reduced (though not eliminated) by

their isolation. Interestingly, the excess of stars found in UGC 4879 at large radius persists in both the single and two component fits.

Wheeler et al. (2015) suggest that dwarf galaxies such as the Solo dwarfs could well host satellites within around 50 kpc of the main dwarfs. Dooley et al. (2017) take this further and explicitly calculate the probability of there being a satellite found around each of the Solo dwarfs within the approximate observational footprint for each of our fields (see their Table 3). For reference, our MegaCam field reaches out to about 0.5 degrees from the centers of each galaxy; for the closest galaxy (Leo T) this corresponds to a maximum (projected) radius of around 3.5 kpc; for the most distant galaxy (UGC 4879), this corresponds to around 10 kpc. Dooley et al. (2017) predict that And XVII, And XXVIII, Sag DIG, Peg DIG and Leo A all have around a 10% chance of having a satellite in this region, and WLM, IC 1613 and UGC 4879 all have around a 10 – 20% chance of having a satellite in this region. Notably, NGC 6822, as one of the most massive dwarfs, has a relatively low probability due to the relatively small radius out to which we probe it.

No definite evidence of satellites or other concentrated substructures are found around any of the galaxies to our surface brightness limits (around 30 – 32 mags sq.arcsec), as inspection of Figures 3.12 and 3.13 makes clear. Candidate features were examined and found to be consistent with fluctuations (statistical or due to irregular features e.g., holes due to bright foreground stars) in the background. The feature in the isophotes around Perseus at ($\xi \simeq -5', \eta \simeq -2.5'$) is tentatively a possible substructure and is discussed in more detail in Section 5.2. Further, the OPTICS clustering algorithm (Ankerst et al. 1999; see its application to a similar dataset in McConnachie et al. 2018) was also applied to the RGB dataset, and no additional significant features were found. We note that this is relatively unsurprising, given that the probabilities given by Dooley et al. (2017) are not large for any single object. Further, we note that these probabilities correspond to satellites with stellar masses as low as $10^4\,M_\odot$. At this limit, detection would be very hard given the data in hand; the lowest stellar mass satellites identified in PAndAS (which used the same instrument, same bands and broadly similar exposure times) were of order $10^{4.2}\,M_\odot$, although most were $> 10^{4.5}\,M_\odot$ (see discussion in Martin et al. 2016). Examination of the numbers in Table 3 of Dooley et al. 2017 suggests that the probability of discovering new satellites around some of the more distant, more massive galaxies in the rest of the Solo dataset remains good.

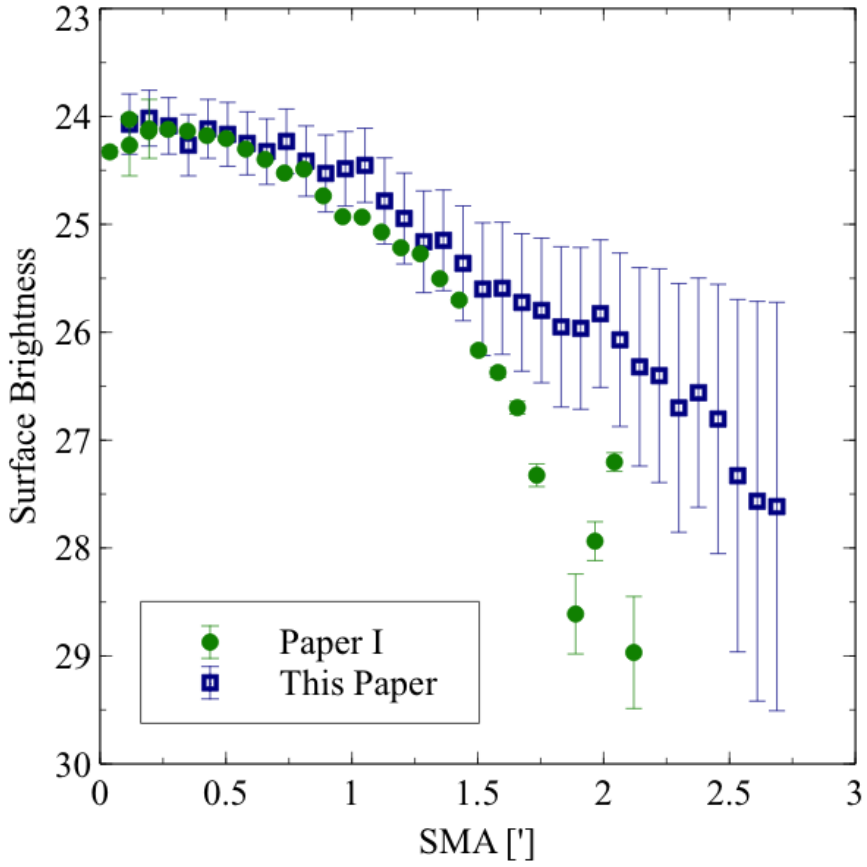

Figure 3.17: Comparison of the (background-subtracted) $i-$band integrated light profiles as a function of radius semi-major axis (SMA) for Sag DIG, derived in this chapter (blue open squares) and in Higgs et al. (2016) (green circles). More robust masking of foreground sources in the current work leads to a more extended surface brightness profile. See text for details.

3.6.2 Specific case studies

Here we present a closer look at our results for three galaxies included in our sample - Sag DIG, WLM and DDO 210 - and use these as case studies to highlight aspects of our approach, interpretation of results, and comparison to previous studies. In particular, Sag DIG was already analysed in Higgs et al. (2016); WLM is a large and very well studied galaxy; DDO 210 has previously been studied with similar observations and methods and is at the faint end of our sample.

Sag DIG

While Sag DIG was extensively studied in Higgs et al. (2016), there are a few important differences between the methodology applied in Paper I and in this current work. The integrated light and resolved RGB profiles were matched in Paper I by matching them "by eye" in the overlapping regions. Archival HST observations were used in order in straddle the region between the resolved stars and integrated light from the CFHT data. However, appropriate HST observations are not available for all targets, and so this method was not used in this current paper. Instead, we make the scaling parameter a free parameter and employ *emcee* to obtain the best fits and explore correlations between parameters.

Critically, the current work takes a more rigorous approach to dealing with the background in the integrated light analysis of the dwarf. In Paper I, masking was applied to all pixels that fell above a certain threshold of counts. In the current work, a threshold is still applied, but also pixels in the neighbourhood of these "hot" pixels are also masked, in order to suppress the effect of halos around bright stars and similar effects. This change in strategy has a significant effect for a galaxy like Sag DIG that is situated at relatively low Galactic latitude, and hence is impacted heavily by (bright) Milky Way foreground stars. In the CMD in Figure 3.8, this foreground is prominent, and even Galactic substructure due to the Sagittarius Stream can be seen.

Figure 3.17 shows the difference in the resulting integrated light profiles for Sag DIG. In particular, the more complete masking of bright sources in the current paper means that the overall background that is estimated for Sag DIG is smaller (by around 20 ADU, or just less than 1 % of the previous background value). This changes the shape of the outer profile considerably, such that the new analysis clearly favors a more extended surface brightness profile. Note also that the uncertainties are much larger in this new analysis, since we explicitly take into account the systematic variation in the background due to the irregular distribution of foreground sources, whereas this was not the case in Paper I. The net flow-down effect of this change in our analysis is considerable for Sag DIG ($R_s = 0.95 \pm 0.01$ in Paper I compared to $R_s = 1.43 \pm 0.08$ arcmins in the current analysis). This emphasises the challenge of integrated light studies of these faint systems, and the need for a homogeneous approach to the analysis.

Beccari et al. (2014) also present a wide and deep study of the resolved stellar

and HI structures of Sag DIG. The Sérsic radius derived from Beccari et al. (2014) is approximately 1.1'; no error bars are given on this measurement but it appears to be in reasonable agreement to that derived here. The TRGB distance estimate $(m-M)_o = 25.39 \pm 0.08$ agrees well with $(m-M)_o = 25.16 \pm 0.11$ from Beccari et al. (2014). Beccari et al. (2014) and Lee & Kim (2000) estimate the position angle to be 90°, which is in agreement with the value (measured East from North) found in this work ($87° \pm 3°$). Similarly the ellipticity from Beccari et al. (2014) and Lee & Kim (2000) is $e = 0.5$, which agrees with 0.56 ± 0.18 estimated here.

WLM

WLM (also known as DDO 221) is one of the more massive dwarfs in the Solo Survey. For comparison of the structural parameters, we focus on the detailed analysis from Leaman et al. (2012, 2013). This deep, wide field analysis also uses resolved RGB stars to study the older stellar populations in addition to including spectroscopy of 180 RGB stars. Leaman et al. (2012) derive the ellipticity and position angle of this dwarf by fitting ellipses using MPFITELLIPSE (Markwardt, 2009), finding $e = 0.55$ and $P.A. = 179°$. These values are in good agreement with $e = 0.54 \pm 0.06$ and $P.A. = 177° \pm 0.5°$ derived here. The ellipticity and position angle of WLM are well defined and do not vary significantly with radius.

The half light radius given for an exponential fit to the overall population in Leaman et al. (2012) is approximately $5.8 \pm 0.2'$, whereas the RGB-only profile has a corresponding radius of approximately $4.7'$; here, we find a slightly smaller half-light radius ($4.10' \pm 0.13'$). As discussed earlier, there is some evidence that the overall profile of WLM is best described by a two-component Sérsic model. We urge caution here, since it is unclear if this is due to the significant number of young stars in WLM, which certainly have a different spatial distribution to the RGB stars used to create the resolved star profile (see Leaman et al. 2012).

DDO 210

DDO 210 (Aquarius) is another well studied dwarf and, prior to the discovery of Leo T, was the smallest known galaxy with a significant gaseous component. We measure the TRGB at $(m-M)_o = 24.97 \pm 0.09$, in excellent agreement with Cole et al. (2014) who measured $(m-M)_o = 24.95 \pm 0.10$ and comparable to McConnachie et al. (2006) with $(m-M)_o = 25.15 \pm 0.08$. The position angle and ellipticity are derived

using the same method in McConnachie et al. (2006) and agree closely. McConnachie et al. (2006) found the ellipticity changed from 0.6 in the inner regions to 0.4 in the outskirts; again, this agrees closely with the current work where we find a median ellipticity of $e = 0.53 \pm 0.05$ and a very modest radial gradient.

McConnachie et al. (2006) demonstrate the complex structure of this galaxy in terms of the differences in the radial gradients of its different stellar populations, and the apparent disconnect between the spatial properties of the stars and HI distribution. Hermosa Muñoz et al. (2020) obtained spectroscopic measurements for 53 RGB stars and determine the axis of rotation for the stellar component to be $139^{\circ}{}^{+17^{\circ}}_{-27^{\circ}}$ in contrast with the HI rotation measured by Iorio et al. (2017) ($77.3^{\circ} \pm 15.2^{\circ}$). In our analysis, we find that this galaxy is possibly better described with a two component profile, but again it is hard to determine if this represents two "old" components, or whether it reflects the age segregation in the stellar populations noted by McConnachie et al. (2006).

3.6.3 Comparing the suite of parameters to the literature

We now compare the global set of parameters derived in this work to previously derived values, particularly the updated compilation of parameters from McConnachie (2012). Figure 3.18 shows the comparison for distance modulus ($(m - M)_o$), central surface brightness (μ_o), V-band magnitude (M_{tot}), ellipticity (e), position angle (P.A.), and half-light radius(R_s). For the central surface brightness and apparent magnitude, μ_o and m_{tot} values in Table 3.4 measured in the $i-$band were converted to their corresponding $g-$band values given the median $(g-i)$ values given in the same table. These values were then transformed to V band using $V = g - 0.098 - 0.544(g-i)$ (Thomas et al., 2021). Points with an "X" have literature values that are highly uncertain, and do not have quoted uncertainties. And XVIII does not have any previous value for its ellipticity or position angle (previous parameters were based on an image where the bulk of the object fell on a chip-gap).

It is worth emphasising that, to the best of our knowledge, some of these galaxies – especially NGC 6822, IC 1613 and Leo A – have not had detailed structural analyses conducted based on resolved stars in the modern era of CCD photometry. The integrated magnitudes of several of these galaxies date back to *The Third Reference Catalogue of Bright Galaxies* (de Vaucouleurs et al. 1991), and in fact the half-light radii quoted in McConnachie (2012) for these three galaxies are estimated by scaling

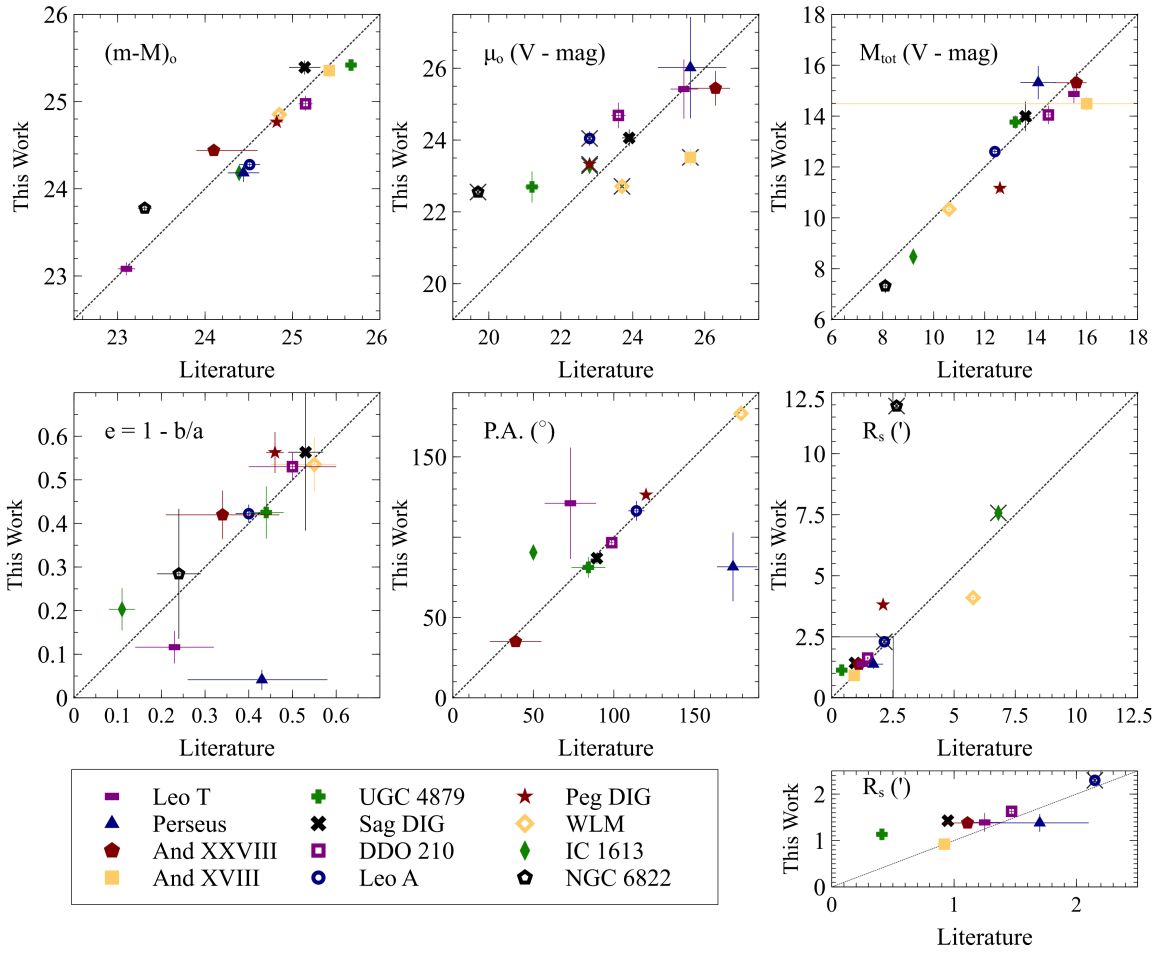

Figure 3.18: Comparison of various structural parameters derived in this paper compared to literature values, taken from the updated compilation in McConnachie (2012). The small panel shows a zoomed version of the R_s panel focused on small radii as indicated with the box. Points with a grey "X" do not have robust literature error estimates. (And XXVIII: Slater et al. 2011, IC 1613: Bernard et al. 2010; de Vaucouleurs et al. 1991, NGC 6822: Gieren et al. 2006; de Vaucouleurs et al. 1991; Dale et al. 2007, Peg DIG: McConnachie et al. 2005; de Vaucouleurs et al. 1991, Leo T: Irwin et al. 2007; de Jong et al. 2008; Muñoz et al. 2018b, WLM: McConnachie et al. 2005; de Vaucouleurs et al. 1991; Leaman et al. 2009, And XVIII:McConnachie et al. 2008; Conn et al. 2012, Leo A: Dolphin et al. 2002; Brown et al. 2007; de Vaucouleurs et al. 1991; Vansevičius et al. 2004; Cole et al. 2007, DDO 210: McConnachie et al. 2005, 2006, Sag DIG: Higgs et al. 2016, UGC 4879: Jacobs et al. 2011; Kopylov et al. 2008; Bellazzini et al. 2011b).

other scale-radii that are measured by de Vaucouleurs et al. (1991). It is clear from the lower right panel of Figure 3.18 that this scaling is distinctly inconsistent for NGC 6822.

Other notably deviant measurements include the central surface brightness of And XVIII, but this is relatively easily understood given that the earlier measurement was affected by an inconvenient chip-gap. Much more difficult to understand is the difference in ellipticity between our measurement of Perseus, which places the galaxy as nearly circular, compared to the measurement by Martin et al. (2013b), which records a notable ellipticity. Inspection of the raw star count map in Figure 3.10 does not suggest that the galaxy is notably elliptical, consistent with our findings, and we speculate that the higher quality photometry for the MegaCam data compared to the discovery PS1 photometry has allowed a cleaner sample of member stars to be selected (this galaxy is at $b \simeq -15$ degrees). Obviously, the poor agreement with the ellipticity measurement correlates with the poor agreement with the position angle measurement.

Generally, we see reasonable agreement between the bulk of our measurements and those from the literature. The only systematic difference that is obvious is that almost all of the effective radii that we derive are systematically larger than previous estimates. We suggest there are two primary factors that contribute. Firstly, some previous work has used observations with a smaller field of view. There is a non-trivial trend in the literature such that when viewing a galaxy out to larger radius, the galaxy is found to be larger than previously estimated. Secondly, and likely more important for the specific systems under study, there is a difference between the half-light radius of a galaxy, and a half-mass radius for any given tracer. Most Solo dwarfs are star forming, and so the central regions (and the light) are dominated by the younger, bluer brighter stars. However, our structural parameters are based on red giant branch stars, belonging to older stellar populations. It is often the case that older stellar populations are more extended than younger populations, and we stress that our results should be viewed as estimates of the older, halo-like populations of these dwarfs. The relative importance of these two factors (field of view verses half light/half mass) likely varies between dwarfs and the estimates used for comparisons. For example, Peg DIG and IC 1613 have a young stellar component (Weisz et al., 2014) and R_s in Figure 3.18 is from de Vaucouleurs et al. (1991) which is based on the integrated light. As a result, the difference between the mass weighted and light weighted profiles is likely the dominant factor. This could also be a factor for

some of the central surface brightness measurements (where integrated light studies will measure the flux density of all the stellar populations in the central regions, whereas our estimates are weighted towards the flux density due to older stellar populations). In contrast, structural parameters for And XVIII were previously based on observations in which the galaxy partially lies over a large chip gap in the MegaCam detector. Here, the differences seen in Figure 3.18 are likely largely due to the wider, more complete Solo observations. In addition, And XVIII has a predominately older SFH (as seen in Weisz et al. 2014), meaning the discrepancy between the mass and lighted weighted profiles is reduced.

3.7 Conclusions

The purpose of this chapter has been to determine a homogeneous set of structural parameters of isolated Local Group galaxies that is suitable for comparison with the well-studied Milky Way and M 31 satellite populations. The diversity of this population of dwarf galaxies leads to considerable complexity in generating a homogeneous dataset, but in general we find good agreement with previous studies. We have focused on their extended stellar structure and morphology and combined information from integrated light analysis of their inner regions with the resolved stellar populations of their outskirts, to parameterize their global structure to very faint surface brightness limits. Both the resolved stars and the integrated light require careful processing due to the intrinsically small and faint nature of these dwarfs. Careful consideration of background subtraction is necessary due to the significant impacts on the resulting structure, particularly on the extended structure. The differences found in the structure of Sag DIG between Paper I and this work highlight these effects. All 12 galaxies are reasonably well described by 1D Sérsic functions, and no prominent or convincing stellar substructures, that could be signs of either faint satellites or recent mergers, are identified in the outer regions of any of systems examined (with the possible exception of Perseus, studied in more detail in Section 5.2.

In Chapter 4, we will use these results in comparison to surveys of Local Group satellite populations to examine differences between the populations of nearby dwarfs that may be attributed to the role of environment.

Chapter 4

Comparing and contrasting satellite and isolated dwarf galaxies in the Local Group

This chapter is published as Higgs & McConnachie (2021). It is entirely my own work, analysis and writing. Some additional figures have been added for increased clarity.

I compare and contrast the stellar structures of isolated Local Group dwarf galaxies, as traced by their oldest stellar populations, with the satellite dwarf galaxies of the Milky Way and M 31. All Local Group dwarfs fainter than the Small Magellanic Cloud (SMC) with $M_v \leq -6$ and $\mu_o < 26.5\,\mathrm{mags\,arcsec^{-2}}$ are considered, taking advantage of measurements from surveys that use similar observations and analysis techniques. For the isolated dwarfs, we use the results from *So*litary *Lo*cal (Solo) Dwarf Galaxy Survey (Higgs et al. 2021; see results presented in Chapter 3). We begin by confirming that the structural and dynamical properties of the two satellite populations are not obviously statistically different from each other, but we note that there many more satellites around M 31 than around the Milky Way under equivalent magnitude and surface brightness limits. We find that dwarfs in close proximity to a massive galaxy generally show more scatter in their Kormendy relations than those in isolation. Specifically, isolated Local Group dwarf galaxies show a tighter trend of half-light radius versus magnitude than the satellite populations, and similar effects are also seen for related parameters. There appears to be a transition in the structural

and dynamical properties of the dwarf galaxy population around ~ 400 kpc from the Milky Way and M 31, such that the smallest, faintest, most circular dwarf galaxies are found closer than this separation. We discuss the impact of selection effects on our analysis, and we argue that our results point to the significance of tidal interactions on the population of systems within approximately 400 kpc from the MW and M 31.

4.1 Introduction

Dwarf galaxies are a product of both their external environment and internally-driven evolutionary processes. A massive galaxy in close proximity to a dwarf can have a significant influence on the latter's evolution, affecting properties such as its overall gas content, its star formation rate, and its global stellar structure. Within the Local Group, there is a unique opportunity to probe the faintest dwarfs, and to compare those that have evolved close to a large host galaxy to those which exist in isolation. Such an approach has the potential to try to disentangle the roles of nature and nurture at the extreme faint end of the galaxy luminosity function.

The results of this type of analysis to date have provided critical insights into the evolution of dwarf galaxies. There is a well known and long observed morphological transition in the Local Group from dwarf spheroidals (dSphs) to dwarf irregulars (dIrrs) with increasing distance from a massive galaxy (Einasto et al., 1974; Spekkens et al., 2014; Putman et al., 2021). The transition from star-forming dwarfs with HI gas (dIrrs) to passive dwarfs devoid of gas (dSphs) broadly aligns with the approximate virial radius of the Milky Way (MW) and the Andromeda galaxy (M 31). Possible mechanisms at play include ram pressure stripping and tidal stripping, which can remove gas (ram pressure and tides) or stars (tides) from the dwarfs. Interactions may trigger star formation, but gas may also be inhibited from being accreted into satellites (strangulation/starvation), ultimately preventing future star formation. In addition, the kinematics of the system may be affected on a global scale via a process like tidal stirring (e.g. Mayer et al. 2006; Kazantzidis et al. 2011; Łokas et al. 2012). Here, the interaction induces a bar instability in the disk of the dwarf that redistributes angular momentum and increases the degree of pressure support among the stars. This restructuring is considered necessary to convert rotationally supported systems into pressure supported systems. However, while it is true that gas in Local Group dIrrs is generally seen to rotate (e.g. LITTLE THINGS survey - Oh et al. 2015), recent analysis of the stellar kinematics of many low mass dIrrs in the Local Group suggest

that the degree of rotation in the old stellar populations is minimal or non-existent (e.g., Kirby et al. 2014 find only Peg DIG has a clearly rotating stellar component and NGC 6822, IC 1613, UGC 4879, Leo A, Cetus, and Aquarius do not). This suggests rotation plays a minimal role in stellar systems at the low mass end (e.g., Kaufmann et al. 2007).

With these considerations in mind, we started Solo Survey. The survey is introduced in (Higgs et al., 2016, hereafter Paper I), and in Chapter 2. It is designed to target only those nearby galaxies that are further than 300 kpc from either M 31 or the Milky Way, and within 3 Mpc. The 300 kpc limit was originally motivated by the expected size of the virial radii of these host dark matter halos (e.g., Klypin et al. 2002, Posti & Helmi 2019). Higgs et al. (2021) (hereafter Paper II) analyses the global stellar structure of the dozen isolated Local Group dwarf galaxies within our sample that are visible from the northern hemisphere, focusing on the old (red giant branch) stellar populations. These results are also available in Chapter 3.

Our original metric for isolation within the Solo sample was based upon the present day position of the dwarf galaxy. As such, a necessary caveat to consider is the presence of "backsplash" galaxies in the isolated sample. These galaxies are often discussed in the context of galaxy clusters, with a significant fraction of galaxies at 1–2 virial radii having had a previous close passage through the center of the cluster (see Balogh et al. 2000; Gill et al. 2005; Smith et al. 2015 among others). It is difficult to rule out the same type of scenario for some of the "isolated" Local Group dwarf galaxies (with respect to a previous close passage with the Milky Way or M 31) without access to the full three-dimension velocities of the dwarfs (however, see Buck et al. 2019; Teyssier et al. 2012, and Blaña et al. 2020 for careful endeavours to do so). We also need to consider the counterpart: dwarfs that are currently within the virial radius of a massive host but are on their first infall and have not yet had an interaction.

Most recently, McConnachie et al. 2021, hereafter Paper III, combines our photometry of isolated Local Group galaxies with astrometry from Gaia Data Release 2 (DR2) (Gaia Collaboration et al. 2018) in order to determine the proper motions, and consequently the orbits, for that small subset of Solo galaxies that have enough bright supergiants that are visible to the Gaia spacecraft (NGC 6822, WLM, IC 1613 and Leo A). For NGC 6822, the Gaia DR2 proper motions appear to favor a scenario where it has never interacted with either of the massive galaxies. However, the updated analysis using Early Data Release 3 shows that NGC 6822 may actually be on

an orbit entirely consistent with being a backsplash system (see Santos et al., *in prep*; also Battaglia et al. 2021).

With these important caveats on the unknown (or only partially known) orbital histories of the systems, this chapter compares the global structural properties of the satellite dwarf galaxies in the Local Group with the isolated Local Group dwarf population. Specifically, we consider their structures as traced via the oldest stellar populations in both sets of galaxies (and as derived for the Solo sample in Paper II and Chapter 3). In Section 4.2, we introduce the datasets used, including discussion of how we deal with selection effects. In Section 4.3, we compare the structural and derived dynamical parameters of the dwarf populations, including their variation as a function of distance from host galaxy. In Section 4.4, we discuss our results, and in Section 4.5 we summarize and conclude.

4.2 Sample definition

The focus of this article is Local Group dwarf galaxies. We consider galaxies to be members of the Local Group if they are within, or at, the zero-velocity surface, as defined by McConnachie (2012). In practice, this puts all galaxies within a heliocentric distance of 1.4 Mpc as Local Group members, with the exception of Antlia, Antlia B and NGC 3109 (all members of the nearby NGC 3109 group).

Our sample of Local Group satellite galaxies is those systems that are within 300 kpc from either M 31 or the Milky Way. Isolated systems are located more than 300 kpc from these large galaxies. We refer to these dwarf subsets as the M 31 satellites, MW satellites and isolated galaxies, and abbreviate to M 31, MW, and ISO, respectively, in figures.

In what follows, we only consider galaxies fainter than the Small Magellanic Cloud (SMC - $M_v \simeq -16.8$; i.e., we exclude M33, the LMC and the SMC from this analysis). We additionally require some faint-end limits to ensure we minimise the effects of varying completeness on our comparisons. For example, the very faintest objects around the MW are more easily found than similar objects around M 31 or in the outer parts of the Local Group. The completeness of the MW satellite system has been the focus of several recent studies (for example, see Drlica-Wagner et al. 2020; Mao et al. 2021; Koposov et al. 2015). It is almost certainly the case that the MW system is complete to fainter levels than that of M 31 or the Local Group as a whole. For M 31, the most complete census of satellites is from the Pan-Andromeda Archaeological Survey

(PAndAS; McConnachie et al. 2009 for example, see discussion in McConnachie et al. (2018)). While a detailed completeness study has not been published, the limiting magnitude of the relevant satellite searches appears to be around $M_V \simeq -6$. For the Local Group, Whiting et al. (2007) estimate that their by-eye search for dwarfs in the Palomar Observatory Sky Survey and ESO/Science Research Council survey plates are complete down to a surface brightness of $26 - 27\,\mathrm{mags\,arcsec^{-2}}$ away from the plane of the Milky Way. This is probably also the appropriate limit for M 31 satellites outside of the PAndAS footprint.

Given the considerations above, we only consider dwarfs with an absolute magnitude $M_v \leq -6$ and $\mu_o < 26.5\,\mathrm{mags\,arcsec^{-2}}$. This includes the faintest Solo dwarf studied by Higgs et al. (2021), Perseus, at $\mu_o = 26.0 \pm 1.7\,\mathrm{mags\,arcsec^{-2}}$. We note that we experimented with various completeness cuts, for example considering only $M_v < -8$, and we found the broad conclusions of this paper unchanged (we note that only 2 galaxies in the Solo sample have $-8 < M_v < -6$). We will discuss remaining issues to do with the completeness of our three samples as they relate to our results at later points in this chapter.

For each dwarf subset, we compile a table of their main global positional, structural and dynamical parameters, trying to draw on studies that use homogeneous and consistent observing methods, data reduction procedures and parameter estimations as much as possible:

- For the isolated dwarfs, we primarily use the recent analysis of structural parameters from Paper II of Solo for the 12 northern Local Group dwarfs (hereafter referred to as the H21 sample; see also Chapter 3). Here, structural parameters were derived on the basis on the spatial distribution of evolved stellar populations (mostly stars on the red giant branch, RGB), though many of these galaxies also contain significant young stellar populations, which are often brighter and more centrally concentrated. This is a particularly important point, given that the satellite dwarfs are generally dominated by older populations, and makes the comparisons in this current chapter less susceptible to being dominated by differences due to only the youngest stars.

- For the M 31 satellites, we primarily use the analysis of 23 dwarfs (all dwarf spheroidals) using PAndAS data by Martin et al. (2016);

- For the MW satellites, we primarily use the homogeneous analysis from the Megacam Survey of Outer Halo Objects (Muñoz et al. 2018a,b; Marchi-Lasch

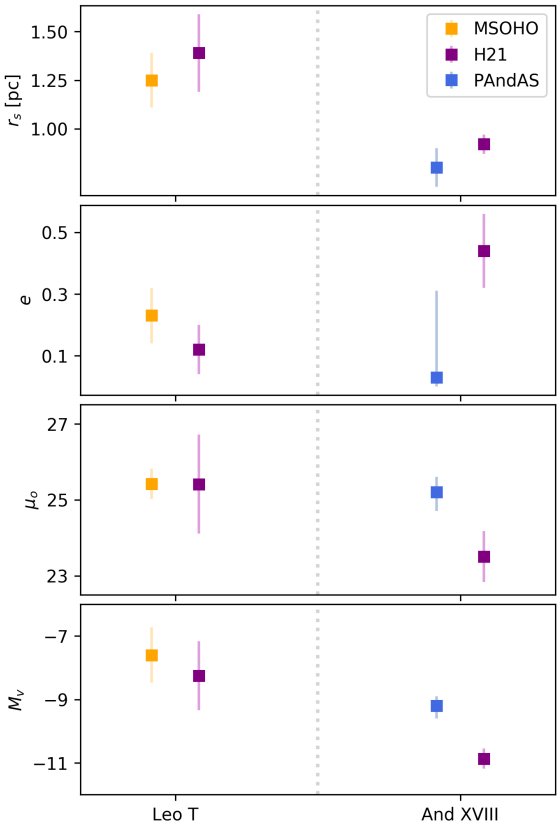

Figure 4.1: A comparison of measured values for various structural parameters for Leo T and Andromeda XVIII between the studies referenced in the text.

et al. 2019; hereafter referred to as MSOHO), selecting only those objects that are confirmed dwarf galaxies.

All three of these data sets were observed with CFHT/MegaCam. H21 and PAndAS used the $g, i-$bands and the MSOHO dataset used the $g, r-$bands (supplemented with some additional DECam observations in equivalent filters). Both MSOHO and PAndAS derived parametric fits to the data using a maximum likelihood method. H21 and MSOHO both fit Sérsic profiles to their dwarfs, whereas the PAndAS subset only used exponential profiles (equivalent to a Sérsic profile with $n = 1$; the Sérsic radius is equivalent to a half-light radius). Finally, we note that, for the H21 subset, the central surface brightness and apparent magnitudes were originally determined in the $i-$band. These values were converted to their corresponding $g-$band values given the median $(g - i)$ values for the dwarfs. All $g-$band values were transformed to $V-$band using $V = g - 0.098 - 0.544(g - i)$ (Thomas et al., 2021).

It is possible to obtain a crude check on the general consistency or otherwise of

the H21, PAndAS and MSOHO studies, since the original papers had a few objects in common. Leo T featured in the MSOHO paper, as well as in H21, and Andromeda XVIII was in the PAndAS paper, as well as H21. Figure 4.1 shows a comparison of various structural parameters between these studies for these two galaxies. We find good agreement between the values derived for Leo T from MSOHO and H21, with measured values lying well within the uncertainties for all parameters. The half-light radius and ellipiticty of Andromeda XVIII also agree between the PAndAS study and H21; the large uncertainty in the ellipticity from Martin et al. (2016) is a result of much of the galaxy lying on a chip gap in their data. For the surface brightness and apparent magnitude, Chapter 3/Paper II measures the galaxy to be considerably brighter than the measurement of Martin et al. (2016)[1]. As discussed in Chapter 3/Paper II, this is almost certainly due to the same chip gap, the significance of which is nicely illustrated in Figure 34 of Martin et al. (2016).

Each of these three primary datasets are supplemented by other works as necessary to ensure all galaxies meeting our selection criteria are included, as well as incorporating velocity dispersion information for each galaxy. Specifically, we use the parameters and references found in the updated McConnachie (2012) catalogue. Tables 4.1, 4.2 and 4.3 list the parameters and sources for the isolated, MW and M 31 dwarf subsets respectively. More specifically, the columns are:

- positions: Right ascension (RA) and declination (Dec.)
- distance moduli: $(m - M)$
- ellipticity: $e = 1 - b/a$
- central surface brightness in the V-band: μ_{vo}
- stellar velocity dispersion: σ_s
- absolute magnitude in the V-band: M_V
- Sérsic index: n (where known)
- half-light radii: r_s

[1]The methodology of both Chapter 3/Paper II and Martin et al. (2016) is such that surface brightness and magnitude are directly correlated, since the central surface brightness is set by the normalization required for the surface integral of the galaxy profile to equal the galaxy magnitude

- dynamical mass within the 3D half light radius: M_{dyn} (computed using Equation 4.1, given later)
- dynamical mass to light ratio within the 3D half light radius: M/L (computed using the dynamical mass and observed luminosity)
- minimum distance to a large galaxy (MW or M 31): D_{min} (computed using positions listed here)

4.3 Comparing and contrasting the dwarf galaxy populations

Here, we compare the distributions of the various parameters listed in Tables 4.1, 4.2 and 4.3 for each of the dwarf populations. We hold off on discussion of the relevant figures until Section 4.4.

4.3.1 Structural comparisons

Figure 4.2 shows histograms of the distribution of dwarfs in each of the three data sets for the four main structural parameters: ellipticity (e), central surface brightness in the V-band (μ_o), half-light radius (r_s), and absolute magnitude in the V-band (M_v). For each of the three populations, the colors indicate the full dataset, and the outlines indicate dwarfs belonging to the three largest, homogeneous, studies (H21, MSOHO and PAndAS, for the isolated dwarfs, MW dwarfs and M 31 dwarfs, respectively).

We attempt to quantitatively compare these histograms through the use of the two-sample Kolmogorov–Smirnov test, which allow us to determine the probability that two datasets are drawn from the same underlying distribution. We note that our sample sizes are not large for any population, and that there are some known "weird" objects in our samples (e.g., M 32 has very few counterparts in the Local Universe, and none in the Local Group). Therefore, to better understand the sensitivity of the derived KS test probability values to individual measurements in our datasets, we perform multiple realisations for each comparison. Specifically, we perform the KS test two hundred times for each comparison, and for each realisation we ignore up to two galaxies in each of the two datasets considered. We then report the median and $16^{th}/84^{th}$ percentiles of the resulting probability values in Table 4.4. Figure 4.5

Name	RA	Dec.	$(m-M)$	e	μ_{vo}	σ_s [km s^{-1}]	M_v	n	r_s [pc]	Ref.	M_{dyn} [10^6 $M_\odot$]	M/L [$M_\odot$ $L_\odot^{-1}$]	D_{min} [kpc]
And XXVIII	$22^h32^m41.2^s$	+31°12′58.0”	24.44±0.04	0.42±0.06	25.5±0.9	$6.6^{+2.9}_{-2.1}$	-9.1±0.5	0.84±0.13	316±22	*1,3*	12.6^{+11}_{-8}	61^{+92}_{-43}	374
And XXXIII (Perseus)	$03^h01^m23.6^s$	+40°59′18.0”	$24.18^{+0.11}_{-0.09}$	0.04±0.08	26.0±1.7	-	-8.9±1.8	0.79±0.63	276±41	*1*	-	-	341
IC 1613 (DDO 8)	$01^h04^m47.8^s$	+02°07′4.0”	24.18±0.06	0.20±0.05	23.3±0.4	$10.8^{+1.0}_{-0.9}$	-15.72±0.09	0.43±0.02	1511±42	*1,5*	164^{+31}_{-28}	2.0±0.4	503
Phoenix	$01^h51^m06.3^s$	−44°26′41.0”	23.06±0.12	0.30±0.03	25.8	9.3±0.7	-9.89±0.42	-	274±18	*10,13,14*	22^{+4}_{-3}	57^{+30}_{-19}	409
NGC 6822 (DDO 209)	$19^h44^m56.6^s$	−14°47′21.0”	23.78±0.05	0.28±0.15	22.5±0.04	23.2±1.2	-16.47±0.08	0.73±0.02	1980±45	*1,5*	992^{+105}_{-101}	$6.0^{+0.8}_{-0.7}$	563
Cetus	$00^h26^m11.0^s$	−11°02′40.0”	24.39±0.07	0.33±0.06	25.0±0.2	8.3±1.0	-11.29±0.21	-	703±32	*5,6,7,15*	45^{+12}_{-10}	32^{+11}_{-9}	679
Peg DIG (DDO 216)	$23^h28^m36.3^s$	+14°44′35.0”	24.77±0.04	0.56±0.05	23.3±0.5	$12.3^{+1.2}_{-1.1}$	-13.6±0.1	0.77±0.03	995±25	*1,5*	140^{+28}_{-25}	12^{+3}_{-2}	463
Leo T	$09^h34^m53.4^s$	+17°03′5.0”	23.08±0.08	0.12±0.08	25.4±1.3	7.5±1.6	-8.3±1.1	0.86±0.36	167±25	*1,4*	9^{+4}_{-3}	100^{+191}_{-67}	418
WLM (DDO 221)	$00^h01^m58.2^s$	−15°27′39.0”	24.85±0.05	0.54±0.06	22.7±0.5	17.5±2.0	-14.52±0.15	0.77±0.04	1114±44	*1,12*	300^{+37}_{-36}	$10^{+1.5}_{-0.9}$	835
And XVIII	$00^h02^m14.5^s$	+45°05′20.0”	25.36±0.08	0.44±0.12	23.5±0.7	9.7±2.3	-10.9±0.3	0.95±0.10	316±22	*1,11*	27^{+15}_{-12}	28^{+20}_{-13}	424
Leo A (DDO 69)	$09^h59^m26.5^s$	+30°44′47.0”	24.28±0.05	0.42±0.05	24.0±0.6	$9.0^{+0.8}_{-0.6}$	-11.7±0.3	0.72±0.72	479±21	*1,2*	36^{+6}_{-5}	18^{+6}_{-5}	722
Aquarius (DDO 210)	$20^h46^m51.8^s$	−12°50′53.0”	24.97±0.05	0.53±0.05	24.7±0.9	$7.8^{+1.8}_{-1.1}$	-10.92±0.18	0.61±0.05	468±26	*1,2*	26^{+11}_{-9}	26^{+15}_{-11}	981
Tucana	$22^h41^m49.6^s$	−64°25′10.0”	24.74±0.12	0.48±0.03	25.0±0.1	$15.8^{+4.1}_{-3.1}$	-9.54±0.23	-	284±54	*8,9,16*	64^{+37}_{-27}	232^{+168}_{-113}	883
Sag DIG	$19^h29^m59.0^s$	−17°40′51.0”	25.39±0.08	0.56±0.18	24.1±0.7	$9.4^{+1.5}_{-1.1}$	-11.4±0.2	0.75±0.07	497±34	*1,2*	40^{+12}_{-11}	26^{+12}_{-9}	1190
UGC 4879 (VV 124)	$09^h16^m02.2^s$	+52°50′24.0”	25.42±0.06	0.43±0.06	22.7±0.9	$9.6^{+1.3}_{-1.2}$	-11.7±0.6	1.28±0.17	400±35	*1,5*	34^{+10}_{-9}	17^{+13}_{-7}	1219

Table 4.1: Relevant observational parameters, and derived quantities, for the isolated dwarf dataset.

1 - H21 (Higgs et al. 2021), *2* - Kirby et al. (2017) *3* - Collins et al. (2013), *4* - Simon & Geha (2007), *5* - Kirby et al. (2014), *6* - McConnachie et al. (2005), *7* - McConnachie & Irwin (2006), *8* - Fraternali et al. (2009), *9* - Saviane et al. (1996), *10* - Battaglia et al. (2012), *11* - Tollerud et al. (2012), *12* - Leaman et al. (2012), *13* - Kacharov et al. (2017), *14* - Martínez-Delgado et al. (1999), *15* - Lewis et al. (2007), *16* - Bernard et al. (2009)

Name	RA	Dec.	$(m-M)$	e	μ_{vo}	σ_s [km s^{-1}]	M_v	n	r_s [pc]	Ref.	M_{dyn} [10^6 $M_\odot$]	M/L [$M_\odot$ $L_\odot^{-1}$]	D_{min} [kpc]
Sag Sph	$18^h55^m19.5^s$	$-30°32'43.0"$	17.10±0.15	0.64±0.02	25.2±0.3	11.4±0.7	-13.5±0.3	-	2600±200	*12,13,14,15*	316^{+48}_{-43}	29^{+12}_{-9}	19
Draco (DDO 208)	$17^h20^m12.4^s$	$+57°54'55.0"$	19.40±0.17	0.30±0.01	25.12±0.07	9.1±1.2	-8.71±0.17	0.96±0.02	219±18	*1,2,3*	17^{+5}_{-4}	128^{+45}_{-36}	76
Ursa Minor (DDO 199)	$15^h09^m08.5^s$	$+67°13'21.0"$	19.40±0.10	0.55±0.01	25.77±0.08	9.5±1.2	-9.03±0.12	0.82±0.01	382±18	*1,3,4,5*	32^{+9}_{-8}	183^{+56}_{-47}	78
Sculptor	$01^h0^m09.4^s$	$-33°42'33.0"$	19.67±0.14	0.37±0.01	23.29±0.15	9.2±0.2	-10.82±0.14	1.16±0.01	308±21	*1,6,10*	26^{+10}_{-8}	27±9	86
Carina	$06^h41^m36.7^s$	$-50°57'58.0"$	20.11±0.13	0.37±0.01	25.35±0.07	6.7±0.3	-9.43±0.15	0.94±0.01	349±22	*1,7,10*	14^{+6}_{-5}	55^{+25}_{-19}	107
Fornax	$02^h39^m59.3^s$	$-34°26'57.0"$	20.84±0.18	0.28±0.01	23.59±0.16	11.8±0.2	-13.46±0.24	0.71±0.01	788±69	*1,7,10*	100^{+19}_{-16}	10^{+3}_{-2}	149
Leo II (DDO 93)	$11^h13^m28.8^s$	$+22°09'06.0"$	21.84±0.13	0.07±0.02	24.24±0.07	6.6±0.7	-9.74±0.16	0.71±0.02	168±11	*1,3,8*	$6.8^{+1.6}_{-1.4}$	20^{+6}_{-5}	236
Leo I (DDO 74)	$10^h08^m28.1^s$	$+12°18'23.0"$	22.02±0.13	0.30±0.01	22.61±0.30	9.2±0.4	-11.78±0.33	0.77±0.02	243±15	*1,9,11*	19±2	9^{+3}_{-2}	257

Table 4.2: Relevant observational parameters, and derived quantities, for the Milky Way satellite dataset.

1 - MSOHO (Muñoz et al. 2018b),*2* - Bonanos et al. (2004), *3* - Walker et al. (2007), *4* - Walker et al. (2009b), *5* - Carrera et al. (2002), *6* - Pietrzyński et al. (2008), *7* - Pietrzyński et al. (2009), *8* - Bellazzini et al. (2005), *9* - Bellazzini et al. (2004), *10* - Walker et al. (2009a), *11* - Mateo et al. (2008), *12* - Monaco et al. (2004), *13* - Ibata et al. (1997), *14* - Mateo et al. (1998), *15* - Majewski et al. (2003)

Name	RA	Dec.	$(m-M)$	e	μ_{vo}	σ_s [km s^{-1}]	M_v	n	r_s [pc]	Ref.	M_{dyn} [10^6 $M_\odot$]	M/L [$M_\odot$ $L_\odot^{-1}$]	D_{min} [kpc]
M 32	$00^h42^m41.8^s$	+40°51′55.0”	24.53±0.21	0.25±0.02	11.1	92.0±5.0	-16.4±0.2	-	110±16	*7,15,16,17*	861^{+164}_{-147}	$5.4^{+1.7}_{-1.3}$	26
NGC 205	$00^h40^m22.1^s$	+41°41′07.0”	24.58±0.07	0.43±0.10	19.2	35.0±5.0	-16.48±0.12	-	590 ± 16	*3,15,16*	667^{+209}_{-178}	$4.0^{+1.4}_{-1.1}$	45
And I	$00^h45^m39.8^s$	+38°02′28.0”	24.36±0.07	0.28±0.3	25.4±0.2	10.2±1.9	-11.2±0.2	-	815±40	*1,3,4*	79^{+32}_{-27}	61^{+28}_{22}	56
And XVII	$00^h37^m07.0^s$	+44°19′20.0”	$24.31^{+0.11}_{-0.08}$	0.50±0.10	$26.4^{+0.4}_{-0.3}$	$2.9^{+2.2}_{-1.9}$	-7.8±0.3	-	285^{+55}_{-45}	*1,2,8*	$2.2^{+4.4}_{-1.9}$	39^{+84}_{-34}	67
And III	$00^h35^m33.8^s$	+36°29′52.0”	24.37±0.07	0.59±0.04	25.1±0.3	9.3±1.4	-9.5±0.3	-	405±35	*1,3,4*	33^{+11}_{-9}	119^{+59}_{-41}	73
And V	$01^h10^m17.1^s$	+47°37′41.0”	24.44±0.08	$0.26^{+0.09}_{-0.07}$	25.6±0.3	$11.5^{+5.4}_{-4.4}$	-9.3±0.2	-	345±40	*1,2,3*	47^{+20}_{-16}	211^{+112}_{-83}	109
And XX	$00^h07^m30.7^s$	+35°07′56.0”	$24.35^{+0.12}_{-0.16}$	$0.11^{+0.41}_{-0.11}$	25.8±0.7	$7.1^{+3.9}_{-2.5}$	$-6.4^{+0.5}_{-0.4}$	-	90^{+35}_{-20}	*1,2,3,8*	4^{+5}_{-3}	242^{+465}_{-197}	128
And XXXII (Cassiopeia III)	$00^h35^m59.4^s$	+51°33′35.0”	24.45±0.14	0.50±0.09	26.4±0.8	8.4±0.6	-12.3±0.7	-	1468^{+288}_{-244}	*6,10*	142^{+40}_{-34}	41^{+42}_{-21}	140
NGC 147 (DDO 3)	$00^h33^m12.1^s$	+48°30′32.0”	24.15±0.09	0.41±0.02	21.2	16.0±1.0	-14.65±0.13	-	623	*3,15,18*	148^{+19}_{-18}	$4.8^{+0.9}_{-0.8}$	140
And XXX	$00^h36^m34.9^s$	+49°38′48.0”	$24.17^{+0.10}_{-0.26}$	$0.43^{+0.10}_{-0.12}$	26.1±0.3	$11.8^{+7.7}_{-4.7}$	$-8.0^{+0.4}_{-0.3}$	-	270±50	*1,2,8*	33^{+47}_{-26}	488^{+957}_{-411}	145
And XIV	$00^h51^m35.0^s$	+29°41′49.0”	$24.50^{+0.06}_{-0.56}$	$0.17^{+0.16}_{-0.17}$	26.3±0.3	5.3±1.0	$-8.5^{+0.4}_{-0.3}$	-	265	*1,4,8*	7^{+3}_{-2}	64^{+36}_{-25}	161
And XV	$01^h14^m18.7^s$	+38°07′03.0”	$23.98^{+0.26}_{-0.12}$	0.24±0.10	26.1±0.3	4.0±1.4	$-8.0^{+0.3}_{-0.4}$	-	230^{+35}_{-25}	*1,4,8*	3^{+3}_{-2}	48^{+53}_{-29}	176
And II	$01^h16^m29.8^s$	+33°25′09.0”	24.07±0.06	0.16±0.02	25.6±0.2	7.8±1.1	-11.6±0.2	-	965±45	*1,3,9*	55^{+17}_{-14}	29^{+11}_{-9}	181
NGC 185	$00^h38^m58.0^s$	+48°20′15.0”	23.95±0.09	0.15±0.01	20.8	24.0±1.0	-14.75±0.13	-	457	*3,15,18*	245±20	$7.2^{+1.1}_{-1.0}$	184
And XXIX	$23^h58^m55.6^s$	+30°45′20.0”	24.32±0.22	0.35±0.06	26.4±0.9	5.7±1.2	-8.3±0.5	-	362^{+57}_{-55}	*13,14*	11^{+6}_{-4}	116^{+93}_{-54}	187
And VII (Cassiopeia)	$23^h26^m31.7^s$	+50°40′33.0”	24.41±0.10	0.13±0.04	23.2±0.2	13.0±1.0	-13.2±0.3	-	775 ±43	*3,4,11,19*	121^{+20}_{-19}	15^{+6}_{-4}	218
IC 10	$00^h20^m17.3^s$	+59°18′14.0”	24.50±0.12	0.19±0.02	24.6±0.2	35.5±16.6	-15.0±0.2	-	612	*5,15,20,21,22*	716^{+796}_{-511}	17^{+20}_{-12}	252
And XXXI (Lacerta I)	$22^h58^m16.3^s$	+41°17′28.0”	24.40±0.12	0.43±0.07	25.8±0.8	10.3±0.9	-11.7±0.7	-	927^{+102}_{-121}	*6,10*	60^{+10}_{-11}	29^{+28}_{-14}	262
LGS 3 (Pisces)	$01^h03^m55.0^s$	+21°53′06.0”	24.43±0.07	0.2±0.1	24.8±0.1	$7.9^{+5.3}_{-2.9}$	-10.13±0.13	-	470 ± 47	*3,12,23*	27^{+36}_{-21}	58^{+99}_{-49}	268
And VI (Peg dSph)	$23^h51^m46.3^s$	+24°34′57.0”	24.47±0.07	0.41±0.03	24.1±0.2	$12.4^{+1.5}_{-1.3}$	-11.5±0.2	-	524 ±49	*2,3,11*	74^{+20}_{-17}	45^{+17}_{-13}	268
And XVI	$00^h59^m29.8^s$	+32°22′36.0”	$23.39^{+0.19}_{-0.14}$	0.29±0.08	25.5±0.3	3.8±2.9	-7.3±0.3	-	130^{+30}_{-15}	*1,4,8*	$1.7^{+3.7}_{-1.5}$	48^{+105}_{-42}	320

Table 4.3: Relevant observational parameters, and derived quantities, for the M 31 satellite dataset.

1 - PAndAS (Martin et al. 2016), *2* - Collins et al. (2013), *3* - McConnachie et al. (2005),*4* - Tollerud et al. (2012), *5* Ho et al. (2009) (based on integrated light rather than resolved stars unlike the rest of the measurements), *6* - Martin et al. (2014), *7* - Fiorentino et al. (2010), *8* - Conn et al. (2012), *9* - Ho et al. (2012), *10* - Martin et al. (2013a), *11* - McConnachie & Irwin (2006), *12* - Lee (1995), *13* - Tollerud et al. (2013), *14* - Bell et al. (2011), *15* - de Vaucouleurs et al. (1991), *16* - Choi et al. (2002), *17* - Grillmair et al. (1996), *18* - Geha et al. (2010), *19* - Kalirai et al. (2010), *20* - Huchra et al. (1999), *21* - Sanna et al. (2010), *22* - Tikhonov & Galazutdinova (2009), *23* - Cook et al. (1999)

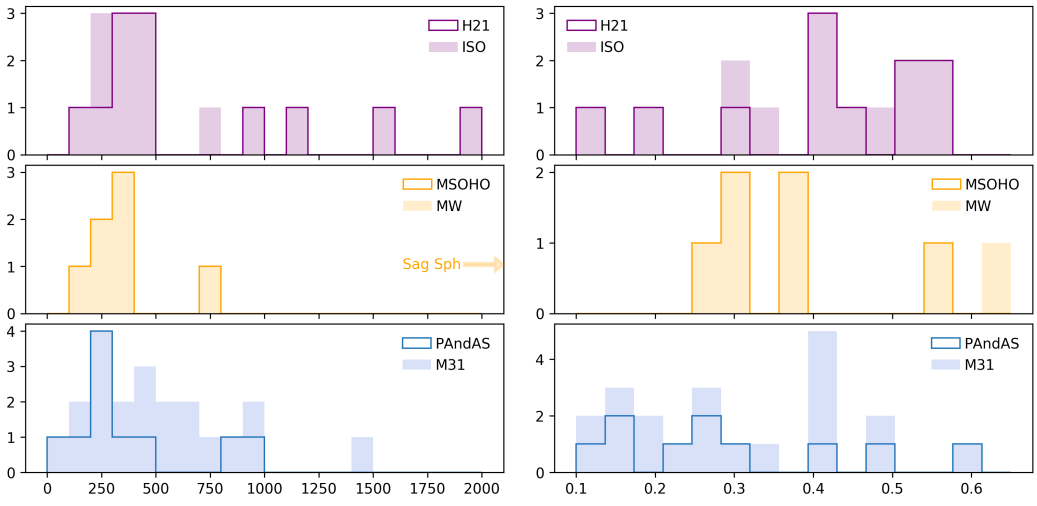

(a) Sérsic radius (r_s,pc) (b) Ellipticity (e)

(c) Surface brightness (μ_o) (d) V-band magnitude (M_v)

Figure 4.2: Histograms of the distribution of structural parameters for isolated (top; purple), MW (middle; yellow) and M 31 (bottom; blue) dwarfs. Dwarfs indicated with arrows lie far outside the range displayed, with actual values listed in Tables 4.1, 4.2 and 4.3.

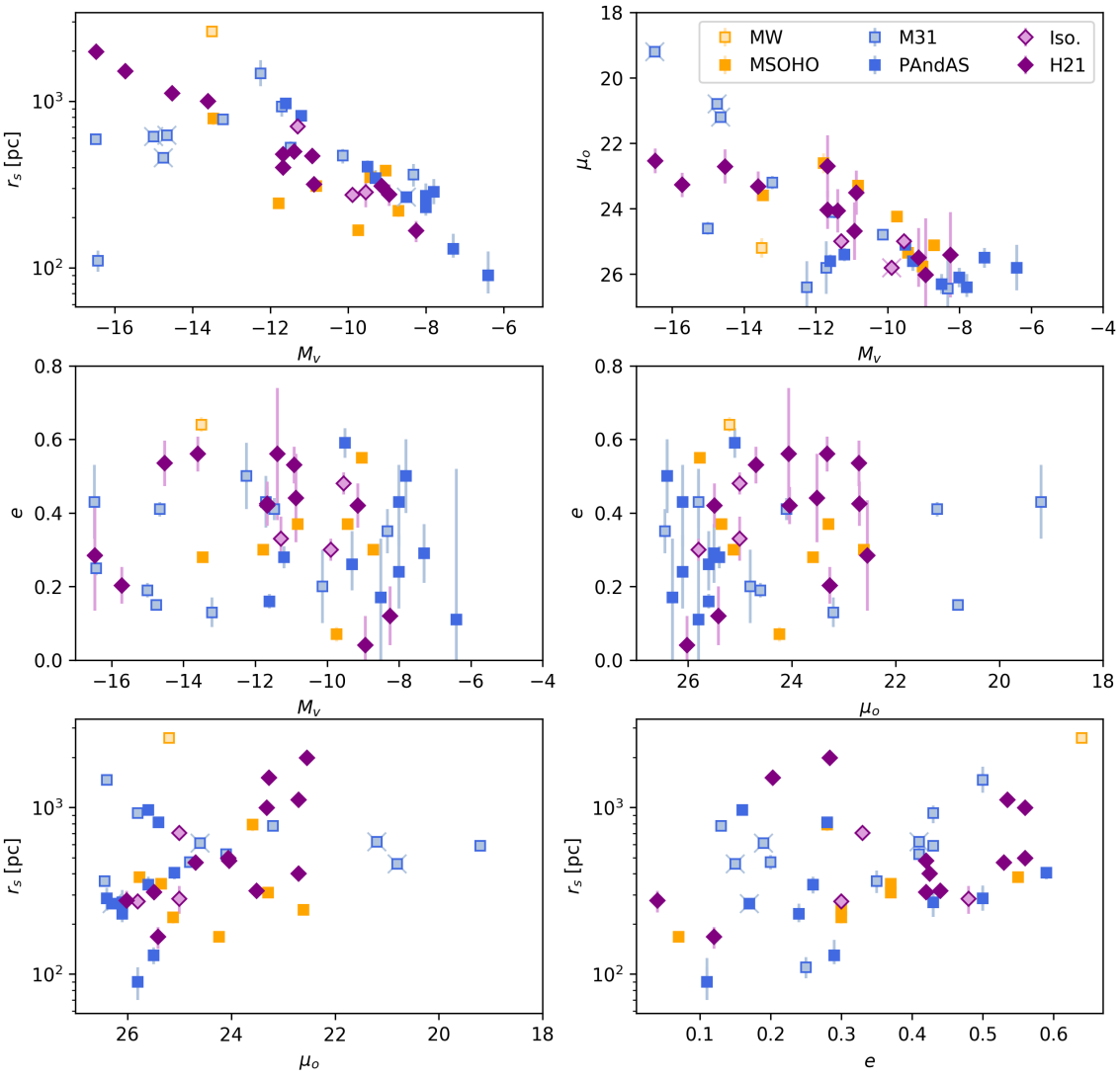

Figure 4.3: Kormendy relations and related trends for the observed structural parameters of the three dwarf populations. The MW population is shown in yellow, the M 31 population is shown in blue and the isolated population is shown in purple. The darker subsets are the uniform surveys (MSOHO, PAndAS and H21 respectively). Points with no error bars are indicated with an X.

shows the distribution of values from this randomized KS test for three parameters (velocity dispersion, dynamical mass and mass-to-light ratios). We also report the "standard value" (a single value derived on application of the test to the full dataset). As expected, the median value derived in this way is always within 1σ of the standard value. We highlight in bold any values of $P \lesssim 0.05$, which indicates our null hypothesis (the two datasets are drawn from the same population) can likely be rejected.

Finally, Figure 4.3 shows the structural parameters discussed in this section plotted against each other. Various, well-known trends can be seen (e.g., Kormendy 1985) in each population, and we discuss these further in Section 4.4.

4.3.2 Dynamical Masses and Kinematics

We now consider the stellar velocity dispersion (σ_s), dynamical masses (M_{dyn}, derived within their 3-D half-light radius, $r_{1/2}$) and dynamical mass-to-light ratios ($M/L = M_{dyn}/L_v$, again derived within $r_{1/2}$) for these dwarfs. We derive M_{dyn} following Kirby et al. (2014):

$$M_{dyn} = 4G^{-1}\sigma_s^2 r_s \text{ , where } \frac{4}{3}r_s \approx r_{1/2} \tag{4.1}$$

from the velocity dispersion and half-light radius. The resulting values of M_{dyn} and M/L are listed in Tables 4.1, 4.2 and 4.3. Histograms are shown in Figure 4.4 and follow the style of Figure 4.2. We perform the same KS tests as described in Section 4.3.1 and tabulate the derived probabilities in Table 4.5. Figure 4.6 shows these dynamical parameters as a function of scale radius and luminosity.

It is worth noting here that the newly derived dynamical masses for all the galaxies considered as dwarf irregular or transition-type studied by H21, use radial velocity dispersions and "half-light" radii measured from the same stellar population (i.e, evolved giants, mostly RGB stars). Previously, for example in Kirby et al. (2014), the radial velocity dispersion based on individual spectroscopic measurements of evolved giants are sometimes (e.g., for IC 1613, NGC 6822) necessarily combined with the half-light radius based on integrated light measurements of the same galaxies. Since dIrrs usually have a prominent young, bright, blue centrally concentrated population, the "half-light" radius that is measured by integrated light measurements does not correspond to the "half-mass radius of the relevant stellar tracer" that is formally required by Equation 4.1. At least for IC 1613 and NGC 6822, this was previously

Data Sets Compared		r_s		e		μ_o		M_v	
		P_{full}	P_{med}	P_{full}	P_{med}	P_{full}	P_{med}	P_{full}	P_{med}
MW	MSOHO	1.00	$1.00^{+0.00}_{-0.05}$	1.00	$1.00^{+0.00}_{-0.02}$	1.00	$1.00^{+0.00}_{-0.01}$	1.00	$1.00^{+0.00}_{-0.05}$
	M 31	0.5	$0.58^{+0.22}_{-0.31}$	0.39	0.43±0.19	0.14	$0.21^{+0.07}_{-013.}$	0.45	$0.51\ ^{+0.14}_{-0.11}$
	PAndAS	0.95	$0.94^{+0.05}_{-0.21}$	0.24	$0.24^{+0.24}_{-0.13}$	**0.00**	**0.01±0.01**	**0.05**	$\mathbf{0.06}^{+0.05}_{-0.03}$
	Solo	0.45	$0.49^{+0.27}_{-0.19}$	0.45	$0.55^{+0.22}_{-0.28}$	0.90	$0.85^{+0.14}_{-0.17}$	0.69	$0.69^{+0.13}_{0.22}$
	H21	0.29	$0.36^{+0.20}_{-0.19}$	0.29	$0.40^{+0.17}_{-0.22}$	0.73	$0.73^{+0.20}_{-0.26}$	0.41	$0.47^{+0.17}_{-0.23}$
MSOHO	M 31	0.22	0.27±0.16	0.51	0.54±0.24	0.22	$0.33^{+0.11}_{-0.16}$	0.51	$0.55^{+0.12}_{-0.08}$
	PAndAS	0.99	$0.94^{+0.04}_{-0.22}$	0.38	$0.51^{+0.22}_{-0.30}$	**0.01**	$\mathbf{0.02}^{+0.02}_{-0.01}$	0.06	$\mathbf{0.08}^{+0.07}_{-0.04}$
	Solo	0.20	$0.27^{+0.11}_{-0.16}$	0.20	$0.28^{+0.19}_{-0.10}$	1.00	$0.98^{+0.02}_{-0.16}$	0.40	0.47±0.26
	H21	0.12	$0.17^{+0.09}_{-0.11}$	0.12	$0.19^{+0.08}_{-0.12}$	0.93	$0.92^{+0.07}_{-0.25}$	0.21	$0.28^{+0.19}_{-0.17}$
M 31	PAndAS	0.40	$0.40^{+0.20}_{-0.17}$	1.00	$1.00^{+0.00}_{-0.04}$	0.22	$0.25^{+0.10}_{-007.}$	0.22	$0.22^{+0.0.07}_{-0.10}$
	Solo	0.74	$0.69^{+0.08}_{-0.09}$	0.26	$0.26^{+0.10}_{-0.08}$	0.10	$0.13^{+0.07}_{-0.05}$	0.50	$0.50^{+011.}_{-0.08}$
	H21	0.49	$0.49^{+0.27}_{-0.10}$	0.17	$0.20^{+0.13}_{-0.09}$	0.07	$\mathbf{0.07}^{+0.07}_{-0.03}$	0.66	$0.66^{+016.}_{-0.15}$
PAndAS	Solo	0.15	$0.20^{+0.15}_{-0.11}$	0.15	$0.20\ ^{+0.13}_{-0.11}$	**0.00**	**0.00±0.00**	**0.01**	$\mathbf{0.02}^{+0.03}_{-0.01}$
	H21	0.19	$0.20^{+0.20}_{-0.09}$	0.37	$0.43^{+0.24}_{-0.21}0$	**0.00**	**0.00±0.00**	**0.05**	$\mathbf{0.05}^{+0.06}_{-0.02}$
Solo	H21	1.00	$1.00^{+0.00}_{-0.02}$	1.00	1.00±0.00	1.00	$1.00^{+0.00}_{-0.11}$	1.00	$1.00^{+0.00}_{-0.02}$
MW & M 31	Solo	0.54	$0.59^{+0.09}_{-0.10}$	0.20	$0.24^{+0.13}_{-0.10}$	0.22	$0.24^{+0.13}_{-0.09}$	0.70	$0.73^{+0.10}_{-0.26}$

Table 4.4: Results of the KS tests between the structural parameter distributions for the different subsets of dwarf populations. P_{full} refers to the KS test preformed using the entire subsets. P_{med} is the median value and associated errors found using the random sampling as described in the text. Values highlighted in bold are deemed statistically significant. The final line of the table (MW & M 31 vs. Solo) compares all satellites to isolated dwarfs without distinguishing between the M 31 and MW satellites.

Data Sets Compared		σ_s		M_{dyn}		M_{dyn}/L_v	
		P_{full}	P_{med}	P_{full}	P_{med}	P_{full}	P_{med}
MW	MSOHO	1.00	$1.00^{+0.00}_{-0.03}$	0.97	$0.95^{+0.05}_{-0.25}$	1.00	$0.99^{+0.01}_{-0.09}$
	M 31	0.18	$0.22^{+0.0.07}_{-0.05}$	0.20	$0.25^{+0.16}_{-0.13}$	0.83	$0.84^{+0.13}_{-0.27}$
	PAndAS	0.38	$0.37^{+0.27}_{-0.09}$	0.38	$0.38^{+0.18}_{-0.10}$	0.11	$0.14^{+0.14}_{-0.09}$
	Solo	0.52	$0.70^{+0.12}_{-0.18}$	0.23	$0.27^{+0.29}_{-0.14}$	1.00	$0.96^{+0.04}_{-0.17}$
	H21	0.57	$0.72^{+0.12}_{-0.20}$	0.19	$0.29^{+0.23}_{-0.14}$	0.88	$0.67^{+0.15}_{-0.28}$
MSOHO	M 31	0.22	$0.22^{+0.12}_{-0.08}$	0.07	$0.12^{+0.07}_{-0.06}$	0.71	$0.77^{+0.17}_{-0.36}$
	PAndAS	0.42	$0.47^{+0.21}_{-0.16}$	0.42	$0.36^{+0.17}_{-0.15}$	0.08	$0.11^{+0.12}_{-0.07}$
	Solo	0.37	$0.52^{+0.24}_{-0.30}$	0.10	$0.14^{+0.15}_{-0.08}$	1.00	$0.92^{+0.05}_{-0.15}$
	H21	0.27	$0.40^{+0.30}_{-0.14}$	0.09	$0.12^{+0.17}_{-0.06}$	0.97	$0.70^{+0.20}_{-0.16}$
M 31	PAndAS	0.36	$0.36^{+0.13}_{-0.06}$	0.22	0.21±0.09	0.24	$0.27^{+0.13}_{-0.14}$
	Solo	0.64	$0.66^{+0.16}_{-0.05}$	0.64	$0.64^{+0.05}_{-0.15}$	0.29	$0.23^{+0.11}_{-0.10}$
	H21	0.72	$0.73^{+0.04}_{-0.09}$ 0.10	0.72	$0.72^{+0.06}_{-0.10}$	**0.05**	**0.03±0.02**
PAndAS	Solo	0.15	$0.19^{+0.15}_{-0.09}$	0.07	$0.08^{+0.10}_{-0.03}$	**0.01**	**0.01**±0.01
	H21	0.23	$0.26^{+0.21}_{-0.10}$	0.09	$0.13^{+0.10}_{-0.06}$	**0.00**	**0.00±0.00**
Solo	H21	1.00	1.00 ± 0.00	1.00	$1.00^{+0.00}_{-0.03}$	0.96	$0.92^{+0.07}_{-0.21}$
MW & M 31	Solo	0.73	$0.78^{+0.11}_{-0.05}$	0.23	$0.26^{+0.10}_{-0.06}$	0.48	$0.34^{+0.18}_{-0.16}$

Table 4.5: As Table 4.4, but for the dynamical parameters.

unavoidable since the relevant measurements did not exist for these galaxies until the analysis by H21.

4.3.3 Trends with distance from the nearest massive galaxy

The focus thus far has been on comparing the satellite population with the isolated population of Local Group dwarf galaxies. However, we also explore the observed structural and dynamical parameters of these galaxies as a function of their "isolation". Obviously, the only massive galaxies in the Local Group relevant to this discussion are the MW and M 31 galaxies. They are broadly the same mass (e.g., Eadie & Jurić 2019; Patel et al. 2017; Bland-Hawthorn & Gerhard 2016; Peñarrubia et al. 2014), and so it is most convenient to examine the dwarf galaxy properties as a function of their distance from these systems, as a proxy for isolation. We determine D_{min} for each dwarf as D_{min} =min(D_{MW}, D_{M31}), the minimum of the dwarf's to the MW and M 31 respectively, adopting a distance modulus of 24.46 (de Grijs & Bono, 2014) for M 31. Figure 4.7 shows r_s, e, μ_o, M_v, σ_s, M_{dyn}, M/L and the Sérsic index n as a function of D_{min}.

An alternative metric for isolation that we considered is the tidal index. The tidal

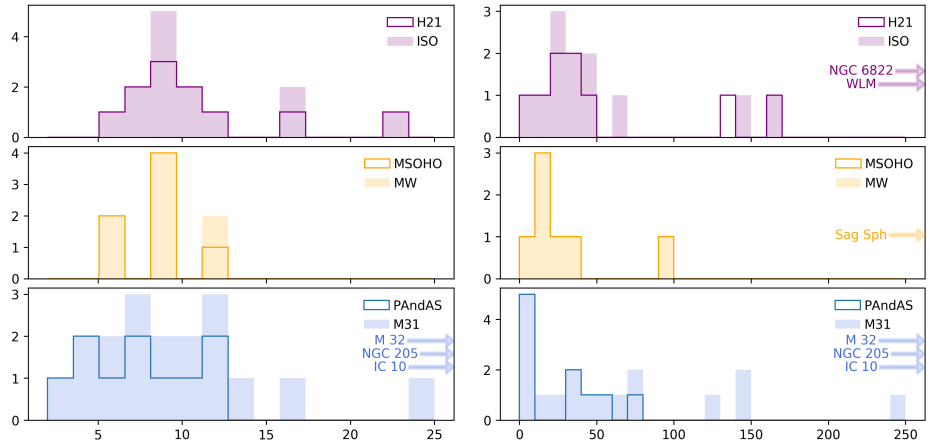

(a) Stellar velocity dispersion (σ_s, km s^{-1})

(b) Dynamical (M_{dyn}, 10^6 $M_\odot$)

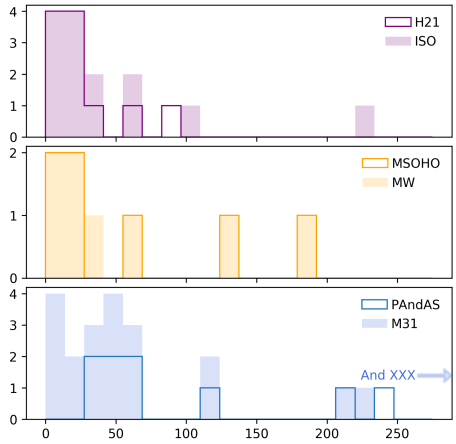

(c) Mass-to-light ratio (M/L, in solar units)

Figure 4.4: Histograms of the distribution of dynamical parameters for isolated (top; purple), MW (middle; yellow) and M 31 (bottom; blue) dwarfs. Dwarfs indicated with arrows lie far outside the range displayed, with actual values listed in Tables 4.2, 4.3 and 4.1.

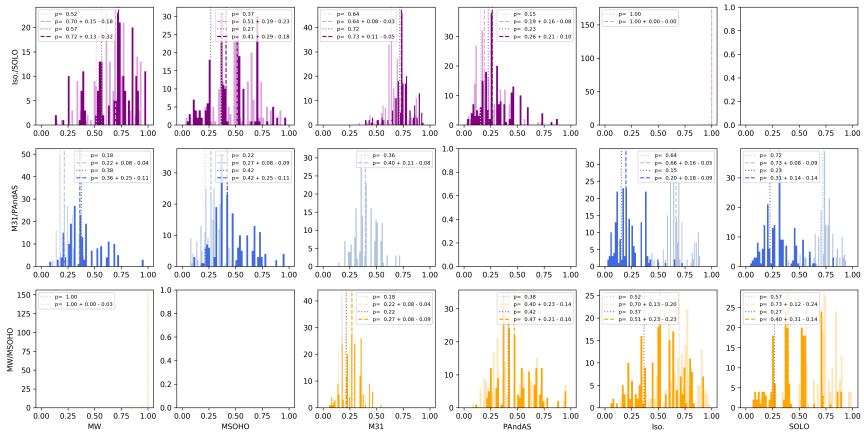

(a) σ_s

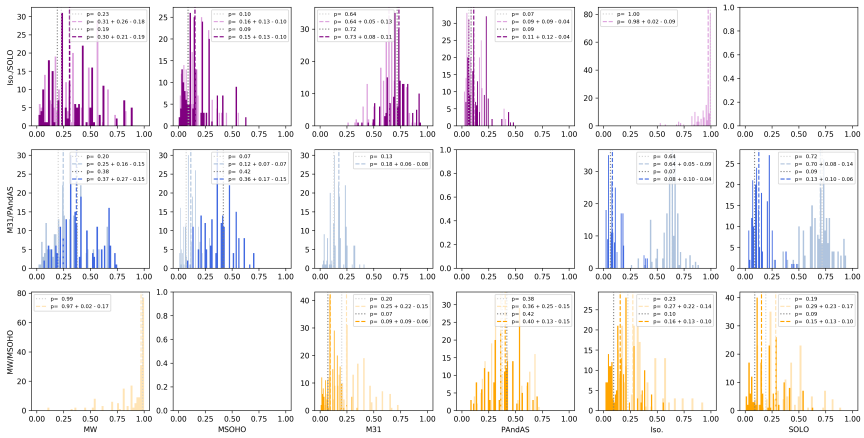

(b) M_{dyn}

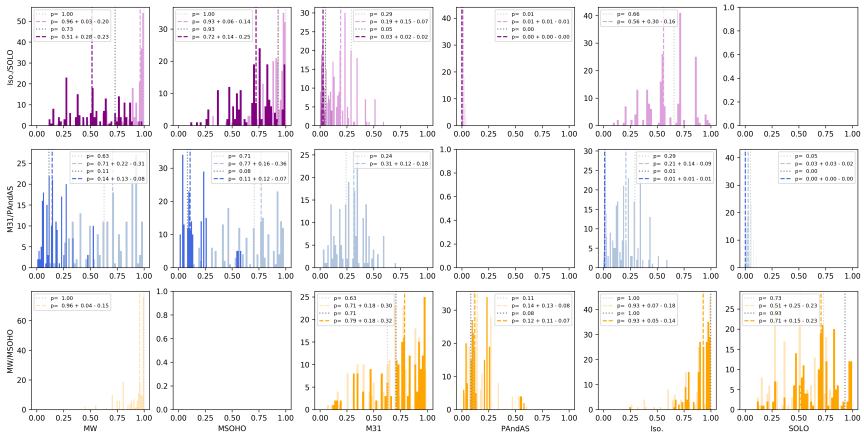

(c) M/L

Figure 4.5: As in Tables 4.4 and 4.5, showing the KS values between each pair of datasets. The darker colours in each row refer to the homogeneous datasets – specifically, from the bottom row to top row: MSOHO, PAndAS and SOLO.

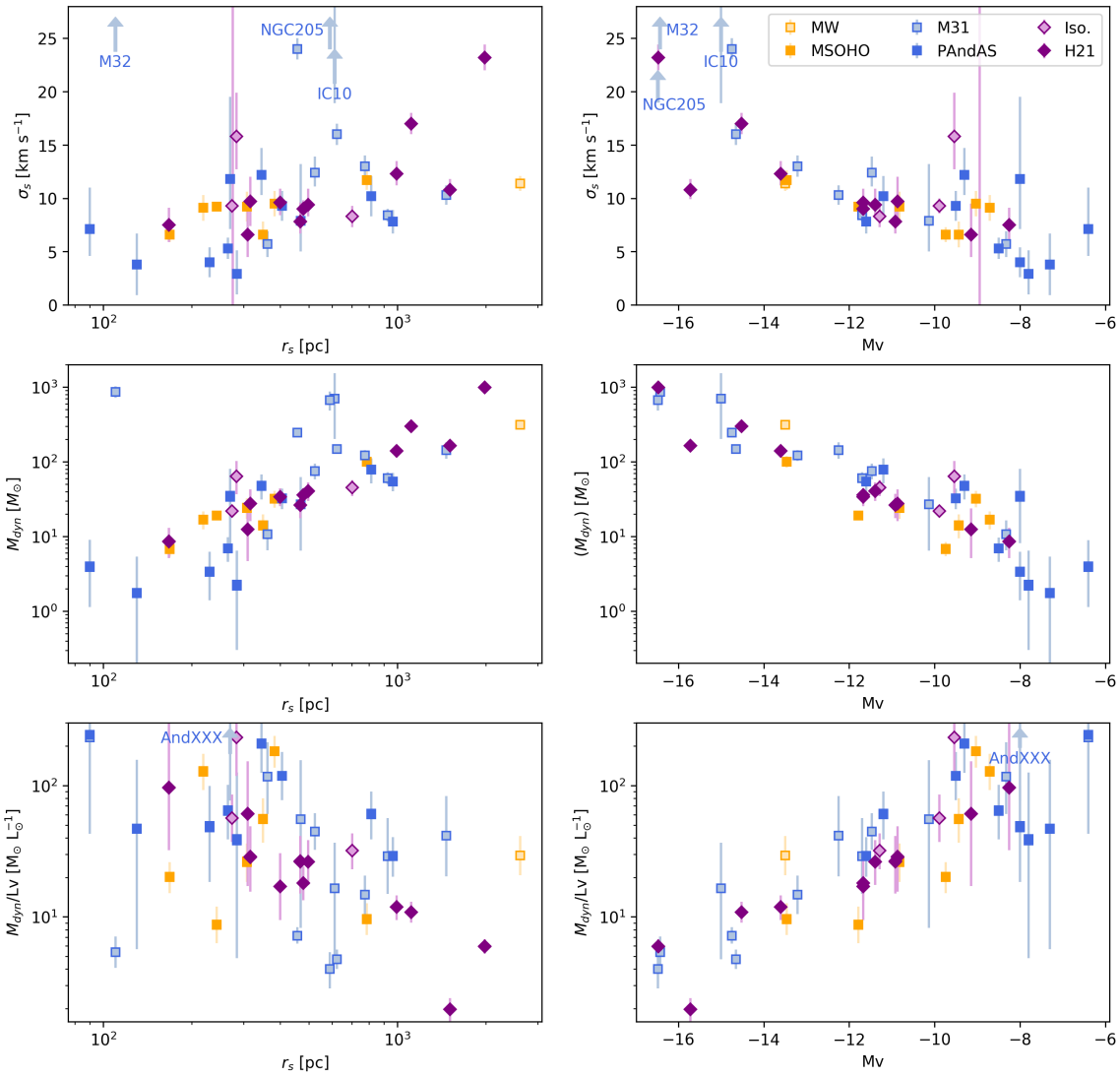

Figure 4.6: Relationships between the dynamical parameters (specifically, velocity dispersion, dynamical mass, and mass-to-light ratio) and key structural parameters (specifically, half-light radii and absolute magnitudes) for the dwarf galaxy populations.

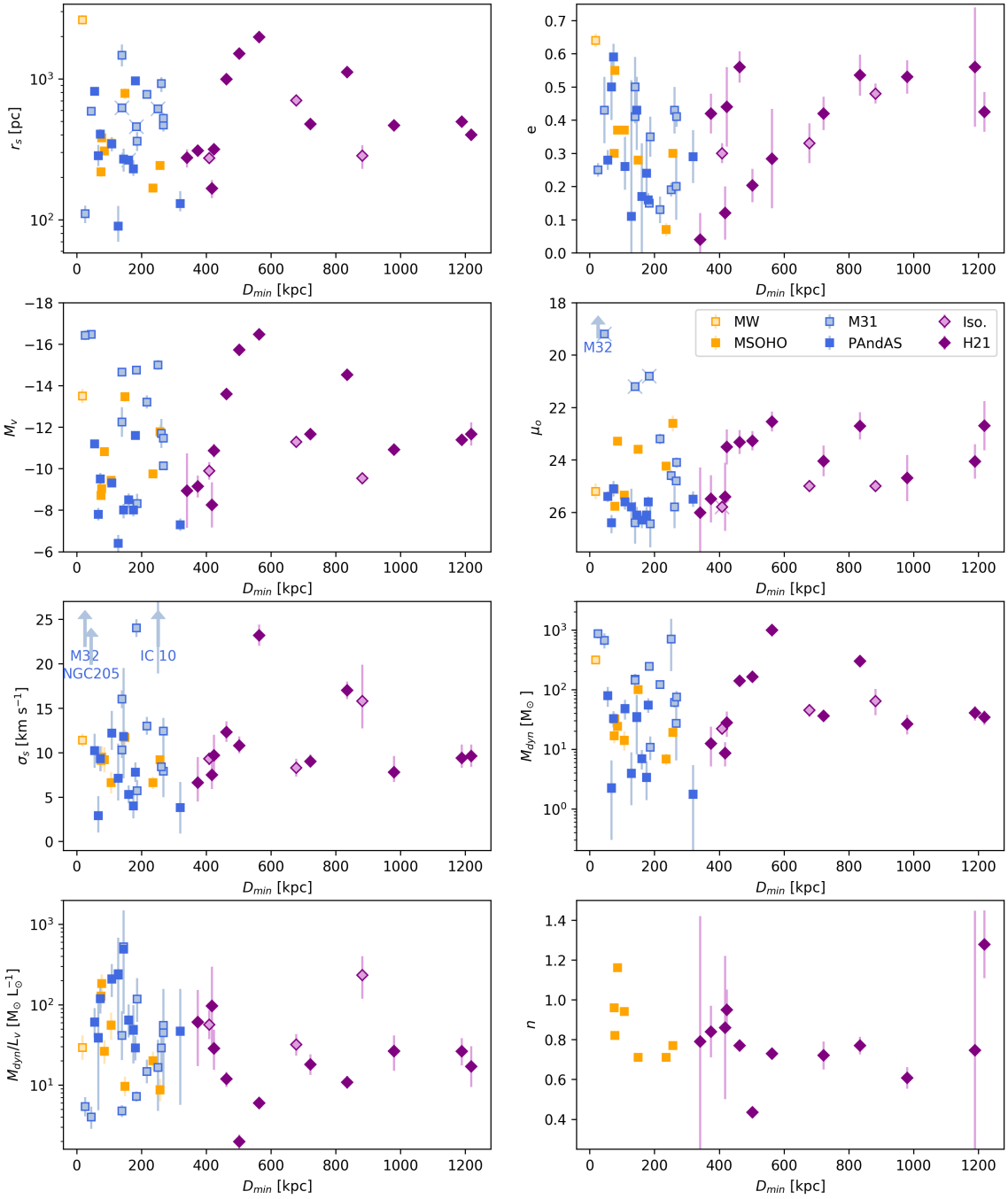

Figure 4.7: Trends of half-light radius (r_s), ellipicity (e), absolute magnitude (M_v), surface brightness (μ_o), stellar velocity dispersion (σ_s), dynamical mass (M_{dyn}), dynamical mass to light ratio (M/L) and Sérsic index (n) with distance to the nearest massive galaxy, D_{min}.

index considers the separation between a dwarf and a perturber, and incorporates the perturber's mass.Karachentsev et al. (2013) give a detailed explanation, where the tidal index (Θ) is dependent on the tidal force (F_n) of its neighbouring galaxy (n), given by:

$$F_n \sim \frac{M_n}{D_n^3} \tag{4.2}$$

for "n" neighbours, where D_n is the from its neighbour between and M_n is the neighbour's mass. We calculated the tidal index between all galaxies in our sample, including also the MW, M31, the Large and Small Magellanic Clouds, and M 33 as possible perturbers. However, for all dwarfs, the largest tidal index is due either to the MW or M 31, with all other galaxies much less significant, by an order of magnitude or more. This result suggests that the MW or M 31 is the dominant perturber for the population and so D_{min} is an appropriate parameter to examine.

4.4 Discussion

4.4.1 Comparing the satellite population of the Milky Way and M 31

Before we compare the satellite population of M 31 and the MW to the isolated Local Group dwarfs, we examine if there exist major differences in the structural and dynamical parameters of the two satellite populations. There are a few notable differences between the two populations in terms of overall morphology, specifically that there are no compact or dwarf elliptical analogs to M 32, NGC 205, NGC 147 and NGC 185 around the MW as found around M 31. At the higher luminosity end, M 31 has M 33 as a companion, whereas the MW has the Magellanic Clouds. While the Magellanic Clouds account for the entire gas-rich population of MW satellites, M 31 additionally has a dwarf starburst satellite (IC 10) in addition to a transition-type satellite (LGS 3). Both M 31 and the MW appear to have planes of satellites (Pawlowski, 2018).

We first examine if there exist any notable differences in the structural and dynamical parameters between the galaxies with parameters derived from MSOHO and PAndAS compared to the full MW and M 31 populations, respectively. Examination of Figures 4.2 and 4.4 and the KS results in Tables 4.4 and 4.5 show that the MSOHO

sample is statistically indistinguishable from the full set of MW satellites, but this is completely unsurprising since there is only 1 additional MW satellite compared to the MSOHO sample. For the M 31 population, Figure 4.2 shows that the PAndAS satellites are generally low luminosity/surface brightness compared to the rest of the M 31 population. Indeed, this is not unexpected: Martin et al. (2017) specifically target the dwarf spheroidal population within the PAndAS footprint. As discussed above, this means that none of the (bright) dwarf elliptical satellites are included. Further, the PAndAS sample misses the gas-rich satellites which are located outside of the PAndAS footprint. As such, we do not further concern ourselves with differences between the PAndAS-studied satellites and the rest of the M 31 population, since the PAndAS-studied sample was never expected to be, nor described as, a representative subset of the diverse M 31 satellite population.

Comparison of the population of the MW and M 31 satellites to each other, both in Figure 4.2 and 4.4 and more quantitatively with the KS results in Table 4.4 and 4.5, reveals that the two populations have statistically indistinguishable structural and dynamical properties across all parameters that we examine. It has previously been noted by McConnachie et al. (2006) and others that M 31 appears to have satellites with considerably larger half-light radii than is found around the MW. Examination of the first panel of Figure 4.2 shows that there is indeed an "excess" of satellites around M 31 with scale radii greater than around 400 pc compared to the MW, although the latter does have two satellites like this (Fornax and the tidally-disrupting Sagittarius dSph). However, these differences do not rise to the level of statistical significance, and we conclude that the MW and M 31 satellites can be considered as a single grouping in our following comparison of satellites and isolated systems.

Prior to this discussion, however, there is a notable difference between the M 31 and MW satellites worth highlighting. Namely, there are only eight MW satellites used in our analysis, and yet there are twenty one analogous systems around M 31. Obscuration by the Galactic plane is clearly an issue for the MW satellites. However, the Galactic plane impacts dwarf detection in, at the most extreme, half the sky (between $-30^\circ < b + 30 <^\circ$). Assuming that satellites are uniformly distributed, this obscuration can account for, at most, a factor of 2 difference between the MW and M 31, whereas we observe a factor of 3 difference.

This difference aligns with other observations of M 31, that together suggest a more active and rich accretion history for this galaxy in comparison to the MW. M 31 is observed to have more halo globular clusters (113 outer halo globular clusters

in M 31 compared to 19 in the MW; Wang et al. 2019), and many more globular clusters are associated with the disk of M 31 compared to the MW. Hammer et al. (2007) compared the integrated properties of the MW and M 31 to other galaxies and concluded that the MW had undergone a relatively passive evolution whereas that of M 31 was more "typical". Indeed, with respect to their satellite populations, Wang et al. (2021) recently compared the MW's satellite luminosity function to other MW-like galaxies and showed that the MW is somewhat unusual insofar as it lacks satellites (considering dwarfs with $M_v > -12$). The Saga Survey (Geha et al., 2017; Mao et al., 2021) also puts the MW and M 31 satellite systems into a broader context, and show that while the MW has a dearth of satellites as compared to M 31, they both lie within the scatter of MW-like analogues. Thus, the difference in the number of brighter satellites observed here aligns with this overall picture of M 31 as galaxy with a more active history than the MW.

4.4.2 Examining the trends of the structural and dynamical parameters

Across all structural and dynamical parameters that we study, neither visual inspection of the histograms in Figures 4.2 and 4.4 nor the KS test results in Tables 4.4 and 4.5 reveals any statistically significant evidence that the one-dimensional parameter distribution functions for satellites compared to isolated systems are different.

Evidence for a more complex story emerges when we consider the Kormendy relations and related diagrams shown in Figure 4.3 and 4.6. Particularly striking is the relation between r_s and $\mathrm{M_v}$ in the top-left panel of Figure 4.3. Here, the isolated dwarfs (purple) define a remarkably linear relation between scale-radius and magnitude. The satellite populations (blue and yellow) follow the same trend, but with notably more scatter around the relation. Inspection of the top-right panel of the same figure shows similar behaviour for the central surface brightness. That is, while all dwarfs appear to follow the same broad trend in surface brightness with luminosity, the relation defined by the isolated systems appears more tightly defined than that for the satellite systems.

This general behaviour is also visible in some of the derived dynamical trends, perhaps most obviously in $\mathrm{M_{dyn}}$ vs. r_s. Indeed, the common element to all of these trends in their reliance on the physical scale of the dwarf ($\mathrm{M_{dyn}}$ is calculated using r_s, and surface brightness is a measure of the concentration of luminosity within a scale

radius). However, we note that we are not able to say that this increased scatter has very high statistical significance. We have tried to use multiple parameterizations of the scatter for these relations, and we find what we can see by eye: the scatter is generally larger for satellites than for isolated systems. In no case, however, are we able to claim this increased scatter is at a high significance. This is likely due to the reality of the Local Group of galaxies: there are simply not enough galaxies in each of our subsets to be able to claim that weak differences in populations are statistically significant. Given the known, observable sample available, only the most extreme differences between populations will ever be classed as statistically significant, although this does not mean that weak differences do not exist, nor that they are uninteresting to consider.

We must use our judgement as to what importance to assign to this apparent increase in scatter. It is interesting to consider that this behaviour may then naturally be explained through a single process, namely the tidal influence of the massive galaxies on the scale radius of the dwarf. For the case of dark matter dominated dwarf spheroidal populations, this has been examined from a theoretical perspective by Peñarrubia et al. (2008). They find that these systems follow remarkably predictable tracks in these 2-parameter plots as mass is stripped. Initially, as the outskirts of the dwarf is stripped (which results in the loss of dark matter but little luminosity), the scale radius of the dwarf will increase as it adjusts to the reduced dark matter content of the dwarf. Then, as stripping proceeds and luminous matter is lost, the scale radius decreases significantly as the overall luminosity decreases. Indeed, following Errani et al. (2015), Fattahi et al. (2018) predict the progenitors of various Local Group dwarfs (especially satellites) prior to tidal stripping, and find the progenitor population occupies a parameter space that is more tightly defined than that occupied by the present-day dwarfs. It seems reasonable to suggest, therefore, that a similar process may be at work here, and could naturally explain why the satellites appear to show some evidence for having a larger scatter in scale radius and related properties. We also note that stripping, while present, is unlikely to be dominant for all satellites, since we might then expect there to be more notable differences in the overall 1-D distributions of these parameters between the populations.

4.4.3 How isolated is isolated?

The original definition of the Solo sample with respect to isolation is $D_{min} > 300\,\mathrm{kpc}$ from the MW or M 31, and was based on the virial radii of the dark matter halos in which these galaxies are expected to reside. We investigate if this "boundary" does indeed represent a meaningful definition of isolation by examination of the trends with distance from the nearest massive galaxy in Figure 4.7.

Examination of the panels in Figure 4.7 consistently show that the identified satellites of M 31 and the Milky Way have generally large spreads on the y-axis of each panel, and that these spreads are much larger than for those dwarfs that have large values of D_{min} (this is true to varying extent for every panel except the last). There appears to be a transition area around $D_{min} \simeq 300-400\,\mathrm{kpc}$, to the left of which dwarf galaxies occupy a broad range of parameter space, and to the right of which the range that is occupied is considerably less. This is consistent with our earlier interpretation of the effect of tides, but what is interesting here is that the effect does not match exactly our original "threshold" for isolation of $D_{min} = 300\,\mathrm{kpc}$. Rather, the parameters of the five isolated galaxies between $D_{min} \simeq 300 - 400\,\mathrm{kpc}$ (Phoenix, Leo T, Perseus, And XVIII and And XXVIII) appear to bear more similarity as a group to the satellite population than the more isolated galaxies; this is most apparent when examining their half-light radius, their magnitudes, and their surface brightnesses.

In addition to these parameters, another feature present in Figure 4.7 is the dearth of low ellipticity dwarfs at large distances visible in the top-right panel. As we get close to the more massive galaxies, we find dwarf galaxies with ellipticities spanning $0 \lesssim e \lesssim 0.6$. However, further than $D_{min} \sim 500\,\mathrm{kpc}$, no low ellipticity systems are found, and indeed all very isolated systems approximately 1 Mpc from either the MW or M 31 have a broadly similar ellipticity of around $e \sim 0.5$. We also emphasise that the ellipticity that we measure is the ellipticity of the older stellar populations in all the dwarfs i.e., for the isolated systems we are not looking at recently formed stars in a young disk, as might be the case if we used integrated light measurements for this comparison.

We conclude from Figure 4.7 that, across all panels, the differences between the "isolated" galaxies and the "satellite" galaxies are maximised if we consider a distance threshold of $D_{min} \simeq 400\,\mathrm{kpc}$, not $300\,\mathrm{kpc}$. The transition distance at which this occurs is occupied by a group of five dwarfs (Phoenix, Leo T, Perseus, And XVIII

and And XXVIII). From simulations, the distance range between 1–2 times the virial radius of the host is populated by many dwarfs which have previously undergone an interaction with the host. Indeed, Gill et al. (2005) suggests that 50% of dwarfs within this distance range have previously interacted with the host. For M 31 and the MW, this distance range corresponds to $D_{min} \sim 300 - 600\,\mathrm{kpc}$. In this range, there are 8 isolated dwarfs in our sample, with possibly 5 looking more similar to satellites than more distant dwarfs. Qualitatively, these findings would seem to align with expectations for backsplash systems.

4.4.4 Building a consistent interpretation

While we do not see any clearly statistically significant differences between satellite and isolated galaxies in any of the parameter space we examine, the items discussed above allow for a consistent interpretation of the data at hand. Specifically:

- Most dwarfs within approximately 400 kpc of the MW and M 31 are satellites or backsplash galaxies. This is consistent with studies of these populations in simulations. Teyssier et al. (2012) suggests that 13% of systems between $300 - 1500\,\mathrm{kpc}$ have actually orbited around the host galaxy. For the Local Group, they suggest that Cetus, Tucana, NGC 6822, Phoenix and Leo T have passed through the Milky Way. This would constitute one-third of our "isolated" sample. A similar study by Buck et al. (2019) reaches similar conclusions regarding NGC 6822 and Leo T, but they find Cetus and Phoenix are slightly less likely to be backsplash systems (with probabilities of $P \simeq 0.36$ and 0.43, respectively; Tucana was not included in their analysis). Further, Blaña et al. (2020) also suggests that Leo T is a backsplash dwarf, while Phoenix is argued to be on its first in-fall. Updated proper motion measurements of NGC 6822, originally made in Paper III, appear to confirm that NGC 6822 is a backsplash system (Santos et al., *in prep*; see also Battaglia et al. 2021). These results highlight the complex and uncertain nature of identifying backsplash galaxies without three dimensional velocity information.

- Interactions of the population of satellite galaxies with their hosts generally causes an increase in the scatter of the underlying trends between the structural and dynamical parameters discussed. This is especially true with respect to the scale radius of the dwarf (e.g., top-left panel of Figure 4.3), as well as surface

brightness (compare the scatter in surface brightness for galaxies interior and exterior to $D_{min} \sim 400\,\mathrm{kpc}$ in Figure 4.7);

- Satellite galaxies have a broader range of ellipticities than isolated systems, and in particular satellite populations have more circular satellites than are found in the field. This is consistent with interactions in the satellite environment making systems more spheroidal, for example as proposed by Kazantzidis et al. (2011), and references therein. These authors invoke a suite of physical processes to "tidally stir" disk-like populations to become spheroidal-like. Interestingly, Łokas et al. (2012) simulate the evolution of various observed parameters for dwarf galaxies ($\mathrm{M_v}$, μ_o, e) as the system is tidally stirred. During these interactions, the ellipticity of the dwarfs are scattered, and are not systematically increased or decreased. Given many of these systems start off with relatively high e, the result is the production of many dwarfs with smaller e, consistent with our findings. But we also note that the assumption that the stars start off in a cold disk is not necessarily correct (e.g., Kaufmann et al. 2007), and this is supported by the fact that the old populations of several isolated dwarf galaxies are not seen to possess any significant rotation (Kirby et al. 2017).

- Given that our interpretation of these plots puts heavy weight on tidal effects, it is also worth noting how the dynamical parameters vary with distance from host. There are only 5 galaxies in our sample that have velocity dispersions $\sigma_v \lesssim 6\,\mathrm{km\,s^{-1}}$. All of them are satellites. Further, examination of the derived dynamical masses for all the dwarfs (which is a function of both σ_v and r_s) shows even more clearly that the galaxies with the smallest dynamical masses are satellites. Again, this is broadly consistent with the idea that the satellite populations contain systems that have been notably affected by tidal stripping.

A consistent picture can therefore emerge from these comparisons, that is also consistent with our general understanding of the likely dominant mechanisms at work for satellites, i.e., tides. The absence of circular galaxies in the field is particularly striking. While it is nearly certainly the case that some highly elliptical satellite galaxies are tidally disrupting (e.g., Hercules; see Deason et al. 2012; Roderick et al. 2015; Garling et al. 2018 among others), it is also clear that many satellites can be intrinsically elliptical, without the need for tides. Our findings suggest that more circular-looking satellites, on the other hand, would not be nearly as circular-looking were it not for their proximity to a massive host.

4.4.5 Revisiting completeness of the sample

As discussed in Section 4.2, the sample on which our analysis and discussion is based is limited in both magnitude and surface brightness, in an attempt to remove the difficulties caused by inhomogeneous detection limits for the three populations. Would our conclusions change significantly if somehow completeness was still an issue, especially for the isolated subset of dwarfs?

With respect to the behaviour of ellipticity, it seems difficult to understand how this would change, since there is no clear reason why nearly circular dwarfs at large distances from either the MW or M 31 would be harder to detect than elliptical ones. Indeed, examination of Figure 4.3 shows there is no trend of ellipticity with either M_v or μ_o (the two parameters on which completeness most likely depends). Completeness would also not change our discussion about the increase in scatter of various parameters, especially r_s, since finding more dwarfs at fainter magnitudes or surface brightnesses will only add new points at the faint end, not change the scatter for any of the systems we already know about. However, regarding Figure 4.7, it could change our ability to discern a distance threshold that distinguishes satellites from field. If there are many systems as faint as Phoenix, Leo T, Perseus, And XVIII and And XXVIII at greater distances from the MW and M 31, then they will likely also have smaller scale radii, lower radial velocity dispersions, and lower dynamical masses (as per the correlations in Figures 4.3 and 4.6). This unseen population could essentially remove the distinguishing features that cause us to conclude that most systems are in fact satellites within $\mathrm{D_{min}} \simeq 400\,\mathrm{kpc}$. We note, however, that the differences in ellipticities would still persist.

Fattahi et al. (2020) argue that, from comparison of the Local Group to cosmological simulations, there may be as many as 50 more dwarfs at least as massive as Draco currently unobserved in the field out to a distance of 3 Mpc (a considerably larger volume than the approximately 1 Mpc distance threshold we use in the current study). However, if we also adopt the best estimates we have for the completeness of the current searches of Local Group satellites, then these systems would mostly have to be very low surface brightness, physically extended, dwarf galaxies like Antlia II, Crater II or Andromeda XIX, and occupy a quite distinct region of parameter space compared to those galaxies studied here. The coming few years, aided by the survey power of the Vera C. Rubin Observatory, the Nancy Grace Roman space telescope, and the Euclid mission, should provide us with the definitive surveys to push searches

of dwarf galaxies to low surface brightness throughout the Local Group.

4.5 Summary and Conclusions

We have used the Solo (*So*litary *Lo*cal) Dwarf Galaxy Survey (Paper I, II/Chapter 3) to compare and contrast isolated dwarfs in the Local Group with those in close proximity to the Milky Way and M 31. In particular, our comparison focuses on the global structural properties of these galaxies as traced by their oldest stellar populations. In addition to their sizes, shapes, luminosities and surface brightnesses, we also examine their global dynamical properties, including their velocity dispersions, implied dark matter masses, and mass-to-light ratios. We attempt to account for different selection effects between our samples by adopting firm faint-end limits in magnitude and surface brightness. Our main findings are:

- The structural and dynamical properties of the satellite populations of the MW and M 31 are not obviously statistically different. However, it is notable that there are a lot more satellites around M 31 than around the MW down to an absolute magnitude $M_v \leq -6$ and $\mu_o < 26.5\,\mathrm{mags\,arcsec^{-2}}$ (21 around M 31 compared to 8 around the MW (considering those satellites fainter than the Magellanic Clouds).

- The proximity of a massive host does not induce any statistically significant offsets between the observed structural or dynamical one-dimensional parameter distributions for satellites compared to isolated systems.

- Dwarfs in close proximity to a massive galaxy generally show more scatter in their Kormendy relations than those in isolation. Specifically, isolated Local Group dwarf galaxies show a much tighter trend of half-light radius versus magnitude than the satellite population, and similar effects are also seen for related and derived parameters (i.e., surface brightness, dynamical mass, and mass-to-light ratio).

- There is an absence of spherical (i.e., $e \lesssim 0.3$) dwarf galaxies far from large galaxies.

- There appears to be a transition in the structural and dynamical properties of the dwarf galaxy population at around $D_{min} \sim 400\,\mathrm{kpc}$ from the MW and

M 31, such that the dwarf population closer than this occupy a broader range of parameter space compared to dwarfs further away, and that the smallest, faintest, most circular systems are found as satellites.

- Differential selection effects between the surveys that have found MW, M 31 and Local Group dwarf galaxies are important to consider, but are unlikely to significantly affect the conclusions of this current study unless our current understanding of the limits of these surveys are significantly flawed.

The limited number of systems that pass our magnitude and surface brightness cuts means that the statistical significance of any one of these findings is not high. However, together they paint a compelling picture that we interpret as pointing to the significance of tidal interactions on the population of systems within approximately 400 kpc from the MW and M 31. These interactions act to increase the scatter in the various relationships we observe, including potentially making some systems more spherical than they might otherwise become if left to nature rather than nurture.

Chapter 5

Stars, gas and the satellites of dwarf galaxies

The analysis in the previous chapter emphasizes the impact of environment by comparing the isolated dwarfs to the satellite dwarfs, with results supporting a narrative where tidal interactions between the satellites and their hosts are likely responsible for an increased scatter in the scaling relations of satellites in comparison to the isolated systems. If true, this supports the contention at the start of the thesis that the isolated systems are most heavily impacted by internally driven processes, while the presence of the host galaxy is the dominant factor for the satellites. Here, we search for additional insights by combining the structural/dynamical analysis of the previous chapter with additional parameters for the dwarfs relating to their star formation (SF), namely their star formation histories (SFH) and the HI gas.

I first examine the HI gas, then the SFHs in these dwarfs, the latter being largely independent of environment. Therefore, by using the SF of a dwarf, we can get a snapshot of the internal processes and compare them to the external impacts already shown in Chapter 4.

Further, we understand that dwarfs should be smaller analogues of more massive galaxies, and so may have their own satellites. I search the surroundings of the Solo dwarfs in the Local Group for their own small satellites, to see if these systems really are as "isolated" as they appear. This includes a brief excursion into searches for globular clusters around these dwarfs.

5.1 Gas and the formation of stars

5.1.1 The gas content of dwarfs

The presence, infall, removal and/or consumption of gas (via SF) is central to how a dwarf evolves. Environment can impact SF (for example, Pearson et al. (2016) conclude that host galaxies prevent dwarfs from re-accreting gas once it is expelled), but it is SF itself that is directly responsible for the cycling of baryons in the galaxy.

One measure of a galaxy's ability to produce future generations of stars is its present HI gas fraction. Putman et al. (2021) compiles the mass of HI (M_{HI}) in almost all of the Local Group dwarfs. In what follows, I use these values to examine the figures originally shown in Figures 4.3, 4.6, and 4.7, but now coding points by their HI mass and HI mass fraction. In particular, Figures 5.1, 5.2, and 5.3 show a subset of the panels originally shown in Chapter 4, where yellow indicates a high HI mass/fraction, and purple indicates a low HI mass/fraction. Diamonds are isolated dwarfs (with "x" indicating upper limits to the HI) and squares are satellites (with "+" indicating upper limits to the HI).

Looking at Figure 5.1, there is a clear trend with M_v, with the brighter dwarfs being more HI rich. This trend is driven by the isolated dwarfs – there is a clear color gradient amongst the diamonds/crosses. There is not such a clear gradient in Figure 5.2, implying that massive dwarfs do not clearly possess more gas per unit stellar mass than smaller systems. Thus, what we recover is an HI mass – M_v relation – more luminous galaxies with gas generally have more gas than less luminous galaxies with gas. No trends are present in any of the other structural parameter plots that have not been reproduced here (e.g., with ellipticity, etc).

Figure 5.3, shows very clearly the distance - morphology relation, whereby the isolated dwarfs have higher HI masses and higher HI mass fractions, than satellites (Einasto et al., 1974; Spekkens et al., 2014; Putman et al., 2021). Importantly, it should be noted that these data support a "binary" relation, as opposed to a continuous trend. That is, if a galaxy is closer than around 300 kpc, it likely does not have gas. If a galaxy is further than around 300 kpc, it likely has gas. However, galaxies beyond this limit do not appear to have more gas (or higher gas fraction) the further from the host they are: there is no clear gradient in the colors of the points for the isolated galaxies with distance.

In Chapter 4, I concluded that the differences between the satellites and the

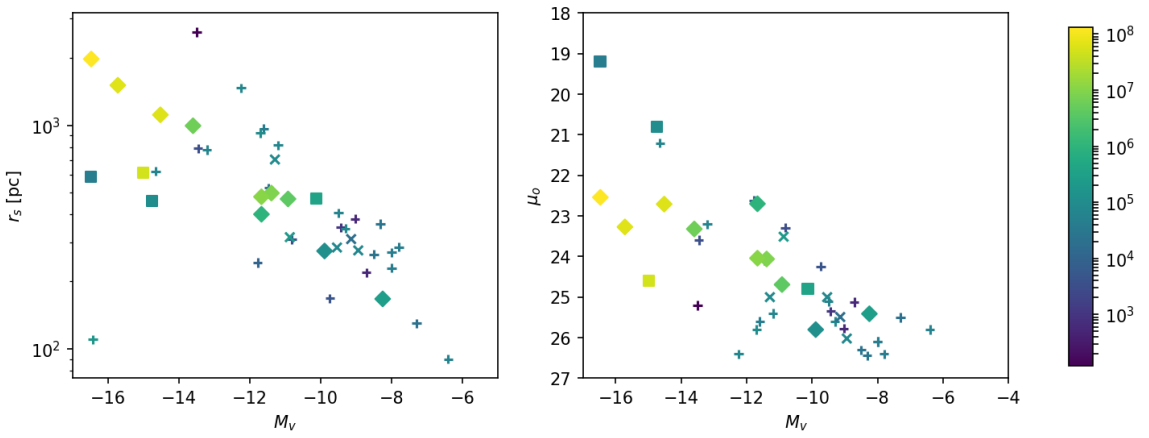

Figure 5.1: Similar to the top panels of Figure 4.3, but color-coded by M_{HI} ($M_\odot$), the HI mass of the dwarf, with values taken from Putman et al. (2021) (and references therein). Diamonds (or "x") are the isolated sample, and the squares (or "+") are the satellites of MW and M31. "x" and "+" denote values that are upper limits only.

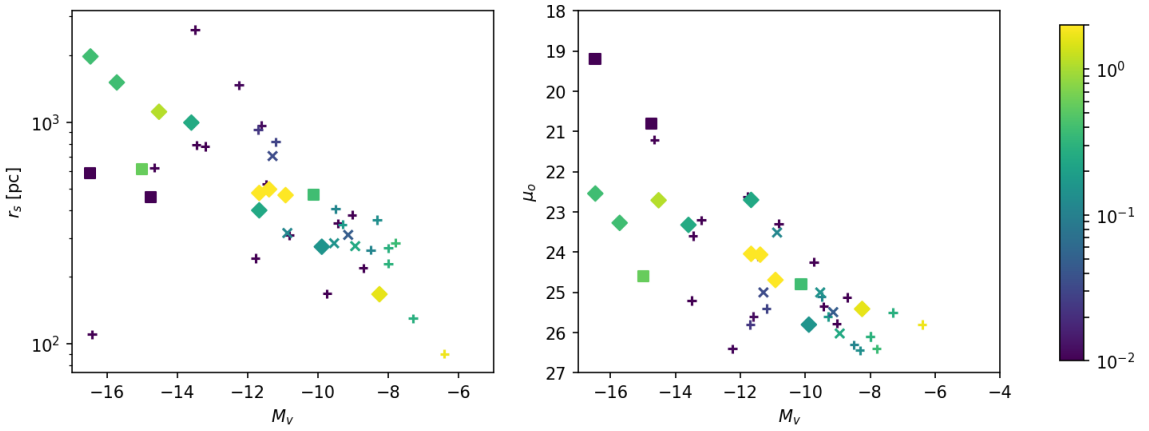

Figure 5.2: Similar to the top panels of Figure 4.3, but color-coded by M_{HI}/L_v [$M_\odot/L_\odot$]. Points are the same as in Figure 5.1.

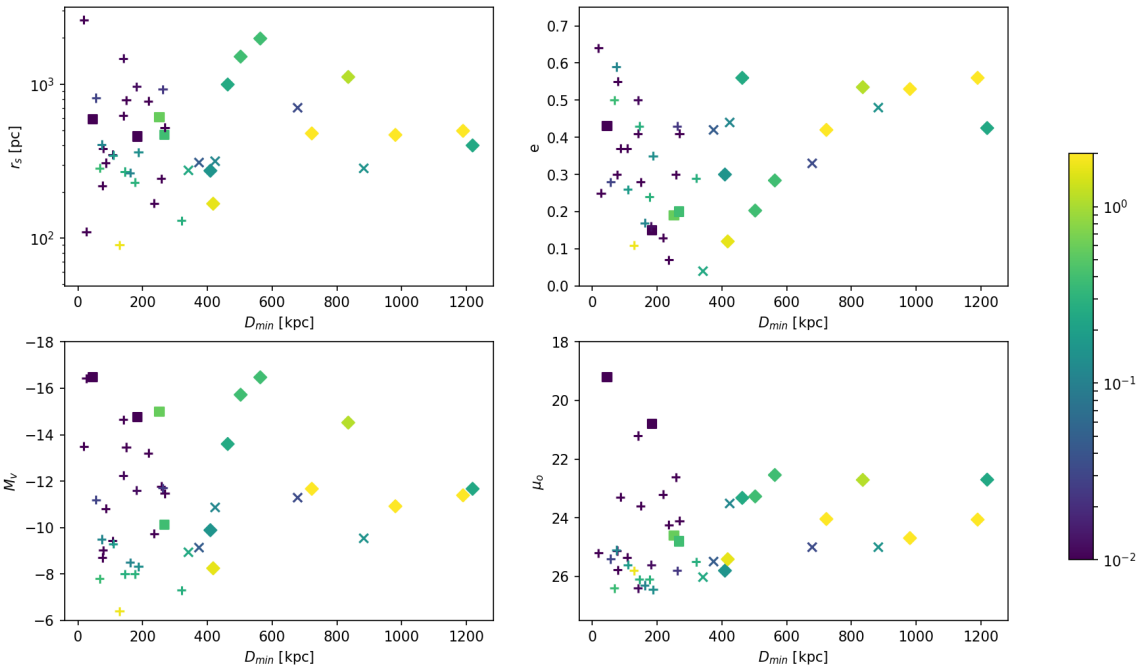

Figure 5.3: Analogous to the top panels of Figure 4.7 but coloured by M_{HI}/L_v $[M_\odot/L_\odot]$ from Putman et al. (2021) (and references therein). Points where M_{HI} is an upper limit are denoted with "x" and "+". As with Figure 4.3, the diamonds (or "x") are the isolated sample, and the squares (or "+") are the satellites of MW and M 31.

"isolated" galaxies set in around 400 kpc, at distances greater than the virial radius of the massive galaxies (in both cases, at approximately 300 kpc). Examination of Figure 5.3 cautiously suggests that, with respect to the gas content of galaxies, the 300 kpc boundary is more appropriate. Due to the (very) low number of dwarfs in this regime, it is clearly not possible to make this statement definitively. However, all of the purple points (essentially no HI gas) are within 300 kpc, and the closest dwarfs with obvious HI (i.e., not upper limits) are found at around 250 kpc (recall, the Magellanic Clouds, as very massive dwarfs, are not shown in this plot). Therefore, there is a tentative suggestion that the regime in which tides observably alter the stellar morphology of dwarfs extends to larger separations from the host galaxy than the regime in which ram pressure stripping removes HI. In some respects, this is not surprising given the very difference physics at play (gravitational interactions versus a hot gaseous halo).

It is worth comparing the Local Group to the more extreme Virgo Cluster environment for a moment. Weżgowiec et al. (2012) use X-ray observations of three galaxies in the Virgo cluster and determine if these galaxies have been predominantly affected by tides or by ram pressure stripping. They find that NGC 4254 (furthest from cluster center) is impacted by tides and not ram pressure stripping, NGC 4569 (closer to the cluster center) is likely influenced by ram pressure stripping and NGC 2276 (closest to the center) shows impacts of both effects, likely dominated by tidal effects. This seems to present a consistent case with the Local Group, where we tentatively propose that there may be a regime just beyond the virial radius where the influence of tidal effects can still be seem, but where there is little evidence of the effects of ram pressure stripping. Bear in mind that the mechanisms in each case are dramatically different, and assuming that both should occur at the same threshold at the virial radius (~ 300 kpc for MW and M 31) is an obvious over-simplification.

5.1.2 The star formation histories of dwarfs

In some respects, the previous analysis involving the current HI content of the dwarfs capture some, but not all, aspects of the dwarfs' star formation histories (SFHs), since galaxies that currently have HI usually have some star formation, whereas galaxies without HI cannot have any current star formation. However, the current gas content is not a good proxy for the historic gas content, and it is worth using a more careful metric to probe star formation at times earlier than the present.

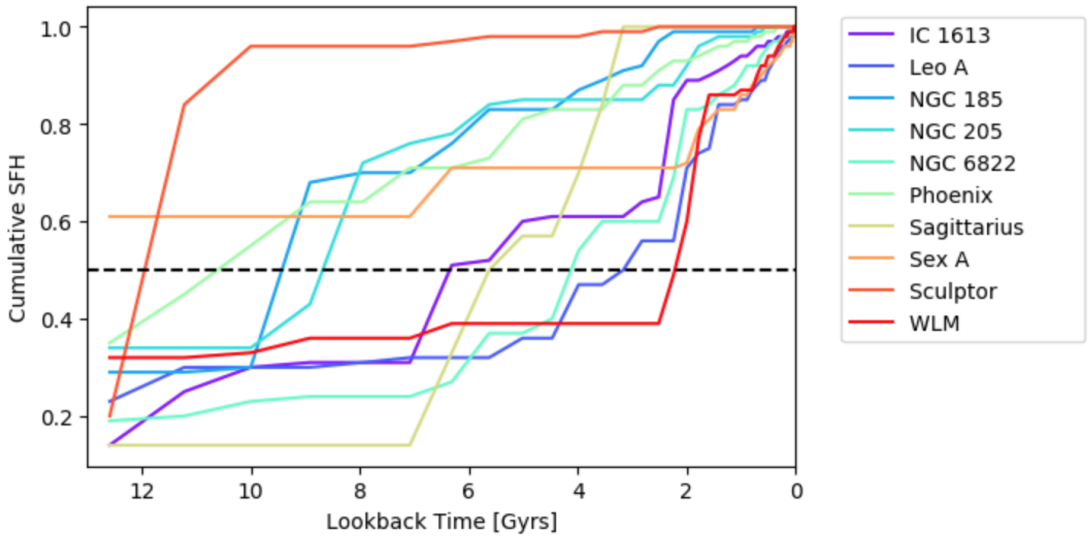

Figure 5.4: A selection of SFHs from Weisz et al. (2014). The dashed line indicates t_{50}, the lookback time when 50% of the stars have formed in the dwarf.

We use the SFHs of nearby dwarfs derived by Weisz et al. (2014, 2019b) (the latter also includes values directly from Skillman et al. 2017). These SFHs, with examples shown in Figure 5.4, are derived by combining single stellar population models to match an observed CMD. The observations required for this require a much deeper CMD than the Solo Survey, at the expense of the field of view. Weisz et al. (2014, 2019b) parameterize these SFHs using the quantity t_{50}, defined as the lookback time at which a dwarf has formed 50% of its stars. Dwarfs with an early burst of star formation, and which are quiescent after, will have an early/large t_{50} (e.g. Sculptor with $t_{50} = 11.9$ Gyrs) whereas those which have had mostly recent or on-going star formation will have a later/smaller t_{50} (e.g. WLM with $t_{50} = 2.2$ Gyrs). Figure 5.4 shows examples of some of the SFHs from Weisz et al. (2014), where I indicate t_{50} as a black dashed line. Clearly, t_{50} does not encapsulate the intricacies and complexities of the widely varying SFHs of the dwarfs but it does allow us to use a single, simple, parameter to explore the impact of historic star formation on a dwarf's observed structural parameters.

First, I compare the parameterized SFHs to the HI contents examined in the previous section. Figure 5.5 shows the HI mass and HI fraction as a function of t_{50}. There is not a simple correlation between these parameters, and most of the points are scattered (for both satellites and isolated systems). Both satellites and isolated systems can have a spread in values for t_{50}, but it is striking that only isolated dwarfs

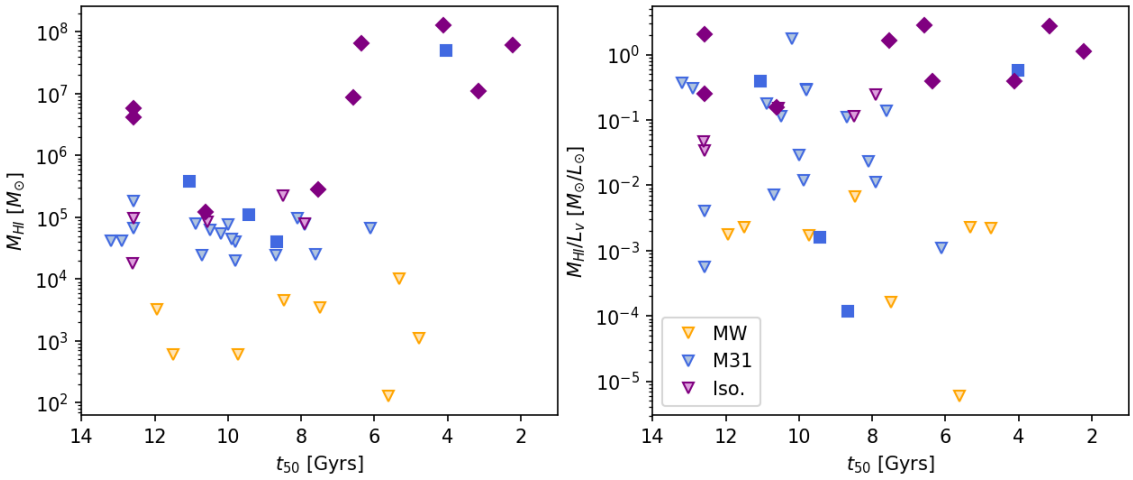

Figure 5.5: Comparing the HI mass and HI mass fraction to t_{50}. Points indicated with arrows are upper limits. The isolated sample is shown in purple, MW satellites are yellow and M 31 satellites are blue.

can have late t_{50} times ($t_{50} < 4$ Gyrs). It is also notable that many of the youngest galaxies have high absolute HI masses, but it is not a "clean" trend: a few other galaxies with HI masses this high have old ages, and a few of the younger (but not youngest) galaxies have no HI. As expected, the current presence of gas in a galaxy, or otherwise, is insufficient to make any claims as to the average age of the stars in the galaxy.

Figure 5.6 shows the same Kormendy relations shown previously, but the points are now color-coded by t_{50}. The dominant trend seen here is a slight correlation between t_{50} and M_v, with brighter dwarfs having a tendency to be younger (as defined by t_{50}). No trends are present in any of the other structural parameter plots that have not been reproduced here (e.g., with ellipticity, etc). Figure 5.7 shows the structural parameters as a function of distance, color-coded by t_{50}. Here, there is no clear trend that distinguishes the satellites and isolated dwarfs. That is, the "age" of the system does not appear to track with distance from the host, irrespective of whether it is a satellite or an isolated system. For example, the group of five isolated dwarfs (Phoenix, Leo T, Perseus, And XVIII and And XXVIII), previously identified as appearing similar to the satellites in terms of their structural properties, are not able to be distinguished by their ages, and look as much like the points to the left of them as they do to the points to the right of them.

In the SFH analysis by Weisz et al. (2014), they conclude by saying that the

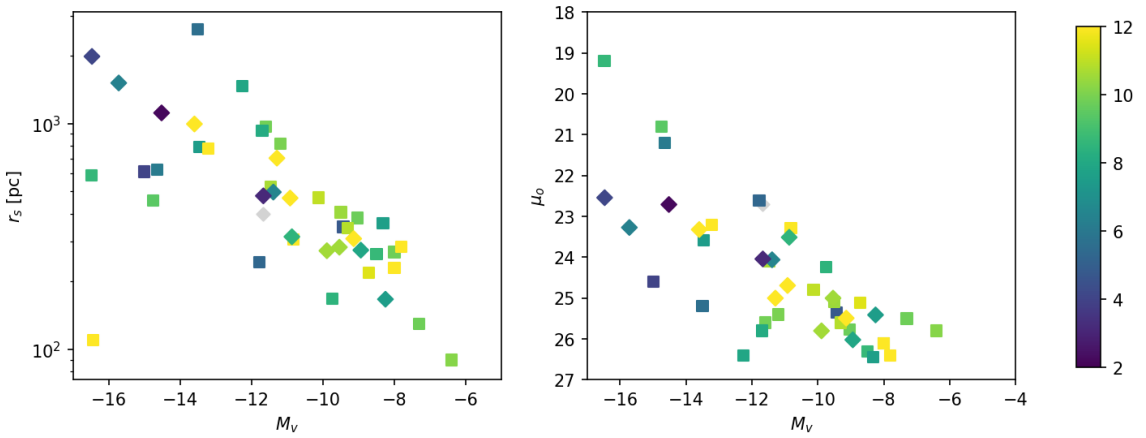

Figure 5.6: Analogous to top panels of Figure 4.3 but coloured by t_{50} from Weisz et al. (2014), Weisz et al. (2019a) (and Skillman et al. 2017 within). t_{50} is the lookback time when 50% of the stars have formed in the dwarf. The grey point is UGC 4879, which has no t_{50} value. As with Figure 4.3, the diamonds are the isolated sample, and the squares are the satellites of MW and M 31.

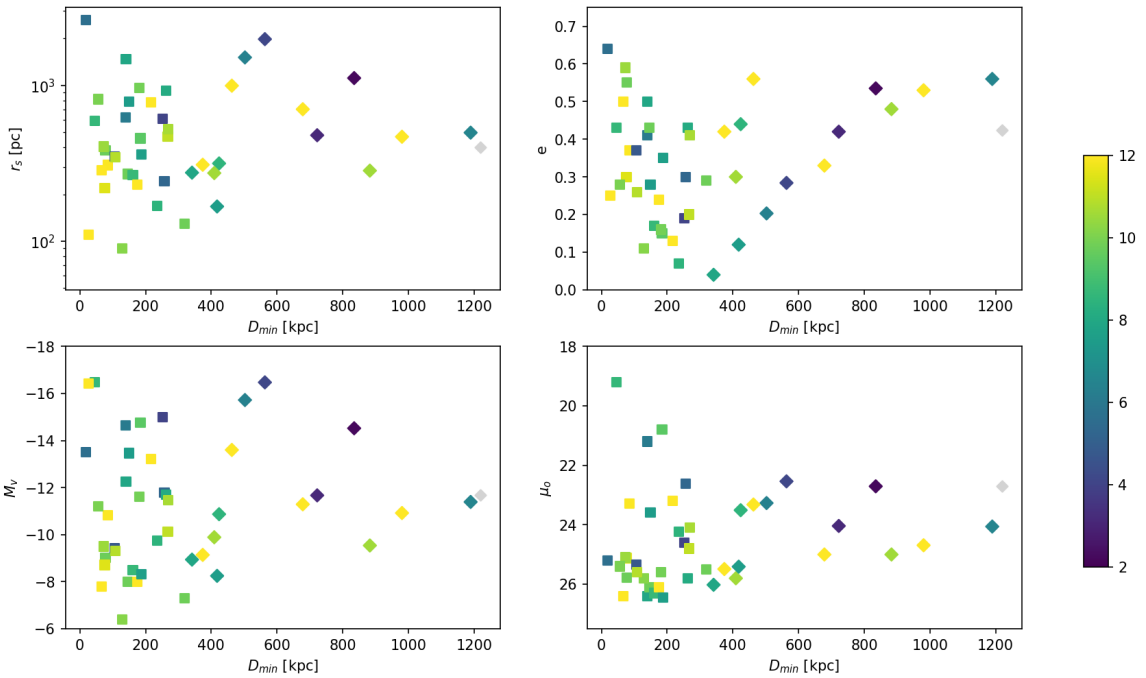

Figure 5.7: Analogous to top panels of Figure 4.7 but coloured by t_{50} from Weisz et al. (2014), Weisz et al. (2019a) (and Skillman et al. 2017 within). t_{50} is the lookback time when 50% of the stars have formed in the dwarf. The grey point is UGC 4879, which has no t_{50} value. As with Figure 4.7, the diamonds are the isolated sample, and the squares are the satellites of MW and M 31.

"[l]ower luminosity dSphs are less likely to have extended SFHs than higher luminosity dSphs. However, the modest scatter in the SFHs suggests that the trend is not a simple function of stellar mass, and that environmental effects (e.g., interaction history) have played an important role in shaping the evolutionary history of any given galaxy." Our brief analysis confirms the trend of age with stellar luminosity, but it does not point to any obvious correlation of age with environment, as least when quantified as distance from nearest massive host. It may well be that full orbital histories of these systems may be necessary to uncover any weaker correlations of age with environment that might exist, something that is now in the realm of possibility with the advent of Gaia and HST proper motion studies of these systems.

5.2 Substructure in the Solo Survey

The extended surroundings of dwarfs is a tantalizing regime in which to look for substructure, be it halos, streams/tidal tails, or faint satellites. I have explored the Solo dataset looking for evidence of interesting substructures, primarily defined as features that cannot be readily matched to a simple, one component fit to radial profiles of these galaxies, and these results are described in detail in Section 3.6. Some of the dwarfs show evidence of extended structure perhaps suggestive that they are not in dynamic equilibrium. Most obvious is UGC 4879 which clearly shows extensions along its semi-major axis ("wings"). Sag DIG also shows these wings while several dwarfs (specifically DDO 210, Leo A, IC 1613) are not ideally characterized by a single Sésric profile, with some "extra-tidal" stars present. Irwin & Hatzidimitriou 1995 posit that these "extra-tidal" stars in Milky Way dSphs may indicate that these stars are being stripped or are evidence that the dwarf is not in dynamic equilibrium. In contrast, we could consider these extended stars as part of a more complex dwarf structure (like Pucha et al. 2019 for IC 1613 or Vansevičius et al. 2004 for Leo A).

In this section, I expand on this previous analysis, but now specifically focus on searches for satellites of these dwarfs i.e., coherent stellar systems that otherwise appear detached from the main dwarf (in contrast to "wings" or extra-tidal stars).

5.2.1 Satellites of dwarfs

The hierarchical nature of galaxies is well established, with dwarfs representing the lowest mass end, and I have extensively discussed the Milky Way and M 31 satellite

dwarf populations. Scaling this to smaller masses, it is entirely plausible that Solo dwarfs could host their own satellites.

At the slightly larger end, there are many studies looking at the LMC and SMC and their satellites (Kallivayalil et al. 2018; Patel et al. 2020; Erkal & Belokurov 2020 among others), clearly showing that low mass galaxies can have their own satellites. Indeed, Wheeler et al. (2015) uses the FIRE simulations to show that dark matter halos appropriate for the Solo dwarfs can host sub-halos that are massive enough to contain baryons, implying that Solo dwarfs could have luminous satellites (rather than halos without a baryonic or stellar component). Such satellites would be at the extremely low mass end of the galaxy mass function, and so would be extremely susceptible to the full range of physical processes at play, particularly feedback from star formation and reionization. However, detection of satellites around isolated dwarfs would be of particular interest in showing, and possibly constraining, the lowest mass end of the galaxy hierarchy. Similar studies like Annibali et al. (2019) of the dwarf DDO 68 have explored this concept beyond the nearest isolated dwarfs. Due to their proximity and our ability to resolve individual stars, the Solo dwarfs present us with the best opportunity to detect the lowest mass satellites for an isolated dwarf and eventually place observational constraints on the presence/absence of these satellites.

Dooley et al. (2017) predict the number of candidate satellites of dwarfs expected to be seen in Solo given our field of view around each galaxy. They address the sensitivity of these extremely low masses by using 4 different abundance matching prescriptions (assigning a baryonic component to the dark matter halos) and include the impacts of reionization. Figure 5.8 shows the probability of a dwarf hosting at least one satellite above a given mass as a function of dwarf mass. Each colour represents a different abundance matching model and the dashed lines indicate the most massive dwarfs (including IC 1613 and NGC 6822).

Figure 5.8 makes clear that, for the most massive Solo dwarfs (notably NGC 6822 and IC 1613), there is a non-negligible possibility for there to be an observable satellite. Specifically, Table 5.1 summarizes results from Dooley et al. (2017), shows the minimum and maximum values (from their four models) for $\bar{N}_{fov}$ for the Solo dwarfs. $\bar{N}_{fov}$ is the mean number of satellites above a mass of $M_\star > 10^4 M_\odot$ within half a degree of the dwarf (i.e. within the Solo field of view). Perseus does not appear as Dooley et al. (2017) did not have a stellar mass available. For Leo T (the closest galaxy), Solo observes a maximum (projected) radius of around 3.5 kpc; and for UGC 4879 (the most distant galaxy), the corresponding radius is approximately 10 kpc.

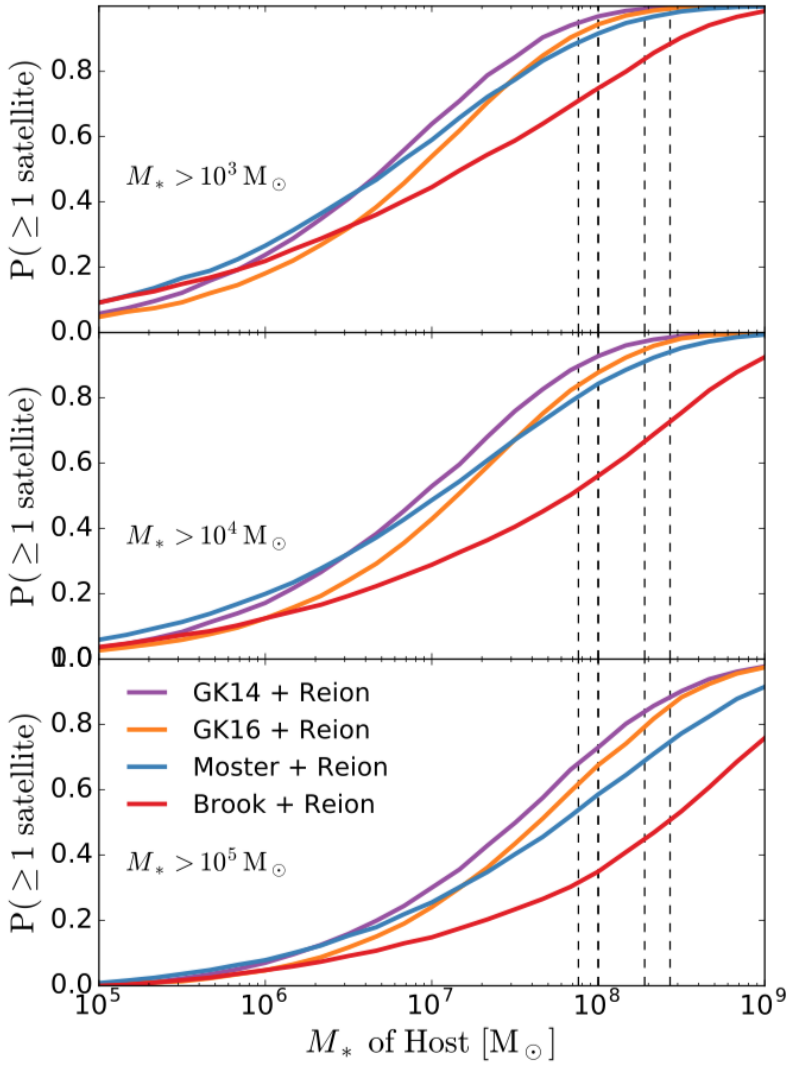

Figure 5.8: Figure 6 from Dooley et al. (2017), showing the probability of a dwarf (with a given stellar mass) hosting a satellite above a certain stellar mass ($M_\star > 10^3 M_\odot$, $M_\star > 10^4 M_\odot$ and $M_\star > 10^5 M_\odot$ from top to bottom respectively). Each colour is a different abundance matching model (with additional effects from reionization). The vertical dashed lines indicate the most massive field dwarfs (IC 5152, IC 4462, IC 1613, NGC 6822 and NGC 3109).

Name	Min. $\bar{N}_{fov}$	Max. $\bar{N}_{fov}$
And XXVIII	0.01	0.02
IC 1613 (DDO 8)	0.06	0.16
Phoenix	0.01	0.02
NGC 6822 (DDO 209)	0.02	0.07
Cetus	0.03	0.06
Peg DIG (DDO 216)	0.05	0.11
Leo T	0.01	0.03
WLM (DDO 221)	0.07	0.16
And XVIII	0.05	0.18
Leo A (DDO 69)	0.04	0.08
Aquarius (DDO 210)	0.05	0.09
Tucana	0.02	0.05
Sag DIG	0.05	0.11
UGC 4879 (VV 124)	0.10	0.21

Table 5.1: From Table 3 in Dooley et al. (2017), where $\bar{N}_{fov}$ is the mean number of satellites above a mass of $M_\star > 10^4 M_\odot$ within half a degree of the dwarf, with the minumum and maximum range selected from their four abundance matching models.

For each of the Solo dwarfs, the likelihood of them hosting a dwarf that could be observed is quite low. Dooley et al. (2017) predict that And XVII, And XXVIII, Sag DIG, Peg DIG and Leo A all have around a 10% chance of having a satellite in this region, and WLM, IC 1613 and UGC 4879 all have around a 10 – 20% chance of having a satellite in this region. Notably, NGC 6822, as one of the most massive dwarfs, has a relatively low probability due to the relatively small radius out to which we probe it. UGC 4879 has the highest chance, both due to its distance and mass.

Dooley et al. (2017) concludes "...we emphasize that discovering no satellites at all is highly unlikely. Nevertheless, a non-detection would imply at least two of the following: a very strong suppression of star formation by reionization, a low $M_\star$ – M_{halo} relationship for low mass galaxies, a $M_\star$ – M_{halo} relationship for galaxies with masses typical of field dwarfs, and a MW which has an abnormally large number of luminous satellites with $M_\star < 10^6 M_\odot$". Clearly, the pursuit of satellites of dwarfs is worth the challenge.

I look for satellites around each Solo dwarf via two methods. As with other structures around these galaxies, they are best traced by their resolved stellar populations. As such, Figures 3.10 and 3.11, which show the spatial distribution of the RGB stars, are especially useful. If we reasonably assume that candidate satellites around dwarfs are dominated by an older stellar population, then they should appear as overdensities

here (the selection of RGB stars for the candidate satellite would be the same as the dwarf as they should lying at largely the same distance). The statistical significance of any overdensity above the background level is quantified via Figures 3.12 and 3.13, which show the RGB star counts as contours above the background. Recall that the first contour in these figures is just 2σ above the background, so many "blobs" appear at this relatively low significance level.

In addition to the contour maps in Figures 3.12 and 3.13, we also explore the use of the OPTICS clustering algorithm (Ankerst et al. 1999; see its application to a similar dataset in McConnachie et al. 2018). OPTICS identifies overdensities relative to their surroundings, and has the nice feature of not requiring a specific spatial scale *a priori* over which it searches (for the contour maps, the choice of pixels and smoothing lengths imposes a spatial scale on which these maps are most sensitive). OPTICS is similar in methodology to other connectivity-based clustering algorithms such as DBSCAN (Ester et al. 1996). However, OPTICS only requires one user-specified parameter (N_{min}); the minimum number of points that can define a substructure. The algorithm works by reordering data such that points in the same neighborhood are physically close together on the x-axis of a dendrogram. The y-axis of the dendrogram is the "reachability distance" of each star, which is the minimum distance required for that star to be considered a member of a cluster with at least N_{min} members. Constructed in this way, physical overdensities stand out in the dendrogram as "valleys", or neighborhoods in which the density is clearly higher than its surroundings. More details on OPTICS can be found in Sans Fuentes et al. (2017); McConnachie et al. (2018) and Oliver et al. (2020). Applied to our problem, we can follow up all major substructures identified in this way by constructing a CMD of the points, and determining if they look like a coherent stellar population.

We searched all the satellites in this way, inspecting both the contour maps and the results of the application of the OPTICS algorithm. In the majority of cases, no convincing evidence of satellites or other concentrated substructures are found around any of the galaxies to our surface brightness limits (around 30 – 32 mags sq.arcsec), with one possible notable exception. We do not go through all of our null detections, for the sake of brevity, but instead we concentrate on two of the dwarfs with the most interesting results (UGC 4879 and Perseus), although only in the latter do we conclude that we might possibly have a real detection.

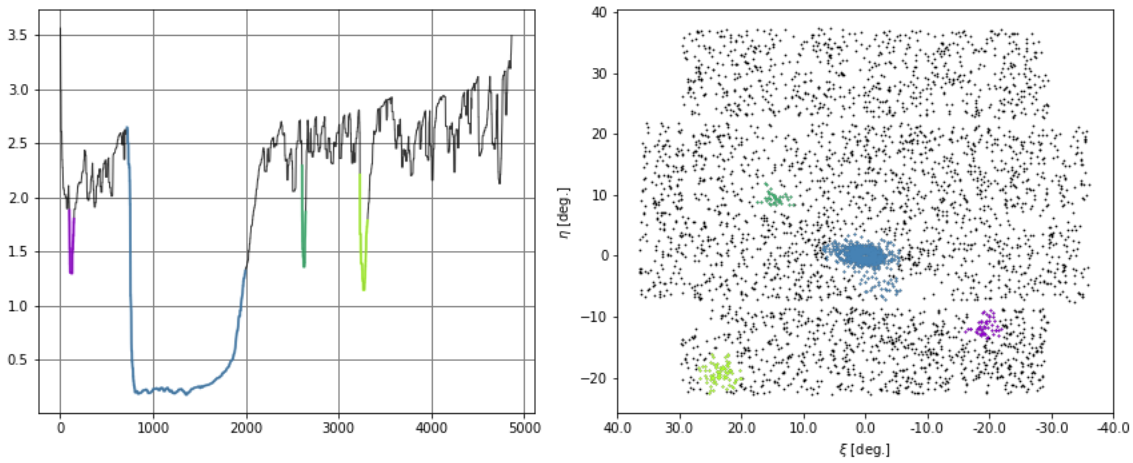

Figure 5.9: Left panel: OPTICS dendrogram of RGB stars in UGC 4879. Valleys are overdensities relative to their surroundings. Right panel: spatial distribution of the RGB stars, where the colours of the stars correspond to the colours of the line in the left panel.

UGC 4879's blobs

UGC 4879 is an interesting case to examine: it has the "wings" mentioned earlier, and it is the most likely to have a satellite according to the analysis by Dooley et al. (2017). Indeed, the RGB maps from Chapter 3 reveal it has intriguing overdensities in its vicinity, clearly visibly in Figure 3.10 at ($\xi \simeq 15', \eta \simeq 10'$) and ($\xi \simeq 23', \eta \simeq -20'$). Indeed, one of these overdensities is along a similar axis as the "wings", which might suggest a common origin. For example, this could point towards UGC 4879 being a less isolated dwarf than it first appears to be, perhaps with its own companion.

We apply the OPTICS algorithm applied to the spatial positions of the RGB stars for UGC 4879. The left panel of Figure 5.9 shows the resulting dendrogram, where clustered points stand out as valleys. The algorithm clearly identifies four significant overdensities, which correspond to the spatial groupings of stars identified in the right panel. Here, the colours of the points in the right panel correspond to the colours of the line in the left panel. The biggest of the four valleys in the dendrogram corresponds to the main body of the dwarf. Two of the other valleys correspond to the previous features highlighted in the RGB map in Figure 3.10. OPTICS also identifies a third, more subtle overdensity.

To follow up on each feature, we construct a CMD of all stellar sources spatially overlapping with the region identified by OPTICS. We also look at the original images.

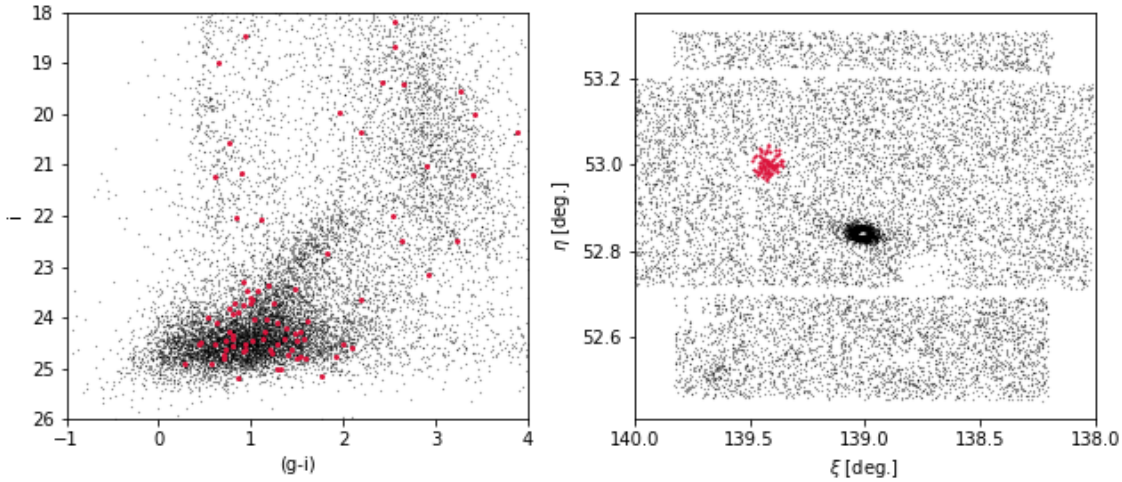

Figure 5.10: CMD and spatial distribution of all stars overlapping spatially with the position of one of the overdensities identified around UGC 4879 are shown in red. Grey points correspond to all stars in the Solo field of view.

In the case of a clear positive detection, we would see a clear RGB, with a few brighter RGB and many fainter RGB, consistent with the luminosity function and stellar populations of an older stellar system. An example of what we actually see is shown in Figure 5.10 for one of the blobs. We do not see any suggestion of a coherent stellar population here - the absence of any brighter RGB candidates given the number of fainter sources is especially notable, and this leaves us to conclude that this particular blob is not a compelling satellite candidate. For the sake of brevity, I do not reproduce the same figures for each of the other overdensities identified by OPTICS, however the conclusion is the same for each.

Perseus's friend

For Perseus, the feature in the contour map of the density of RGB stars in Figure 3.12 at ($\xi \simeq -5', \eta \simeq -2.5'$) appears reasonably significant, with the contours reaching up to $5\,\sigma$ above the background. We run OPTICS on the RGB spatial distribution as before and we show the results in the left panel of Figure 5.11. The right panel shows the corresponding spatial distribution of the points corresponding to each of the highlighted valleys in the left panel. Interestingly, from the OPTICS algorithm, the prominent group of stars visible in the isophote map is not particularly obvious as a stand-out feature in the OPTICS dendrogram, although it is present, mostly as a small dip within the larger valley (OPTICS can identify substructure within a

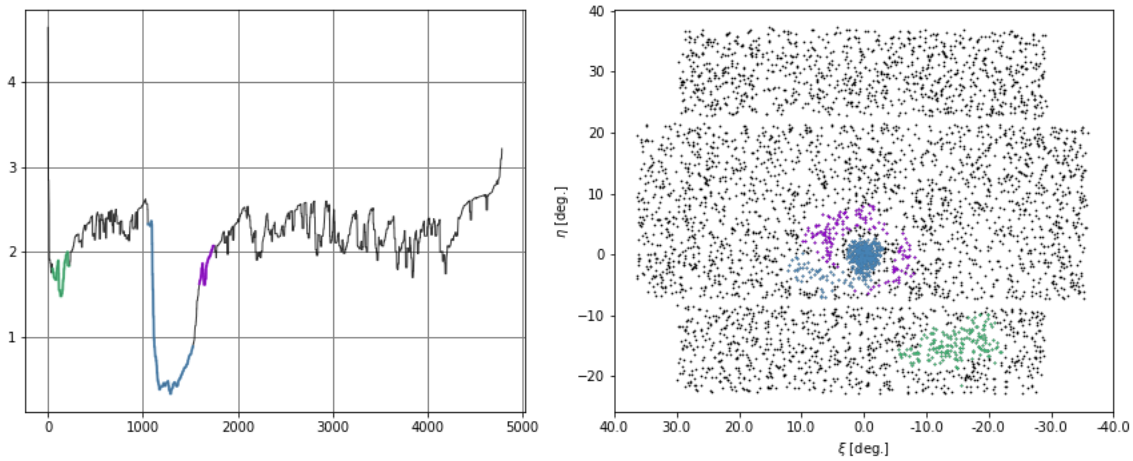

Figure 5.11: Left panel: OPTICS dendrogram of RGB stars in Perseus. Valleys are overdensities relative to their surroundings. Right panel: spatial distribution of the RGB stars, where the colors of the stars correspond to the colors of the line in the left panel.

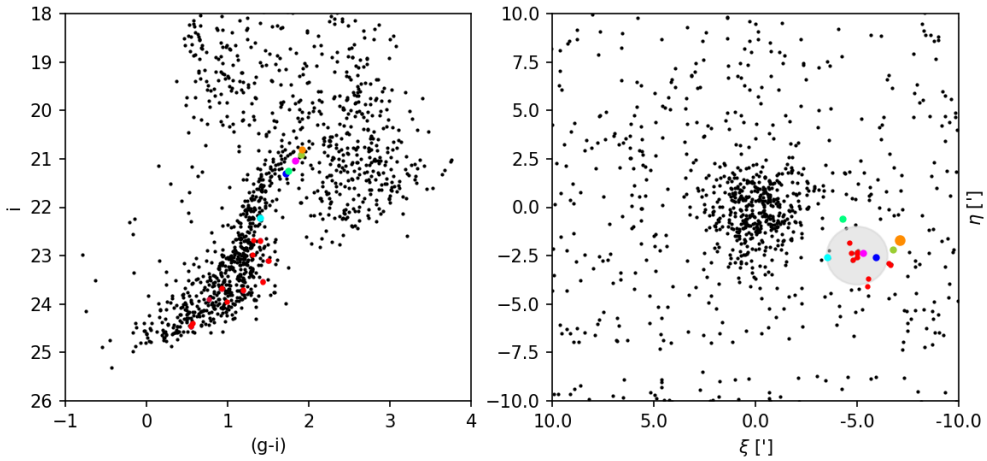

Figure 5.12: On the left, the CMD for Perseus (in black) with the RGB stars selected from the overdensity over plotted in colour. On the right, the spatial distribution of RGB stars, centered on Perseus, with the same stars highlighted in colour. The grey shading represents the overdensity as seen in the contours.

substructure, which appears in the dendrogram as a valley within a valley). Also identified at significant levels are the main body of the galaxy, and a large diffuse blob. CMD analysis of the latter does not imply it is a strong candidate for a real satellite.

For the feature that is prominent in the isophote map, we do find a very subtle suggestion of an RGB, shown in Figure 5.12. The grey shaded region shows the approximate overdensity from the contour plot. We can see that, in this region, there a few stars (in colour) that trace a possible RGB. I compare this CMD with other CMDs of random regions, of the same size and separation from Perseus, as controls, and this candidate feature is certainly unusual. The few bright stars that are present (with the numerous fainter stars) appear to trace out a path in color-magnitude space that could be consistent with a narrow RGB. Inspection of the image does not reveal any obvious feature like a star cluster, implying that this is a plausible candidate for a satellite of the Perseus dwarf galaxy.

However, this detection seems less plausible when we select all stars (not just RGB stars) in the region just within the over density, as shown in Figure 5.13. Now we see the CMD and spatial distribution and the possible RGB branch is much less convincing. It is important to note that Perseus itself (which is a clear and obvious object) is also essentially indistinguishable in the CMD, while apparent in the stellar

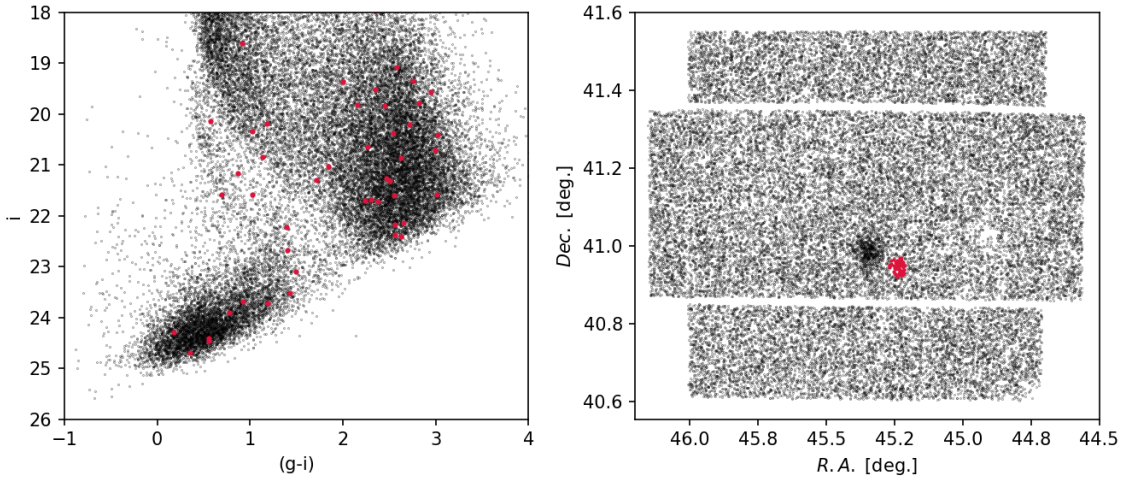

Figure 5.13: On the left, the CMD for all stars in the Perseus field of view (in black) with stars selected from the overdensity over plotted in red. The right panel shows the spatial distribution of all the stars, with the over density again coloured red.

distribution.

This tentative detection requires follow up, specifically deeper photometry to confirm its reality and spectroscopy to determine if it corresponds to a dynamically cold stellar population. This marginal and subtle detection emphasizes again the real challenge to detect objects of this type, and the various methods that must be employed to search for them. It also emphasizes the challenges in establishing a spatially complete sample of isolated dwarfs to faint magnitude limits.

5.2.2 Globular clusters in dwarfs

Having searched for satellite galaxies to the Solo dwarfs, it is natural to enquire as to the prevalence, or otherwise, of globular clusters around these galaxies. After all, the Milky Way's outer halo GC population is believed to have largely been accreted via disrupted dwarf galaxies. Around M 31, the PAndAS has revealed very strong evidence for the majority of GCs beyond ∼30 kpc being originally associated with dwarfs of a range of masses (Mackey et al., 2010; Veljanoski et al., 2014).

Despite the importance of nearby dwarfs as a source of Galactic GCs, remarkably few GCs are known around Local Group dwarfs (excluding the Magellanic Clouds and M 33). The Sagittarius dSph likely has/had 5 GCs (e.g., see discussion in Bellazzini et al. 2020, and the Fornax dSph has 6 (see discussion in Huang & Koposov 2021).

NGC 6822 has 8 reported GCs, and WLM has one. Some star clusters have been reported around IC10 (Lim & Lee, 2015), although it is unclear how many of these are GCs, similarly with a young stellar cluster in Leo A (Stonkutė et al., 2015). DDO 210 is known to have a GC, while the recently discovered Eri II also has a cluster (which is notable due to Eri II's low mass; see discussion in Crnojević et al. 2016). Andromeda I has also been shown to have a GC (Caldwell et al. 2017) as well as Peg DIG's GC (Cole et al., 2017; Leaman et al., 2020). This is almost a complete inventory of known GCs in isolated Local group dwarfs. The extent to which the dearth of GCs in Local Group dwarfs is evidence for a physical absence of GCs is difficult to quantify given the lack of any systematic study.

The Solo Survey is an ideal data set to systematically identify the presence (or absence) of GCs in the nearest but unperturbed dwarf galaxies. I have conducted a first examination of the feasibility of finding GCs around Solo dwarfs, by looking at a few dwarfs with known GCs (NGC 6822 and WLM) to determine if the known population could be retrieved. GCs at distances of $\sim 500 - 1$ Mpc are notoriously difficult to identify since they may be fully resolved, fully unresolved or partially resolved into stars depending on their spatial extent (see Cockcroft et al. 2011 for a discussion).

Our identification technique is based upon the PAndAS survey (Huxor et al., 2014) that has successfully identified nearly 100 GCs in the halo of M 31 based on near-identical data to that of Solo. Previous work has confirmed 8 GCs around NGC 6822 (see Hubble 1925; Krienke & Hodge 2004; Hwang et al. 2011; Huxor et al. 2013 with follow up by Veljanoski et al. 2015). We successfully identified all 6 known GCs that fall within our field of view around NGC 6822, shown in Figure 5.14, in the $i-$band. We also find ten novel GC candidates, with the three most likely candidates shown in Figure 5.15, in the $u-, g-$ and $i-$bands.

The candidates identified in NGC 6822 and shown here are the most likely GCs in the Solo dataset, with by-eye searches of the other dwarfs resulting in few likely candidates. Requests for follow-up observations to try to better determine the reality, or otherwise, of the Solo GC candidates in NGC 6822, have been pursued and are on-going. As with the search for satellites to dwarfs, identifying (or systematically ruling out the presence of) GCs remains an elusive task.

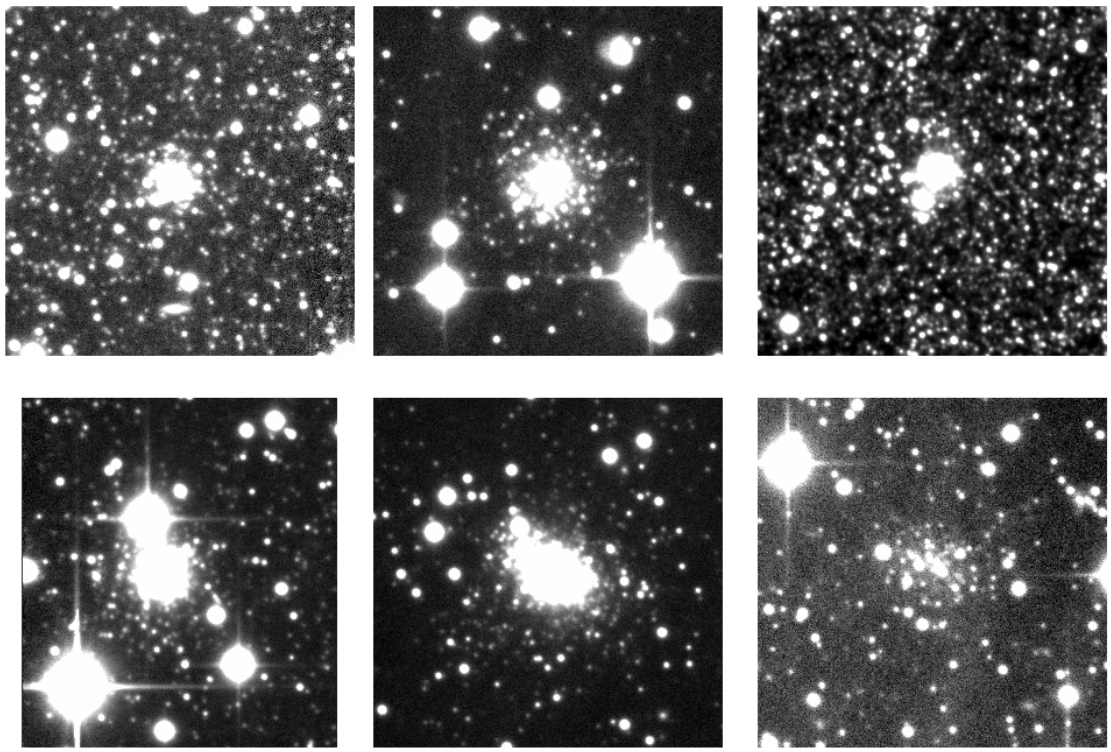

Figure 5.14: The 6 known GCs in NGC 6822, shown in the $i-$band from the Solo observations.

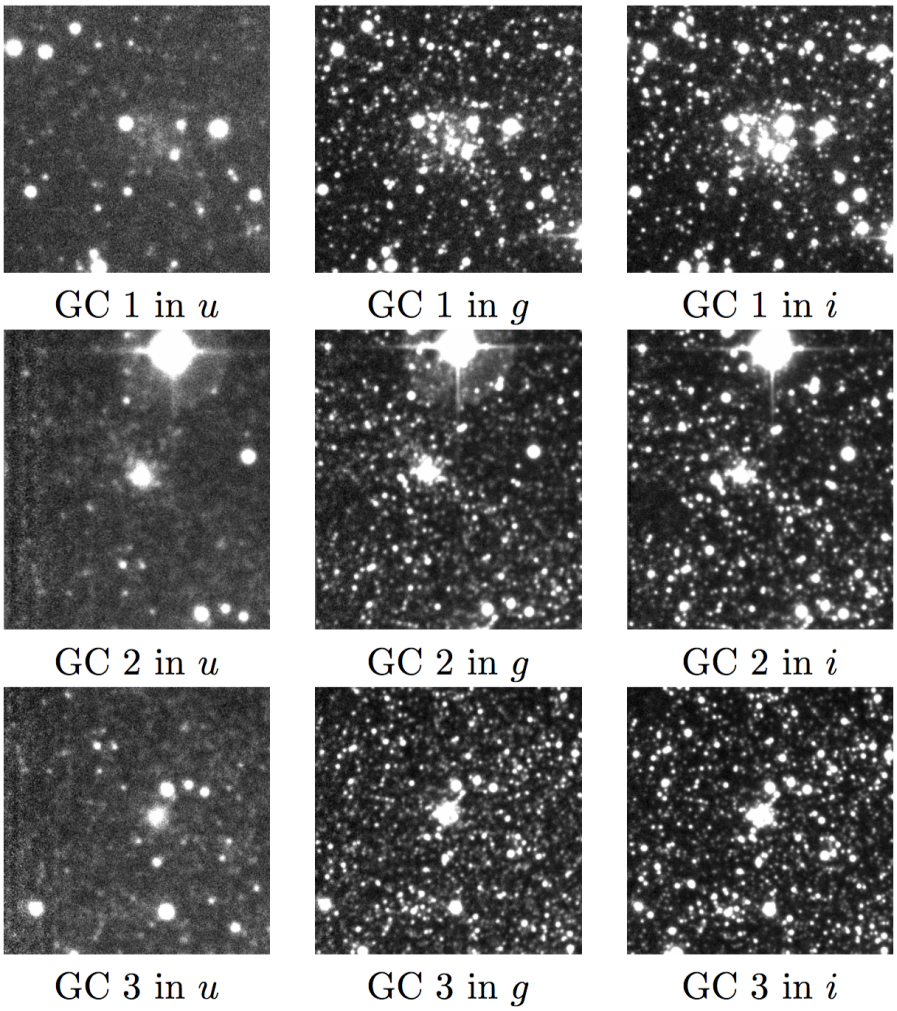

Figure 5.15: Three candidate GCs in NGC 6822 (out of 10 candidates in total), shown in $u-, g-$ and $i-$band from the Solo observations.

5.3 Conclusions

Our focus here has been to incorporate HI and stellar ages into our analysis, with the intent of gaining insight into star formation and its effects on the Local Group dwarf population. We recover the well known distance-morphology relation, where dwarfs within ~ 300 kpc are generally devoid of HI gas, but those more distant generally have gas. But the relation is binary, insofar as the 300 kpc threshold essentially only distinguishes the "haves" from the "have-nots", and that there is not a trend such that beyond this radius, more isolated systems are more gas rich. We also propose that there is very weak observational evidence to suggest that the regime of ram-pressure stripping does not extend as far as the regime of gravitational (tidal) interactions. For both HI and stellar ages, the dominant (only) trend that we observe is with luminosity, such that brighter systems generally have younger ages and more gas. Note, there is no evidence to suggest that brighter systems generally have higher gas *fractions*. Environment, at least as characterised by the distance to the nearest large galaxy, does not appear to have any impact on stellar ages, as defined by t_{50}. The existence of trends between environment and star formation histories seems a reasonable expectation, however, and it might be that more detailed parameterizations of SFHs and of environment, will be required if we are to observationally uncover such relationships in the Local Group.

Additionally, we look for satellites around the Solo dwarfs, utilizing the large field of view to look for satellite galaxies and to conduct a preliminary investigation of the suitability of our data for globular cluster surveys. We find a hint of a possible candidate dwarf galaxy in the vicinity of Perseus, and are using this to motivate follow up imaging and spectroscopy to confirm its reality and derive its basic properties. No other clear candidate satellite galaxies exist around the Solo dwarfs to the limiting surface brightness of our survey, and this is generally consistent with expectations on the frequency of satellites around dwarf galaxies. With respect to globular clusters, we recover the known GC population of NGC 6822 and identify 10 new candidate clusters. This highlights the great merit in GCs searches around nearby dwarfs using the Solo dataset, which could provide a deep and systematic study, but which is well beyond the scope of this current exercise.

Chapter 6

Conclusions

6.1 In summary

Using the Solo Survey, I have gained insights into the impact of massive host galaxies on dwarf galaxy evolution. The detailed structural analysis from Chapter 3 generated a foundation upon which I based comparisons to the satellite dwarfs of the MW and M 31, studied in detail in Chapter 4 and expanded on in Chapter 5.

For each of the 12 dwarfs analyzed in detail in **Chapter 3**, their resolved RGB stars were used in combination with integrated light to parameterize their structure, quantifying their extent (Sérsic radius), shape (ellipticity), size (central surface brightness and absolute magnitude), and environment (distance using the TRGB). The resulting parameters were found to be, generally, in agreement with previous studies, with some exceptions. Further, these parameters were now derived in a consistent manner across this diverse dataset. Using the resolved stars, the faint, highly extended regions were examined for evidence of interactions and other features. Each dwarf was fit with both a single Sérsic profile and a combination of two Sérsic profiles to explore the presence of substructures (e.g., "bulge and disk", stellar halos, etc), finding that they are generally best fit as a population with a single component. Despite the large variations in luminosity (Leo T with $M_v = -8.5$ to NGC 6822 with $M_v = -16.5$) and size ($r_s \approx 170\,\mathrm{pc}$ to $r_s \approx 1800\,\mathrm{pc}$ for Leo T and NGC 6822 respectively), the same analysis was applied to all Solo dwarfs, allowing for comparisons within, and beyond, the Solo dataset.

The limited number of dwarfs observable in the Local Group increases the importance of this homogeneous analysis. Without careful consideration, we can easily

emphasize "irrelevant" differences, comparing "apples-to-oranges". Specifically, many of the Solo dwarfs are dominated by their young, blue, centrally concentrated stellar populations, as they are primarily dIrrs. In contrast, the satellites are mostly dSphs and generally have only older stellar populations. It has been well understood that dIrrs and dSphs are different, and it is not the point of this thesis to rediscover this difference. Differences between the brightest stellar populations in dIrrs and dSphs can also permeate to the dynamical mass estimates (and mass-to-light ratios), as the M_{dyn} depends on the radius and velocity dispersion. The velocity dispersion is measured using the RGB stars in all galaxy types. However, for the dIrrs, the radius measured should be that of the same population (the RGB stars), rather than the more centrally concentrated, younger, brighter population. Radii measured using the integrated light, or by not specifically selecting the older stars, are likely to be biased towards the younger population. My emphasis on the RGB stars generates a consistent and reliable focus on the old stellar populations of all galaxies, permitting like-with-like comparisons, measuring "apples-to-apples".

The homogeneous set of derived parameters was then compared to the satellites of the MW and M 31 in **Chapter 4** using the MegaCam Survey of Outer Halo objects (MSOHO; Muñoz et al. 2018a,b) and the Pan-Andromeda Survey (PAndAS; McConnachie et al. 2009; Martin et al. 2016), with additional dwarfs included from the compilation of McConnachie (2012). We also considered their global dynamical properties, including their velocity dispersions, implied dark matter masses, and mass-to-light ratios. Together, we consider all Local Group dwarfs with $M_v \leq -6$ and $\mu_o < 26.5\,\mathrm{mags\,arcsec^{-2}}$.

The main conclusions from these comparisons are:

- There is no statistically significant difference between the satellite and isolated dwarf populations. The satellites of the MW and M 31 are consistent with each other. This consistency indicates that isolated and satellite dwarfs are not distinguishable by one observed parameter, and the impact of a massive host does not cause an observed shift in properties (using the properties measured here.

- Within our selection criteria ($M_v \leq -6$ and $\mu_o < 26.5\,\mathrm{mags\,arcsec^{-2}}$ and fainter than the SMC), there are notably more satellites of M 31 as opposed to MW by a factor of ~ 3. This difference is larger than expected given the possible obstruction of MW satellites by the MW itself, perhaps indicative of M 31's

more active merger history.

- We see evidence for an increase in the scatter between related parameters in the Kormendy relations for the satellite dwarfs as compared to the isolated population. Specifically, isolated Local Group dwarf galaxies appear to show a tighter trend of half-light radius versus magnitude than the satellite population, and similar effects are also seen for related and derived parameters (i.e., surface brightness, dynamical mass, and mass-to-light ratio). This scattering suggests that massive galaxies do, indeed, alter nearby dwarfs and these changes increase the diversity of properties of the satellites.

- We observe a lack of dwarfs with $e \lesssim 0.3$ far from massive galaxies. This surprising lack of dwarfs with an apparently circular structure is not due to completeness.

- There appears to be a transition in the structural and dynamical properties of the dwarf galaxy population at around $D_{min} \sim 400\,\mathrm{kpc}$ from the MW and M 31, such that the dwarf population closer than this occupy a broader range of parameter space compared to dwarfs further away. This boundary is not aligned with the well-observed transition from dIrrs to dSphs around $\sim 300\,\mathrm{kpc}$.

Our comparisons of the isolated and satellite dwarfs emphasizes the "chaotic" influences of tides. Specifically, we find that tides do not produce systematic shifts in the values of the parameters but rather increase the scattering in trends between parameters. Figure 6.1 from Łokas et al. (2011) shows simulations of the evolution of a dwarf's ellipticity during an interaction with a massive host. The "scattering" that they observe is reflected in our results here.

Applebaum et al. (2021) use the the Mint Condition DC Justice League Simulations, looking at very low mass dwarfs around MW-type galaxies. They find "one of the primary drivers of the variety seen in nearby galaxies is due to interaction with the Milky Way galaxy". This agrees with our observations of Local Group dwarfs.

I have discussed at length the limitations of the small number of dwarfs observable, the possibility of backsplash galaxies, and observational completeness. I argue that each of these challenges has been minimized and appropriately addressed and the results are as robust as possible given the known population of dwarfs.

In **Chapter 5**, we extend beyond comparisons involving the structural and dynamical properties of the dwarf populations, to consider the dwarfs' HI gas content

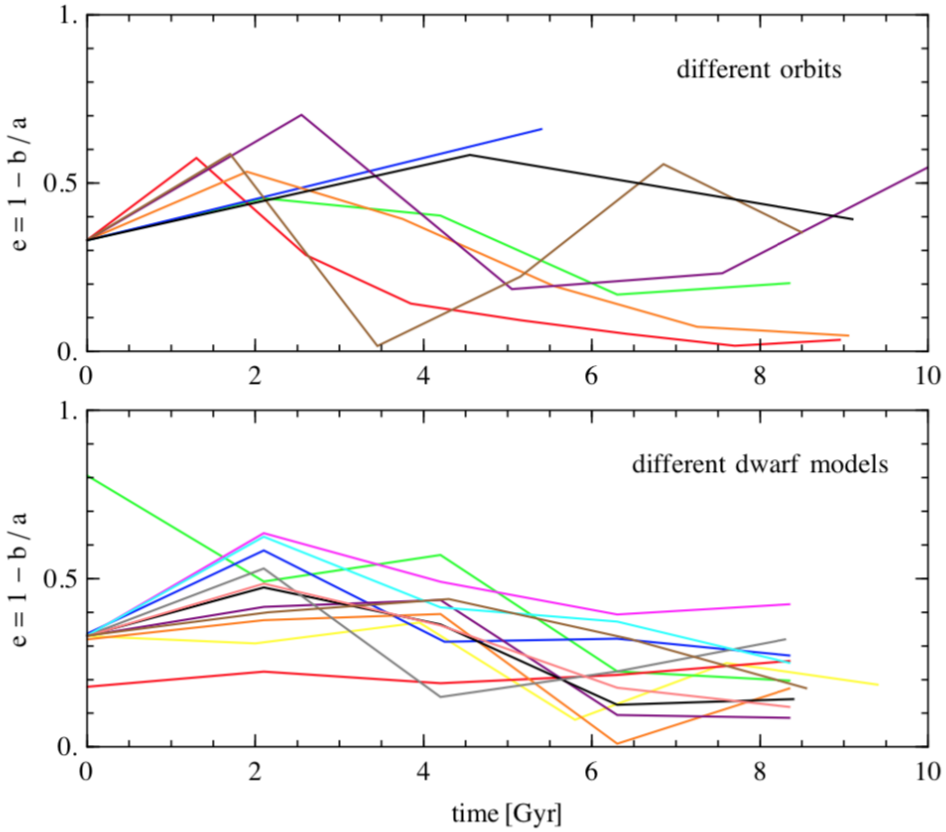

Figure 6.1: From Łokas et al. (2011), showing the evolution of a dwarf's ellipicity during an interaction with a massive galaxy, for different dwarf orbits (top) and different dwarf models (bottom).

and their star formation histories. Finally, we search for companions around the dwarfs, both in terms of dwarf galaxy satellites and globular cluster populations.

With respect to the gas content and star formation histories of dwarfs, I draw the following conclusions:

- The well studied distance-morphology relation, where dwarfs within ~ 300 kpc are devoid of HI gas, is recovered. The ~ 300 kpc boundary aligns with the virial radius of the MW/M 31, rather than the ~ 400 kpc seen in the structural analysis.

- We see a clear relation between M_v and both t_{50} and HI mass, finding brighter dwarfs have more recent SF and more HI, while the HI fraction shows no trend.

- While both the satellites and isolated dwarfs have a range in t_{50}, we find that only the isolated dwarfs have late t_{50} times.

- We do not find obvious distinctions between satellites and isolated dwarfs in terms of their SFH/"age" (t_{50}) or HI mass/fraction.

Together, these results suggest that environment plays a significant role in the presence/lack of HI gas, but we do not observe more subtle trends with isolation.

Given the hierarchical nature of galaxy formation, we expect dwarfs to have some satellites. The number and masses of these satellites are a direct constraint on how far down in mass the hierarchy extends. Further, the presence of satellites or tidal tails or other extended features could call these dwarfs' apparent isolation into question. Throughout this work, I have considered isolation as the separation of a dwarf from a more massive galaxy, however, a dwarf can clearly have it's own satellites, which could, in theory, cause observable morphological changes. Our wide field observations are ideal for searches of these satellites, but I only find one possible candidate for a dwarf galaxy satellite: a faint overdensity near the Perseus dwarf. My searches illustrate the challenges of finding, and later confirming, these extremely faint sources. My "by-eye" searches for GCs find a handful of candidates in NGC 6822 (and retrieve the known GCs) and illustrate the usefulness of Solo in this regard. My preliminary finding suggest that there are few compelling candidates in the other Local Group dwarfs, although this needs to be revisited using a more robust identification methodology, something that is beyond the scope of this current study.

6.2 Dwarfs in the Local Group in the future

A notable consideration throughout this analysis has been the issue of completeness. I have carefully selected the isolated and satellite populations compared to minimize differential completeness effects. I argue that the results are likely robust to this effect. This analysis benefits from the fact that the populations of known dwarfs has recently massively increased due to wider, deeper, more complete or more extensive surveys (e.g. SDSS; Willman et al. 2005; Belokurov et al. 2007 and DES; Bechtol et al. 2015; Koposov et al. 2015), especially with respect to the satellite population. Any further increase in the number of known isolated Local Group dwarfs would be a welcome addition, as there are indications that there are potentially a significant number of dwarfs remain yet to be discovered (e.g. see discussion in Fattahi et al. 2020; Garrison-Kimmel et al. 2019; Newton et al. 2018).

The benefits of more complete surveys including fainting objects are twofold. First and most simply, with an increased number of galaxies, our statistics improve. Certainly, the limited number of isolated dwarfs studied limits the statistical significance of the conclusions drawn. Secondly, robust completeness limits with surface brightness and/or magnitude are essential. In Chapter 4, much care was taken to appropriately compare the three groups (isolated dwarfs, MW and M31 satellites) despite the distinctly different selection effects affecting each population. For the MW, we can see much fainter satellites as compared to M 31, with the isolated dwarfs are at distances more analogous to M31. I used a surface brightness limit of 26.5 mags. arcsec^{-2}, as established by Whiting et al. (2007), for the isolated dwarfs. This is similar to what Carlsten et al. (2021) quotes as the 90% completeness limit, 26.0 – 26.5 mags. arcsec^{-2}, around 10 massive galaxies in the Local Volume, observed with CFHT imaging.

Our adopted surface brightness threshold appears to be a conservative limit for completeness in the Local Group, particularly for the satellites of the MW and M 31 where there are a considerable number of satellites fainter than this threshold. Specifically, the number of MW satellites increases from 8 to 11, M31 satellites from 21 to 32 and isolated dwarfs from 15 to 16 by altering the surface brightness limit from 26.5 to 28.5 mag. arcsec^{-2}. Establishing a deeper, robust, completeness limit will allow us to extend these comparisons to even smaller dwarfs. Furthermore, establishing a deficit (or excess) of the faintest dwarfs will assist in placing the MW, M 31 and, indeed the whole Local Group, in the context of other systems (e.g, Geha et al. 2017; Smercina et al. 2018).

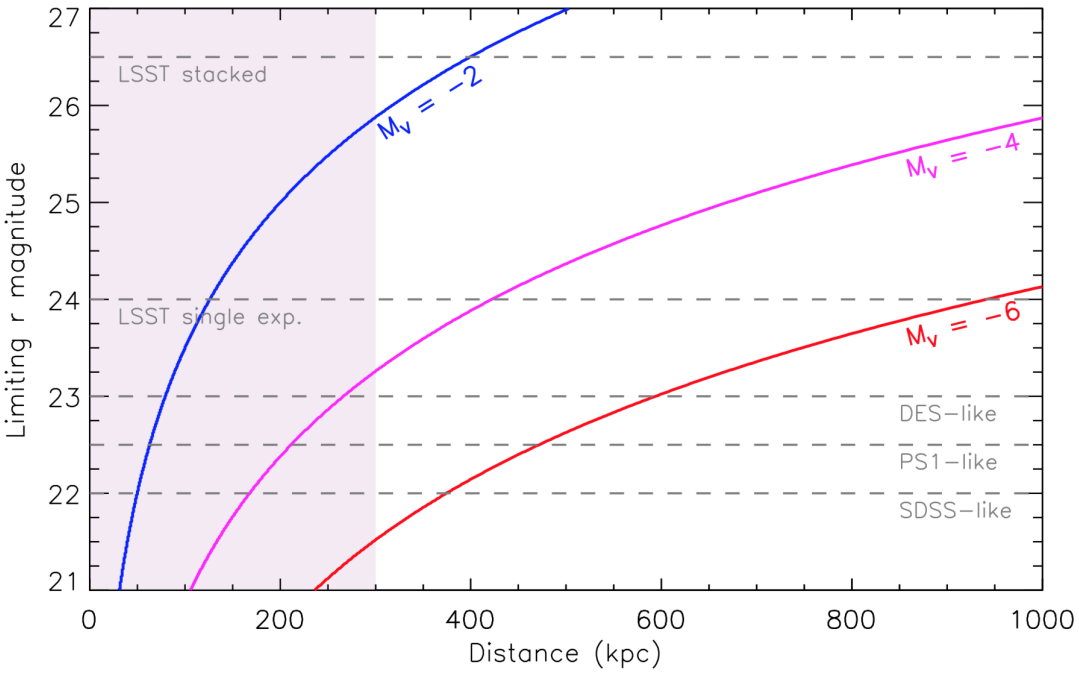

Figure 6.2: From Simon (2019), the magnitude of the 20th brightest star in M_v =-2, -4 and -6 dwarf as a function of distance.

There is the additional challenge for the isolated dwarfs in that they lack a concentrated area in which to complete a deeper, conclusive search. The UNIONS (Ultraviolet Near Infrared Optical Northern Survey, includes Canada France Imaging Survey - CFIS Ibata et al. 2017, see discussion in Bickley et al. 2021) presents an intriguing possibility for establishing new and deeper completeness limits for the isolated Local Group dwarfs. With these observations, it is possible to do a systematic search for both satellites and isolated dwarfs, perhaps with a more automated machine learning approach. Another revolutionary change will be observations by the Vera C. Rubin Observatory, previously known as Large Synoptic Survey Telescope (LSST). This telescope will be able to find faint dwarfs around the Local Group, and provide robust completeness limits. Figure 6.2 shows the observing depth of LSST as compared to SDSS, DES and Pan-STARRS. LSST will dramatically improve our understanding the faintest dwarfs. Newton et al. (2018) predicts an additional $\sim$ 60 "hyperfaint" dwarfs in the Local Group and suggests that LSST's observing capabilities will be able to detect half of this possible population. Similarly, Applebaum et al. (2021) suggests that the majority of nearby dwarfs that exist will be observable with LSST.

Gaia (Gaia Collaboration et al., 2018, 2021) has already revolutionized our understanding of Local Group dwarfs by providing proper motions (McConnachie & Venn 2020; McConnachie et al. 2021; Battaglia et al. 2021) of the nearest dwarfs, and interesting constraints on more isolated ones (McConnachie et al. 2021; Battaglia et al. 2021). With this new information, we can establish orbits and place more strict constraints on those which are fundamentally isolated and which have had prolonged interactions with the MW. Using the results from Battaglia et al. (2021), Figures 6.3 and 6.4 show panels from Figures 4.3 and 4.7 but coloured by the dwarf's orbital distance at pericenter and time since last pericenter. Clearly, these figures are highly incomplete, with the majority of dwarfs lacking orbital values. At present, determining these orbits, particularly of the isolated dwarfs (arguably the most interesting sample in this context), is at the outermost limits of Gaia's capabilities, and systematic uncertainties dominate the measurements.

However, this type of analysis illustrates future opportunities. Really, a dwarf's orbit (and orbital history) is the ideal fundamental property that we would like to use to constrain the environmental effects relevant to that particular dwarf. In Figures 6.3 and 6.4, we see that dwarfs at larger separations from host galaxies are, in fact, those with greater distances at pericenter. This, again, broadly highlights the fact that separation is a good metric for isolation, despite the confusion with backsplash galaxies. With the addition (and refinement) of dwarfs' orbital parameters, we will be able to generate more nuanced discussions of isolation and perhaps values like "time since last pericentric passage" will become increasingly informative. Importantly, discussions of orbital timescales become possible with robust orbital measurements. Rather than looking for evidence of past interactions, we can constrain the time and magnitude of the interaction to search for residual effects.

6.3 The big picture with little galaxies

I hope that this thesis has successfully shown the value of the Solo Survey, provided a useful, homogeneous dataset of the structures of the isolated dwarfs in our Local Group, and offered interesting insights into the intrinsic nature of dwarf galaxies when removed from the substantial environmental effects induced by large host galaxies. I have endeavoured to use the wealth of detail available by studying the galaxies in our own backyard, which will always be the galaxies we can explore and understand in the greatest detail due to their proximity. Throughout this work, the complexity of

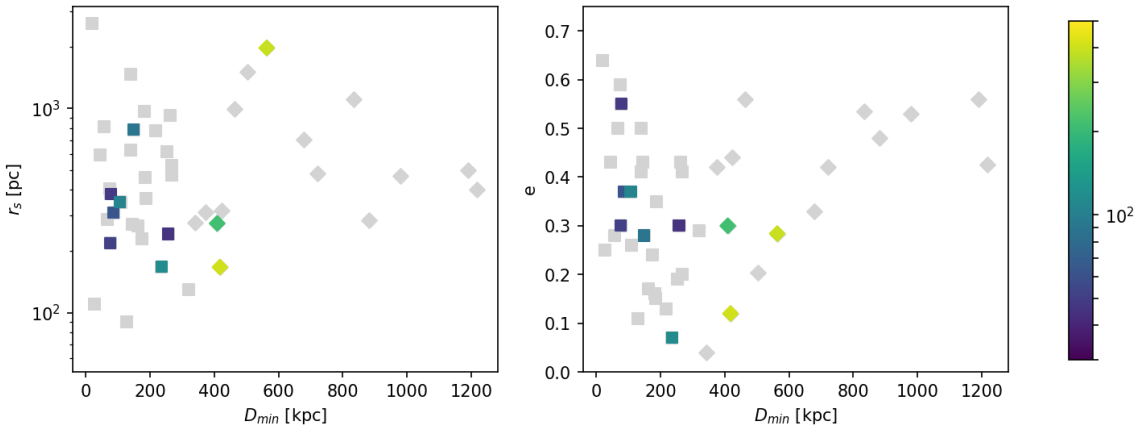

Figure 6.3: Subset of Figure 4.7, coloured by the pericentric distance from Battaglia et al. (2021) ("light" MW version).

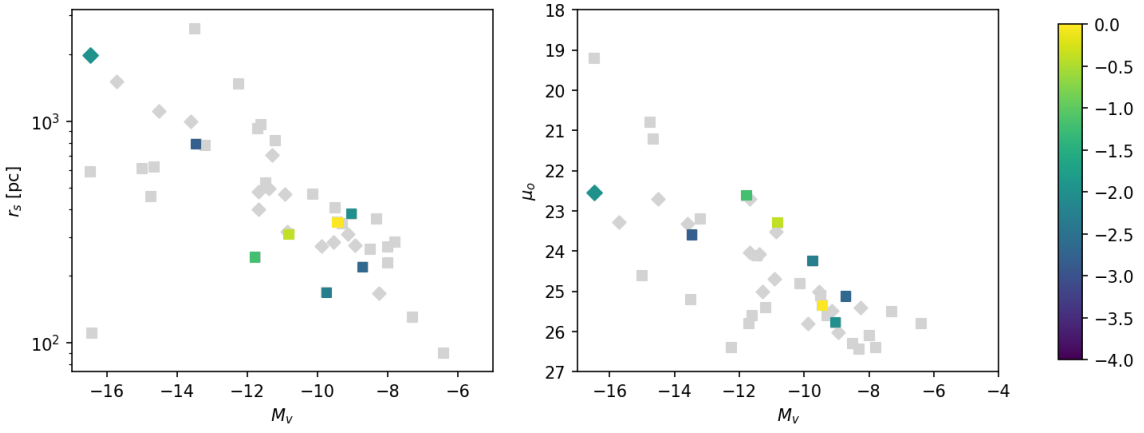

Figure 6.4: Subset of Figure 4.3, coloured by time since last pericentric passage from Battaglia et al. (2021) ("light" MW version).

these small galaxies and the roles of the complementary and competing evolutionary effects has been emphasized. Dwarfs may be low mass, but their origins and our interpretations of their observed state are far from simple.

Bibliography

Abraham, R. G., & van Dokkum, P. G. 2014, Publications of the ASP, 126, 55

Adams, E. A. K., & Oosterloo, T. A. 2018, Astronomy and Astrophysics, 612, A26

Albers, S. M., Weisz, D. R., Cole, A. A., et al. 2019, Monthly Notices of the RAS, 490, 5538

Amorisco, N. C., & Evans, N. W. 2012, Astrophysical Journal, Letters to the Editor, 756, L2

Amorisco, N. C., Evans, N. W., & van de Ven, G. 2014, Nature, 507, 335

Ankerst, M., Breunig, M. M., Kriegel, H.-P., & Sander, J. 1999, in Proceedings of the 1999 ACM SIGMOD International Conference on Management of Data, SIGMOD '99 (New York, NY, USA: Association for Computing Machinery), 49–60

Annibali, F., Bellazzini, M., Correnti, M., et al. 2019, Astrophysical Journal, 883, 19

Applebaum, E., Brooks, A. M., Christensen, C. R., et al. 2021, Astrophysical Journal, 906, 96

Balogh, M. L., Navarro, J. F., & Morris, S. L. 2000, Astrophysical Journal, 540, 113

Bastian, N., & Lardo, C. 2018, Annual Review of Astronomy and Astrophysics, 56, 83

Battaglia, G., Helmi, A., Tolstoy, E., et al. 2008, Astrophysical Journal, Letters to the Editor, 681, L13

Battaglia, G., Rejkuba, M., Tolstoy, E., Irwin, M. J., & Beccari, G. 2012, Monthly Notices of the RAS, 424, 1113

Battaglia, G., Taibi, S., Thomas, G. F., & Fritz, T. K. 2021, arXiv e-prints, arXiv:2106.08819

Battinelli, P., Demers, S., & Kunkel, W. E. 2006, Astronomy and Astrophysics, 451, 99

Beccari, G., Bellazzini, M., Fraternali, F., et al. 2014, Astronomy and Astrophysics, 570, A78

Bechtol, K., Drlica-Wagner, A., Balbinot, E., et al. 2015, Astrophysical Journal, 807, 50

Behroozi, P. S., Wechsler, R. H., & Conroy, C. 2013, Astrophysical Journal, 770, 57

Bekki, K., Couch, W. J., & Shioya, Y. 2002, Astrophysical Journal, 577, 651

Bell, E. F., Slater, C. T., & Martin, N. F. 2011, Astrophysical Journal, Letters to the Editor, 742, L15

Bellazzini, M., Ferraro, F. R., & Pancino, E. 2001, Astrophysical Journal, 556, 635

Bellazzini, M., Gennari, N., & Ferraro, F. R. 2005, Monthly Notices of the RAS, 360, 185

Bellazzini, M., Gennari, N., Ferraro, F. R., & Sollima, A. 2004, Monthly Notices of the RAS, 354, 708

Bellazzini, M., Ibata, R., Malhan, K., et al. 2020, Astronomy and Astrophysics, 636, A107

Bellazzini, M., Perina, S., Galleti, S., & Oosterloo, T. 2011a, Astronomy and Astrophysics, 533, A37

Bellazzini, M., Beccari, G., Oosterloo, T. A., et al. 2011b, Astronomy and Astrophysics, 527, A58

Belokurov, V., Erkal, D., Evans, N. W., Koposov, S. E., & Deason, A. J. 2018, Monthly Notices of the RAS, 478, 611

Belokurov, V., Zucker, D. B., Evans, N. W., et al. 2007, Astrophysical Journal, 654, 897

Benítez-Llambay, A., Navarro, J. F., Abadi, M. G., et al. 2016, Monthly Notices of the RAS, 456, 1185

Bernard, E. J., Aparicio, A., Gallart, C., Padilla-Torres, C. P., & Panniello, M. 2007, Astronomical Journal, 134, 1124

Bernard, E. J., Gallart, C., Monelli, M., et al. 2008, Astrophysical Journal, Letters to the Editor, 678, L21

Bernard, E. J., Monelli, M., Gallart, C., et al. 2009, Astrophysical Journal, 699, 1742

—. 2010, Astrophysical Journal, 712, 1259

—. 2013, Monthly Notices of the RAS, 432, 3047

Bickley, R. W., Bottrell, C., Hani, M. H., et al. 2021, Monthly Notices of the RAS, 504, 372

Binggeli, B. 1994, in European Southern Observatory Conference and Workshop Proceedings, Vol. 49, European Southern Observatory Conference and Workshop Proceedings, 13

Blaña, M., Burkert, A., Fellhauer, M., Schartmann, M., & Alig, C. 2020, Monthly Notices of the RAS, 497, 3601

Bland-Hawthorn, J., & Gerhard, O. 2016, Annual Review of Astronomy and Astrophysics, 54, 529

Blumenthal, G. R., Faber, S. M., Primack, J. R., & Rees, M. J. 1984, Nature, 311, 517

Bonaca, A., Hogg, D. W., Price-Whelan, A. M., & Conroy, C. 2019, Astrophysical Journal, 880, 38

Bonanos, A. Z., Stanek, K. Z., Szentgyorgyi, A. H., Sasselov, D. D., & Bakos, G. Á. 2004, Astronomical Journal, 127, 861

Borukhovetskaya, A., Errani, R., Navarro, J. F., Fattahi, A., & Santos-Santos, I. 2021, arXiv e-prints, arXiv:2104.00011

Bower, R. G., Benson, A. J., Malbon, R., et al. 2006, Monthly Notices of the RAS, 370, 645

Boylan-Kolchin, M. 2018, Monthly Notices of the RAS, 479, 332

Boylan-Kolchin, M., Bullock, J. S., & Kaplinghat, M. 2011, Monthly Notices of the RAS, 415, L40

Bradford, J. D., Geha, M. C., Greene, J. E., Reines, A. E., & Dickey, C. M. 2018, Astrophysical Journal, 861, 50

Brasseur, C. M., Martin, N. F., Rix, H.-W., et al. 2011, Astrophysical Journal, 729, 23

Bresolin, F., Pietrzyński, G., Urbaneja, M. A., et al. 2006, Astrophysical Journal, 648, 1007

Brodie, J. P., & Strader, J. 2006, Annual Review of Astronomy and Astrophysics, 44, 193

Brown, T. M., Tumlinson, J., Geha, M., et al. 2014, Astrophysical Journal, 796, 91

Brown, W. R., Geller, M. J., Kenyon, S. J., & Kurtz, M. J. 2007, Astrophysical Journal, 666, 231

Buck, T., Macciò, A. V., Dutton, A. A., Obreja, A., & Frings, J. 2019, Monthly Notices of the RAS, 483, 1314

Bullock, J. S., & Boylan-Kolchin, M. 2017, Annual Review of Astronomy and Astrophysics, 55, 343

Bullock, J. S., Kravtsov, A. V., & Weinberg, D. H. 2000, Astrophysical Journal, 539, 517

Butler, K. M., Obreschkow, D., & Oh, S.-H. 2017, Astrophysical Journal, Letters to the Editor, 834, L4

Byun, W., Sheen, Y.-K., Park, H. S., et al. 2020, Astrophysical Journal, 891, 18

Caldwell, N., Strader, J., Sand, D. J., Willman, B., & Seth, A. C. 2017, PASA, 34, e039

Carlin, J. L., & Sand, D. J. 2018, Astrophysical Journal, 865, 7

Carlsten, S. G., Greco, J. P., Beaton, R. L., & Greene, J. E. 2020, Astrophysical Journal, 891, 144

Carlsten, S. G., Greene, J. E., Peter, A. H. G., Beaton, R. L., & Greco, J. P. 2021, Astrophysical Journal, 908, 109

Carrera, R., Aparicio, A., Martínez-Delgado, D., & Alonso-García, J. 2002, Astronomical Journal, 123, 3199

Carroll, B., & Ostlie, D. 2006, An Introduction to Modern Astrophysics and Cosmology, Vol. -1

Chiti, A., Frebel, A., Simon, J. D., et al. 2021, Nature Astronomy, 5, 392

Choi, P. I., Guhathakurta, P., & Johnston, K. V. 2002, Astronomical Journal, 124, 310

Chowdhury, A., & Chengalur, J. N. 2017, Monthly Notices of the RAS, 467, 3856

Cicuéndez, L., & Battaglia, G. 2018, Monthly Notices of the RAS, 480, 251

Cockcroft, R., Harris, W. E., Ferguson, A. M. N., et al. 2011, Astrophysical Journal, 730, 112

Cohen, Y., van Dokkum, P., Danieli, S., et al. 2018, Astrophysical Journal, 868, 96

Cole, A. A., Weisz, D. R., Dolphin, A. E., et al. 2014, Astrophysical Journal, 795, 54

Cole, A. A., Skillman, E. D., Tolstoy, E., et al. 2007, Astrophysical Journal, Letters to the Editor, 659, L17

Cole, A. A., Weisz, D. R., Skillman, E. D., et al. 2017, Astrophysical Journal, 837, 54

Collins, M. L. M., Chapman, S. C., Rich, R. M., et al. 2013, Astrophysical Journal, 768, 172

Collins, M. L. M., Read, J. I., Ibata, R. A., et al. 2021, Monthly Notices of the RAS, 505, 5686

Conn, A. R., Ibata, R. A., Lewis, G. F., et al. 2012, Astrophysical Journal, 758, 11

Cook, K. H., Mateo, M., Olszewski, E. W., et al. 1999, Publications of the ASP, 111, 306

Crnojević, D., Sand, D. J., Zaritsky, D., et al. 2016, Astrophysical Journal, Letters to the Editor, 824, L14

Crnojević, D., Sand, D. J., Bennet, P., et al. 2019, Astrophysical Journal, 872, 80

Cutri, R. M., Skrutskie, M. F., van Dyk, S., et al. 2003, 2MASS All Sky Catalog of point sources.

Dale, D. A., Gil de Paz, A., Gordon, K. D., et al. 2007, Astrophysical Journal, 655, 863

de Blok, W. J. G. 2010, Advances in Astronomy, 2010, 789293

de Grijs, R., & Bono, G. 2014, Astronomical Journal, 148, 17

de Jong, J. T. A., Harris, J., Coleman, M. G., et al. 2008, Astrophysical Journal, 680, 1112

de Vaucouleurs, G., de Vaucouleurs, A., Corwin, Jr., H. G., et al. 1991, Third Reference Catalogue of Bright Galaxies (Volume 1-3, XII, 2069 pp. 7 figs.. Springer-Verlag Berlin Heidelberg New York)

Deason, A., Wetzel, A., & Garrison-Kimmel, S. 2014, Astrophysical Journal, 794, 115

Deason, A. J., Belokurov, V., Evans, N. W., Watkins, L. L., & Fellhauer, M. 2012, Monthly Notices of the RAS, 425, L101

Demers, S., Battinelli, P., & Kunkel, W. E. 2006, Astrophysical Journal, Letters to the Editor, 636, L85

D'Ercole, A., Vesperini, E., D'Antona, F., McMillan, S. L. W., & Recchi, S. 2008, Monthly Notices of the RAS, 391, 825

Di Cintio, A., Brook, C. B., Macciò, A. V., et al. 2014, Monthly Notices of the RAS, 437, 415

Di Matteo, T., Springel, V., & Hernquist, L. 2005, Nature, 433, 604

Dolphin, A. E., Saha, A., Claver, J., et al. 2002, Astronomical Journal, 123, 3154

D'Onghia, E., Besla, G., Cox, T. J., & Hernquist, L. 2009, Nature, 460, 605

Dooley, G. A., Peter, A. H. G., Yang, T., et al. 2017, Monthly Notices of the RAS, 471, 4894

Dotter, A., Chaboyer, B., Jevremović, D., et al. 2008, Astrophysical Journal, Supplement Series, 178, 89

Drinkwater, M. J., Jones, J. B., Gregg, M. D., & Phillipps, S. 2000, PASA, 17, 227

Drlica-Wagner, A., Bechtol, K., Rykoff, E. S., et al. 2015, Astrophysical Journal, 813, 109

Drlica-Wagner, A., Bechtol, K., Mau, S., et al. 2020, Astrophysical Journal, 893, 47

Eadie, G., & Jurić, M. 2019, Astrophysical Journal, 875, 159

Efstathiou, G. 1992, Monthly Notices of the RAS, 256, 43P

Einasto, J., Saar, E., Kaasik, A., & Chernin, A. D. 1974, Nature, 252, 111

El-Badry, K., Bradford, J., Quataert, E., et al. 2018a, Monthly Notices of the RAS, 477, 1536

El-Badry, K., Quataert, E., Wetzel, A., et al. 2018b, Monthly Notices of the RAS, 473, 1930

Erkal, D., & Belokurov, V. 2015, Monthly Notices of the RAS, 454, 3542

Erkal, D., & Belokurov, V. A. 2020, Monthly Notices of the RAS, 495, 2554

Errani, R., Penarrubia, J., & Tormen, G. 2015, Monthly Notices of the RAS, 449, L46

Ester, M., Kriegel, H.-P., Sander, J., & Xu, X. 1996, in Proc. of the Second International Conference on Knowledge Discovery and Data Mining, 226–231

Evstigneeva, E. A., Drinkwater, M. J., Peng, C. Y., et al. 2008, Astronomical Journal, 136, 461

Fattahi, A., Navarro, J. F., & Frenk, C. S. 2020, Monthly Notices of the RAS, 493, 2596

Fattahi, A., Navarro, J. F., Frenk, C. S., et al. 2018, Monthly Notices of the RAS, 476, 3816

Ferrarese, L., Côté, P., Jordán, A., et al. 2006, Astrophysical Journal, Supplement Series, 164, 334

Ferrarese, L., Côté, P., Cuillandre, J.-C., et al. 2012, Astrophysical Journal, Supplement Series, 200, 4

Ferrarese, L., Côté, P., Sánchez-Janssen, R., et al. 2016, Astrophysical Journal, 824, 10

Ferrarese, L., Côté, P., MacArthur, L. A., et al. 2020, Astrophysical Journal, 890, 128

Fiorentino, G., Monachesi, A., Trager, S. C., et al. 2010, Astrophysical Journal, 708, 817

Fitts, A., Boylan-Kolchin, M., Bullock, J. S., et al. 2018, Monthly Notices of the RAS, 479, 319

Foreman-Mackey, D., Hogg, D. W., Lang, D., & Goodman, J. 2013, Publications of the ASP, 125, 306

Fraternali, F., Tolstoy, E., Irwin, M. J., & Cole, A. A. 2009, Astronomy and Astrophysics, 499, 121

Freedman, W. L. 2017, Nature Astronomy, 1, 0169

Freedman, W. L., Madore, B. F., Hoyt, T., et al. 2020, Astrophysical Journal, 891, 57

Freeman, K. C. 1993, in Astronomical Society of the Pacific Conference Series, Vol. 48, The Globular Cluster-Galaxy Connection, ed. G. H. Smith & J. P. Brodie, 608

Gaia Collaboration, Brown, A. G. A., Vallenari, A., et al. 2018, Astronomy and Astrophysics, 616, A1

—. 2021, Astronomy and Astrophysics, 649, A1

Gallart, C., Martínez-Delgado, D., Gómez-Flechoso, M. A., & Mateo, M. 2001, Astronomical Journal, 121, 2572

Gallart, C., Monelli, M., Mayer, L., et al. 2015, Astrophysical Journal, Letters to the Editor, 811, L18

Garling, C., Willman, B., Sand, D. J., et al. 2018, Astrophysical Journal, 852, 44

Garrison-Kimmel, S., Hopkins, P. F., Wetzel, A., et al. 2019, Monthly Notices of the RAS, 487, 1380

Geha, M., Blanton, M. R., Yan, R., & Tinker, J. L. 2012, Astrophysical Journal, 757, 85

Geha, M., van der Marel, R. P., Guhathakurta, P., et al. 2010, Astrophysical Journal, 711, 361

Geha, M., Willman, B., Simon, J. D., et al. 2009, Astrophysical Journal, 692, 1464

Geha, M., Wechsler, R. H., Mao, Y.-Y., et al. 2017, Astrophysical Journal, 847, 4

Gerbrandt, S. A. N., McConnachie, A. W., & Irwin, M. 2015, Monthly Notices of the RAS, 454, 1000

Gieren, W., Pietrzyński, G., Nalewajko, K., et al. 2006, Astrophysical Journal, 647, 1056

Gill, S. P. D., Knebe, A., & Gibson, B. K. 2005, Monthly Notices of the RAS, 356, 1327

Gilmore, G., Wilkinson, M. I., Wyse, R. F. G., et al. 2007, Astrophysical Journal, 663, 948

Gnedin, O. Y., Hernquist, L., & Ostriker, J. P. 1999a, Astrophysical Journal, 514, 109

Gnedin, O. Y., Lee, H. M., & Ostriker, J. P. 1999b, Astrophysical Journal, 522, 935

Gnedin, O. Y., & Ostriker, J. P. 1997, Astrophysical Journal, 474, 223

Graham, A. W., & Driver, S. P. 2005, PASA, 22, 118

Graham, A. W., & Guzmán, R. 2003, Astronomical Journal, 125, 2936

Gratton, R. G., Carretta, E., & Bragaglia, A. 2012, Astronomy and Astrophysics Reviews, 20, 50

Graus, A. S., Bullock, J. S., Kelley, T., et al. 2019, Monthly Notices of the RAS, 488, 4585

Gravity Collaboration, Abuter, R., Amorim, A., et al. 2018, Astronomy and Astrophysics, 615, L15

Grebel, E. K., Gallagher, J. S., & Harbeck, D. 2003, Astronomical Journal, 125, 1926

Greisen, E. W., & Calabretta, M. R. 2002, Astronomy and Astrophysics, 395, 1061

Grillmair, C. J. 2009, Astrophysical Journal, 693, 1118

Grillmair, C. J., Lauer, T. R., Worthey, G., et al. 1996, Astronomical Journal, 112, 1975

Gunn, J. E., & Gott, J. Richard, I. 1972, Astrophysical Journal, 176, 1

Hammer, F., Puech, M., Chemin, L., Flores, H., & Lehnert, M. D. 2007, Astrophysical Journal, 662, 322

Harbeck, D., Grebel, E. K., Holtzman, J., et al. 2001, Astronomical Journal, 122, 3092

Harrison, C. M. 2017, Nature Astronomy, 1, 0165

Helmi, A. 2020, Annual Review of Astronomy and Astrophysics, 58, 205

Helmi, A., Babusiaux, C., Koppelman, H. H., et al. 2018, Nature, 563, 85

Helmi, A., Sales, L. V., Starkenburg, E., et al. 2012, Astrophysical Journal, Letters to the Editor, 758, L5

Hermosa Muñoz, L., Taibi, S., Battaglia, G., et al. 2020, Astronomy and Astrophysics, 634, A10

Hidalgo, S. L., Aparicio, A., Skillman, E., et al. 2011, Astrophysical Journal, 730, 14

Hidalgo, S. L., Monelli, M., Aparicio, A., et al. 2013, Astrophysical Journal, 778, 103

Higgs, C. R., & McConnachie, A. W. 2021, Monthly Notices of the RAS, 506, 2766

Higgs, C. R., McConnachie, A. W., Annau, N., et al. 2021, Monthly Notices of the RAS, 503, 176

Higgs, C. R., McConnachie, A. W., Irwin, M., et al. 2016, Monthly Notices of the RAS, 458, 1678

Hilker, M., Infante, L., Vieira, G., Kissler-Patig, M., & Richtler, T. 1999, Astronomy and Astrophysics, Supplement Series, 134, 75

Ho, L. C., Greene, J. E., Filippenko, A. V., & Sargent, W. L. W. 2009, Astrophysical Journal, Supplement Series, 183, 1

Ho, L. C., Li, Z.-Y., Barth, A. J., Seigar, M. S., & Peng, C. Y. 2011, Astrophysical Journal, Supplement Series, 197, 21

Ho, N., Geha, M., Munoz, R. R., et al. 2012, Astrophysical Journal, 758, 124

Hodge, P. W., Smith, T. R., Eskridge, P. B., MacGillivray, H. T., & Beard, S. M. 1991, Astrophysical Journal, 369, 372

Homma, D., Chiba, M., Okamoto, S., et al. 2018, Publications of the ASJ, 70, S18

Homma, D., Chiba, M., Komiyama, Y., et al. 2019, Publications of the ASJ, 71, 94

Hopkins, P. F., Wetzel, A., Kereš, D., et al. 2018, Monthly Notices of the RAS, 480, 800

Huang, K.-W., & Koposov, S. E. 2021, Monthly Notices of the RAS, 500, 986

Hubble, E. P. 1925, Astrophysical Journal, 62, 409

Huchra, J. P., Vogeley, M. S., & Geller, M. J. 1999, Astrophysical Journal, Supplement Series, 121, 287

Hunter, D. A., Ficut-Vicas, D., Ashley, T., et al. 2012, Astronomical Journal, 144, 134

Huxor, A. P., Ferguson, A. M. N., Veljanoski, J., Mackey, A. D., & Tanvir, N. R. 2013, Monthly Notices of the RAS, 429, 1039

Huxor, A. P., Mackey, A. D., Ferguson, A. M. N., et al. 2014, Monthly Notices of the RAS, 442, 2165

Hwang, N., Lee, M. G., Lee, J. C., et al. 2011, Astrophysical Journal, 738, 58

Hwang, N., Park, H. S., Lee, M. G., et al. 2014, Astrophysical Journal, 783, 49

Ibata, R., Bellazzini, M., Thomas, G., et al. 2020, Astrophysical Journal, Letters to the Editor, 891, L19

Ibata, R., Malhan, K., Martin, N., et al. 2021, Astrophysical Journal, 914, 123

Ibata, R. A., Gilmore, G., & Irwin, M. J. 1994, Nature, 370, 194

Ibata, R. A., Wyse, R. F. G., Gilmore, G., Irwin, M. J., & Suntzeff, N. B. 1997, Astronomical Journal, 113, 634

Ibata, R. A., McConnachie, A., Cuilland re, J.-C., et al. 2017, Astrophysical Journal, 848, 128

Ideta, M., & Makino, J. 2004, Astrophysical Journal, Letters to the Editor, 616, L107

Iorio, G., Fraternali, F., Nipoti, C., et al. 2017, Monthly Notices of the RAS, 466, 4159

Irwin, M., & Hatzidimitriou, D. 1995, Monthly Notices of the RAS, 277, 1354

Irwin, M., & Lewis, J. 2001, NAR, 45, 105

Irwin, M. J. 1985, Monthly Notices of the RAS, 214, 575

—. 1997, Detectors and data analysis techniques for wide field optical imaging., ed. J. M. Rodríguez Espinosa, A. Herrero, & F. Sánchez, 35–74

Irwin, M. J., Lewis, J., Hodgkin, S., et al. 2004, in Society of Photo-Optical Instrumentation Engineers (SPIE) Conference Series, Vol. 5493, Optimizing Scientific Return for Astronomy through Information Technologies, ed. P. J. Quinn & A. Bridger, 411–422

Irwin, M. J., Belokurov, V., Evans, N. W., et al. 2007, Astrophysical Journal, Letters to the Editor, 656, L13

Jacobs, B. A., Tully, R. B., Rizzi, L., et al. 2011, Astronomical Journal, 141, 106

Ji, A. P., Frebel, A., Chiti, A., & Simon, J. D. 2016, Nature, 531, 610

Kacharov, N., Battaglia, G., Rejkuba, M., et al. 2017, Monthly Notices of the RAS, 466, 2006

Kalirai, J. S., Beaton, R. L., Geha, M. C., et al. 2010, Astrophysical Journal, 711, 671

Kallivayalil, N., Sales, L. V., Zivick, P., et al. 2018, Astrophysical Journal, 867, 19

Kang, H. D., & Ricotti, M. 2019, Monthly Notices of the RAS, 488, 2673

Karachentsev, I. D., Makarov, D. I., & Kaisina, E. I. 2013, Astronomical Journal, 145, 101

Karachentsev, I. D., & Makarova, L. N. 2019, Astrophysics, 62, 293

Kass, R. E., & Raftery, A. E. 1995, Journal of the American Statistical Association, 90, 773

Kaufmann, T., Wheeler, C., & Bullock, J. S. 2007, Monthly Notices of the RAS, 382, 1187

Kawata, D., & Mulchaey, J. S. 2008, Astrophysical Journal, Letters to the Editor, 672, L103

Kazantzidis, S., Łokas, E. L., Callegari, S., Mayer, L., & Moustakas, L. A. 2011, Astrophysical Journal, 726, 98

Kim, S. Y., Peter, A. H. G., & Hargis, J. R. 2018, Phys. Rev. Lett., 121, 211302

Kirby, E. N., Bullock, J. S., Boylan-Kolchin, M., Kaplinghat, M., & Cohen, J. G. 2014, Monthly Notices of the RAS, 439, 1015

Kirby, E. N., Cohen, J. G., & Bellazzini, M. 2012, Astrophysical Journal, 751, 46

Kirby, E. N., Rizzi, L., Held, E. V., et al. 2017, Astrophysical Journal, 834, 9

Klypin, A., Kravtsov, A. V., Valenzuela, O., & Prada, F. 1999, Astrophysical Journal, 522, 82

Klypin, A., Zhao, H., & Somerville, R. S. 2002, Astrophysical Journal, 573, 597

Kniazev, A. Y., Brosch, N., Hoffman, G. L., et al. 2009, Monthly Notices of the RAS, 400, 2054

Koposov, S. E., Casey, A. R., Belokurov, V., et al. 2015, Astrophysical Journal, 811, 62

Kopylov, A. I., Tikhonov, N. A., Fabrika, S., Drozdovsky, I., & Valeev, A. F. 2008, Monthly Notices of the RAS, 387, L45

Kormendy, J. 1985, Astrophysical Journal, 295, 73

Koutsouridou, I., & Cattaneo, A. 2019, Monthly Notices of the RAS, 490, 5375

Krienke, K., & Hodge, P. 2004, Publications of the ASP, 116, 497

Kruijssen, J. M. D. 2015, Monthly Notices of the RAS, 454, 1658

Kruijssen, J. M. D., Pfeffer, J. L., Chevance, M., et al. 2020, Monthly Notices of the RAS, 498, 2472

Laevens, B. P. M., Martin, N. F., Bernard, E. J., et al. 2015, Astrophysical Journal, 813, 44

Larson, R. B., Tinsley, B. M., & Caldwell, C. N. 1980, Astrophysical Journal, 237, 692

Leaman, R., Cole, A. A., Venn, K. A., et al. 2009, Astrophysical Journal, 699, 1

Leaman, R., Venn, K. A., Brooks, A. M., et al. 2012, Astrophysical Journal, 750, 33

—. 2013, Astrophysical Journal, 767, 131

Leaman, R., Ruiz-Lara, T., Cole, A. A., et al. 2020, Monthly Notices of the RAS, 492, 5102

Lee, M. G. 1995, Astronomical Journal, 110, 1129

Lee, M. G., Freedman, W. L., & Madore, B. F. 1993, Astrophysical Journal, 417, 553

Lee, M. G., & Kim, S. C. 2000, Astronomical Journal, 119, 777

Letarte, B., Chapman, S. C., Collins, M., et al. 2009, Monthly Notices of the RAS, 400, 1472

Lewis, G. F., Ibata, R. A., Chapman, S. C., et al. 2007, Monthly Notices of the RAS, 375, 1364

Li, Z.-Y., Ho, L. C., Barth, A. J., & Peng, C. Y. 2011, Astrophysical Journal, Supplement Series, 197, 22

Lim, S., & Lee, M. G. 2015, Astrophysical Journal, 804, 123

Łokas, E. L., Kazantzidis, S., & Mayer, L. 2011, Astrophysical Journal, 739, 46

Łokas, E. L., Majewski, S. R., Kazantzidis, S., et al. 2012, Astrophysical Journal, 751, 61

Ma, X., Quataert, E., Wetzel, A., Faucher-Giguère, C.-A., & Boylan-Kolchin, M. 2021, Monthly Notices of the RAS, 504, 4062

Mackey, A. D., Huxor, A. P., Ferguson, A. M. N., et al. 2010, Astrophysical Journal, Letters to the Editor, 717, L11

Madore, B. F., & Freedman, W. L. 1995, Astronomical Journal, 109, 1645

Madore, B. F., Mager, V., & Freedman, W. L. 2009, Astrophysical Journal, 690, 389

Majewski, S. R., Skrutskie, M. F., Weinberg, M. D., & Ostheimer, J. C. 2003, Astrophysical Journal, 599, 1082

Man, A., & Belli, S. 2018, Nature Astronomy, 2, 695

Mao, Y.-Y., Geha, M., Wechsler, R. H., et al. 2021, Astrophysical Journal, 907, 85

Marchi-Lasch, S., Muñoz, R. R., Santana, F. A., et al. 2019, Astrophysical Journal, 874, 29

Markwardt, C. B. 2009, Astronomical Society of the Pacific Conference Series, Vol. 411, Non-linear Least-squares Fitting in IDL with MPFIT, ed. D. A. Bohlender, D. Durand, & P. Dowler, 251

Martin, N. F., de Jong, J. T. A., & Rix, H.-W. 2008, Astrophysical Journal, 684, 1075

Martin, N. F., Slater, C. T., Schlafly, E. F., et al. 2013a, Astrophysical Journal, 772, 15

Martin, N. F., Schlafly, E. F., Slater, C. T., et al. 2013b, Astrophysical Journal, Letters to the Editor, 779, L10

Martin, N. F., Chambers, K. C., Collins, M. L. M., et al. 2014, Astrophysical Journal, Letters to the Editor, 793, L14

Martin, N. F., Ibata, R. A., Lewis, G. F., et al. 2016, Astrophysical Journal, 833, 167

Martin, N. F., Weisz, D. R., Albers, S. M., et al. 2017, Astrophysical Journal, 850, 16

Martínez-Delgado, D., Gallart, C., & Aparicio, A. 1999, Astronomical Journal, 118, 862

Martínez-Delgado, D., Romanowsky, A. J., Gabany, R. J., et al. 2012, Astrophysical Journal, Letters to the Editor, 748, L24

Massey, P., Olsen, K. A. G., Hodge, P. W., et al. 2007, Astronomical Journal, 133, 2393

—. 2006, Astronomical Journal, 131, 2478

Mastropietro, M., De Rijcke, S., & Peletier, R. F. 2021, Monthly Notices of the RAS, 504, 3387

Mateo, M., Olszewski, E. W., & Morrison, H. L. 1998, Astrophysical Journal, Letters to the Editor, 508, L55

Mateo, M., Olszewski, E. W., & Walker, M. G. 2008, Astrophysical Journal, 675, 201

Mateo, M. L. 1998, Annual Review of Astronomy and Astrophysics, 36, 435

Mayer, L., Governato, F., Colpi, M., et al. 2001a, Astrophysical Journal, 559, 754

—. 2001b, Astrophysical Journal, Letters to the Editor, 547, L123

Mayer, L., Mastropietro, C., Wadsley, J., Stadel, J., & Moore, B. 2006, Monthly Notices of the RAS, 369, 1021

McConnachie, A. W. 2012, Astronomical Journal, 144, 4

McConnachie, A. W., Arimoto, N., Irwin, M., & Tolstoy, E. 2006, Monthly Notices of the RAS, 373, 715

McConnachie, A. W., Ferguson, A. M. N., Irwin, M. J., et al. 2010, Astrophysical Journal, 723, 1038

McConnachie, A. W., Higgs, C. R., Thomas, G. F., et al. 2021, Monthly Notices of the RAS, 501, 2363

McConnachie, A. W., & Irwin, M. J. 2006, Monthly Notices of the RAS, 365, 1263

McConnachie, A. W., Irwin, M. J., Ferguson, A. M. N., et al. 2004, Monthly Notices of the RAS, 350, 243

—. 2005, Monthly Notices of the RAS, 356, 979

McConnachie, A. W., Peñarrubia, J., & Navarro, J. F. 2007a, Monthly Notices of the RAS, 380, L75

McConnachie, A. W., & Venn, K. A. 2020, Astronomical Journal, 160, 124

McConnachie, A. W., Venn, K. A., Irwin, M. J., Young, L. M., & Geehan, J. J. 2007b, Astrophysical Journal, Letters to the Editor, 671, L33

McConnachie, A. W., Huxor, A., Martin, N. F., et al. 2008, Astrophysical Journal, 688, 1009

McConnachie, A. W., Irwin, M. J., Ibata, R. A., et al. 2009, Nature, 461, 66

McConnachie, A. W., Ibata, R., Martin, N., et al. 2018, Astrophysical Journal, 868, 55

Melotte, P. J. 1926, Monthly Notices of the RAS, 86, 636

Mercado, F. J., Bullock, J. S., Boylan-Kolchin, M., et al. 2020, arXiv e-prints, arXiv:2009.01241

Mezcua, M., & Domínguez Sánchez, H. 2020, Astrophysical Journal, Letters to the Editor, 898, L30

Miralda-Escudé, J., Haehnelt, M., & Rees, M. J. 2000, Astrophysical Journal, 530, 1

Monachesi, A., Bell, E. F., Radburn-Smith, D. J., et al. 2016, Monthly Notices of the RAS, 457, 1419

Monaco, L., Bellazzini, M., Ferraro, F. R., & Pancino, E. 2004, Monthly Notices of the RAS, 353, 874

Monelli, M., Hidalgo, S. L., Stetson, P. B., et al. 2010a, Astrophysical Journal, 720, 1225

Monelli, M., Gallart, C., Hidalgo, S. L., et al. 2010b, Astrophysical Journal, 722, 1864

Monelli, M., Martínez-Vázquez, C. E., Bernard, E. J., et al. 2016, Astrophysical Journal, 819, 147

Moore, B., Ghigna, S., Governato, F., et al. 1999, Astrophysical Journal, Letters to the Editor, 524, L19

Moore, B., Katz, N., & Lake, G. 1996, Astrophysical Journal, 457, 455

Moore, B., Lake, G., & Katz, N. 1998, Astrophysical Journal, 495, 139

Moster, B. P., Naab, T., & White, S. D. M. 2013, Monthly Notices of the RAS, 428, 3121

Muñoz, R. R., Côté, P., Santana, F. A., et al. 2018a, Astrophysical Journal, 860, 65

—. 2018b, Astrophysical Journal, 860, 66

Muñoz, R. R., Majewski, S. R., Zaggia, S., et al. 2006, Astrophysical Journal, 649, 201

Müller, O., Rejkuba, M., Pawlowski, M. S., et al. 2019, Astronomy and Astrophysics, 629, A18

Müller, O., Scalera, R., Binggeli, B., & Jerjen, H. 2017, Astronomy and Astrophysics, 602, A119

Myeong, G. C., Vasiliev, E., Iorio, G., Evans, N. W., & Belokurov, V. 2019, Monthly Notices of the RAS, 488, 1235

Necib, L., Ostdiek, B., Lisanti, M., et al. 2020, Nature Astronomy, 4, 1078

Newberg, H. J., Yanny, B., & Willett, B. A. 2009, Astrophysical Journal, Letters to the Editor, 700, L61

Newton, O., Cautun, M., Jenkins, A., Frenk, C. S., & Helly, J. C. 2018, Monthly Notices of the RAS, 479, 2853

Nidever, D. L., Ashley, T., Slater, C. T., et al. 2013, Astrophysical Journal, Letters to the Editor, 779, L15

Oh, S.-H., Hunter, D. A., Brinks, E., et al. 2015, Astronomical Journal, 149, 180

Oliver, W. H., Elahi, P. J., Lewis, G. F., & Power, C. 2020, Monthly Notices of the Royal Astronomical Society, 501, 4420

Ordoñez, A. J., & Sarajedini, A. 2015, Astronomical Journal, 149, 201

Patel, E., Besla, G., & Mandel, K. 2017, Monthly Notices of the RAS, 468, 3428

Patel, E., Kallivayalil, N., Garavito-Camargo, N., et al. 2020, Astrophysical Journal, 893, 121

Patra, N. N., Chengalur, J. N., Karachentsev, I. D., & Sharina, M. E. 2016, Astrophysical Bulletin, 71, 408

Paudel, S., Smith, R., Yoon, S. J., Calderón-Castillo, P., & Duc, P.-A. 2018, Astrophysical Journal, Supplement Series, 237, 36

Paudel, S., Smith, R., Duc, P.-A., et al. 2017, Astrophysical Journal, 834, 66

Paust, N. E. Q., Chaboyer, B., & Sarajedini, A. 2007, Astronomical Journal, 133, 2787

Pawlowski, M. S. 2018, Modern Physics Letters A, 33, 1830004

Pawlowski, M. S., & McGaugh, S. S. 2014, Monthly Notices of the RAS, 440, 908

Peñarrubia, J., Ma, Y.-Z., Walker, M. G., & McConnachie, A. 2014, Monthly Notices of the RAS, 443, 2204

Peñarrubia, J., Navarro, J. F., & McConnachie, A. W. 2008, Astrophysical Journal, 673, 226

Peñarrubia, J., Pontzen, A., Walker, M. G., & Koposov, S. E. 2012, Astrophysical Journal, Letters to the Editor, 759, L42

Pearson, S., Besla, G., Putman, M. E., et al. 2016, Monthly Notices of the RAS, 459, 1827

Peng, Y., Maiolino, R., & Cochrane, R. 2015, Nature, 521, 192

Peng, Y.-j., Lilly, S. J., Kovač, K., et al. 2010, Astrophysical Journal, 721, 193

Pietrzyński, G., Górski, M., Gieren, W., et al. 2009, Astronomical Journal, 138, 459

Pietrzyński, G., Gieren, W., Szewczyk, O., et al. 2008, Astronomical Journal, 135, 1993

Polzin, A., van Dokkum, P., Danieli, S., Greco, J. P., & Romanowsky, A. J. 2021, Astrophysical Journal, Letters to the Editor, 914, L23

Pontzen, A., & Governato, F. 2012, Monthly Notices of the RAS, 421, 3464

Posti, L., & Helmi, A. 2019, Astronomy and Astrophysics, 621, A56

Pucha, R., Carlin, J. L., Willman, B., et al. 2019, Astrophysical Journal, 880, 104

Putman, M. E., Zheng, Y., Price-Whelan, A. M., et al. 2021, Astrophysical Journal, 913, 53

Read, J. I., Wilkinson, M. I., Evans, N. W., Gilmore, G., & Kleyna, J. T. 2006a, Monthly Notices of the RAS, 367, 387

—. 2006b, Monthly Notices of the RAS, 366, 429

Reines, A. E., Condon, J. J., Darling, J., & Greene, J. E. 2020, Astrophysical Journal, 888, 36

Reines, A. E., Greene, J. E., & Geha, M. 2013, Astrophysical Journal, 775, 116

Richardson, J. C., Irwin, M. J., McConnachie, A. W., et al. 2011, Astrophysical Journal, 732, 76

Ricotti, M., & Gnedin, N. Y. 2005, Astrophysical Journal, 629, 259

Roderick, T. A., Jerjen, H., Mackey, A. D., & Da Costa, G. S. 2015, Astrophysical Journal, 804, 134

Rodriguez Wimberly, M. K., Cooper, M. C., Fillingham, S. P., et al. 2019, Monthly Notices of the RAS, 483, 4031

Roychowdhury, S., Chengalur, J. N., Begum, A., & Karachentsev, I. D. 2010, Monthly Notices of the RAS, 404, L60

Ruiz-Lara, T., Gallart, C., Beasley, M., et al. 2018, Astronomy and Astrophysics, 617, A18

Safarzadeh, M., & Loeb, A. 2021, arXiv e-prints, arXiv:2107.03478

Safarzadeh, M., Ramirez-Ruiz, E., Andrews, J. J., et al. 2019, Astrophysical Journal, 872, 105

Saifollahi, T., Janz, J., Peletier, R. F., et al. 2021, Monthly Notices of the RAS, 504, 3580

Sakai, S., Madore, B. F., & Freedman, W. L. 1996, Astrophysical Journal, 461, 713

Sanna, N., Bono, G., Stetson, P. B., et al. 2010, Astrophysical Journal, Letters to the Editor, 722, L244

Sans Fuentes, S. A., De Ridder, J., & Debosscher, J. 2017, Astronomy and Astrophysics, 599, A143

Saviane, I., Held, E. V., & Piotto, G. 1996, Astronomy and Astrophysics, 315, 40

Schlegel, D. J., Finkbeiner, D. P., & Davis, M. 1998, Astrophysical Journal, 500, 525

Schönrich, R., Binney, J., & Dehnen, W. 2010, Monthly Notices of the RAS, 403, 1829

Simon, J. D. 2019, Annual Review of Astronomy and Astrophysics, 57, 375

Simon, J. D., & Geha, M. 2007, Astrophysical Journal, 670, 313

Skillman, E. D., Hidalgo, S. L., Weisz, D. R., et al. 2014, Astrophysical Journal, 786, 44

Skillman, E. D., Monelli, M., Weisz, D. R., et al. 2017, Astrophysical Journal, 837, 102

Slater, C. T., Bell, E. F., & Martin, N. F. 2011, Astrophysical Journal, Letters to the Editor, 742, L14

Slater, C. T., Bell, E. F., Martin, N. F., Tollerud, E. J., & Ho, N. 2015, Astrophysical Journal, 806, 230

Smercina, A., Bell, E. F., Price, P. A., et al. 2018, Astrophysical Journal, 863, 152

Smith, R., Sánchez-Janssen, R., Beasley, M. A., et al. 2015, Monthly Notices of the RAS, 454, 2502

Spekkens, K., Urbancic, N., Mason, B. S., Willman, B., & Aguirre, J. E. 2014, Astrophysical Journal, Letters to the Editor, 795, L5

Stierwalt, S., Besla, G., Patton, D., et al. 2015, Astrophysical Journal, 805, 2

Stonkutė, R., Arimoto, N., Hasegawa, T., et al. 2014, Astrophysical Journal, Supplement Series, 214, 19

Stonkutė, R., Narbutis, D., Bridžius, A., Leščinskaitė, A., & Vansevičius, V. 2015, Baltic Astronomy, 24, 293

Stonkutė, R., Čeponis, M., Leščinskaitė, A., Naujalis, R., & Vansevičius, V. 2018, Astronomy and Astrophysics, 614, A144

Teyssier, M., Johnston, K. V., & Kuhlen, M. 2012, Monthly Notices of the RAS, 426, 1808

Thomas, G. F., Martin, N. F., Fattahi, A., et al. 2021, Astrophysical Journal, 910, 92

Thompson, G. P., Ryan, S. G., & Sibbons, L. F. 2016, Monthly Notices of the RAS, 462, 3376

Tikhonov, N. A., & Galazutdinova, O. A. 2009, Astronomy Letters, 35, 748

Tollerud, E. J., Bullock, J. S., Graves, G. J., & Wolf, J. 2011, Astrophysical Journal, 726, 108

Tollerud, E. J., Geha, M. C., Vargas, L. C., & Bullock, J. S. 2013, Astrophysical Journal, 768, 50

Tollerud, E. J., & Peek, J. E. G. 2018, Astrophysical Journal, 857, 45

Tollerud, E. J., Beaton, R. L., Geha, M. C., et al. 2012, Astrophysical Journal, 752, 45

Tolstoy, E., Hill, V., & Tosi, M. 2009, Annual Review of Astronomy and Astrophysics, 47, 371

Tolstoy, E., Irwin, M. J., Helmi, A., et al. 2004, Astrophysical Journal, Letters to the Editor, 617, L119

Tomozeiu, M., Mayer, L., & Quinn, T. 2016, Astrophysical Journal, Letters to the Editor, 827, L15

Torrealba, G., Koposov, S. E., Belokurov, V., & Irwin, M. 2016, Monthly Notices of the RAS, 459, 2370

Torrealba, G., Belokurov, V., Koposov, S. E., et al. 2019, Monthly Notices of the RAS, 488, 2743

Urbaneja, M. A., Kudritzki, R.-P., Bresolin, F., et al. 2008, Astrophysical Journal, 684, 118

van den Bergh, S. 1999, Astrophysical Journal, Letters to the Editor, 517, L97

van der Marel, R. P. 2006, in The Local Group as an Astrophysical Laboratory, ed. M. Livio & T. M. Brown, Vol. 17, 47–71

van Dokkum, P. G., Abraham, R., Merritt, A., et al. 2015, Astrophysical Journal, Letters to the Editor, 798, L45

van Zee, L., Skillman, E. D., & Haynes, M. P. 2006, Astrophysical Journal, 637, 269

Vansevičius, V., Arimoto, N., Hasegawa, T., et al. 2004, Astrophysical Journal, Letters to the Editor, 611, L93

Veljanoski, J., Mackey, A. D., Ferguson, A. M. N., et al. 2014, Monthly Notices of the RAS, 442, 2929

Veljanoski, J., Ferguson, A. M. N., Mackey, A. D., et al. 2015, Monthly Notices of the RAS, 452, 320

Venhola, A., Peletier, R., Laurikainen, E., et al. 2018, Astronomy and Astrophysics, 620, A165

Venn, K. A., Tolstoy, E., Kaufer, A., et al. 2003, Astronomical Journal, 126, 1326

Verbeke, R., Papastergis, E., Ponomareva, A. A., Rathi, S., & De Rijcke, S. 2017, Astronomy and Astrophysics, 607, A13

Vollmer, B., Marcelin, M., Amram, P., et al. 2000, Astronomy and Astrophysics, 364, 532

Walker, M. G., Mateo, M., & Olszewski, E. W. 2009a, Astronomical Journal, 137, 3100

Walker, M. G., Mateo, M., Olszewski, E. W., et al. 2007, Astrophysical Journal, Letters to the Editor, 667, L53

—. 2009b, Astrophysical Journal, 704, 1274

Walsh, S. M., Jerjen, H., & Willman, B. 2007, Astrophysical Journal, Letters to the Editor, 662, L83

Wang, L., Dutton, A. A., Stinson, G. S., et al. 2015, Monthly Notices of the RAS, 454, 83

Wang, S., Ma, J., & Liu, J. 2019, Astronomy and Astrophysics, 623, A65

Wang, W., Takada, M., Li, X., et al. 2021, Monthly Notices of the RAS, 500, 3776

Weisz, D. R., Dolphin, A. E., Skillman, E. D., et al. 2014, Astrophysical Journal, 789, 147

Weisz, D. R., Dolphin, A. E., Martin, N. F., et al. 2019a, Monthly Notices of the RAS, 489, 763

Weisz, D. R., Martin, N. F., Dolphin, A. E., et al. 2019b, Astrophysical Journal, Letters to the Editor, 885, L8

Westmeier, T., Staveley-Smith, L., Calabretta, M., et al. 2015, Monthly Notices of the RAS, 453, 338

Weżgowiec, M., Bomans, D. J., Ehle, M., et al. 2012, Astronomy and Astrophysics, 544, A99

Wheeler, C., Oñorbe, J., Bullock, J. S., et al. 2015, Monthly Notices of the RAS, 453, 1305

Wheeler, C., Hopkins, P. F., Pace, A. B., et al. 2019, Monthly Notices of the RAS, 490, 4447

White, S. D. M., & Frenk, C. S. 1991, Astrophysical Journal, 379, 52

White, S. D. M., & Rees, M. J. 1978, Monthly Notices of the RAS, 183, 341

Whiting, A. B., Hau, G. K. T., Irwin, M., & Verdugo, M. 2007, Astronomical Journal, 133, 715

Williams, M. E. K., Steinmetz, M., Sharma, S., et al. 2011, Astrophysical Journal, 728, 102

Willman, B., & Strader, J. 2012, Astronomical Journal, 144, 76

Willman, B., Blanton, M. R., West, A. A., et al. 2005, Astronomical Journal, 129, 2692

Wise, J. H., Demchenko, V. G., Halicek, M. T., et al. 2014, Monthly Notices of the RAS, 442, 2560

Wolf, M. 1909, Astronomische Nachrichten, 183, 187

Zhang, H.-X., Paudel, S., Smith, R., et al. 2020, Astrophysical Journal, Letters to the Editor, 891, L23

Zoutendijk, S. L., Brinchmann, J., Boogaard, L. A., et al. 2020, Astronomy and Astrophysics, 635, A107